NMR Study of ^{3}He Adsorbed on Exfoliated Graphite

By

Laila Ibrahim Abou-El-Nasr

Royal Holloway and Bedford New College

A Thesis submitted For The Degree Of

Doctor Of Philosophy

To

University Of London

January 1989

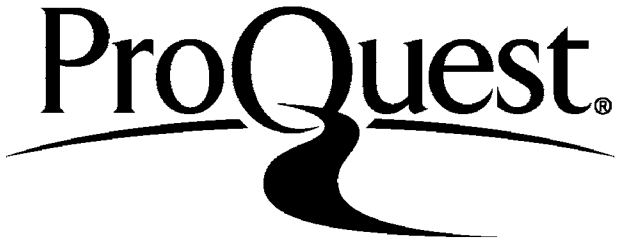

To

My Dearest Family

and to

The Memory of My Father and Sister

ACKNOWLEDGEMENTS

I wish to express my deep gratitude to my supervisor Brian Cowan, for his constant help, discussions and directions throughout the period of my study. My greatest debt is for his insight, support and friendship.

Special thanks should also go to Prof. E.R. Dobbs for his encouragement and support at different stages of my stay here.

My thanks to A. Kent, who showed me around the cryostat and helped me to understand the experimental techniques I used. I am grateful to Francis Greenough and A. Betts who always responded actively and quickly to solve the technical problems.

Thanks to M. Richards who arranged useful seminars between our group and his group. His concern and encouragement were of great help.

Countless thanks go to Mike Fardis for developing the NMR theory and for his interesting discussions and friendship. Thanks to Tom Crane as well for his encouragement and valuable discussions.

I would like to thank S. May for taking photos of the sample chamber, W. Ellis who helped in analyzing the grafoil specimen and G. Lawes who made the grafoil micrograph.

I am grateful to P. Taylor, P. Pal and L. Nodes from the computer centre, for their invaluable assistance and support.

Many thanks to Sheila Pearson for her friendship and help, she was always there when I needed a real friend.

Many people in and around the lab, who with their encouragement,

help and friendship have really made my stay most enjoyable and useful. Amongst these I would like to mention Rawia Abd-El-Monem, S. Abboudy, I. Al-Qaradawi, L. Miljko, S. Simon, P. Fozooni, B. El-Gamal, E. Abd-El-Hady, S. Abou-El-Gheit, A. Hatem, V. Leach, R. White, F. Bayouk, A. Laggetter, O. Stone, J. Frost, J. Saunders, M. Lea, C. Lusher, D. Smith and J. Watt.

I am grateful to the people in Alexandria University and Faculty of Science and to the family of The Egyptian Education Bureau (London) for all sorts of help they have offered me.

All my love and warmest thanks should go to my husband Farid, my daughter Heba and my son Ibrahim who shared a lot with me throughout the years of my study. I am indebted to them for their love, moral support, encouragement, patience and help.

Finally, financial support from The Ministry of Higher Education of Egypt and The Overseas Research Students Award Scheme (ORS) of U.K., is gratefully acknowledged.

ABSTRACT

The present work has been carried out to investigate the dynamic properties of ^{3}He film adsorbed on an exfoliated graphite substrate, using pulsed NMR techniques. It has been found that the dipolar interaction is the dominant mechanism for the spin relaxation, although the effect of the grafoil local fields can not be ignored. The spin-lattice relaxation time T_1 and the spin-spin relaxation time T_2 which characterize the spin system were determined.

The study has been concentrated on two phases. The registered phase and the solid phase. Some data were taken at the mixed phase which lies between them. Both relaxation times were determined as functions of monolayer capacity, frequency, temperature and spin orientations. For temperatures less than 2 K, the spins exhibit quantum motion behaviour. The frequency of this motion was determined and was found to be inversely proportional to the spin density.

At the registered phase, the activation temperature was determined, where it was a maximum corresponding to perfect registry. Special attention was given to the T_1 data at the minima in the solid phase since there the frequency of the motion is comparable to the Larmor frequency.

CONTENTS

CHAPTER 1

Introduction

1.1 The Physisorption Phenomenon:

When one speaks about physisorption it implies a two dimensional (2D) system which consists of two substances. One of them; *the adsorbate*; is held to the surface of the other; *the adsorber*. So, if an atom or molecule approaches the surface of a solid, it will experience a net attractive potential of Van-der-Waals nature. As a result, there will be an appreciable probability for the adsorbate to be trapped on the surface (Somorjai 1981) and the phenomenon of adsorption will occur. The adsorber serves only as a substrate to confine the adsorbate to a plane to obtain a 2-d system.

The adsorption happens when the equilibrium temperature of the system is comparable or less than the attractive potential between the adsorbate and the adsorber. As a result, if enough adatoms (adsorbate) are available and the temperature is low enough; then the surface can completely covered by a layer of adsorbed atoms (Dash 1978). Different techniques have been used to study the properties of physisorbed systems, such as Heat Capacity, Positron Annihilation, Mössbauer Effect, Low Energy Electron Diffraction (LEED), Neutron Scattering and Nuclear Magnetic Resonance (NMR). ^{3}He adsorbed on exfoliated graphite is considered as an excellent combination to study such phenomenon.

1.2 The Choice of ^{3}He:

It is well known that noble gases are attracted to other substances more than to each other. When the gas is cooled (Dash 1973) it is adsorbed as a thin film on the wall of the vessel rather than to condense into droplets or crystals so it makes an ideal adsorbate.

Helium is one of these gases, the element has two isotopes namely ^{3}He and ^{4}He. ^{3}He is a Fermion which has two electrons, two protons and one neutron. The atomic mass is $\approx$ 3.016 and the gyromagnetic ratio is (-3.244 $\times 10^7$) Hz T^{-1}.

1.3 Grafoil as a Convenient Substrate:

The use of graphitized carbon black is very common because the adsorption isotherm data (Thomy and Duval 1969) have shown that the basal planes of graphite offer a uniquely uniform surface to rare gas adatoms. The adsorption isotherm of Kr adsorbed on graphite shows as many as seven steps (Thomy and Duval 1970) corresponding to the clear build-up of distinguishable layers. Building such steps, is the behavior expected from adsorption on a uniform surface.

Another form of graphite is used as a successful substrate, known as *grafoil* (a trade name). This substrate (Bretz et al, errata 1973); (Dash and Schick 1978) is the graphite which has been exfoliated in a strongly oxidizing medium then rinsed and rapidly heated. The expanded particles are pressed together and rolled into binderless flexible sheets which has more surface area than the prototype graphite.

These sheets are composed of graphite crystallites in the form of platelets as shown in the electron micrograph figure (1.3.1). These crystallites tend

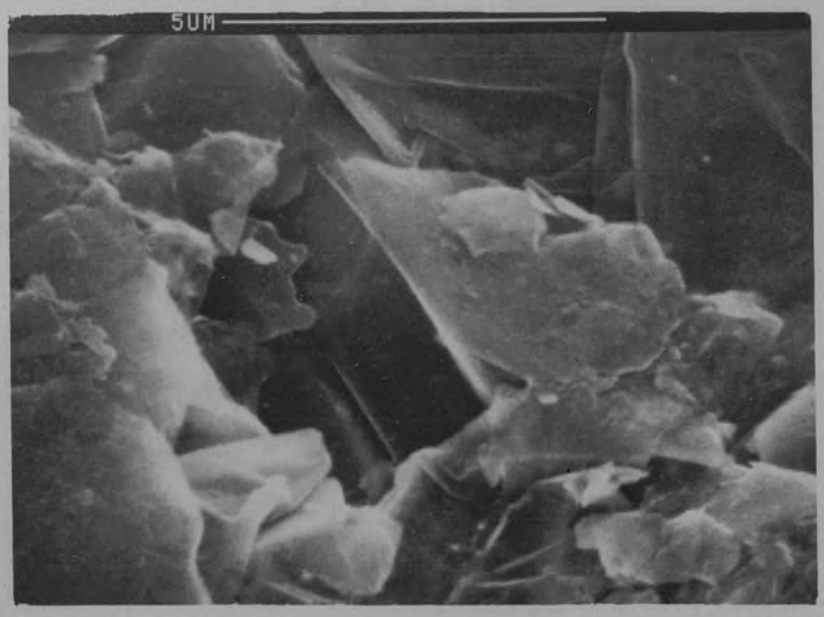

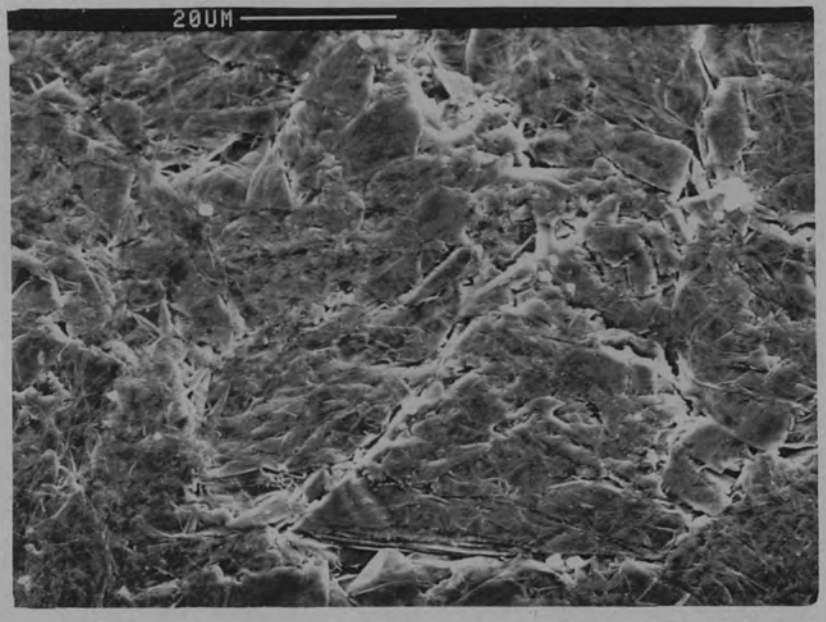

Figure 1.3.1

Electron Micrograph of the Grafoil Specimen with different Magnifications.

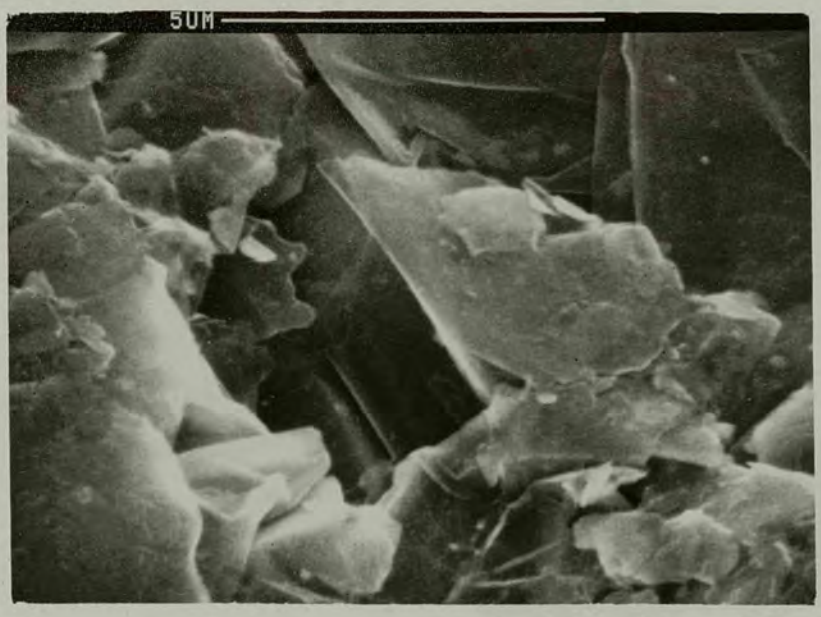
50M

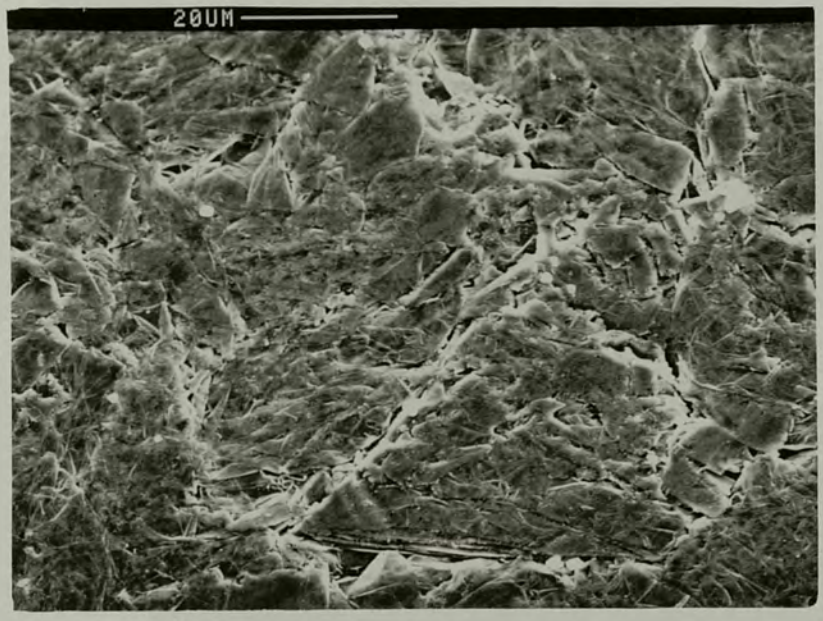
20UM

to align with their C-axes normal to the foil plane (Kjems et al 1976) i.e., their basal planes preferentially oriented parallel to the plane of the foil. The distribution of the C-axes seems to consist of two parts, a purely random part and an oriented part. The full width at half maximum of the C-axes distribution was observed to be 30° which is considered as the substrate mean mis-orientation. The basal plane consists of hexagonal arrays of carbon atoms (Novaco 1973), with a point of minimum potential energy to trap the helium atom through the center of the hexagon (the adsorption site). However the actual length of the exposed basal planes (Kjems et al 1976) is of the order of 100 Å, while the specific area of grafoil is $\approx 20\ m^2/g$ and the area per ^3He atom is about 9.95 $Å^2$ (Grimmer and Luszczynski 1973).

Grafoil is diamagnetic material and its magnetic susceptibility is anisotropic. Although the substrate is quite uniform, it is not ideal and it has varying densities and different types of imperfections and impurities. Before using grafoil in experiments it should be heated in vacuum for several hours to eliminate water vapour and the impurities adsorbed on the surface. It was found that even with the heat treatment, grafoil still has traces of impurities mainly silicon and iron. The analysis of the grafoil used in this work has been done before and after the heat treatment (Hilger & Watts) and the result is shown in table (1.3.1).

1.4 The Phase Diagram:

The monolayer of ^3He film adsorbed on grafoil exhibits several distinct phases. These phases have been investigated by different methods. One of the most effective methods is heat capacity measurements. The first experimental studies have been made by Bretz and Dash (1971). Later on, a phase

Element	Before Heating	After Heating
Silver	2	<1
Gold	<1	<1
Aluminium	200	5
Boron	10	3
Bismuth	1	<1
Calcium	3	3
Cobalt	<1	<1
Chromium	50	5
Copper	1	<1
Iron	≈100	20
Mercury	30	<1
Magnesium	30	5
Manganese	3	<1
Molybdenum	<1	<1
Nickel	10	10
Lead	<1	10
Antimony	<1	<1
Silicon	>500	≈200
Zinc	<1	<1

Table 1.3.1

The chemical analysis of impurities (ppm) contained in the grafoil specimen. Before and after heat treatment.

diagram of this system was constructed (Bretz et al 1973), a reproduction of which is displayed in figure (1.4.1). Bearing in mind that the monolayer is completed at $n = 0.108$ Å^{-2}, where n is the number of atoms per unit area; the different phases could be mainly classified according to coverage and temperature dependence as follows:

1.4.1 The Gas Phase; $x < 0.5$ monolayer:

In this region the ^{3}He atoms exhibit 2D gas behaviour. The heat capacity measurements (Bretz et al 1973) showed that the specific heat is of the order of Boltzmann's constant. Except for very low and high coverage, the film displays 2D gas signature for some range of temperature and the atoms are highly mobile. This behaviour was not seen for any other physisorbed system and it has been considered as a proof of the substrate uniformity.

1.4.2 The Registered Phase; $0.5 < x < 0.66$ monolayer:

This phase is characterised by its regular adatom arrangement with respect to the substrate lattice. Hence the substrate structure affects the behavior of the film as shown in §4.2.

A series of strong heat capacity peaks around 3 K have been observed by Hickernell et al (1972) and Bretz et al (1973) at this region. These peaks are very sensitive to coverage, but the sensitivity is less with the change of temperature. The peak region of this critical coverage was described by a logarithmic temperature dependence of the specific heat (Bretz et al 1973).

$$\frac{C}{Nk_B} = -A \ln | t | + B$$

where $t = (T - T_c)/T_c$, T_c is the temperature at the critical density and A, B are critical parameters, their values were given by (Bretz et al 1973) for different

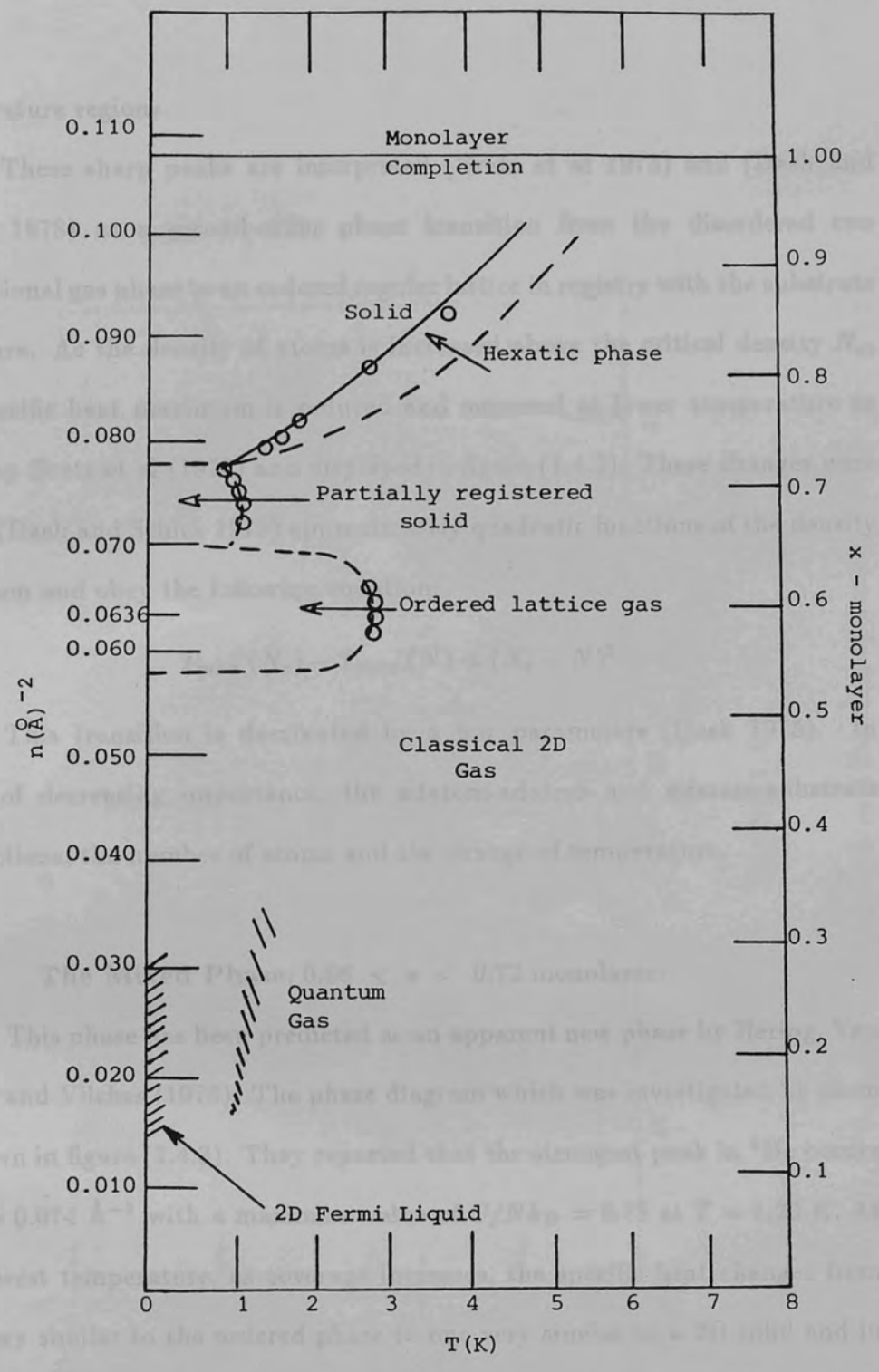

Figure 1.4.1

Phase Diagram of ^{3}He adsorbed on Grafoil as obtained from Heat Capacity Measurements (Bretz et al. 1973)

temperature regions.

These sharp peaks are interpreted (Bretz et al 1973) and (Dash and Schick 1978) as a second-order phase transition from the disordered two dimensional gas phase to an ordered regular lattice in registry with the substrate structure. As the density of atoms is increased above the critical density N_c, the specific heat maximum is reduced and occurred at lower temperature as given by Bretz et al (1973) and displayed in figure (1.4.2). These changes were found (Dash and Schick 1978) approximately quadratic functions of the density deviation and obey the following equation:

$$T_{max.}(N_c) - T_{max.}(N) \propto (N_c - N)^2$$

This transition is dominated by a few parameters (Dash 1975). In order of decreasing importance, the adatom-adatom and adatom-substrate interactions, the number of atoms and the change of temperature.

1.4.3 The Mixed Phase; $0.66 < x < 0.72$ monolayer:

This phase has been predicted as an apparent new phase by Hering, Van Sciver and Vilches (1976). The phase diagram which was investigated by them is shown in figure (1.4.3). They reported that the strongest peak in ^{3}He occurs at $n = 0.074$ Å^{-2} with a maximum value of $C/Nk_B = 0.75$ at $T = 1.23$ K. At the lowest temperature, as coverage increases, the specific heat changes from one very similar to the ordered phase to one very similar to a 2D solid and in between there is a range where the specific heat is independent of the number of atoms. This would suggest a form of coexistence of a solid and registered phases. This coexistence was found in the calculations done by Campbell and Schick (1972) as well.

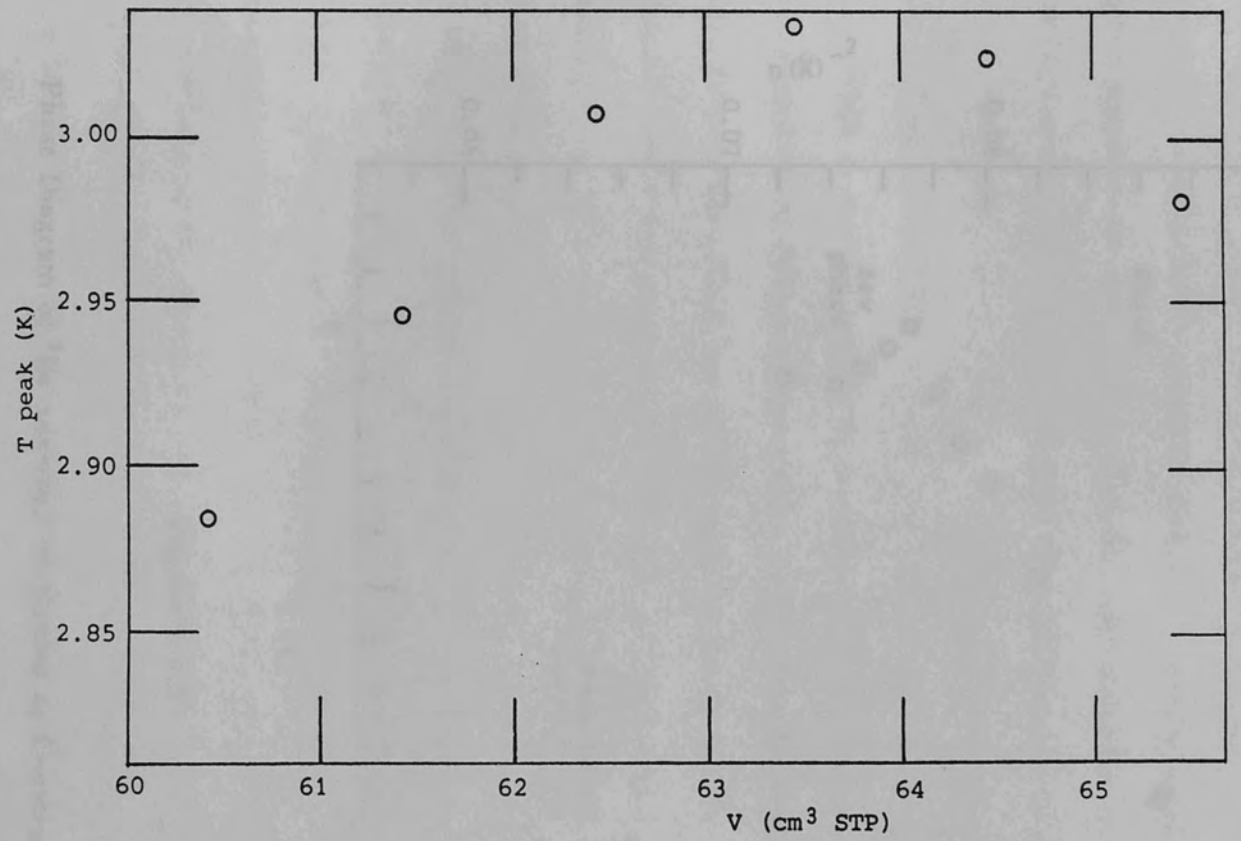

Figure 1.4.2

Temperature of the Peak as a Function of Sample Volume

Bretz et al.(1973)

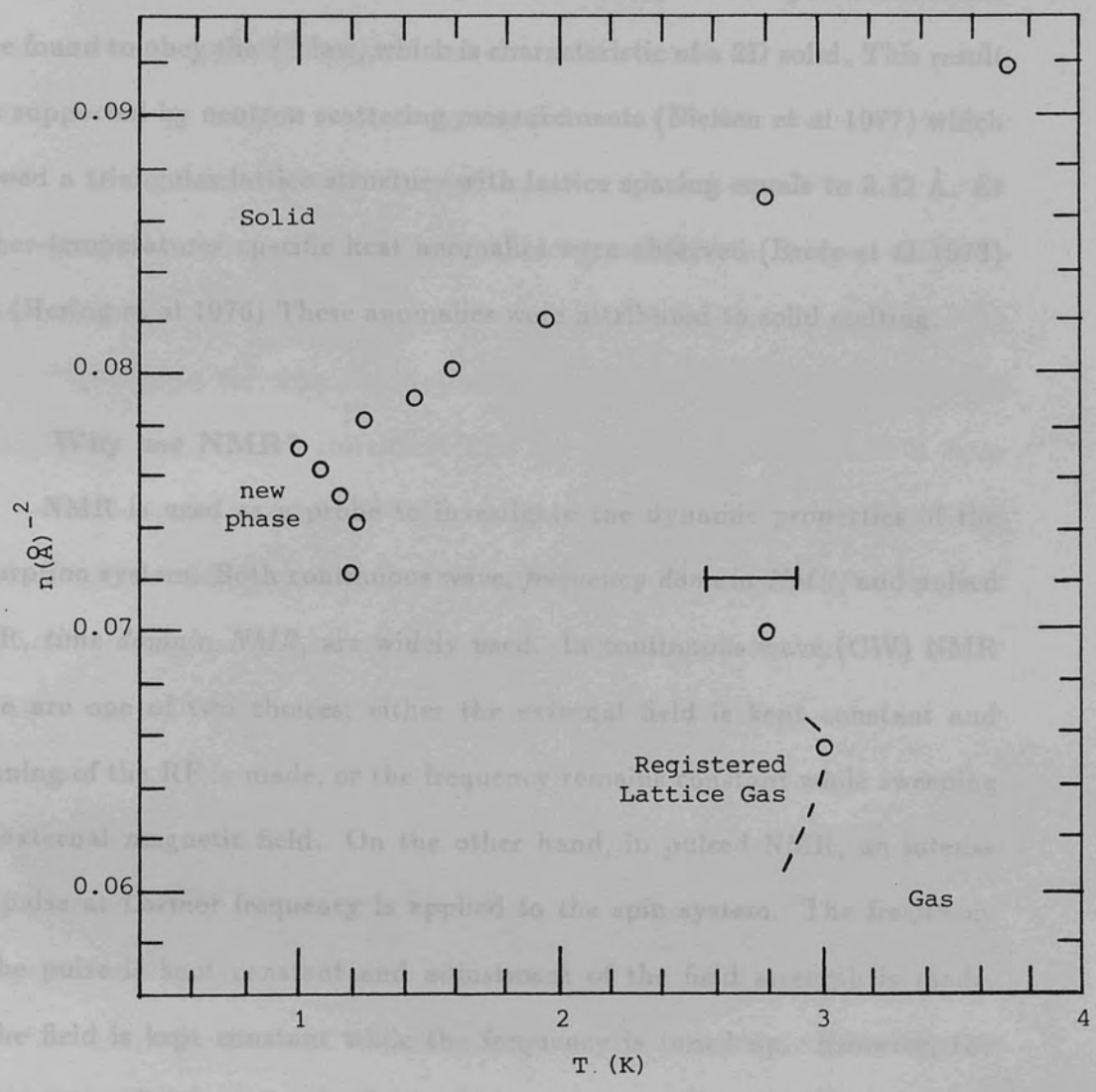

Figure 1.4.3

Phase Diagram of ^{3}He adsorbed on Grafoil as Constructed by Hering et al. (1976)

1.4.4 The Solid Phase; $0.72 < x < 1$ monolayer:

For these high densities coverage, the low temperature specific heat data were found to obey the T^2 law, which is characteristic of a 2D solid. This result was supported by neutron scattering measurements (Nielsen et al 1977) which showed a triangular lattice structure with lattice spacing equals to 3.32 Å. At higher temperatures specific heat anomalies were observed (Bretz et al 1973) and (Hering et al 1976) These anomalies were attributed to solid melting.

1.5 Why use NMR?

NMR is used as a probe to investigate the dynamic properties of the adsorption system. Both continuous wave, *frequency domain NMR*, and pulsed NMR, *time domain NMR*, are widely used. In continuous wave (CW) NMR there are one of two choices; either the external field is kept constant and scanning of the RF is made, or the frequency remains constant while sweeping the external magnetic field. On the other hand, in pulsed NMR, an intense RF pulse at Larmor frequency is applied to the spin system. The frequency of the pulse is kept constant and adjustment of the field strength is made, or the field is kept constant while the frequency is tuned up. However, the resonance condition; $\Delta E = \hbar\gamma B_0$ should be satisfied. Where ΔE is the energy difference between the energy levels, $\hbar$ is Plank's constant divided by 2π, γ is the gyromagnetic ratio of the adsorbate and B_0 is the external magnetic field. Hence both frequency and field are kept constant. These two approaches to resonance are Fourier Transform (FT) of each other, and hence, they lead to the same sort of information.

To use any NMR technique; the requirement of an adsorbate which posses a magnetic moment and an adsorber with a large specific area is essential. Hence

^{3}He and grafoil adsorption system is preferably used. Different informations could be gained by using NMR. Knowledge about spin-dependent interactions either adatom-adatom or adatom-substrate interactions are obtained. The activation energy of the atoms may be determined. The correlation time τ_c of local fields modulation as well as the diffusion coefficient D could give information about the adatoms mobility, so different phases could be distinguished.

^{3}He being a Fermion with a spin half makes NMR studies of its mobility and phase diagram very suitable. The low mass of ^{3}He leads to a large zero point energy (Richards 1971) which results in a significant overlapping of the single particle wave function. Hence the quantum effects are very clear and the exchange motion in solid could be studied which is dominant at low temperature.

1.6 Previous Work:

Using NMR as a tool of investigation, experiments on ^{3}He film adsorbed on various substrates have been carried out. Zeolite molecular sieve substrates were first used (Careri et al 1965), then followed by porous vycor glass (Brewer et al 1970). Nevertheless, both substrates suffered from inhomogeneity.

With graphitized carbon black as a substrate, Rollefson (1972) has done interesting work at 20.5 MHz using CW technique. He observed broadening in the linewidth at perfect registry, which indicates the slow down of the motion of ^{3}He atoms at this region. At $T > 3$ K and $x_{reg.} > x > x_{reg.}$, the reduction of the linewidth was interpreted as motional narrowing due to atomic mobility. These results however were not reproduced by any other group.

Several groups have used grafoil as a substrate which has been proved

to be an excellent candidate for NMR experiments. Richards and his group (Cowan 1976), (Owers-Bradley 1978) (Owers-Bradley et al 1978) have made measurements at 1 MHz and 1 K using both CW and pulsed techniques. They observed a small minimum for both T_1 and T_2 at the density corresponding to registry. While in the solid phase T_1 has a minimum and T_2 decays as coverage increases to reach a minimum value at complete layer. From the T_1 and T_2 dependence on temperature they determined the activation energy corresponding to each coverage. On the other hand, pulsed NMR work was done at 10 MHz and 1 K by Sato and Sugawara (1980). In this work, sharp minimum in T_2 was observed while there was not a lot of change of T_1 with the change of coverage at registry. The activation energy was independent of coverage. Minimum in T_1 was observed in the solid phase as well and T_2 has its lowest value at one layer completion. The results obtained by both groups were compared with the present work.

1.7 Outline of the work:

This thesis has been divided into six chapters. As it has been shown, chapter (1) is a general introduction for the physisorbed system. A description of the phase diagram of ^{3}He adsorbed on grafoil as predicted by heat capacity measurements is done. The reason for the popularity of using NMR to investigate the two dimensional systems is discussed, and why does the ^{3}He-grafoil combination is considered as a good example for such study. Then a review of the previous work is given.

Chapter (2) discuss the NMR theory in two dimensional mater; while chapter (3) is devoted to describe the equipment used in the experimental work, the preparation for the run and how the monolayer is determined using

the adsorption isotherm. Different sequences used to determine T_1 and T_2 are described as well.

Details, analyses and discussion of the experimental data taken at the registered phase and the solid phase are presented in chapter (4) and chapter (5) respectively. Finally, chapter (6) gives a summary for the experimental work discussed previously as well as suggestions for further work.

CHAPTER 2

ASPECTS OF THE NMR THEORY

2.1 Introduction:

The NMR phenomenon is based on the effect of the external magnetic field applied to the spins system. In the absence of the magnetic field, the spins are randomly oriented, while the application of the field causes splitting of the energy levels. If a static magnetic field B_0 is applied to a nucleus with a spin 1/2, its energy levels split into two sub levels with distribution of the spins governed by Boltzmann law:

$$\frac{N_1}{N_2} = exp(\frac{-\Delta E}{k_B T})$$

where N_1 and N_2 are the population of each level, and the energy difference between these levels is $\Delta E = \gamma \hbar B_0$. This implies that each spin should adopt one of the two orientations.

If the nucleus has an angular momentum **I** and magnetic moment $\boldsymbol{\mu}$, it will precess around the field at Larmor frequency $\omega_0 = -\gamma B_0$ where $\gamma = \mu/\hbar I$ is the gyromagnetic ratio which is a characteristic parameter for the nucleus. If the field is chosen to be in the z-direction, in bulk matter the equilibrium magnetization M_z parallel to the field will be given by:

$$M_z = M_0 = \frac{\chi_0}{\mu_0} B_0$$

where χ_0 is the equilibrium magnetic susceptibility.

It is well known that the condition for the magnetic absorption to occur, is the existence of a population difference between the energy levels. Therefore,

to introduce this transition, an oscillating field should be applied to the system. Hence an RF field B_1 is applied perpendicular to the steady field B_0.

It is helpful if the motion of the magnetization is viewed in a coordinate system (x', y', z') which rotates about B_0 in the same direction as the nuclear moments precess and with the same angular frequency ω_0. This rotating frame has its z' axis parallel to the steady field B_0 and its x' axis in the same direction as B_1. Hence, the field B_1 could be thought of as rotating in x-y plane with an angular frequency ω_0. As a result; the effect of B_0 could be cancelled and after a time t the net magnetization would precess about B_1 with an angle $\beta = \gamma B_1 t$.

If this angle is chosen to be 90°, the magnetization M_z will be tipped to the x-y plane. The *transverse magnetisation* will shrink to zero because of the effect of the inhomogeneity of the magnet. The time constant for this shrinking is T_2^* and the observed time varying signal is the FID. On the other hand, if the angle β is chosen as 180°, the *longitudinal magnetisation* will rotate to the -z-direction. In this case the magnetisation will relax back to its equilibrium value in time T_1.

The theoretical approach to the NMR problems has been done quantum mechanically by different groups such as Bloembergen, Purcell and Pound (1948); Van vleck (1948); Kubo and Tomita (1954) and Cowan (1980).

2.2 Quantum Mechanical Approach:

In quantum theory; a system is specified by its Hamiltonian operator. Hence, for an assembly of nuclear spins the general form of the Hamiltonian is given by:

$$\mathcal{H} = \mathcal{H}_z + \mathcal{H}_d + \mathcal{H}_m \qquad (2.2.1)$$

where $\mathcal{H}_z$ is the Zeeman part which represents the interactions between the

individual magnetic moments and the applied static magnetic field. Since the magnetic energy is given as $(-\mathbf{B}_0 \cdot \mathbf{M})$, the Zeeman Hamiltonian can be written in the following form:

$$\mathcal{H}_z = -B_0 \gamma \hbar I_z = \hbar \omega_0 I_z$$

where I_z is the operator of z-component of the spin angular momentum of the system.

The Hamiltonian $\mathcal{H}_d$ represents all the inter-spin interactions, mainly the dipole-dipole interaction which is given as:

$$\mathcal{H}_d = \hbar^2 \gamma^2 \left(\frac{\mu_0}{4\pi}\right) \sum_{i<j} \left\{ \mathbf{I}_i . \mathbf{I}_j - 3 \frac{(\mathbf{I}_i . \mathbf{r}_{ij})(\mathbf{I}_j \cdot \mathbf{r}_{ij})}{r_{ij}^2} \right\} \Big/ r_{ij}^3 \qquad (2.2.2)$$

where $\mathbf{I}_i$ is the angular momentum operator of the i^{th} spin and $\mathbf{r}_{ij}$ is the distance between the i^{th} and the j^{th} spins. It is convenient for the sake of simplicity; to expand $\mathcal{H}_d$ into its various spin-flip components (Landesman 1973),

$$\mathcal{H}_d = \sum_{m=-2}^{2} D_m$$

$$D_m = \hbar^2 \gamma^2 \left(\frac{\mu_0}{4\pi}\right) \left(\frac{4\pi}{5}\right)^{1/2} \sum_{i<j} Y_2^{-m}(\mathbf{\Omega}_{ij}) T_{ij}^m (-1)^m / r_{ij}^3$$

where $\mathbf{\Omega}_{ij}$ is the direction of $\mathbf{r}_{ij}$, Y_2^{-m} is a spherical harmonic of the second order and T_{ij}^m is a tensor spin operator. T_{ij} is given by:

$$T_{ij}^0 = \mathbf{I}^i . \mathbf{I}^j - 3 I_z^i I_z^j$$

$$T_{ij}^1 = (3/2)^{1/2} (I_z^i \, I_+^j \; + \; I_z^j \, I_+^i) = -(T_{ij}^{-1})^+$$

$$T_{ij}^2 = -(3/2)^{1/2} \, I_+^i \, I_+^j \; = (T_{ij}^{-2})^+$$

The significance of these terms is that, due to the properties of the operators I_+ and I_-, they couple together different eigenstates of $\mathcal{H}_z$ separated in energy by $m\hbar\omega_0$. So T_{ij}^2 flips two spins and T_{ij}^1 flips only one spin while the adiabatic

term T_{ij}^0 implies that there is no net spin flip and hence the Zeeman energy is conserved.

The use of such spin operator is particularly convenient since they satisfy the following angular momentum commutation relations:

$$[I_z, T_{ij}^m] = mT_{ij}^m$$

$$[I_\pm, T_{ij}^m] = [6 - m(m \pm 1)]^{1/2}\ T_{ij}^\pm.$$

Finally, the motion Hamiltonian $\mathcal{H}_m$ generates various motions of the spins and most generally contains their potential and kinetic energies. As a special case, in solid helium-3 the small mass of the atoms results in a large zero point motion and a consequent overlap of the wave functions of nearest neighbour particles (Richards 1971). This results in quantum mechanical tunneling whereby the atoms of the solid are able to exchange places and thus possess a degree of mobility. Pairwise exchange motion is described by the Heisenberg Hamiltonian (Landesman 1973),

$$\mathcal{H}_x = -2\sum_{i<j} J_{ij}\mathbf{I}^i \,.\, \mathbf{I}^j$$

Where J_{ij} is the exchange parameter which is constant for nearest neighbour exchange known as the exchange frequency J and zero otherwise. Such a Hamiltonian generates the exchange of two particles i and j at an (angular) frequency J_{ij}. Early treatments of exchange in solid ^{3}He was based on such a two particle description of motion. However, particularly as a result of the new ordered phases (Roger et al 1980) it seems that this description is inadequate. Therefore, the hierarchy of multiple exchange motion must be introduced. From energetic considerations (Roger 1984), it appears that three particle exchange is dominant in two dimensional triangular lattice. The Hamiltonian for this

process may be written as,

$$\mathcal{H}_3 = -2 \sum_{i<j<k} J_{ijk} \left(\mathbf{I}^i \,.\, \mathbf{I}^j + \mathbf{I}^j \,.\, \mathbf{I}^k + \mathbf{I}^k \,.\, \mathbf{I}^i \right)$$

and thus the three particle exchange Hamiltonian could be written as an effective two particle exchange Hamiltonian (Roger 1984) with different frequency,

$$\begin{aligned} \mathcal{H}_3 &= \mathcal{H}_x \\ &= -2J \sum_{i<j} \mathbf{I}^i \,.\, \mathbf{I}^j \end{aligned}$$

where,

$$J = 3J_3$$

for this reason, the simple two particle exchange Hamiltonian will be used in all the following.

2.3 Evaluation of the Relaxation Functions:

If the spin system described by the previous Hamiltonian $\mathcal{H}$ is disturbed; then the evolution of the system is governed by the transverse relaxation function $F(t)$ and the longitudinal relaxation function $L(t)$. To evaluate these functions, the following procedures (Cowan 1987) have been followed.

The magnetization of the spins $M(t)$ is a result of the disturbance of the spins equilibrium state. Appendix A is devoted for the mathematical derivation of such state. The resultant magnetization is given by equations (A3) and (A4) for the transverse magnetization and by equation (A5) for the longitudinal magnetization. The Larmor precession is included in a term such as $(exp\ i\omega t)$ in the transverse magnetization. Therefore to extract this term, it is required to introduce the complex magnetization.

$$m_+ = m_x + i m_y$$

and the spin raising and lowering operators

$$I_+ = I_x + iI_y$$

$$I_- = I_x - iI_y$$

From equations (A3) and (A4), the transverse magnetization can be written as:

$$m(t)_+ = \frac{\gamma\beta\hbar^2\omega_0}{V}\,(\frac{\mu_0}{4\pi})\,Tr\,\{I_+(t)\,I_x(0)\}\,/Tr\,\{1\}$$

which can be proved (Appendix B) to be as follows:

$$m(t)_+ = \frac{\gamma\beta\hbar^2\omega_0}{2V}\,(\frac{\mu_0}{4\pi})\,Tr\,\{I_+(t)\,I_-(0)\}\,/Tr\,\{1\} \qquad (2.3.1)$$

where $\beta = 1/K_BT$ and V is a unit volume of the sample.

The major part of the motion of the transverse magnetization is the Larmor precession. Superimposed on this is the actual relaxation. The following procedures were made to distinguish both terms.

Recall that the total Hamiltonian for the spin system is given by equation (2.2.1),

$$\mathcal{H} = \mathcal{H}_z + \mathcal{H}_d + \mathcal{H}_m$$

If $\mathcal{H}_d = 0$, we are left with the Larmor precession part only as will be shown. The Heisenberg equation of motion of I_+ is given by

$$\frac{d}{dt}I_+(t) = \frac{i}{\hbar}[\mathcal{H}_z + \mathcal{H}_m\,,\,I_+(t)]$$

Since $\mathcal{H}_m$ operates in the real space and I_+ operates in spin space then, $[I_+, \mathcal{H}_m] = 0$ and the equation of motion becomes,

$$\frac{d}{dt}I_+(t) = i\omega_0[I_z, I_+(t)]$$

$$= i\omega_0 I_+$$

integrating this equation we obtain:

$$I_+(t) = exp(i\omega_0 t) I_+(0)$$

substituting in equation (2.3.1),

$$m_+(t) = \frac{\gamma\beta\hbar^2\omega_0}{2V} \left(\frac{\mu_0}{4\pi}\right) exp(-i\omega_0 t)\, Tr\left\{I_+(0)\, I_-(0)\right\} / Tr\left\{1\right\} \qquad (2.3.2)$$

It is clear that the time dependence is contained in the oscillatory factor $(exp - i\omega_0 t)$ only; no relaxation term is included yet.

To introduce the relaxation term we should transfer to the *interaction representation* where the time evolution is contained in both the operator and the wave function. The operator $U(t) = exp\frac{i}{\hbar}\mathcal{H}\ t$, is defined such that the time dependence of $I_+(t)$ could be expressed as:

$$I_+(t) = U(t) I_+(0) U^{-1}(t)$$

Now, $\mathcal{H}_{\ d}$ is included to the Hamiltonian, which effect is to give the relaxation part; while $\mathcal{H}_{\ m}$ is excluded because there is no lattice motion.

$U(t)$ is factorized such that:

$$U(t) = S(t) exp - \frac{i}{\hbar}\mathcal{H}_{\ z}\ t$$

and

$$U^+(t) = exp\frac{i}{\hbar}\mathcal{H}_{\ z}\ tS^+(t)$$

It was found that $(exp\frac{i}{\hbar}\mathcal{H}_{\ z}\ t)$ represents Larmor precession, hence $S(t)$ represents the decay of the magnetization vector. Therefore equation (2.3.2) could be written as:

$$m_+(t) = \frac{\gamma\beta\hbar^2\omega_0}{2V} \left(\frac{\mu_0}{4\pi}\right) exp(-i\omega_0 t) Tr\left\{S(t) I_+(0) S^+(t) I_-(0)\right\} / Tr\left\{1\right\}$$

or

$$m_+(t) = \frac{\gamma\beta\hbar^2\omega_0}{2V} \left(\frac{\mu_0}{4\pi}\right) exp(-i\omega_0 t) Tr\left\{I_+(t)\, I_-(0)\right\} / Tr\left\{1\right\}$$

This relaxation term $[Tr\{I_+(t)I_-(t)\}]$ represents the decay of the envelope which is observed experimentally. This relaxation term is normalized to unity at zero time. Hence the fundamental transverse relaxation function is obtained as:

$$F(t) = Tr\{I_+(t)I_-(0)\} / \{I_+I_-\}$$

Following the same fashion, the fundamental longitudinal relaxation function is given by:

$$L(t) = Tr\{I_z(t)I_z(0)\} / \{I_z^2\}$$

Finally the actual transverse and longitudinal magnetization were given as follows:

$$\begin{aligned} m_+(t) &= \frac{\gamma\beta\hbar^2\omega_0}{2V} \frac{Tr\{I_+(0)\, I_-(0)\}}{Tr\{1\}} exp(-i\omega_0 t)F(t) \\ m_z(t) &= \frac{\gamma\beta\hbar^2\omega_0}{2V} \frac{Tr\{I_z^2(0)\}}{Tr\{1\}} L(t) \end{aligned} \tag{2.3.3}$$

2.4 The Cumulant Approximation:

The normalized FID function in x-direction is given (Abragam 1961) by the spin torque correlation function $G(t)$. Instead of evaluating $G(t)$ by using the method of moments or by applying the perturbation theory, the *cumulant method* (Kubo and Tomita 1954) has been employed. The reason was that; for long-time the expansion diverges unless an infinite number of terms is included, while in cumulant method the high-order terms are approximated in terms of the lower-order ones.

Assuming high temperature limit:

$$G(t) = Tr\{I_x(t)\, I_x(0)\}/Tr\, I_x^2$$

where the time development of I_x is generated by the coupling Hamiltonian

$\mathcal{H}_1$ which includes both $\mathcal{H}_d$ and $\mathcal{H}_z$,

$$i\dot{I}(t) = [I_x(t) \,.\, \mathcal{H}_1(t)]$$

hence,

$$G(t) = Tr\left\{ I_x exp\left(i\varepsilon \int_0^t \mathcal{H}_1(t)\, dt \right) I_x \left[exp\left(i\varepsilon \int_0^t \mathcal{H}_1\, dt \right) \right]^+ \right\} \Big/ TrI_x^2 \tag{2.4.1}$$

the expansion parameter ε has been introduced to keep track of the powers of $\mathcal{H}_1$ in a perturbation expansion.

The function $\Psi(t)$ defined by

$$G(t) = exp\Psi(t) \tag{2.4.2}$$

is evaluated in different order of ε. From equations (2.4.1) and (2.4.2) the expression for $\Psi(t)$ (Cowan 1977) is given as follows:

$$\Psi(t,\varepsilon) = \ln Tr\left\{ I_x\, exp\left(i\varepsilon \int_0^t \mathcal{H}_1(\tau)\, d\tau \right) I_x \left[exp\left(i\varepsilon \int_0^t \mathcal{H}_1\, d\tau \right) \right]^+ \right\} \Big/ TrI_x^2$$

expanding $\Psi(t,\varepsilon)$ in a power series in ε gives,

$$\Psi(t,\varepsilon) = \Psi(t,0) \;+\; \varepsilon \frac{d}{d\varepsilon}\Psi(t,0) \;+\; \frac{\varepsilon^2}{2}\,\frac{d^2}{d\varepsilon^2}\Psi(t,0) \;+\cdots$$

It has been found (Kubo and Tomita 1954) that expanding to the lowest-order non-vanishing term which is the second order of ε is sufficient. After ignoring the small imaginary terms (Cowan 1977), the transverse relaxation function took the form,

$$F(t) = exp\left[-\int_0^t (t-\tau) \sum_{m=-2}^{2} (3 - \frac{m^2}{2})\, G_m(\tau)\, exp(im\omega_0\tau)\, d\tau \right] \tag{2.4.3}$$

and similarly, the longitudinal relaxation function could be written as,

$$L(t) = exp\Big[-\int_0^t (t-\tau) \sum_{m=-2}^{2} m^2\, G_m(\tau)\, exp(im\omega_0\tau)\, d\tau\Big] \qquad (2.4.4)$$

One should bear in mind that the spin-torque correlation functions $G_m(t)$ are the autocorrelation functions of the dipolar Hamiltonian components (Cowan 1980),

$$G_m(t) = Tr\{D_m(0)\, D_{-m}(\tau)\}/TrI_z^2 \qquad (2.4.5)$$

and that the time dependence of the D_m being generated only by the motion Hamiltonian. In general, in both direct space where r_{ij} varies and spin space where the spin operator varies, one could write:

$$G_m(t) = \frac{4\pi\hbar^2\gamma^4}{5N} \left(\frac{\mu_0}{4\pi}\right)^2 \sum_{\substack{i<j \\ k<l}} \frac{Y_2^{-m}\,(\Omega_{ij}(0))\; Y_2^{m}\,(\Omega_{kl}(t))}{r_{ij}^3(0)\; r_{kl}^3(t)}\; \Gamma_{ijkl}(t)$$

where $\Gamma_{ijkl}(t)$ is a symmetric four spin correlation function which describes the motion in the spin space and defined as:

$$\Gamma_{ijkl}(t) = N\; Tr\{T_{ij}^{m}(0)\; T_{kl}^{-m}(t)\}/TrI_z^2$$

Assuming that $G_m(\tau)$ decays to zero sufficiently fast; the upper limit of the integrals in equations (2.4.3) and (2.4.4) would be extended to infinity (Cowan 1980) leading to exponential relaxation,

$$L(t) \sim exp(-t/T_1)$$

$$F(t) \sim exp(-t/T_2)$$

where T_1 and T_2, the spin-lattice and spin-spin relaxation times are given by,

$$\begin{aligned} \frac{1}{T_1} &= J_1(\omega_0) \;+\; 4J_2(2\omega_0) \\ \frac{1}{T_2} &= \frac{3}{2}J_0(0) \;+\; \frac{5}{2}J_1(\omega_0) \;+\; J_2(2\omega_0) \end{aligned} \qquad (2.4.6)$$

where the spectral density functions $J_m(\omega_0)$ are the *Fourier Transform* of the correlation functions and given by:

$$J_m(\omega) = \int_{-\infty}^{\infty} G_m(t)\ exp(i\omega t)\ dt$$

2.5 Transformation into Two Dimensions:

The long time behaviour of the correlation function depends crucially on the dimensionality ($\sim\ t^{-d/2}$). In three dimensions, the decay of $G_m(t)$ is sufficiently fast and the previous condition is verified. In case of 2D, this dependence causes some functions to diverge. The non-adiabatic part ($m \neq 0$) will ensure convergence through the oscillating factor $exp(im\omega_0 t)$. The problem is created from the adiabatic term ($m = 0$) in the transverse relaxation function. Hence there is a need of special treatment for 2D.

Transformation into 2D system and using a reference frame based on the substrate surface, the orientation of the spins is then given by the azimuthal angle in this plane and the $G_m(t)$ functions will take the following form:

$$\begin{aligned}
G_0(t) &= \frac{27}{64}\hbar^2\gamma^4\,(\frac{\mu_0}{4\pi})^2\left\{(\sin^2\beta - \frac{2}{3})^2\ g_0(t)\ +\ \frac{\sin^4\beta}{2}\ g_2(t)\right\}\\
G_1(t) &= \frac{9}{32}\hbar^2\gamma^4\,(\frac{\mu_0}{4\pi})^2\left\{\cos^2\beta\ \sin^2\beta\ g_0(t)\ +\ \frac{\sin^2\beta(1+\cos^2\beta)}{2}\ g_2(t)\right\}\\
G_2(t) &= \frac{9}{128}\hbar^2\gamma^4\,(\frac{\mu_0}{4\pi})^2\left\{\sin^4\beta\ g_0(t)\ +\ \frac{\cos^4\beta + 6\cos^2\beta + 1}{2}\ g_2(t)\right\}
\end{aligned} \tag{2.5.1}$$

where the positional correlation functions $g_n(t)$ are given as follows:

$$g_n(t) = \frac{4}{3N}\sum_{\substack{i<j\\k<l}} \frac{exp(-in\phi_{ij}(0))\ exp(in\phi_{kl}(t))}{r_{ij}^3(0)\ r_{kl}^3(t)}\ \Gamma_{ijkl}(t) \tag{2.5.2}$$

As it has been shown from the previous treatment, the problem of determining the relaxation functions has been reduced to evaluate the functions $g_0(t)$ and $g_2(t)$ for specific models for the motion.

2.6 Different Models for the Motion:

2.6.1 Diffusion:

In the case of random motion of the spins, the correlation functions $g_n(t)$ are completely classical. It is extremely difficult to solve equation (2.5.2), so replacing the summation with an integral over a probability function (Cowan 1980) gives:

$$g_n(t) = \frac{2\pi\alpha}{a^4} \int_0^\infty dx\, x^3 p(x/a,t) \left[\int_x^\infty \frac{J_n(y)\, dy}{y^2} \right]^2$$

where the probability function is given by,

$$p(r,t) = (1/8\pi Dt)\, exp(-r^2/8Dt)$$

If the motion of the spins could be described by a two dimensional diffusion equation, $g_n(t)$ are given by (Cowan 1980),

$$g_n(t) = \frac{2\pi\alpha}{a^4} \int_0^\infty dx\, x^3 exp - \frac{tx^2}{\tau_c} \left[\int_x^\infty \frac{J_n(y)\, dy}{y^2} \right]^2 \qquad (2.6.1)$$

Bearing in mind that $p(x/a,t)$ is the spatial Fourier Transform of $p(r,t)$ and α is the assumed uniform spin density within a hard core sphere of radius a while τ_c is the time which is taken by the spin to diffuse a distance a and given as $\tau_c = \frac{a^2}{2D}$ where D is the two dimensional diffusion coefficient and $J_n(y)$ is the n^{th} order Bessel function.

The above integrals cannot be evaluated analytically as in the case of three dimensions. However, numerical evaluation was performed by Avogadro and Villa (1977) and the reference in their paper. These calculations showed that the decay of $g_0(t)$ is much slower than that of $g_2(t)$.

2.6.1a Long-Time Behaviour:

To find the long-time behaviour of the correlation functions; integrating equation (2.6.1) by parts series expansion for $J_n(y)$, then integrate over x term by term. Therefore, the long time decay of $g_n(t)$ is given as,

$$g_0(t) = g(0)\left\{2\frac{\tau_c}{t} - 2\sqrt{\pi}\left(\frac{\tau_c}{t}\right)^{3/2} + 3\left(\frac{\tau_c}{t}\right)^{2} + \cdots\right\}$$

$$g_2(t) = g(0)\left\{\frac{2}{9}\frac{\tau_c}{t}^{2} - \frac{\sqrt{\pi}}{8}\left(\frac{\tau_c}{t}\right)^{5/2} + \frac{1}{16}\left(\frac{\tau_c}{t}\right)^{3} + \cdots\right\}$$

if $t \gg \tau_c$, the leading term will be dominant and hence

$$\begin{aligned} g_0(t) &\sim g(0)2\frac{\tau_c}{t} \\ g_2(t) &\sim g(0)\frac{2}{9}\left(\frac{\tau_c}{t}\right)^{2} \end{aligned} \tag{2.6.2}$$

2.6.1b Short-Time Behaviour:

It is a great difficulty to examine the short-time behaviour of the correlation functions since the diffusion is a hydrodynamic concept which is valid only for long time.

However, with suitable approximations the short-time spatial correlation functions were found (Cowan 1980) as:

$$g_n(t) = g(0) \times 4\int_0^{\infty} dx\, x^3 exp - \frac{t^2x^2}{\tau_c\tau_0}\left[\int_x^{\infty} \frac{J_n(y)\, dy}{y^2}\right]^2$$

where $g(0) = \pi\alpha/2a^4$ and τ_0 is the mean time between atomic collisions.

The transverse relaxation is dominant by the long tail of $g_0(t)$ while the short-time behaviour affects the longitudinal relaxation time in the high frequency/slow motion limit.

2.6.1c Longitudinal Relaxation:

From equation (2.4.6) T_1 is given by the following expression:

$$\frac{1}{T_1} = J_1(\omega_0) + 4J_2(2\omega_0)$$

the spectral densities $J_n(\omega_0)$ are the Fourier Transform of

the autocorrelation functions $G_n(t)$,

$$J_0(\omega) = \frac{27}{64}\hbar^2\gamma^4 \left(\frac{\mu_0}{4\pi}\right)^2 \left\{(\sin^4\beta - \frac{2}{3})^2 j_0(\omega) + \frac{1}{2}\sin^4\beta j_2(\omega)\right\}$$

$$J_1(\omega) = \frac{9}{32}\hbar^2\gamma^4 \left(\frac{\mu_0}{4\pi}\right)^2 \left\{\cos^2\beta \sin^2\beta j_0(\omega) + \frac{1}{2}\sin^4\beta(1+\cos^2\beta)\, j_2(\omega)\right\}$$

$$J_2(\omega) = \frac{9}{128}\hbar^2\gamma^4 \left(\frac{\mu_0}{4\pi}\right)^2 \left\{\sin^4\beta j_0(\omega) + \frac{1}{2}(\cos^4\beta + 6\cos^2\beta + 1)\, j_2(\omega)\right\}$$

where the spectral functions $j_n(\omega)$ are the Fourier Transform of the spatial correlation functions $g_n(t)$.

It was found (Cowan 1980) that the $n = 2$ term exhibits normally of being flat for $\omega_0\tau_c < 1$. While there is the logarithmic divergence of $n = 0$ term which reduces the value of T_1 in the low frequency/fast motion limit.

2.6.1d Transverse Relaxation:

It is clear that equation (2.4.3) splits into two parts; the adiabatic part where $m = 0$ and the non-adiabatic part where $m \neq 0$, therefore we can write:

$$F(t) = exp\left(-t/T_2^{na}\right) exp\left(-3\int_0^t (t-\tau)\, G_0(\tau)\, d\tau\right) \qquad (2.6.3)$$

where the non-adiabatic part is given by,

$$\frac{1}{T_2^{na}} = \frac{5}{2}J_1(\omega_0) + J_2(2\omega_0)$$

This equation looks similar to that of $\frac{1}{T_1}$, so it was treated in a similar fashion to give a relaxation rate,

$$\frac{1}{T} = \frac{81}{256}\hbar^2\gamma^4 \left(\frac{\mu_0}{4\pi}\right)^2 \sin^4\beta j_2(0)$$

or by substituting the value of $j_2(0)$

$$\frac{1}{T} = 0.237\hbar^2\gamma^4 (\frac{\mu_0}{4\pi})^2 \frac{\alpha\tau_c}{a^4} \sin^4\beta \qquad (2.6.4)$$

Now the adiabatic part has contributions from both $g_0(t)$ and $g_2(t)$ functions. Since there is no divergence in the integral of $1/t^2$ in $g_2(t)$, the limit of the integral could be extended to infinity and the result is an exponential contribution to the relaxation.

On the other hand, the $g_0(t)$ correlation function gives a non-exponential contribution to the relaxation because it does not decay to zero fast enough. This component of the relaxation function is,

$$f(t) = exp - \left\{ \frac{81}{64}\hbar^2\gamma^4 (\frac{\mu_0}{4\pi})^2 \left(\sin^2\beta - \frac{2}{3}\right)^2 \int_0^t (t-\tau)\, g_0(\tau) d\tau \right\}$$

this function $f(t)$ is the dominant part of the relaxation. Since it is not exponential it cant be characterised by a relaxation time. Instead; the *instantaneous* relaxation rate $1/T(t)$ is introduced;

$$\frac{1}{T(t)} = \frac{81}{64}\hbar^2\gamma^4 (\frac{\mu_0}{4\pi})^2 \left(\sin^2\beta - \frac{2}{3}\right)^2 \int_0^t g_0(\tau) d\tau$$

Hence,

$$\frac{1}{T_2} = \frac{1}{T(T_2)}$$

and

$$\frac{1}{T_2} = \frac{81}{64}\hbar^2\gamma^4 (\frac{\mu_0}{4\pi})^2 (\sin^2\beta - \frac{2}{3})^2 \int_0^{T_2} g_0(\tau) d\tau \qquad (2.6.5)$$

Now from equations (2.6.4) and (2.6.5), the following definition were made (Cowan 1980),

$$M_2' = \frac{81}{128} \frac{\pi\alpha\hbar^2\gamma^4}{a^4} (\frac{\mu_0}{4\pi})^2 \left(\sin^2\beta - \frac{2}{3}\right)^2$$

$$M_2'' = \frac{81}{256} \frac{\pi\alpha\hbar^2\gamma^4}{a^4} (\frac{\mu_0}{4\pi})^2 \sin^4\beta$$

where the second moment is defined as,

$$M_2 = M_2' + M_2''$$

So equation (2.6.4) tends to be

$$\frac{1}{T} = 0.329\, M_2''\, \tau_c$$

which takes the form of the NMR rule of thumb,

$$\frac{1}{T_2} = M_2\, \tau \tag{2.6.6}$$

where M_2 is the second moment which is the mean square value of the local fields multiplied by γ^2. While τ is the characteristic time associated with the motion.

To study the general feature of the relaxation (Cowan 1980), $g_0(t)$ could be approximated to:

$$g_0(t) \sim \frac{g(0)}{1 + t/2\tau_c}$$

this analytical expression has the correct value at $t = 0$ and is asymptotically correct at long times. Therefore integrating equation (2.6.5) for the adiabatic part and add the non-adiabatic contribution of equation (2.6.4) to it,

$$\frac{1}{T_2} = 2\ln(T_2/2\tau_c e)\, M_2'\tau_c + 0.329 M_2''\tau_c$$

the logarithmic dependence in the $n = 0$ part implies the insensitivity to the motion, specially that it is affected only by the internuclear separation and not the orientation.

2.6.2 Exchange:

As mentioned previously §2.2, the Heisenberg exchange Hamiltonian for two particle exchange could be introduced for three particle exchange but with different frequency,

$$\mathcal{H}_x = -2\sum_{i<j} J_{ij}\mathbf{I}^i.\mathbf{I}^j$$

it is known that this exchange Hamiltonian leads to the same result as the spin diffusion (Cowan 1977) for long time.

The exchange frequency J_{ij} is a constant equals to J for nearest neighbour and zero otherwise. The diffusion coefficient D is related to J through the following equation,

$$D = cJd^2 \tag{2.6.7}$$

where d is the nearest neighbour separation and c is a numerical factor which depends on the lattice structure and the method of calculations. For triangular lattice its value has been estimated to be of the order of unity (Cowan 1980) and calculated exactly (Mullin and Cowan 1989) and was found to be 1.005.

2.6.2a Short-time Behaviour:

The general expression of the $g_n(t)$ for motion in spin space, equation (2.5.2) is reduced to the form,

$$g_n(t) = \frac{4}{3N} \sum_{\substack{i<j \\ k<l}} \frac{exp\Big[-in(\phi_{ij} - \phi_{kl})\Big]}{r_{ij}^3 \quad r_{kl}^3} \Gamma_{ijkl}(t)$$

where the time dependence is included in the symmetric four-spin correlation functions $\Gamma_{ijkl}(t)$ only.

For short-time the behaviour of $g_n(t)$ could be described by an expansion of $g_n(t)$ in powers of t. Bearing in mind that the odd powers vanish and excluding the term $i = j$, the derivatives of $g_n(t)$ for $t = 0$ are given as:

$$g_n^{(m)}(0) = \frac{4}{3N} \sum_{\substack{i<j \\ k<l}} \frac{exp\Big[-in(\phi_{ij} - \phi_{kl})\Big]}{r_{ij} \quad r_{kl}} \Gamma_{ijkl}(0) \tag{2.6.8}$$

First term gives,

$$g(0) = \sum_{i \neq j} r_{ij}^{-6} \tag{2.6.9a}$$

which is for triangular lattice with spacing d (Cowan 1980) equals to

$$g(0) = 6.36\, d^{-6} \qquad (2.6.9b)$$

Evaluating the second coefficient of $g_n(t)$ from equation (2.6.8); the lattice sums may be evaluated for nearest- neighbour exchange and the expression for short-time is given as,

$$\frac{g_0(t)}{g(0)} = 1 - 6\, J^2\, t^2 + \cdots$$
$$\frac{g_2(t)}{g(0)} = 1 - 12.5\, J^2\, t^2 + \cdots$$

2.6.2b Long-time Behaviour:

Long-time spin diffusion leads to equation (2.6.2). The diffusion time τ_c is of the same order as the exchange time $1/J$. From the relation $\tau_c = a^2/2D$ and equation (2.6.7) we find,

$$\tau_c = \frac{1}{J} \times \frac{a^2}{2cd^2} \qquad (2.6.10)$$

equating equation (2.6.9a) and equation (2.6.9b) and changing the summation into integral

$$6.36\, d^{-6} = \alpha \int_a^{\infty} \frac{2\pi r\, dr}{r^6}$$

substituting the value of α for triangular lattice $\alpha = 2/\sqrt{3}\, d^2$. The hard core a (the smallest distance the spin can diffuse) is related to the nearest neighbour distance d (the distance between two exchange spins) by the expression,

$$a = 0.7308\, d$$

Hence by substituting in equation (2.6.10), we concluded that:

$$\tau_c = \frac{0.267}{J} \qquad (2.6.11)$$

Therefore for Heisenberg exchange, the long-time behaviour of the correlation functions is given by:

$$\frac{g_0(t)}{g(0)} \sim \frac{1}{1.87\,Jt}$$
$$\frac{g_2(t)}{g(0)} \sim \frac{1}{63\,J^2t^2}$$

2.6.2c The Interpolation Procedure:

In case of two dimensions; since the tail of the correlation function goes as $1/t$, any approximation procedures for $G(t)$ should respect both short-time and long-time behaviour. Hence, to join these two behaviours, interpolation was made and different formulae were used. The following form of correlation functions were established by Cowan (1980),

$$\begin{aligned}\frac{g_0(t)}{g(0)} &= \frac{P(1+2aJt)}{(1+aJt)^2} + Qexp(-bJ^2t^2)\\ \frac{g_2(t)}{g(0)} &= \frac{P}{(1+J^2t^2)} + Qexp(-bJ^2t^2)\end{aligned} \tag{2.6.12}$$

where the values of the constants for both $n = 0$ and $n = 2$ are,

$$P = 0.3338$$

$$Q = 0.6662$$

$$b = 8.2255$$

and $a = 1.2485$ for $n = 0$, while $a = 21.03$ for $n = 2$.

A better choice was made (Cowan et al 1987a) and the correlation functions are expressed as:

$$\begin{aligned}\frac{g_0(t)}{g(0)} &= \frac{P_0}{[1+a_0^2t^2/\tau^2]^{1/2}} + \frac{Q_0}{[1+b_0^2t^2/\tau^2]}\\ \frac{g_2(t)}{g(0)} &= \frac{P_2}{[1+a_2^2t^2/\tau^2]}\end{aligned} \tag{2.6.13}$$

where the constants have the following values:

$$P_0 = 0.524 \qquad P_2 = 1.0$$

$$a_0 = 0.262 \qquad a_2 = 0.944$$

$$b_0 = 0.928 \qquad Q_0 = 0.476$$

where τ is the correlation time which measure the speed of the motion.

When the correlation functions of both choice are expanded, they contain the term $(J^2\ t^2)$ which is of the same order as in the calculated short time expansion. On the other hand, the linear term does not exist in the short time expansion; so the correlation functions (Cowan et al 1987) which do not contain the linear term as well, give powerful results when they are used in the analyses.

To evaluate T_1 and T_2, the Fourier Transform of $g_0(t)$ and $g_2(t)$ namely $j_0(\omega)$ and $j_2(\omega)$ should be determined. Similar to diffusion, the $n = 2$ term exhibits normal behaviour while the $n = 0$ function diverges at low frequency.

2.6.2d Longitudinal Relaxation:

Except of using the expressions of $j_n(\omega)$ for exchange; the treatment of the longitudinal relaxation followed the same procedures as diffusion. Since the short-time behaviour of the correlation functions is considered, T_1 at the minimum and above the minimum (high frequency) could be determined, so the whole frequency range could be covered.

Using the correlation functions equation (2.6.12), T_1 was inspected at different angles and a plot of $1/T_1$ as a function of exchange frequency J at constant Larmor frequency is demonstrated in figure (2.6.1). The behaviour at angle of orientation $\beta = 0$ was seen to be normal because the contribution comes from $j_2(2\omega)$ only (the non-zero term). By increasing β to 45 and 90 degrees, the $j_2(\omega)$ term will also takes part and T_1 is no longer flat at low frequency.

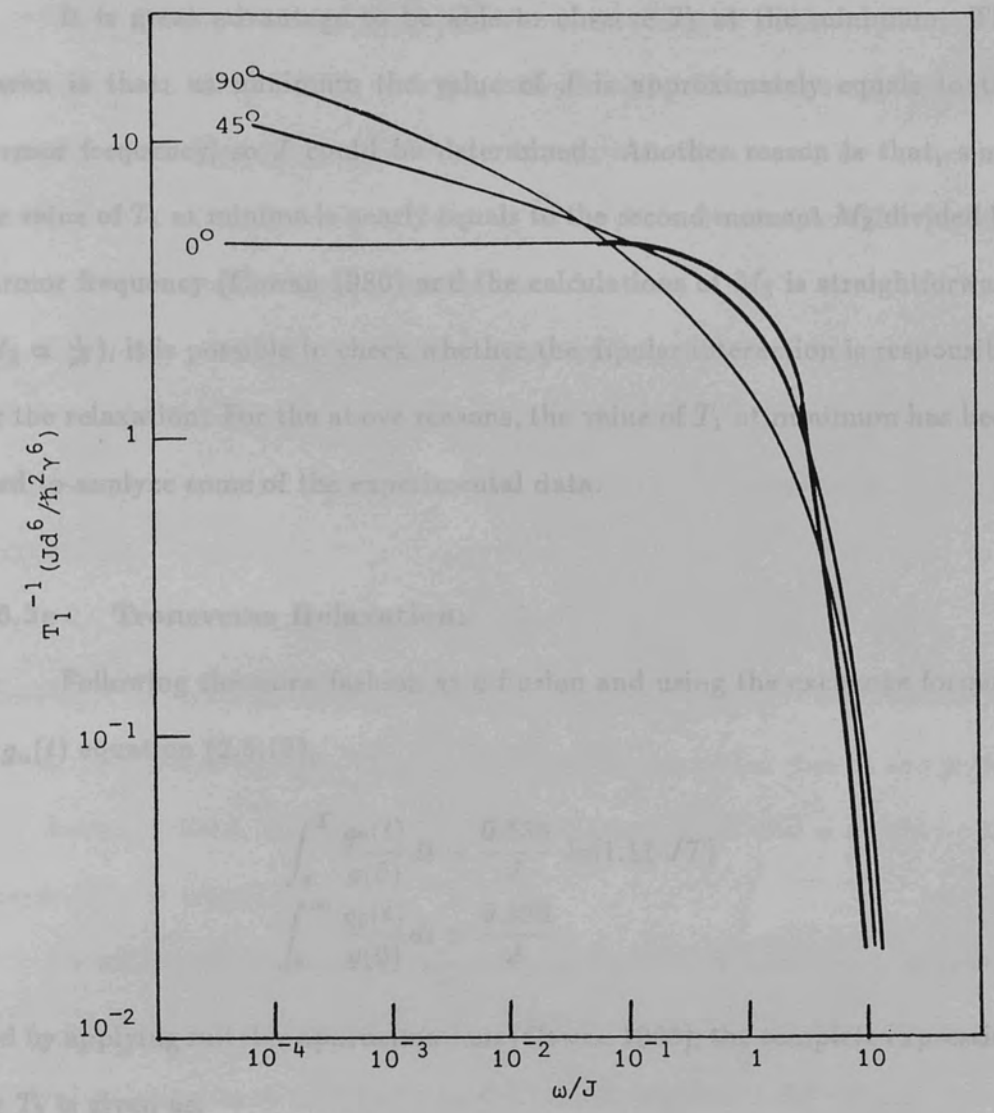

Figure 2.6.1

Theoretical Plot of the Spin-Lattice Relaxation Time as a Function of Exchange Frequency for Different Orientations (Cowan 1980).

It is great advantage to be able to observe T_1 at the minimum. The reason is that; at minimum the value of J is approximately equals to the Larmor frequency, so J could be determined. Another reason is that, since the value of T_1 at minima is nearly equals to the second moment M_2 divided by Larmor frequency (Cowan 1980) and the calculations of M_2 is straightforward ($M_2 \propto \frac{1}{r^6}$), it is possible to check whether the dipolar interaction is responsible for the relaxation. For the above reasons, the value of T_1 at minimum has been used to analyze some of the experimental data.

2.6.2e Transverse Relaxation:

Following the same fashion as diffusion and using the exchange formula of $g_n(t)$ equation (2.6.12),

$$\int_0^T \frac{g_0(t)}{g(0)} dt \simeq \frac{0.535}{J} \ln[1.11\ JT]$$
$$\int_0^\infty \frac{g_2(t)}{g(0)} dt \simeq \frac{0.320}{J}$$

and by applying suitable approximations (Cowan 1980), the complete expression for T_2 is given as:

$$\frac{1}{T_2} = 0.535\frac{M_2'}{J} \ln\frac{J^2}{4M_2'} + 0.93\frac{M_2''}{J} + \frac{5}{2}J_1(\omega_0) + J_2(2\omega_0)$$

The first two terms can be calculated from the experimental details while the last two terms (the non-adiabatic part) are calculated in a similar way to the calculation of T_1 but with different coefficients.

2.7 Relaxation due to Grafoil platelets:

Besides the dipolar interactions, there is another mechanism for spin relaxation in the ^{3}He adsorbed on grafoil system which results from the

anisotropic diamagnetism of the graphite surface. Because of the application of the steady magnetic field B_0, each graphite platelet will have a certain induced magnetisation. This magnetisation, in turn, produces a small magnetic field normal to the platelet surface. Motion of the helium spins in this spatially varying field is another mechanism for the relaxation.

Robertson (1966) has considered a model for relaxation through bounded diffusion. In this model, the field gradient is assumed to be constant but alternating in sign with a period a. In this case the transverse relaxation time is given by:

$$\frac{1}{T_2^{exp.}} = \frac{1}{T_2^{dip.}} + \frac{a^4 \gamma^2 G^2}{120\ D}$$

where $T_2^{exp.}$ is the observed transverse relaxation time and $T_2^{dip.}$ is the relaxation due to the dipolar motion. The last term is the relaxation due to the grafoil local fields gradient, where D is the diffusion coefficient and a would be the typical platelet length.

A more realistic model of the local field spatial variation is a sinusoidal curve, which has been treated by Cowan (1976). The relaxation due to this mechanism is similar to that found by Robertson, but with a different numerical coefficient. This similarity is an evidence that any model for relaxation through motion in spatially varying fields will yield a transverse relaxation rate of the form:

$$\frac{1}{T_2} \sim < \omega_{loc.}^2 > \ \tau_c$$

where τ_c is the time for a spin to diffuse across a platelet and $\gamma^2 < \omega_{loc.}^2 >$ is a measure of the mean square of the associated fields.

It is clear that these two models imply a transverse relaxation rate proportional to *square* of the applied magnetic field (or the Larmor frequency). However, all experimental data clearly indicate a *linear* variation of $1/T_2$ with

ω_0. This is still a major unsolved problem in interpreting the relaxation data in the fluid phase of ^{3}He adsorbed on grafoil.

CHAPTER 3

APPARATUS AND EXPERIMENTAL TECHNIQUES

(i) THE APPARATUS

3.1 The Cryostat:

The cryostat used in this work was built in the college's physics workshop. It was designed to support an Oxford Instruments 7 mK dilution refrigerator. A schematic diagram of the cryostat is displayed in figure (3.1.1).

It has a copper 0.5 litre ^{4}He pot. A large vacuum can *inner vacuum can* (IVC) is bolted directly to the pot and sealed with an indium "O-ring". This can contains the sample chamber and the exchange gas. Surrounding the ^{4}He pot and the IVC there is another large can which is the *outer vacuum can* (OVC).

The OVC was evacuated to rather low pressure ($\sim 10^{-5}$ Torr) to maintain thermal isolation between the pot and ^{4}He bath. The IVC was filled with low pressure ($\sim$ 1 Torr) exchange ^{4}He gas to thermally anchor the ^{4}He pot with the sample chamber. To achieve the required temperature, the pot was filled with ^{4}He from the bath through a needle valve to reach 4.2 K, then pumped with a large rotary pump (Edward 1sc 450B) to reduce the temperature.

The ^{4}He bath is contained within a special dewar which has super insulation and a nitrogen jacket. The cryostat service lines are of thin walled stainless steel tubing to minimize thermal conduction.

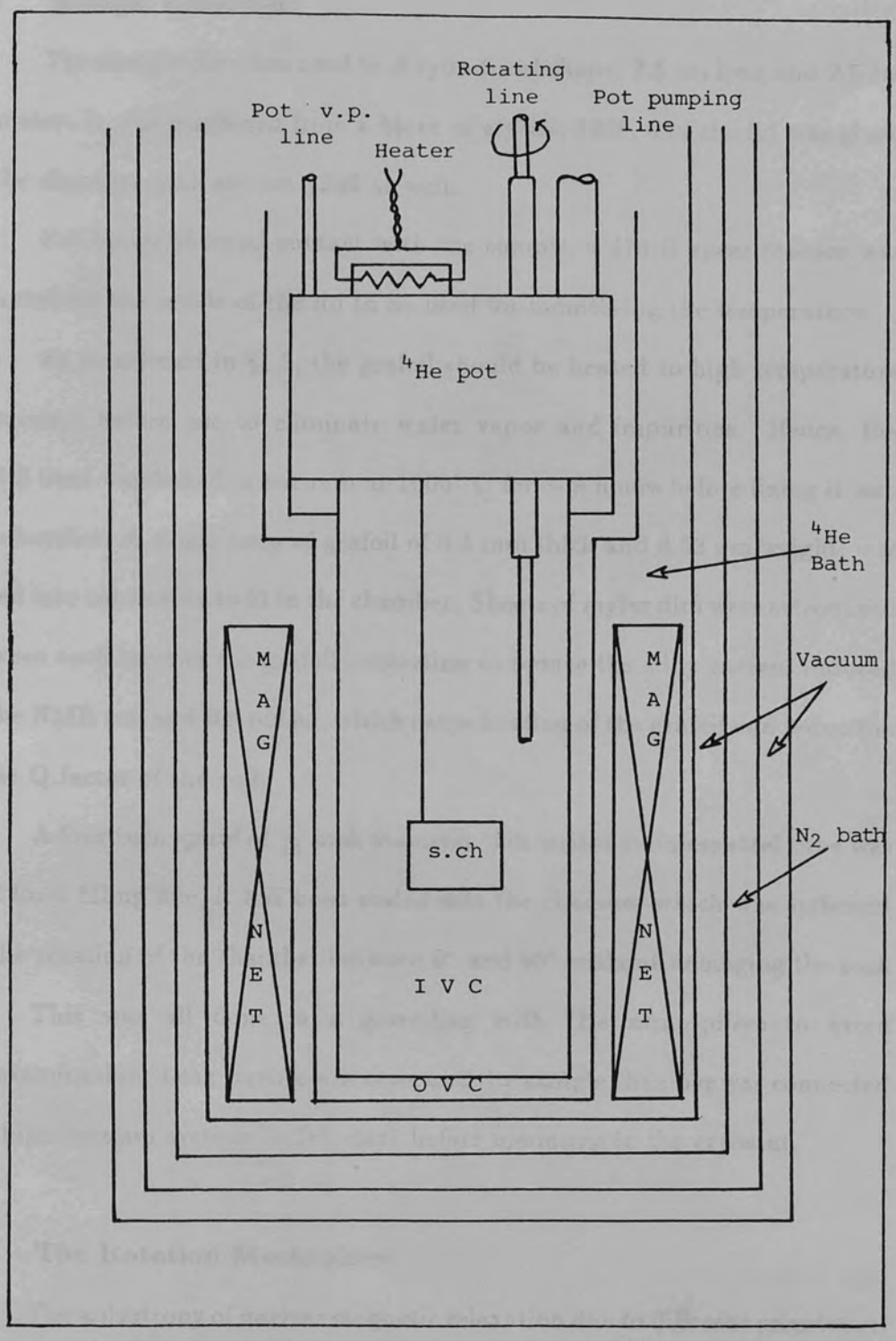

Figure 3.1.1

Schematic Diagram of the Cryostat

3.2 Sample Chamber:

The sample chamber used is of cylindrical shape, 2.5 cm long and 2.5 cm diameter. It was machined from a block of stycast 1266, and the lid was glued to the chamber with stycast 1266 as well.

For better thermal contact with the sample, a 470 Ω speer resistor was mounted on the inside of the lid to be used for monitoring the temperature.

As mentioned in §1.3, the grafoil should be heated to high temperature in vacuum before use to eliminate water vapor and impurities. Hence, the grafoil used was baked in vacuum at 1000° C for ~ 8 hours before fixing it into the chamber. A single strip of grafoil of 0.4 mm thick and 8.53 gm weight; was folded into concertina to fit in the chamber. Sheets of mylar film were introduced between each layer of the grafoil concertina to reduce the eddy current induced by the NMR coil and RF pulses, which cause heating of the grafoil and reduction of the Q_factor of the coil.

A four turn spiral of $\frac{1}{16}$ inch diameter thin walled stainless steel tube was used for a filling line, it has been sealed into the chamber which was sufficient for the rotation of the chamber between 0° and 90° without damaging the seal.

This was all done in a glove_bag with ^{4}He atmosphere to avoid recontamination. Leak testing was done and the sample chamber was connected to a high vacuum system for few days before mounting in the cryostat.

3.3 The Rotation Mechanism:

The anisotropy of nuclear magnetic relaxation due to different orientation of the substrate planes with the magnetic field has been studied. It was desirable to rotate the sample chamber without opening the cryostat. For this reason, a home made rotating mechanism which is shown in figure (3.3.1) has been

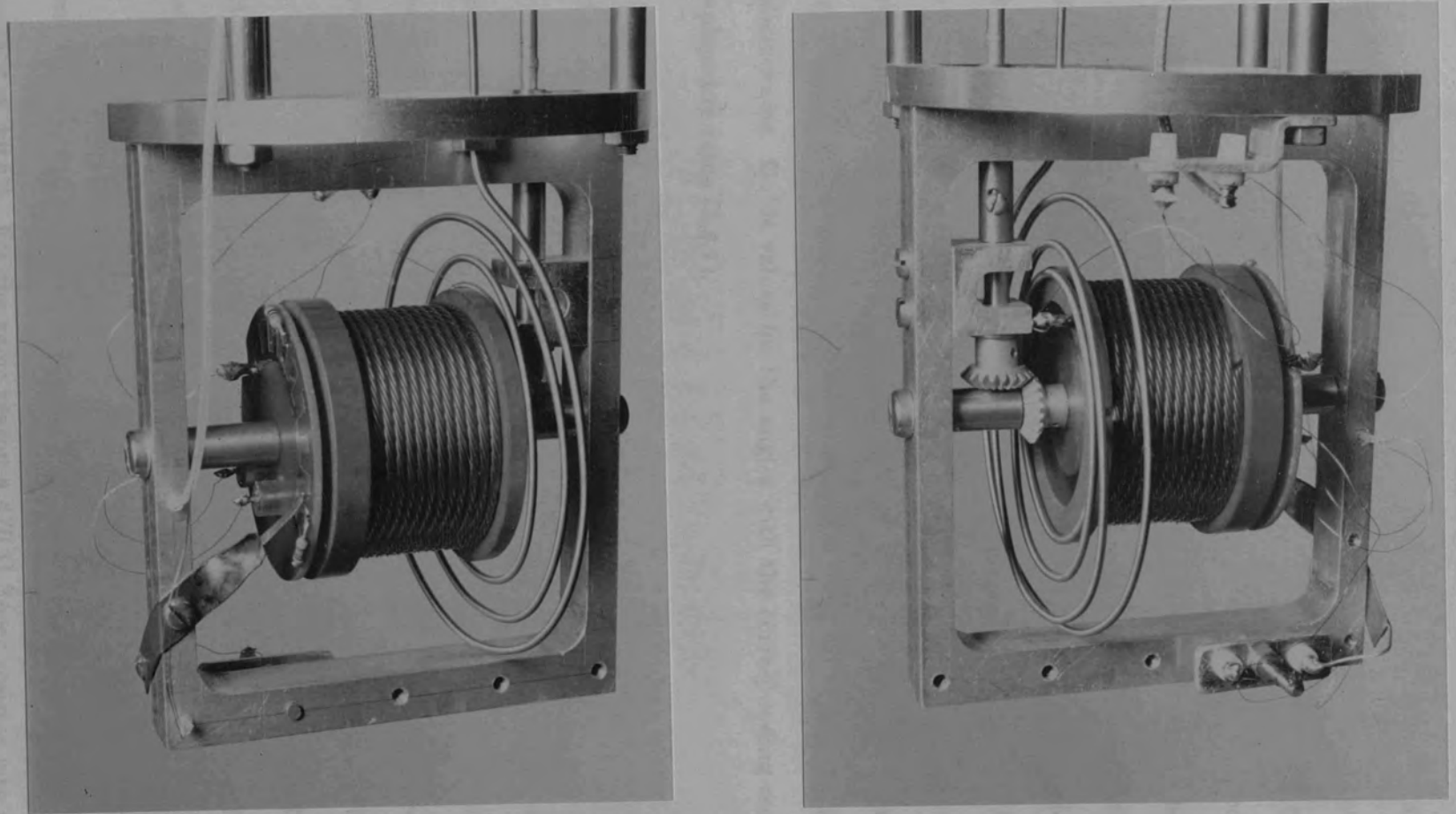

a b

Figure 3.3.1

The Rotating Mechanism shows; a) The Position Sensor, b) The Bevel Driver Gears and the Filling Line.

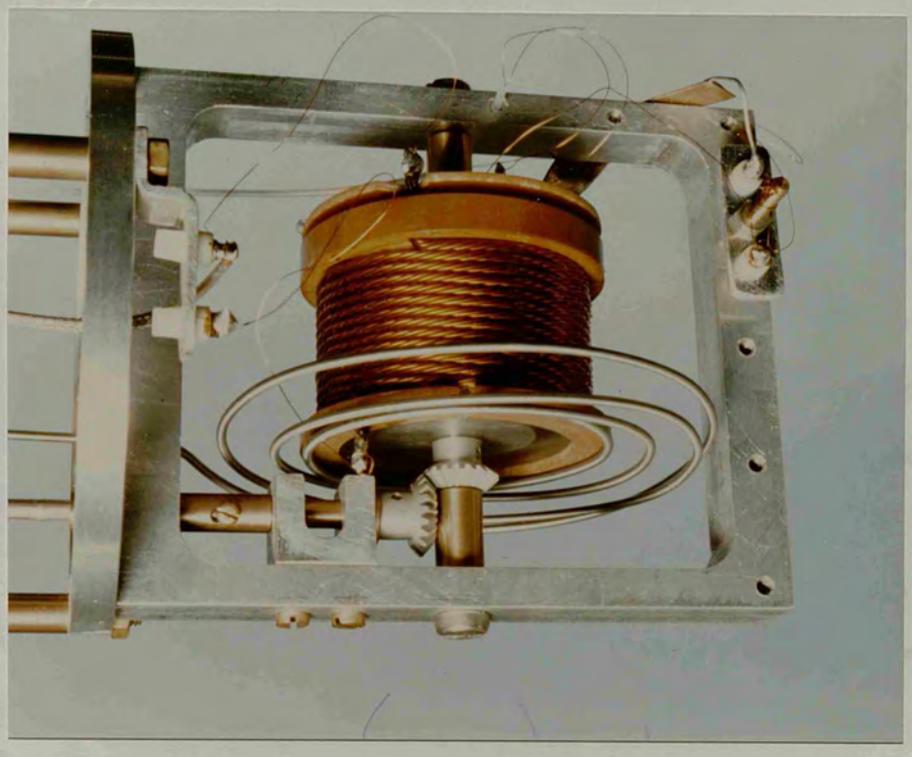

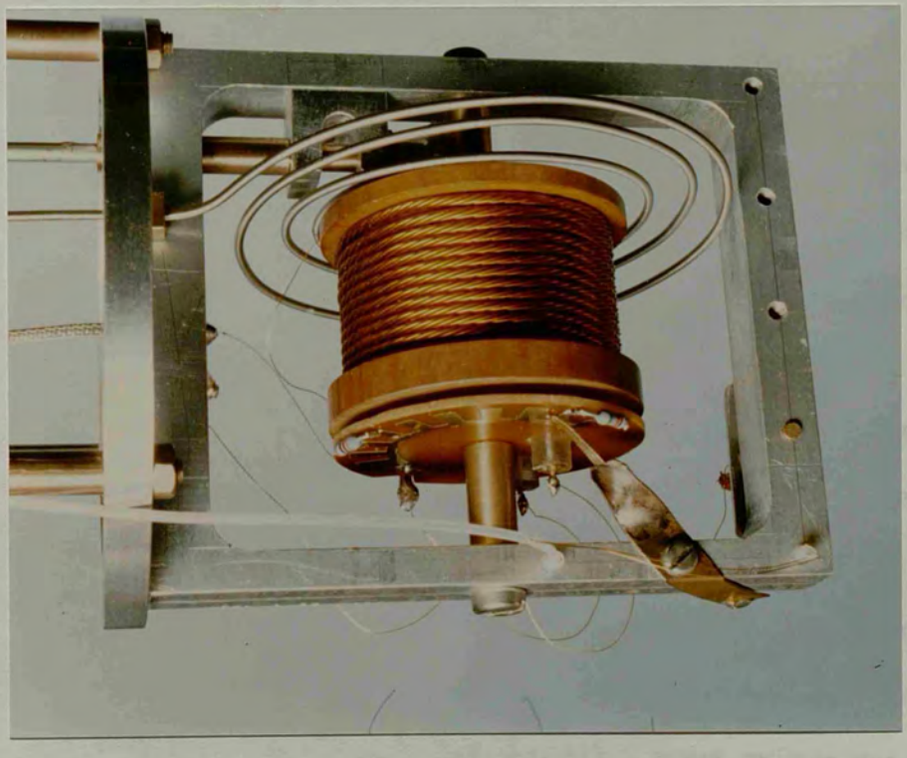

constructed to support and rotate the sample chamber.

The rotating mechanism consists of bevel gears to change the drive axis from vertical to horizontal direction. To indicate the substrate orientation, a disc of paxolin printed circuit board is fitted to the end of sample chamber. This board is etched to leave a set of radially distributed gold plated copper pads electrically connected. Two metal film resistors were fixed to the board; a 1 K Ω resistor is fixed before the zero angle indicator, while a resistor of 500 Ω was fixed after the location of the 90° angle to simplify the detection. Between zero and 90, angles could be varied in steps of 9 degrees. This was obtained by monitoring the *conducting* position corresponding to zero ohm and the following *non-conducting* position with ∞ ohm using an ohm meter. Hence a precise orientation angle could be obtained by starting the rotation from 90° anticlockwise. Guide values for the angles with the corresponding resistors is displayed in table (3.3.1).

3.4 The Temperature Regulation System:

At the start of each run, the calibration of thermometers was performed. Oil manometer, Mercury_manometer and Wallace & Tiernan capsule gauge were used to calibrate the Speer (SP) and Allen_Bradley (AB) resistors which are attached to different places in the cryostat with thermally anchor leads.

The manometers and the gauge measure the ^{4}He vapor pressure in the pot, then temperature was determined numerically using the T_{54} temperature scale (Rusby 1985).

A 47 Ω Allen_Bradley resistor was used to measure the pot's temperature over the range of 2 to 20 K, where its change with temperature is rapid and the accuracy is $\pm$0.5%. For the same reason a 470 Ω Speer resistor was used for

Angle (deg.)	**Resistance** (Ω)
> 99	500
99	∞
90	0
81	∞
72	0
63	∞
54	0
45	∞
36	0
27	∞
18	0
9	∞
0	0
< 0	1000

Table (3.3.1)

Angles of the substrate orientation with the corresponding resistances.

temperatures below 2 K.

The following formulae were used for computing temperatures in the range above 2 K (Hoare et al 1961) and below 2 K (Rose-Innes 1973) respectively.

$$\frac{1}{T} = a_2(\log_{10} R)^{-1} + b_2 + c_2(\log_{10} R) \tag{3.4.1}$$

$$\log_{10} T = a_1(\log_{10} R)^{-1} + b_1 + c_1(\log_{10} R) \tag{3.4.2}$$

The resistances values as a function of temperatures were fitted to the above equations using the method of least squares. The constants were computed and found to be:

$$a_1 = 6.3641 \qquad a_2 = 0.5029$$

$$b_1 = -46.2145 \qquad b_2 = -1.4984$$

$$c_1 = 83.4158 \qquad c_2 = 1.0985$$

Temperatures between 1.1 K and 4.2 K were controlled by regulating the ^{4}He pot pumping rate with a needle valve and a solenoid valve On the other hand, temperatures above 4.2 K were obtained by using a power supply driving a heater resistance attached to the ^{4}He pot, where a small voltage of about 2 V was enough to raise the temperature of the pot to the required value, provided that the pot is completely empty. A microcomputer unit (RML- 380Z) was used to control the temperature during either cooling down or worming up the pot. The computed temperature was written via the interface unit to a digital display mounted in the resistor selector unit adjacent to the SHE conductance bridge/Model PCB.

3.5 The Gas Handling System:

The basic function of the gas handling system is to admit a measured amount of ^{3}He gas into the sample chamber. It also enables the vapor pressure of the adsorbed gas to be measured on a Druck gauge for the isotherm measurements.

A block diagram of the gas handling system has been drawn in figure (3.5.1). The ^{3}He gas is kept in a special cylinder. The Druck digital pressure indicator was used for measuring the gas pressure through the needle valve with resolution of 0.0001 bar. There are two Druck gauge heads, head 1 is connected to the store of ^{3}He gas to enable reading the pressure of the gas inside. While head 2 is attached to the sample line to monitor the pressure in the sample chamber. A charcoal trap in a nitrogen bath (77 K) was connected to the system to clean the sample when it passes through it.

3.6 The NMR Magnet:

The NMR magnet consists of three parts. First, is the main solenoid which provides the static magnetic field B_0. The solenoid, a superconducting magnet works in persistent mode, so it is immersed in liquid helium at 4 K. It produces a field up to two Tesla at a current of 50 amp.

Second part is the Z_1 shim coil which operates in the persistent mode as well. This coil was provided to improve the inhomogeneity of the main magnet or to narrow the echo when the motion of the spins slow down. The third part of the magnet is a pair of helmholtz coils which are not working in the persistent mode. They are used to provide a field gradient or shift, but they were not used through this work.

A current regulated power supply was used to energise the magnet. It

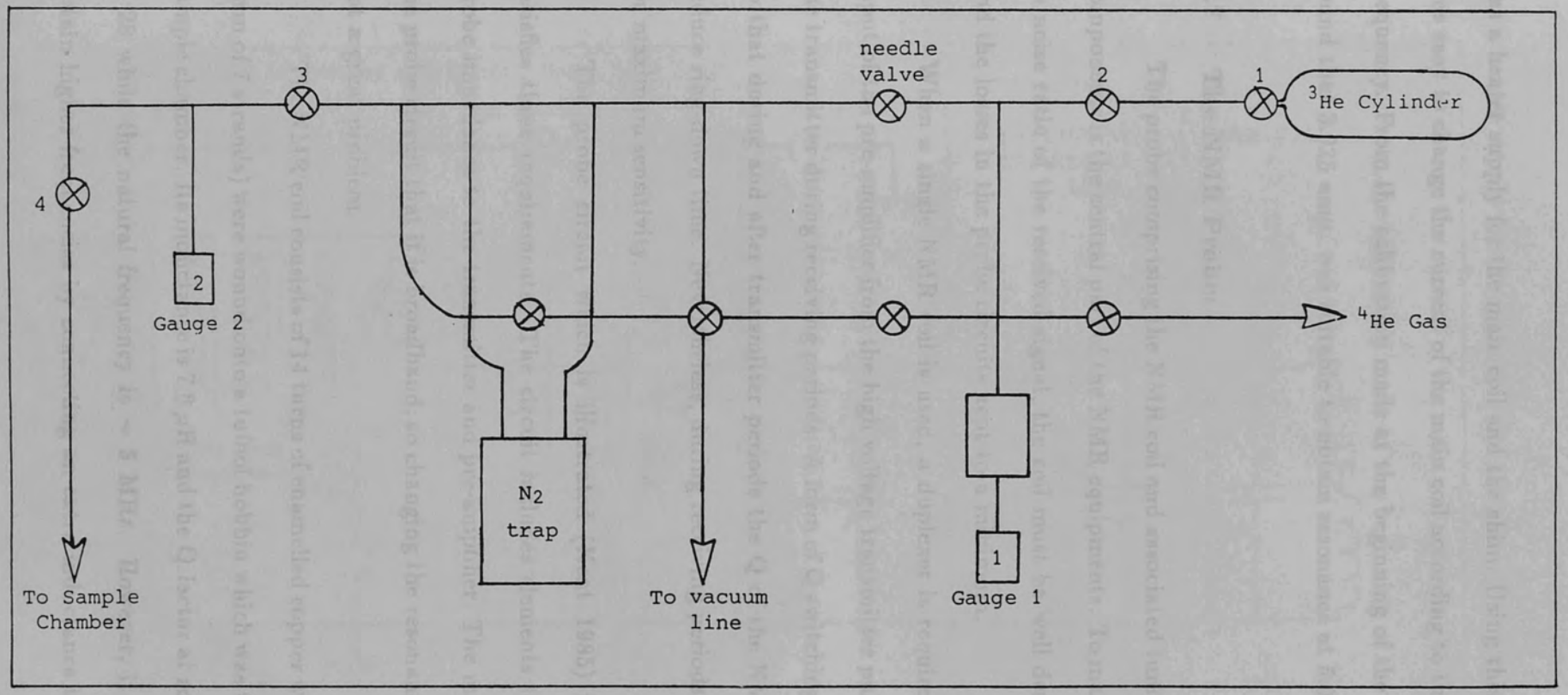

Figure 3.5.1

The Sample Gas Handling System.

has a heater supply for the main coil and the shim. Using this power supply it was easy to change the current of the main coil according to the chosen Larmor frequency. From the calibration made at the beginning of the run; it has been found that 3.925 amp. was suitable to obtain resonance at 5.0477 MHz.

3.7 The NMR Probe:

The probe comprising the NMR coil and associated tuning and matching components is the central part of the NMR equipments. To maximize the signal to noise ratio of the received signal, the coil must be well designed of high Q and the losses in the probe circuits kept to a minimum.

When a single NMR coil is used, a duplexer is required to protect the input of the pre-amplifier from the high voltage transmitter pulse and to isolate the transmitter during receiving periods. A form of Q switching is also required, so that during and after transmitter periods the Q of the NMR coil is low to reduce ring-down time. Nevertheless, during receiving periods Q must be high for maximum sensitivity.

The probe circuit which is illustrated (Kent 1985) in figure (3.7.1) satisfies these requirements. The circuit includes elements for matching the probe impedance to the transmitter and pre-amplifier. The main advantage of the probe circuit that it is broadband, so changing the resonance frequency was not a great problem.

The NMR coil consists of 14 turns of enamelled copper wire. The wire (in form of 7 strands) were wound onto a tufnol bobbin which was fitted around the sample chamber. Its inductance is 7.8 μH and the Q_factor at room temperature is 28 while the natural frequency is $\sim$ 5 MHz. However, it was possible to obtain higher frequencies by connecting an extra inductance to point A figure

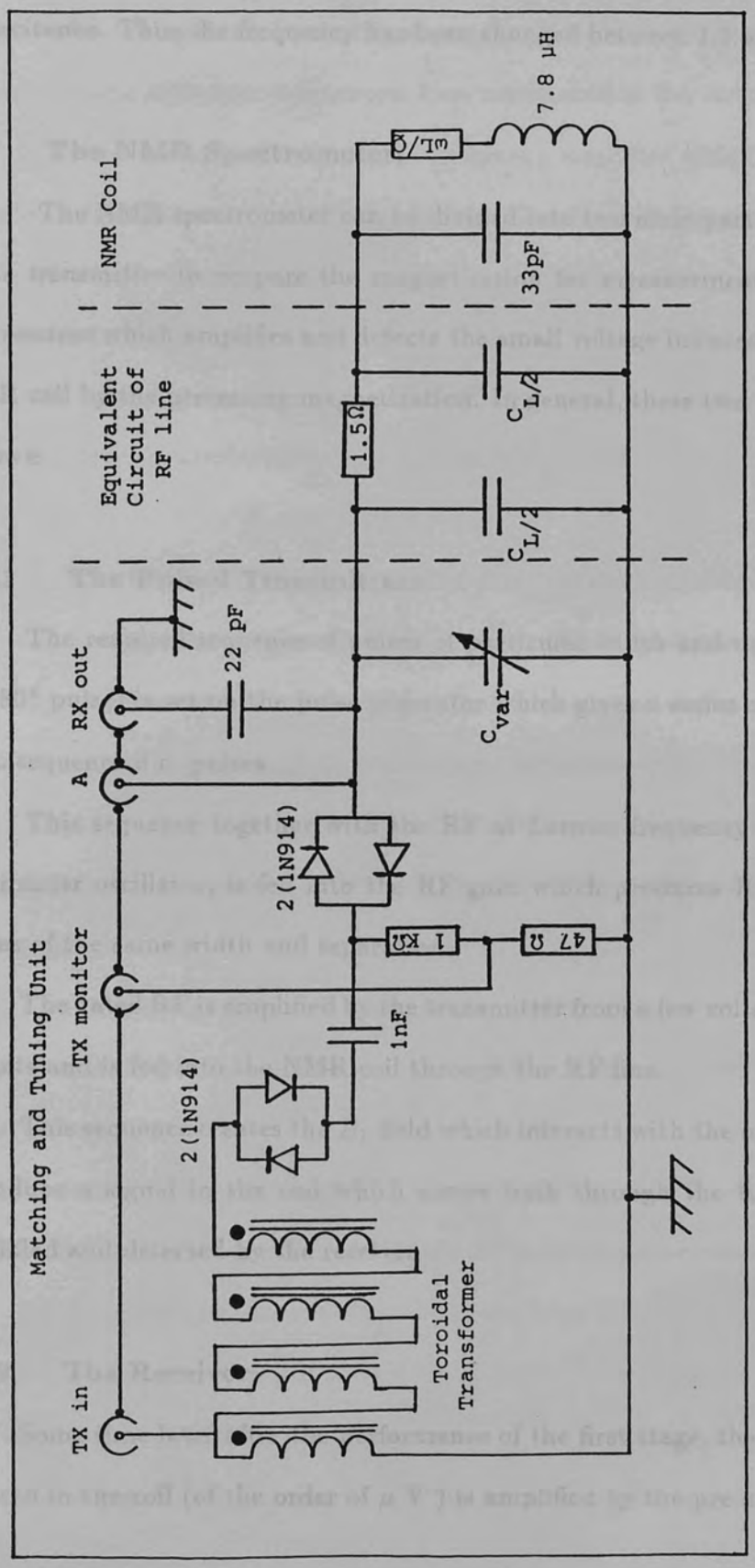

Figure 3.7.1

Circuit of the Matching and Tuning Unit and the Equivalent Circuit of NMR Probe.

(3.7.1), while lower frequencies could be achieved by the connection of a suitable capacitance. Thus the frequency has been changed between 1.3 and 10.2 MHz.

3.8 The NMR Spectrometer:

The NMR spectrometer can be divided into two main parts. First is the *pulse transmitter* to prepare the magnetisation for measurements. Second is the *receiver* which amplifies and detects the small voltage induced in the single NMR coil by the precessing magnetization. In general, these two parts work as follows:

3.8.1 The Pulsed Transmitter:

1) The required sequence of pulses of particular width and delay (e.g. 90° or 180° pulse) is set on the pulse generator which gives a series of rectangular TTL sequence d.c. pulses.

2) This sequence together with the RF at Larmor frequency coming from the master oscillator, is fed into the RF gate which produces RF modulated pulses of the same width and separation.

3) The gated RF is amplified by the transmitter from a few volts to hundreds of volts and is fed into the NMR coil through the RF line.

4) This sequence creates the B_1 field which interacts with the magnetization to induce a signal in the coil which comes back through the RF line to be amplified and detected by the receiver.

3.8.2 The Receiver:

1) Some time later after the performance of the first stage, the tiny voltage induced in the coil (of the order of μ V) is amplified by the pre-amplifier.

2) The resultant RF signal goes to the mixer to be multiplied by the steady reference RF voltage with Larmor frequency produced by the master oscillator. Hence *sum* and *difference* frequencies were introduced in the output.

3) The two parts go to the audio frequency amplifier which has variable range of gain and bandwidth. The gain amplifies the "difference" part and the FID is obtained. On the other hand the low pass filter eliminates the "sum" part which is of high frequency (2ω).

4) The last stage is to average this AF signal as many times as required. Then the signal is displayed on the oscilloscope.

3.8.3 The Essential Requirements of a Pulsed NMR Spectrometer:

The minimum requirements of pulsed NMR spectrometer could be summarized (Farrar and Becker 1971) as follows:

1) The transmitter should be able to produce pulses of hundreds of volts to ensure that the B_1 field is greater than the inhomogeneity of the static field B_0, i.e. $B_1 \gg \Delta B_0$. This condition is important for all the spins to rotate with the same angle.

2) After switching off the RF pulse its power must be quickly dissipated and the receiver must recover as soon as possible. Hence low Q is needed at the end of the pulse.

3) In conflict with condition (3), the tank circuit must have as high Q as possible in the receiving mode for best signal to noise performance.

4) The receiver must be protected from the large RF pulses.

5) The sample must be efficiently coupled to the receiver to obtain maximum S/N from the nuclear induction signal.

6) The receiver and the transmitter should be well isolated from one another,

in order to achieve minimum overload conditions and faster recovery time.

7) The pulse generator must have a very stable time base and allow for precise setting of all time intervals.

8) The master oscillator must have a very stable frequency.

9) The B_1 and the B_0 fields must be homogeneous as possible over the sample volume to insure that all spins will precess with the same frequency.

10) There should not be any radiation of the RF energy at the resonance frequency in the laboratory.

3.9 Details of the Spectrometer Used:

A block diagram of the pulsed NMR spectrometer used in this work is illustrated in figure (3.9.1). To achieve the essential conditions required of the pulsed spectrometer, our home made spectrometer was built which worked satisfactorily.

To deal with condition (1); the transmitter circuits used the TTL pulses to gate the RF pulses at Larmor frequency. These pulses were then amplified up to power of 1 kW before passing to the NMR coil.

The power amplifier delivers peak pulse amplitude of up to 250 V into 50 Ω load. The circuit is different of the usual ones by having the output transformer untuned which results in a broad band transmitter. This allows the easy change of Larmor frequency.

The pulsed NMR receiver has a high sensitivity and signal to noise ratio. The dead time, which is the time taken to recover full signal sensitivity following a transmitter pulse, is less than the time taken for the probe voltage to ring down to the noise level which satisfies condition (2).

Conditions (3) and (4) were achieved by special design of the NMR probe

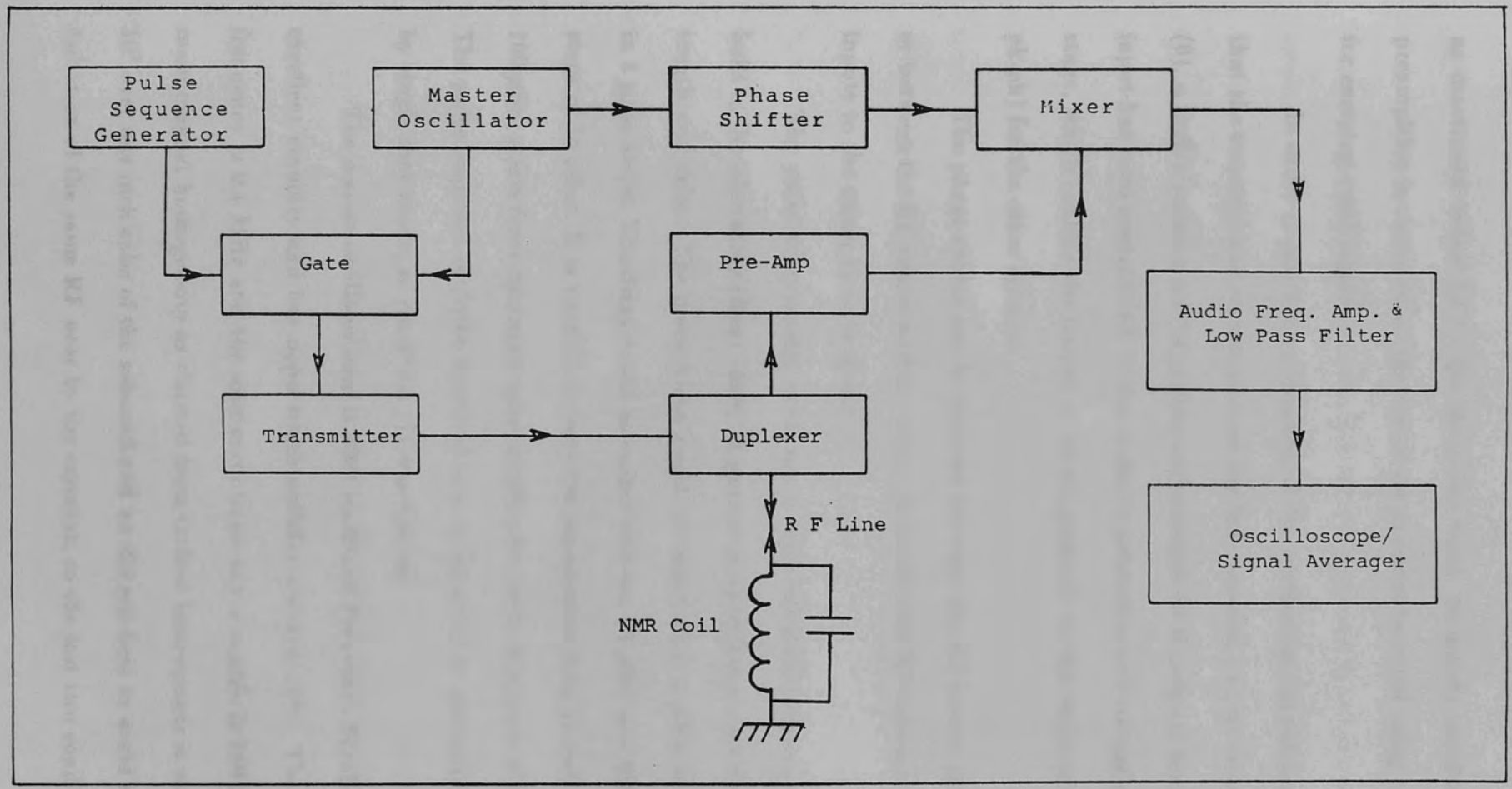

Figure 3.9.1

Schematic Diagram of the Pulsed NMR Spectrometer.

as mentioned before §3.7. On the other hand, to satisfy condition (5) the preamplifier is mounted on the top of the cryostat to avoid using coaxial lines for carrying small signals.

In order to prevent overloading of the synthesizer output and to ensure that the transmit and receive sections are fully isolated, i.e., to verify condition (6), a buffer/isolator providing four independent 50 Ω outputs from one 50 Ω input has been constructed. It also includes a detector and voltage comparator stage, which enables the output to be set precisely to the optimum level (1 V pk-pk) for the other circuits.

The phase shifter can be inserted between the RF source and the gate, or between the RF source and the mixer. It enables the RF reference and signal inputs to the mixer to be in phase.

The pulse programmer used was a digitized pulse sequence generator built in the laboratory (Kent 1985). It generates up to four pulses with different length and delay. The pulse width could be varied from 1 μSec to 9900 μSec in 1 μSec steps. The delay could be varied between 10 μSec and 9900 mSec in steps of 10 μSec. It is possible to vary the repeatation time as well in steps of 100 μSec starts from minimum value at 100 μSec with maximum of 9900 mSec. The pulse sequence could be operated in a cyclic mode or manually controlled by single shot mode, so condition (7) was fulfilled

The master oscillator used is 5600 Rockland Frequency Synthesizer with excellent stability and low noise which satisfies condition (8). The minimum frequency is 0.1 MHz and the maximum frequency available is 160 MHz. The main magnet homogeneity as claimed from Oxford Instruments is one part per 10^5 over one inch cube of the solenoid and we did our best to avoid having any radiation of the same RF near by the cryostat, so the last two conditions were

verified.

By using our home made signal averager it was possible to detect the weak signals at very low coverage, high temperature and from both low and high frequencies. The signal was averaged as much as it is needed with maximum of 2048 times.

The last stage of detecting the signal was to display it on the Digital Storage Oscilloscope (Gould 054100) where it becomes ready for measurements.

(ii) REVIEW ON THE EXPERIMENTAL TECHNIQUES

3.10.1 Introduction:

In this part, a short note will be given about the preparation usually made before starting the run, how the monolayer capacity is determined by the adsorption isotherm and then how the sample is admitted to the chamber. Finally, the methods which were used to determine the relaxation times T_1 and T_2 are explained.

3.10.2 Preparation for the Run:

After closing the cryostat up; the dewar, the IVC and the OVC must be evacuated. Then the sample chamber was pumped out as well. While the needle valve is closed the ^{4}He pot was evacuated using its own rotary pump. All these were done at room temperature. ^{4}He exchange gas of 1 Torr pressure was admitted to both vacuum cans.

When the system reached suitable vacuum $\approx 10^{-5}$ Torr, pre-cooling to 77 K was begun. This was done by filling the nitrogen jacket and the ^{4}He bath by liquid nitrogen. After 24 hours the nitrogen was blown out from the helium bath using a current of ^{4}He gas. The first ^{4}He transfer then starts using about 25 litres to cool the system to 4.2 K. The temperature of the system was recorded at room temperature, nitrogen temperature and helium temperature to calibrate the thermometers, these values are shown in table (3.10.1) for a specific run. After temperature stabilization, the ^{4}He exchange gas was removed from the OVC. During the run, automatic transfer of nitrogen was done every night while nearly 14 litres of ^{4}He was transferred every other day to keep the cryostat at 4.2 K.

Position of resistors	Cond. at Room Temp.	Cond. at N_2 Temp.	Cond. at ^4He Temp.
Top Baffle	3.549	3.138	2.578
Middle Baffle	3.677	2.895	1.369
Bottom Baffle	9.346	7.850	2.849
Flange	17.766	16.326	2.402
Pot (SP)	1.934	1.663	1.017
Pot (AB)	17.187	15.918	3.415
Sample Chamber	1.973	1.752	1.028
Magnet (Top)	4.092	3.245	0.264
Magnet (Bottom)	4.055	3.273	0.268

Table 3.10.1

Typical values of Conductance (mho) Sensors at Room Temperature, Nitrogen Temperature and Helium Temperature.

3.10.3 Adsorption Isotherm:

For a uniform surface with a number N_s of equivalent adsorption sites, the ratio of the number of adsorbed atoms N to N_s is defined as *coverage*, $x = N/N_s$ (Somorjai 1981). At the same time $x = V/V_m$ where V is the volume of the ^{3}He admitted gas at STP and V_m is the volume of monolayer capacity (STP). The monolayer completion ($x = 1$) could be determined by calibrating a certain volume of ^{3}He gas (which is admitted to the sample chamber) with its vapor pressure at 4.2 K.

According to (Bretz et al 1973), point A or point B criterion is used to determine the volume of ^{3}He gas corresponding to a complete monolayer. Point A is the extrapolation of the linear region pressure to zero pressure. While point B is approximately the point where the pressure changes from very low value to the linear region of low pressure points above them. Using point B criterion, it was found experimentally that the volume of ^{3}He gas corresponding to monolayer completion equals to 59.5 cc STP as shown in figure (3.10.1).

3.10.4 Admittance of The Sample:

A store of volume 18.83 cm^3 was filled with the sample which is pure ^{3}He gas through the needle valves 1 and 2 as illustrated in figure (3.5.1). The initial pressure of the store was read from the Druck gauge through the head (1). The sample volume V measured in (cc @ STP) is combined with pressure by the following equation (Kay and Laby 1975).

$$V = \frac{18.83\ \Delta P}{1013.25(1 + 0.00367\ T)} \qquad (3.10.1)$$

Where $\Delta P = P_{final} - P_{intial}$ is the change of the pressure of the store in mbars. T in degree Celsius is the store temperature which equals to room temperature.

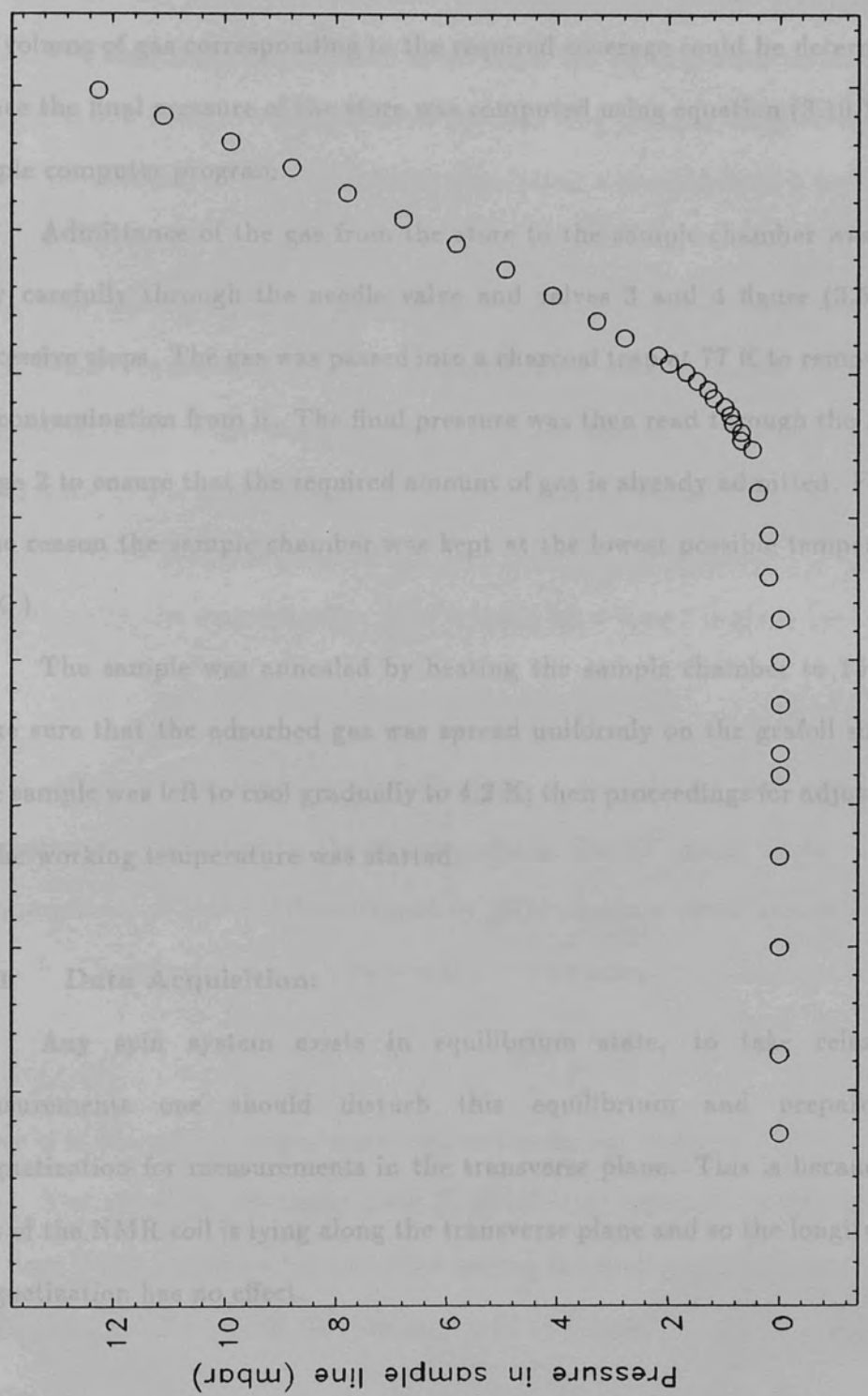

Figure 3.10.1

4.2 K Isotherm for He-3 adsorbed on grafoil

Bearing in mind that one layer completion is equivalent to 59.5 cc STP of the gas as determined from the adsorption isotherm in the previous section; the volume of gas corresponding to the required coverage could be determined. Hence the final pressure of the store was computed using equation (3.10.1) in a simple computer program.

Admittance of the gas from the store to the sample chamber was done very carefully through the needle valve and valves 3 and 4 figure (3.5.1) in successive steps. The gas was passed into a charcoal trap at 77 K to remove any air contamination from it. The final pressure was then read through the Druck gauge 2 to ensure that the required amount of gas is already admitted. For the same reason the sample chamber was kept at the lowest possible temperature (1 K).

The sample was annealed by heating the sample chamber to 15 K to make sure that the adsorbed gas was spread uniformly on the grafoil surface. The sample was left to cool gradually to 4.2 K; then proceedings for adjustment of the working temperature was started.

3.11 Data Acquisition:

Any spin system exists in equilibrium state, to take relaxation measurements one should disturb this equilibrium and prepare the magnetization for measurements in the transverse plane. This is because the axis of the NMR coil is lying along the transverse plane and so the longitudinal magnetization has no effect.

3.11.1 T_1 and T_2 Measurements:

The spin-lattice relaxation time is the time which the spins take to

reach equilibrium with the environment by transferring energy to the lattice. To measure this time, the *saturation recovery* method (90-90 sequence) was used. The first pulse disturbs the spins while the second pulse measures the magnetization after a waiting period by observing the size $M(t)$ of the FID. Hence the recovery of the nuclear spin population is monitored as a function of time.

The use of the 90-90 pulse sequence is preferable over the use of the usual 180-90 sequence. The reason is that (Fukushima and Roeder 1981) the z-component of the magnetisation is reduced to zero after any $\pi/2$ pulse regardless of the state of the magnetisation before the pulse, so no need for long waiting period between the pulse pairs.

Ideally, the magnetization after waiting for a time t is given by:

$$M(t) = M_0\ [1 - exp(-\frac{t}{T_1})]$$

where $M(t)$ is the magnetisation at time t and M_0 is the equilibrium magnetisation. Practically, the inaccuracies in the 90° pulse length and the inhomogeneity of the NMR coil result in $M(t)$ does not equal exactly to zero at $t = 0$. Therefore, a small correction is made by using the following equation:

$$M(t) = M_0[1 - \alpha\ exp(\frac{-t}{T_1})]$$

where α is the correction parameter which ideally equals to one.

The spin-spin relaxation time T_2 is intrinsic relaxation time, i.e. it is the time which the spins take to relax among themselves without any change in their energy. Two methods were employed to determine T_2 depending on its value.

At very high coverage it was difficult to observe the echo because T_2 was short due to the slowing down of the motion ($\sim$ 500 μS), which is comparable

to the instrumental dead time. Therefore, the method of FID was applied. But when T_2 was long enough, the spin echo technique has been used.

In the first case; data were taken at 4 K, where it was possible to determine T_2 by spin echo and T_2^* using the FID method. Thus, if T_2^* is the total spin-spin relaxation time decomposed into two parts; the relaxation time $T_2^{dip.}$ due to dipolar interaction and $T_2^{mag.}$ due to the inhomogeneity of the magnet, then

$$\frac{1}{T_2^*} = \frac{1}{T_2^{dip.}} + \frac{1}{T_2^{mag.}} \tag{3.11.1}$$

by substituting with the value of $T_2^{dip.}$ and T_2^*; it was possible to calculate $T_2^{mag.}$. Thus by measuring T_2^* and using the value of $T_2^{mag.}$ which is constant for each frequency; $T_2^{dip.}$ could be determined even when the signal is weak.

For long T_2, the pulse sequence 90-180 was used and the echo has been observed. The magnetization decay satisfies the following relaxation equation:

$$M(t) = M_0 \; exp(\frac{-2t}{T_2})$$

where $M(t)$ is the echo height at time t.

The advantage of using the spin echo technique which was first introduced by Hahn (1950), was to eliminate the influence of the inhomogeneity of the applied magnetic field. This was made because the effect of the inhomogeneity is reversible, so the decrease of the echo height with time is due to the interaction of the spins which decays exponentially with time constant T_2.

The consequence of this method is described (Fukushima Roeder 1981) as follows. Assuming that a 90° pulse has been applied along the x′ axis to the spin system at zero time. Shortly after; the spin isochromats will precess with different Larmor frequencies according to the field they see. Some of these

isochromats will get ahead of the average and some will be behined. Hence, the spin isochromats will be dephased in the x´-y´ plane and the net magnetisation in this plane will be zero, although the individual isochromats are not dephased. A time τ later, a 180 ° pulse is applied along the x´-axis as well. As a result, each spin isochromat would be rotated 180° along the x´-axis. Any magnetisation along z-axis would be inverted to the -z direction and be of no consequence of the magnetisation remaining in the x´-y´ plane. The spin isochromats which were ahead the average by a certain angle will be behined the average by the same amount, while those who were behind, now will become ahead the average and so the spins catch each other and rephase to form a net magnetisation in the x´-y´ plane. As a result, the magnetisation would be rebuilt at -y´-axis at time 2 τ and form an inverted spin echo. The height of this echo is given by:

$$E(2\tau) = E(0)\ exp(\frac{-2\tau}{T_2})$$

Hence to determine either relaxation time, the data were collected using the suitable sequence for certain period and the height of magnetisation was plotted as a function of delay time on a semilogarithmic paper. It was considered that the ratio S/N decreases with the increase of time, so cutoff of the data was useful after certain time. The data points were fed to a least square fitting program and the relaxation times were computed.

CHAPTER 4

THE REGISTERED PHASE

4.1 Introduction:

The registered phase is considered as an attractive area for studying NMR properties of the spin system in two dimensions. The reason is that it has a characterized structure where the ^{3}He atoms are regularly distributed on the grafoil mesh.

This phase, as observed from heat capacity measurements (Bretz et al 1973) (Hickernell et al 1972) and shown in figure (1.4.1) extends in a narrow range between $x = 0.56$ and $x = 0.625$ monolayer approximately and below temperature of 3 K.

4.2 Concept of the Registered Phase:

The adatoms have a regular arrangement with the substrate lattice. Therefore, the nature of the film and its properties depend crucially on the substrate structure. In the case of ^{3}He adsorbed on grafoil, the amount of helium three atoms is just enough for each atom to occupy one out of each three sites of the hexagons of grafoil to form a triangular lattice. The lattice spacing has been found to be equal to 4.26 $\mathring{A}$ (Nielsen et al 1977). The surface spacing is $\sqrt{3}$ larger than the grafoil mesh and only 1/3 of the adsorption sites are occupied. This registered structure which is known as $\sqrt{3} \times \sqrt{3}$ structure is illustrated in figure (4.2.1). Therefore, for such a system; the following equation

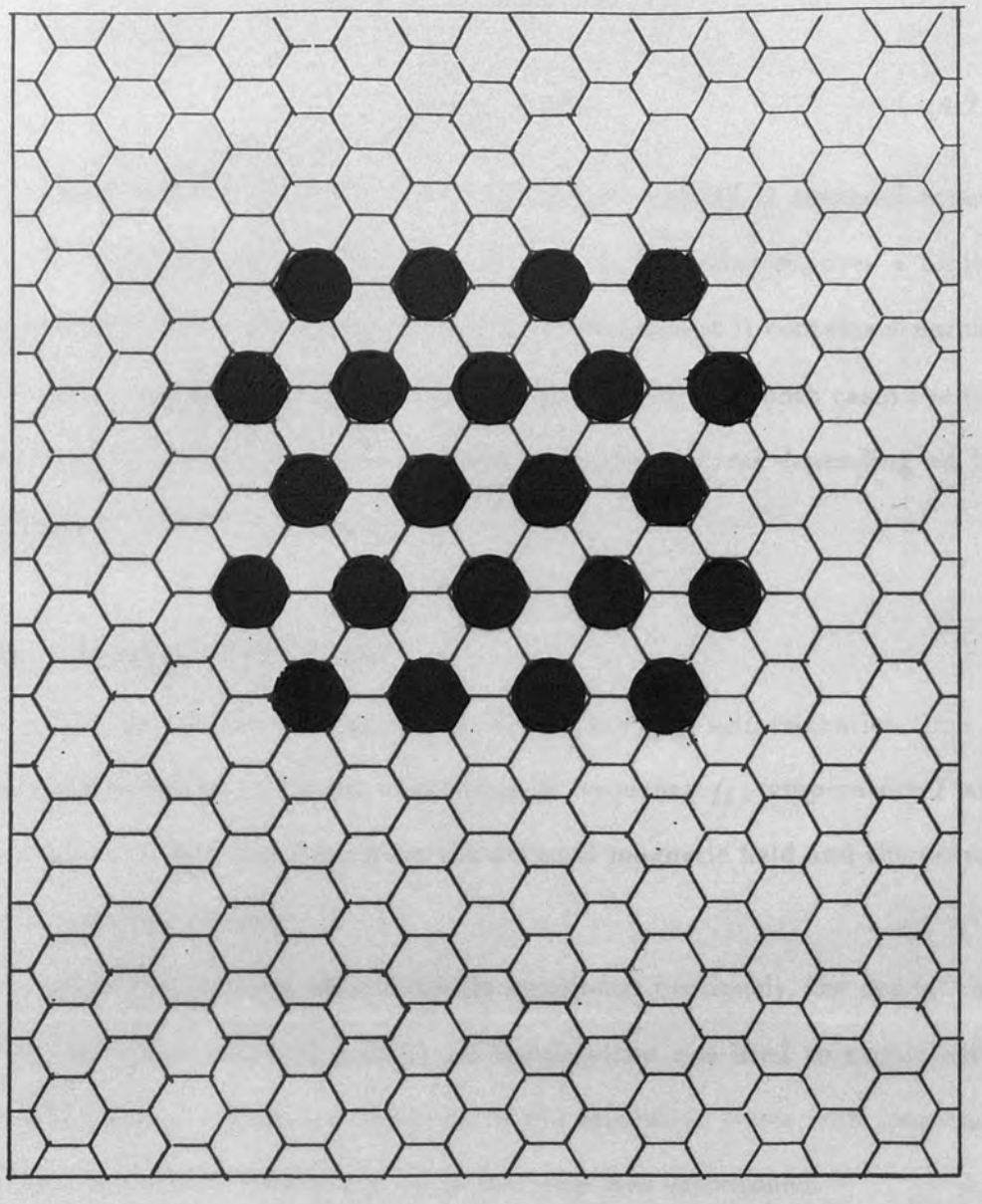

Figure 4.2.1

Regular Structure of ^{3}He Atoms on the Grafoil Lattice.

is verified :

$$x = \frac{N}{N_s} = 1/3 \tag{4.2.1}$$

According to Bretz et al (1973), perfect registry is centered around $x \approx 0.6$ monolayer and temperature $T < 3$ K. Nevertheless, over a limited range at lower densities, the phase is still present except it contains a number of vacancies, while at higher densities interstitials exist. In both cases the film is affected by the registered phenomena to various degrees depending on the proximity to the perfect registry.

4.3 Display of the Data:

The spin-lattice relaxation time T_1 and the spin-spin relaxation time T_2 were determined as a function of coverage x, frequency f_0, temperature T and the angle of orientation β between the external magnetic field and the normal to the substrate surface.

Besides the direct measurements mentioned previously, the dependence of the relaxation times T_1 and T_2 on temperature was used to evaluate the activation energy. From the variation of the relaxation times with frequency, the correlation time for the motion of the spins was determined.

Some T_1 and T_2 data were taken at the mixed phase, which lies between the registered and the solid phases. These data have been analysed and interpreted.

4.4 The Coverage Dependence:

A display of the variation of T_1 and T_2 with coverage was illustrated in figure (4.4.1) and (4.4.2). The NMR frequency was 5.1 MHz and the substrate orientation was 90° while the temperature was 1.2 and 4.2 K respectively. Data

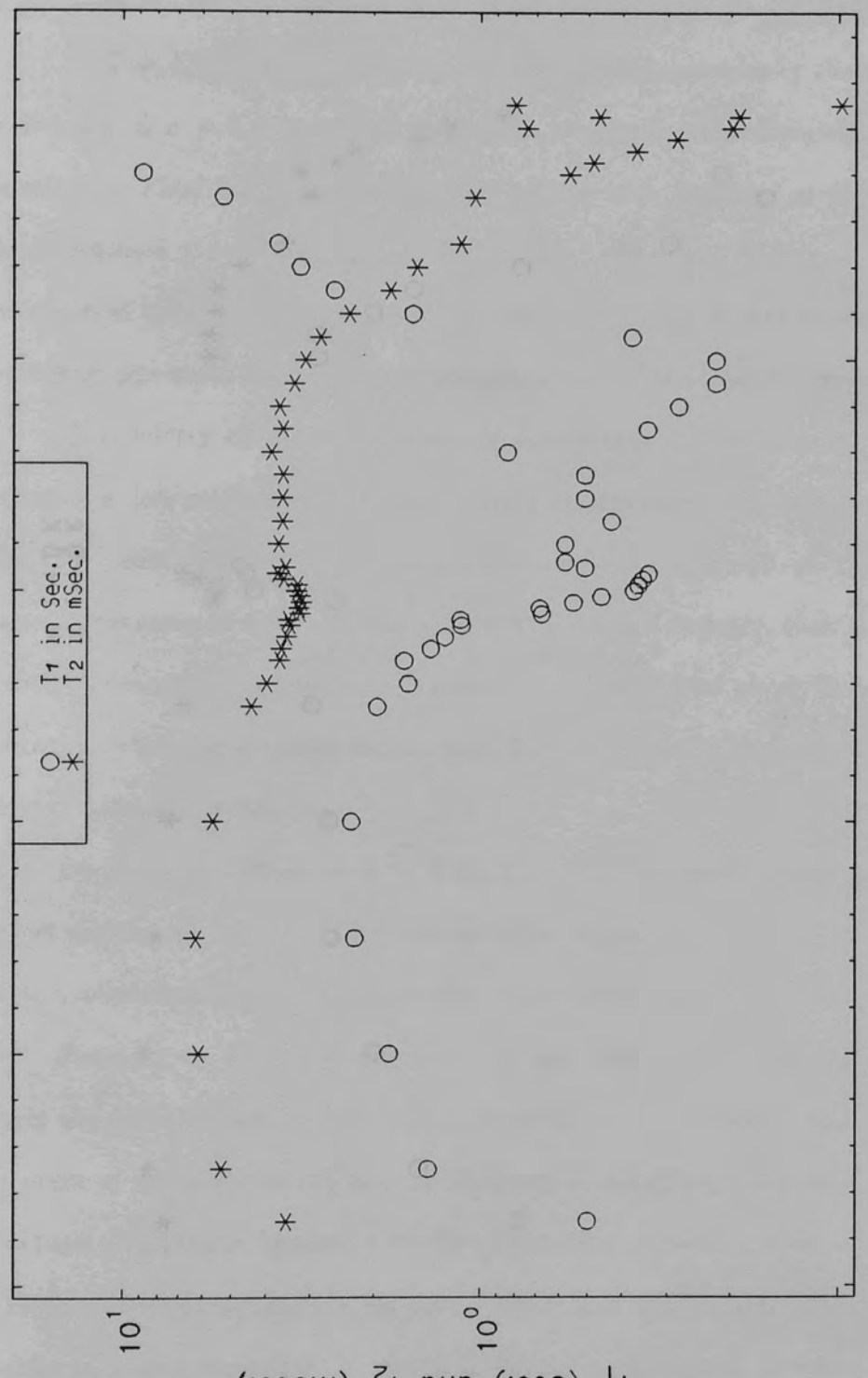

Figure 4.4.1

T_1 and T_2 as a function of coverage at f_o=5.1 MHz, T=1.2 K and β=90 deg.

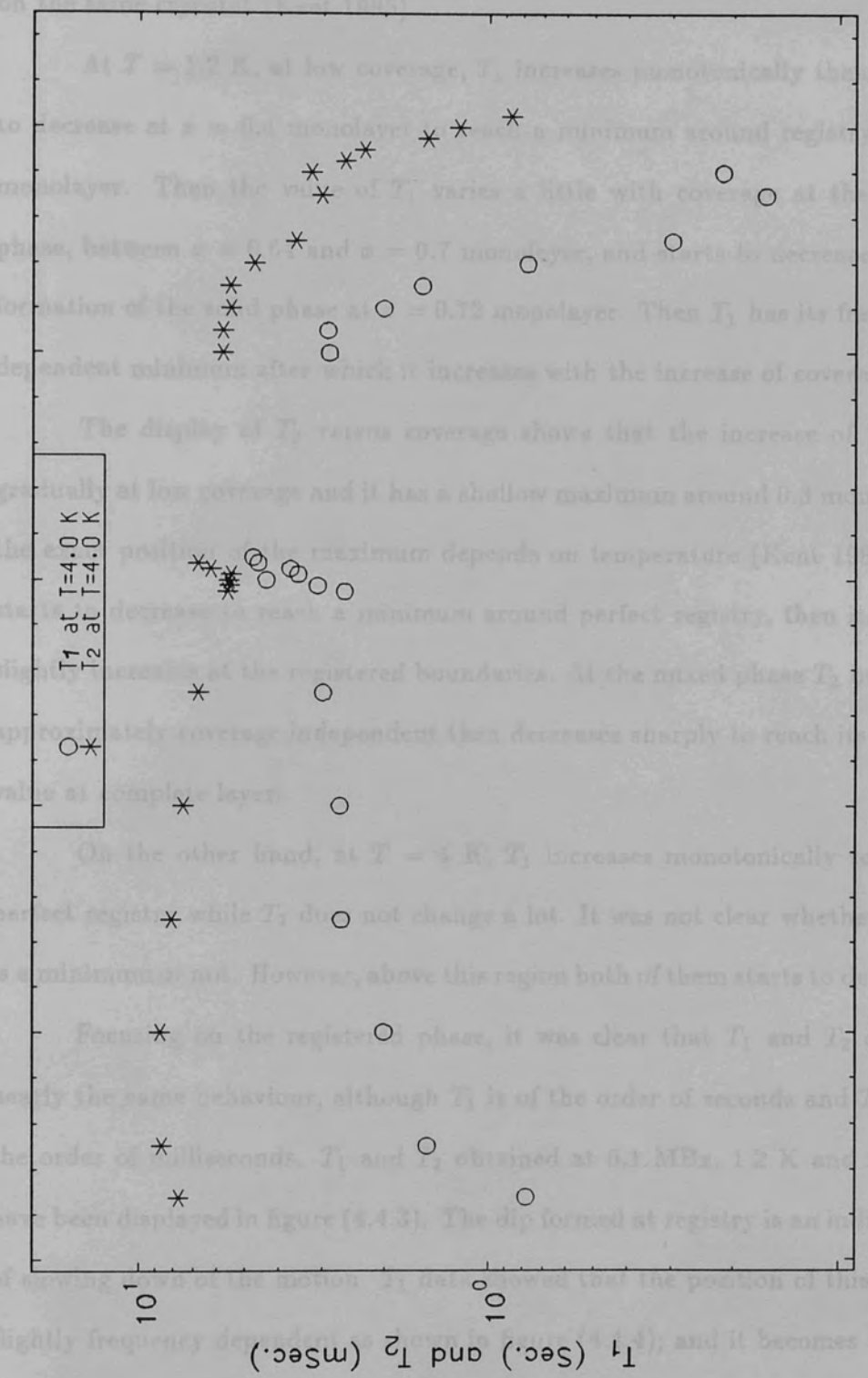

Figure 4.4.2

T_1 and T_2 as a function of coverage at f_o=5.1 MHz, T=4.0 K and β=90 deg.

for coverage less than 0.5 monolayer were taken from the previous work done on the same cryostat (Kent 1985).

At $T = 1.2$ K, at low coverage, T_1 increases monotonically then begins to decrease at $x = 0.4$ monolayer to reach a minimum around registry at 0.6 monolayer. Then the value of T_1 varies a little with coverage at the mixed phase, between $x = 0.64$ and $x = 0.7$ monolayer, and starts to decrease at the formation of the solid phase at $x = 0.72$ monolayer. Then T_1 has its frequency dependent minimum after which it increases with the increase of coverage.

The display of T_2 versus coverage shows that the increase of T_2 was gradually at low coverage and it has a shallow maximum around 0.3 monolayer, the exact position of the maximum depends on temperature (Kent 1985). T_2 starts to decrease to reach a minimum around perfect registry, then its value slightly increases at the registered boundaries. At the mixed phase T_2 becomes approximately coverage independent then decreases sharply to reach its lowest value at complete layer.

On the other hand, at $T = 4$ K, T_1 increases monotonically to reach perfect registry while T_2 does not change a lot. It was not clear whether there is a minimum or not. However, above this region both of them starts to decrease.

Focusing on the registered phase, it was clear that T_1 and T_2 exhibit nearly the same behaviour, although T_1 is of the order of seconds and T_2 is of the order of milliseconds. T_1 and T_2 obtained at 5.1 MHz, 1.2 K and 90 deg have been displayed in figure (4.4.3). The dip formed at registry is an indication of slowing down of the motion. T_1 data showed that the position of this dip is slightly frequency dependent as shown in figure (4.4.4); and it becomes dipper for smaller Larmor frequency. While T_2 data indicated that the position of the dip is shifted towards higher coverage for smaller Larmor frequencies; and

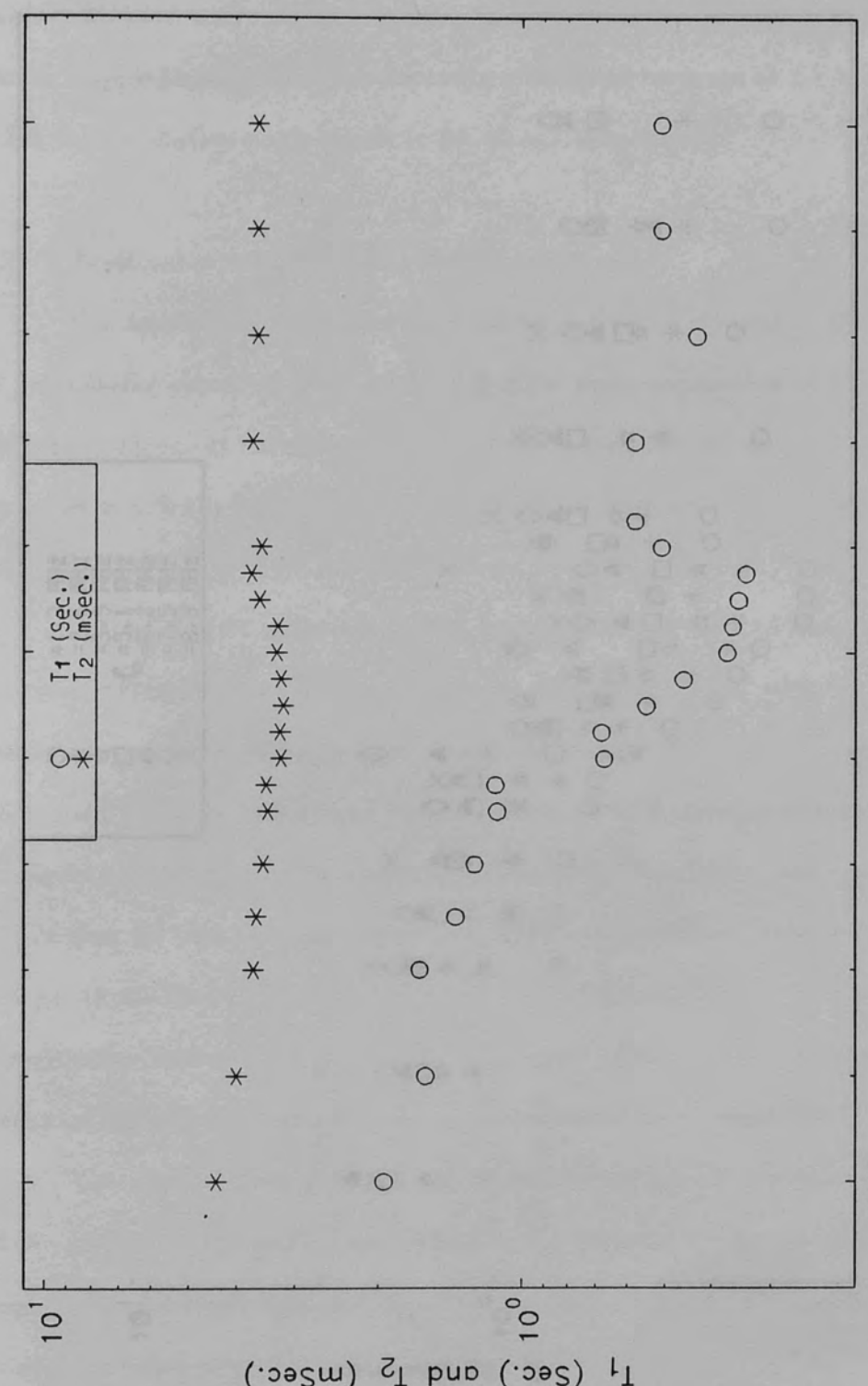

Figure 4.4.3

T_1 and T_2 as a function of coverage at f_o=5.1 MHz, T=1.2 K and β=90 deg.

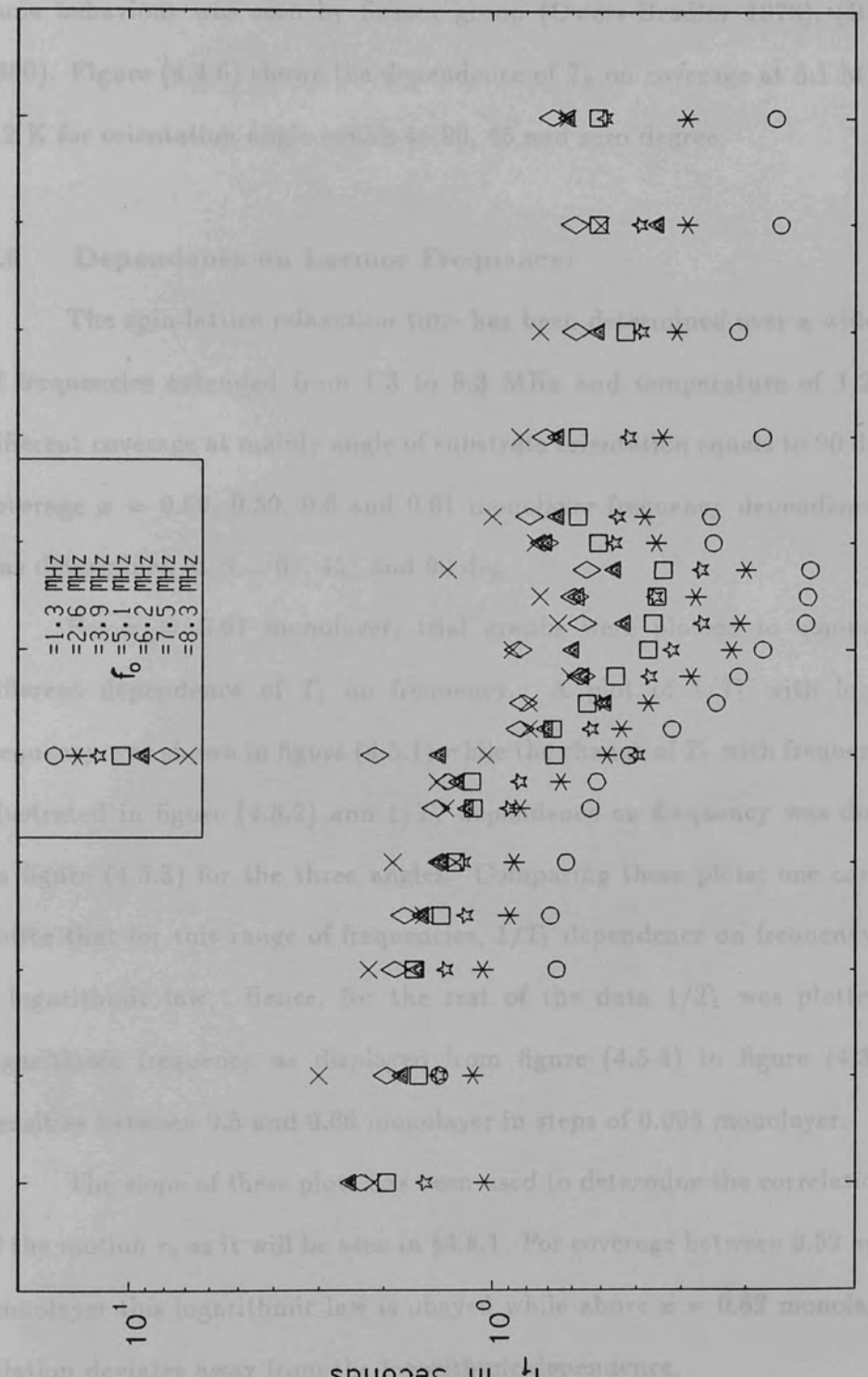

Figure 4.4.4

Spin–lattice relaxation time as a function of coverage at different frequencies.

becomes dipper as well. This dependence was displayed in figure (4.4.5). The same behaviour was seen by Sussex group (Owers-Bradley 1978), (Richards 1980). Figure (4.4.6) shows the dependence of T_2 on coverage at 5.1 MHz and 1.2 K for orientation angle equals to 90, 45 and zero degree.

4.5 Dependence on Larmor Frequency:

The spin-lattice relaxation time has been determined over a wide range of frequencies extended from 1.3 to 8.3 MHz and temperature of 1.2 K for different coverage at mainly angle of substrate orientation equals to 90 deg. For coverage x = 0.58, 0.59, 0.6 and 0.61 monolayer frequency dependence of T_1 was determined at $\beta = 0°$, 45° and 90 deg.

For x = 0.61 monolayer, trial graphs were plotted to compare the different dependence of T_1 on frequency. A plot of $1/T_1$ with logarithm frequency was shown in figure (4.5.1) while the change of T_1 with frequency was illustrated in figure (4.5.2) and $1/T_1$ dependence on frequency was displayed on figure (4.5.3) for the three angles. Comparing these plots; one can easily notice that for this range of frequencies, $1/T_1$ dependence on frequency obeys a logarithmic law. Hence, for the rest of the data $1/T_1$ was plotted with logarithmic frequency as displayed from figure (4.5.4) to figure (4.5.9) for densities between 0.5 and 0.66 monolayer in steps of 0.005 monolayer.

The slope of these plots has been used to determine the correlation time of the motion τ_c as it will be seen in §4.8.1. For coverage between 0.52 and 0.62 monolayer this logarithmic law is obeyed while above x = 0.62 monolayer the relation deviates away from the logarithmic dependence.

It has been found experimentally that $1/T_2$ has linear dependence on ω_0. The linearity was shown in figures (4.5.10), (4.5.11), (4.5.12) and (4.5.13) for

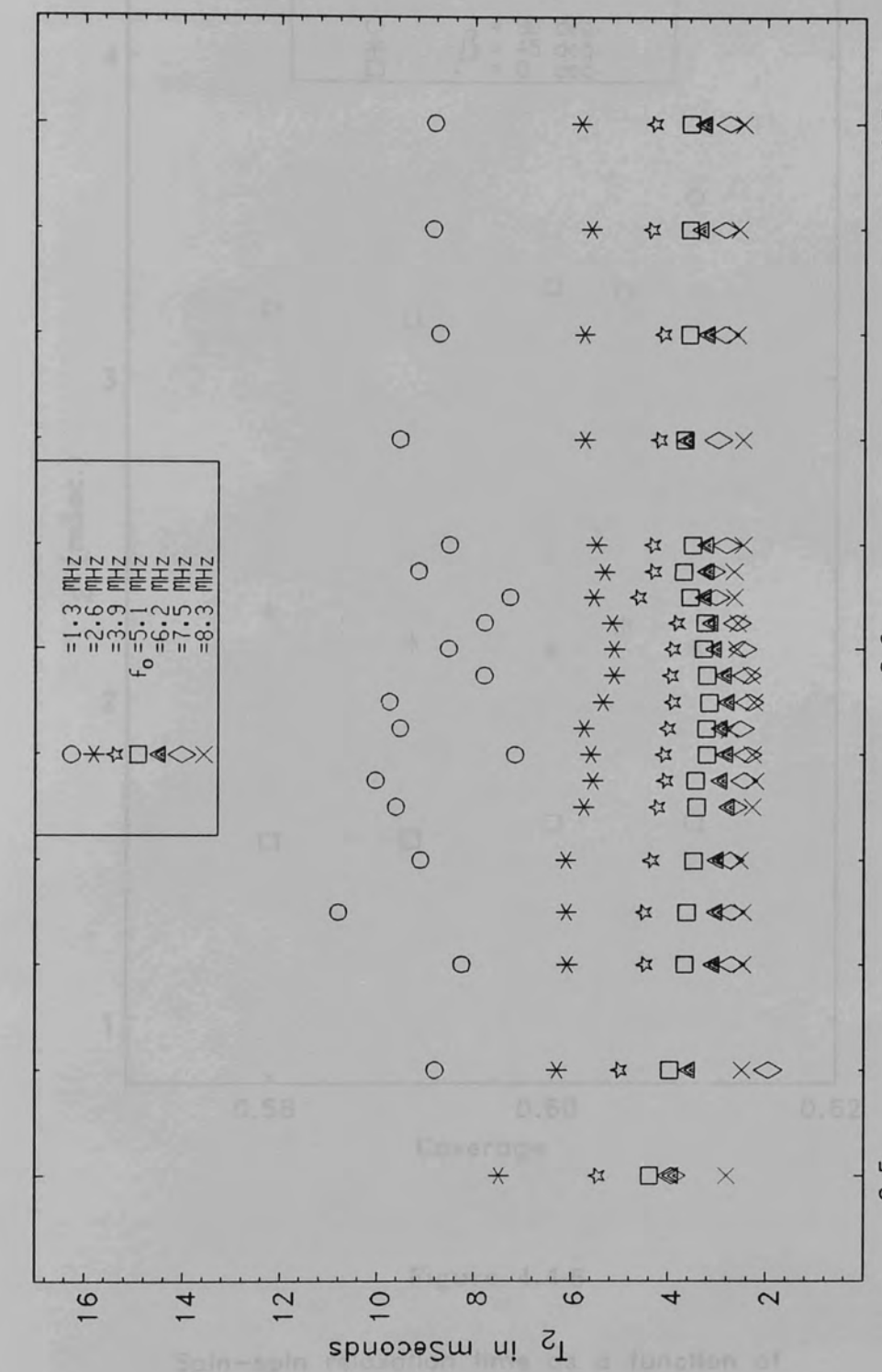

Figure 4.4.5

Spin-spin relaxation time as a function of coverage at different frequencies. T=1.2 K & $\beta = 90^{\circ}$

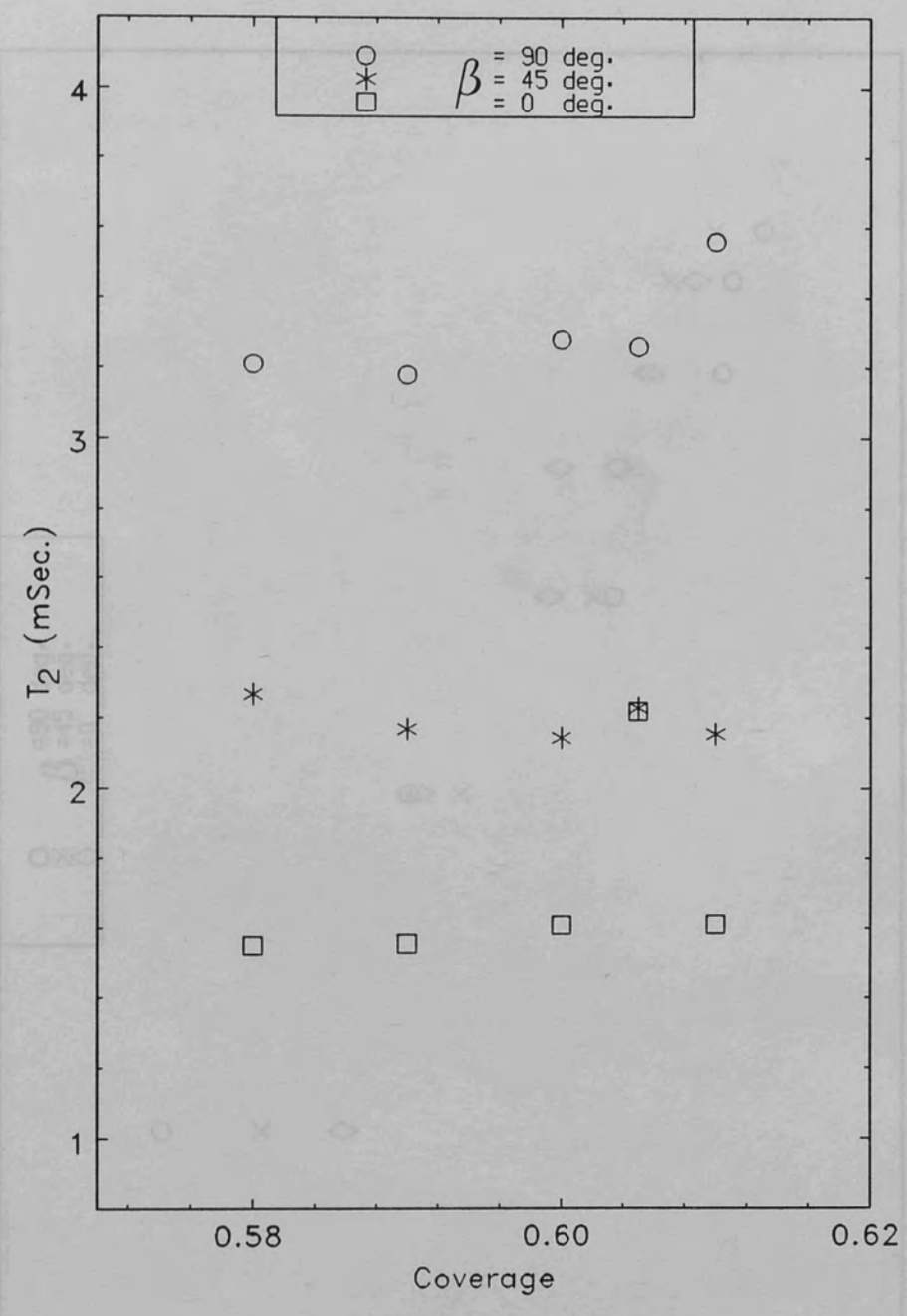

Figure 4.4.6

Spin–spin relaxation time as a function of coverage at β= 0, 45 and 90 deg. T=1.2 K, f_o =5.1 MHz.

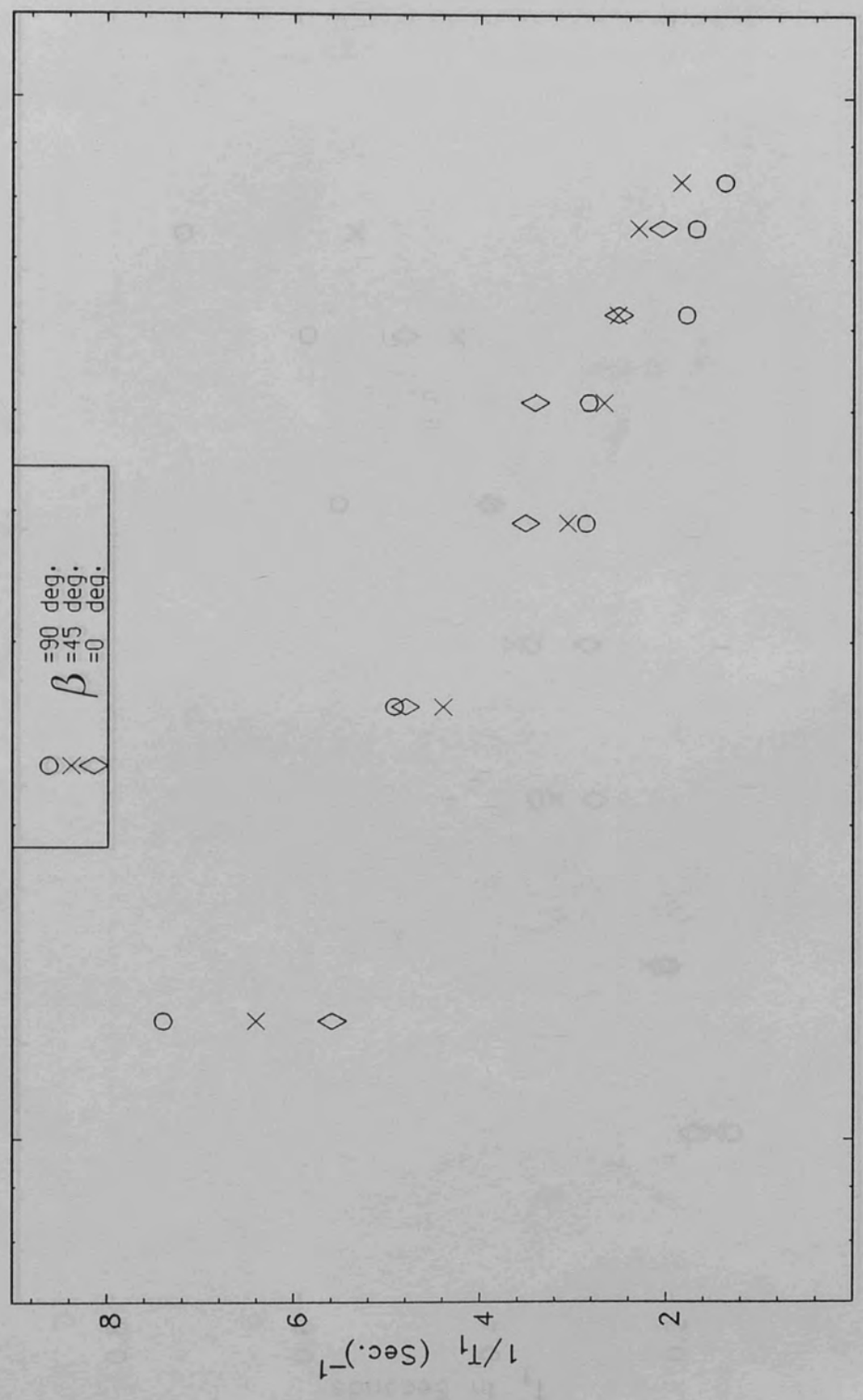

Figure 4.5:1

Spin-lattice relaxation rate as a function of frequency. T=1.2 K and x=0.61 monolayer.

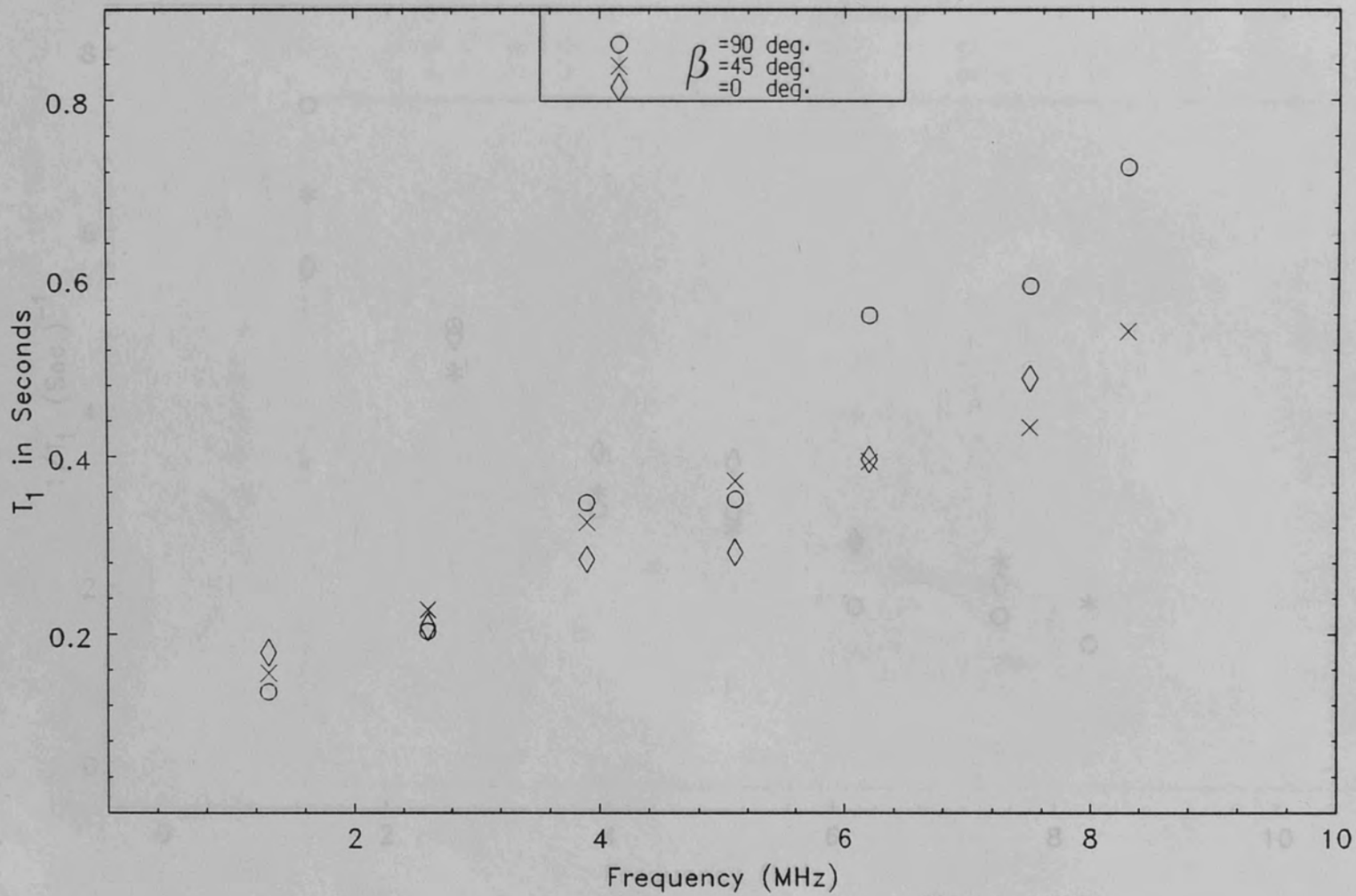

Figure 4.5.2

Spin-lattice relaxation time as a function of frequency. T=1.2 K and x=0.61 monolayer

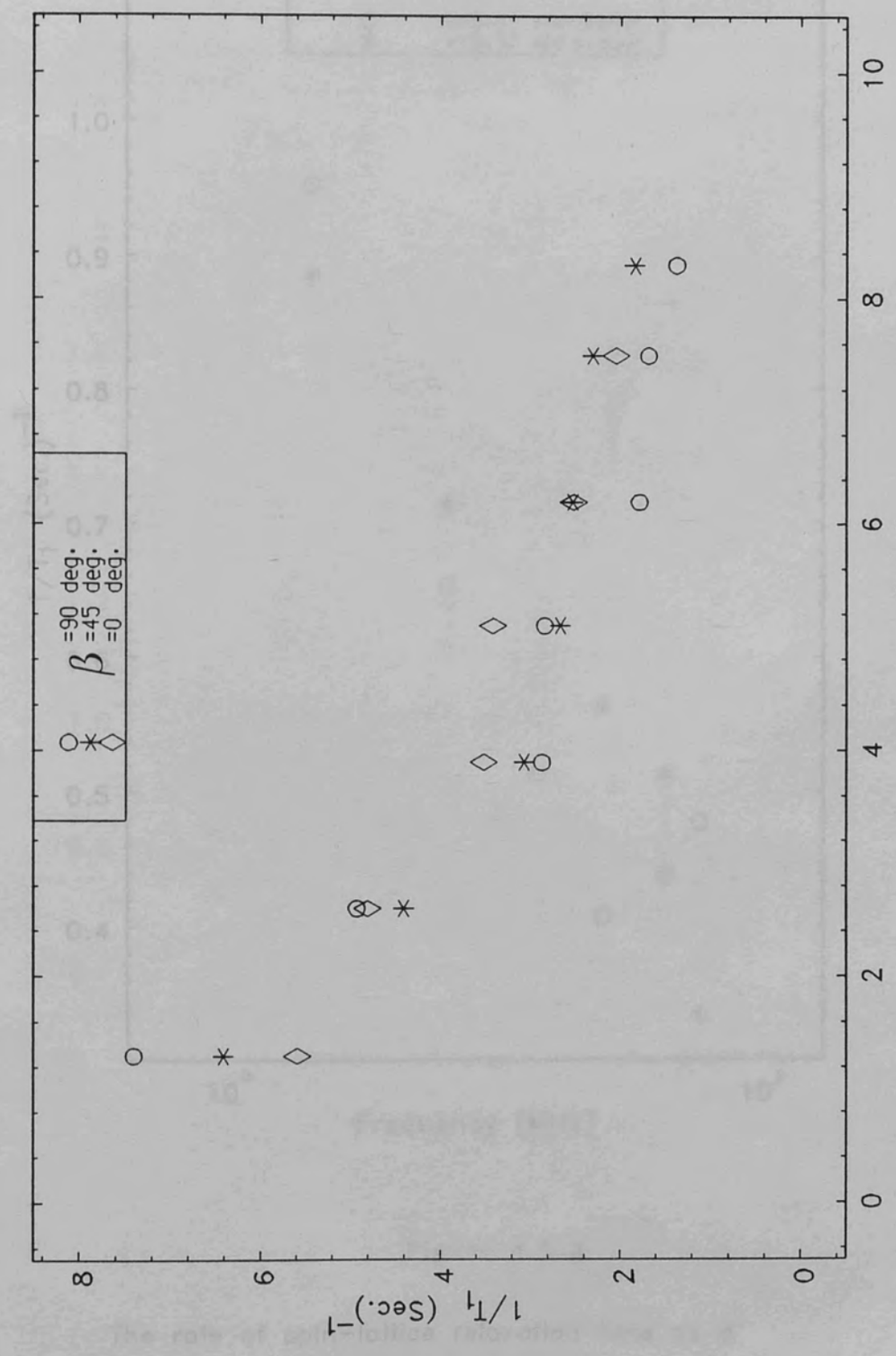

Figure 4.5.3

$1/T_1$ as a function of frequency. x=0.61 monolayer and T=1.2 K.

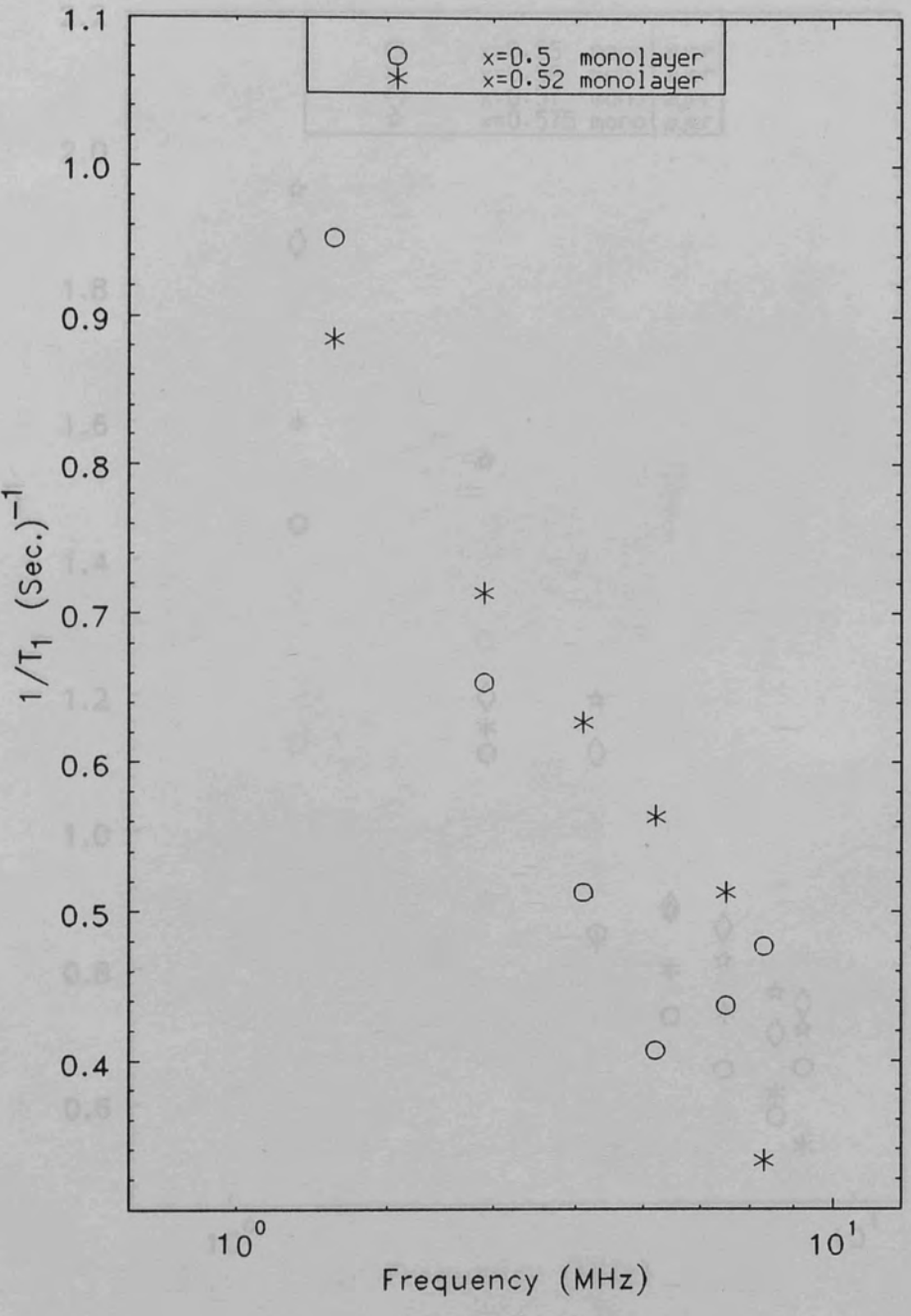

Figure 4.5.4

The rate of spin-lattice relaxation time as a function of coverage. T=1.2 K and β=90 deg.

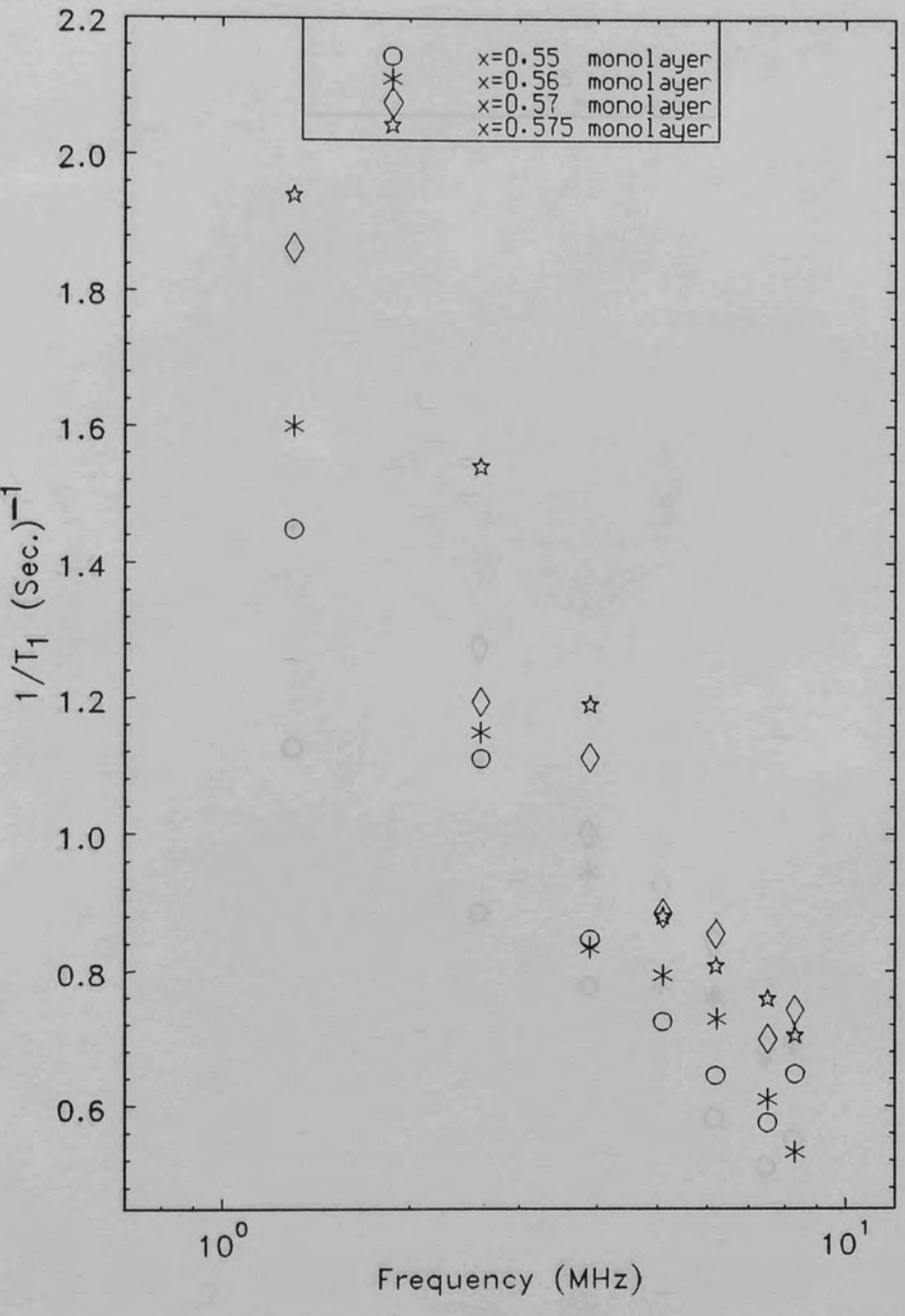

Figure 4.5.5

The rate of spin-lattice relaxation time as a function of Larmor frequency. T=1.2 K and $\beta = 90^{o}$

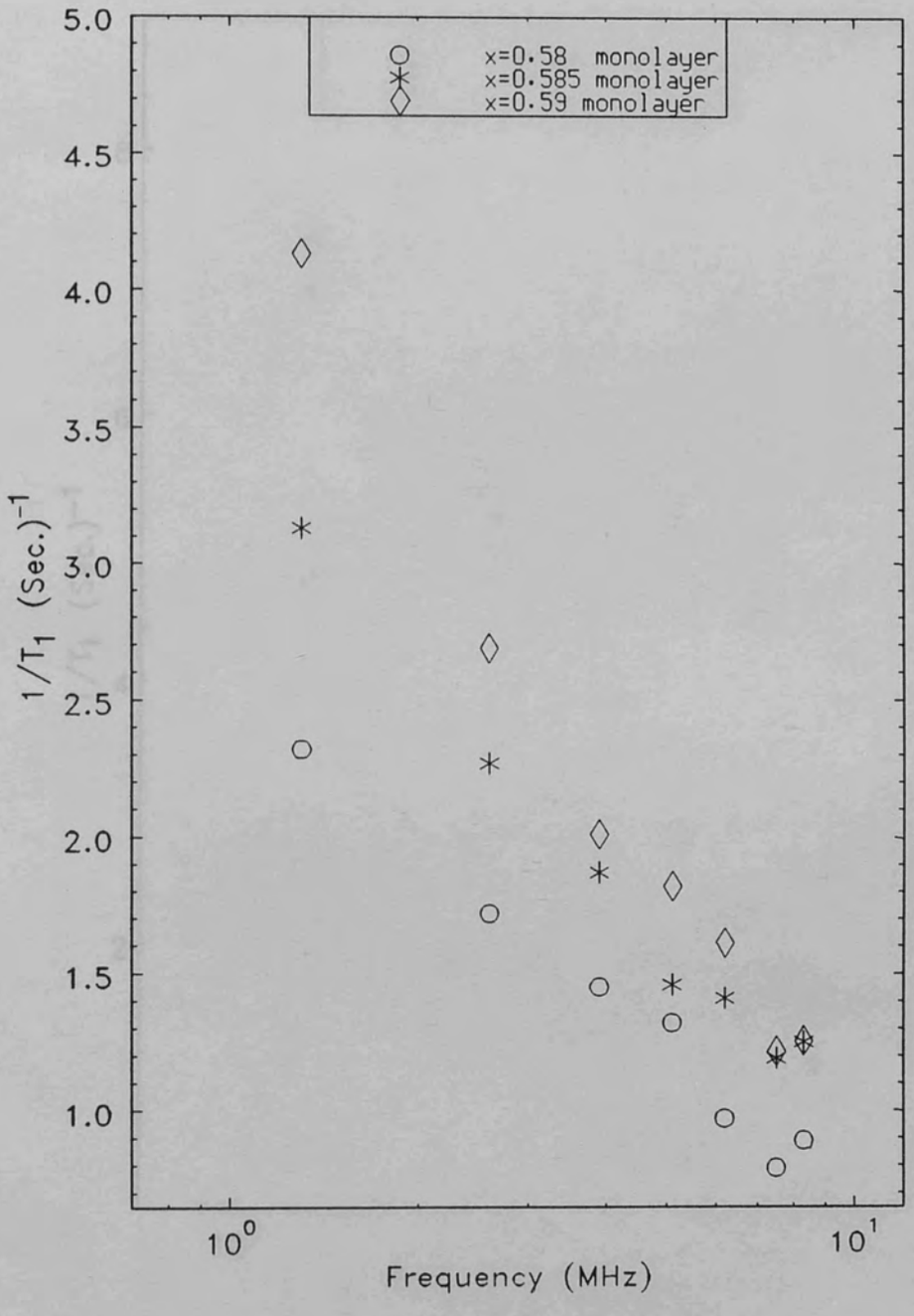

Figure 4.5.6

The rate of spin–lattice relaxation time as a function of coverage.
T=1.2 K and β=90 deg.

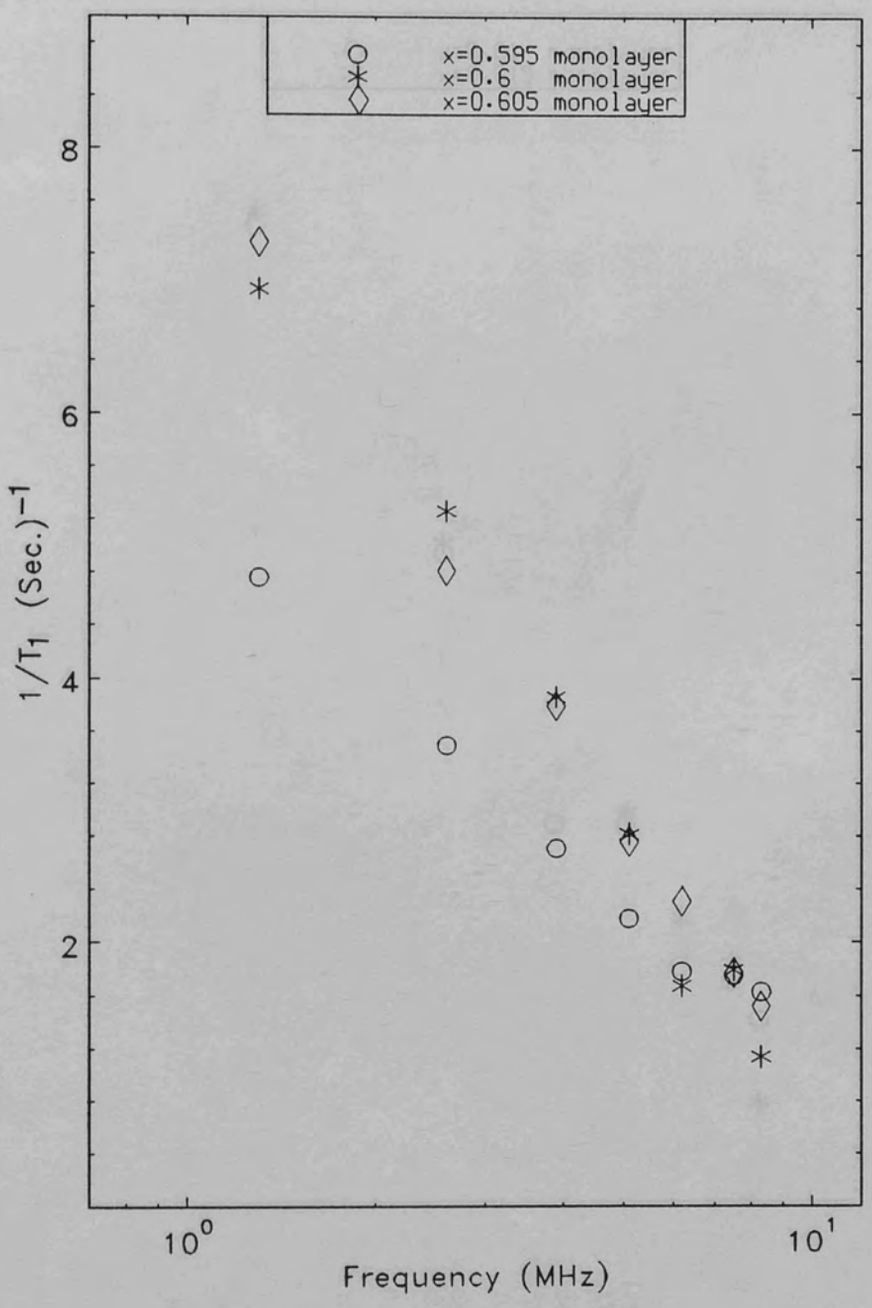

Figure 4.5.7

The rate of spin-lattice relaxation time as a function of coverage. T=1.2 K and β=90 deg.

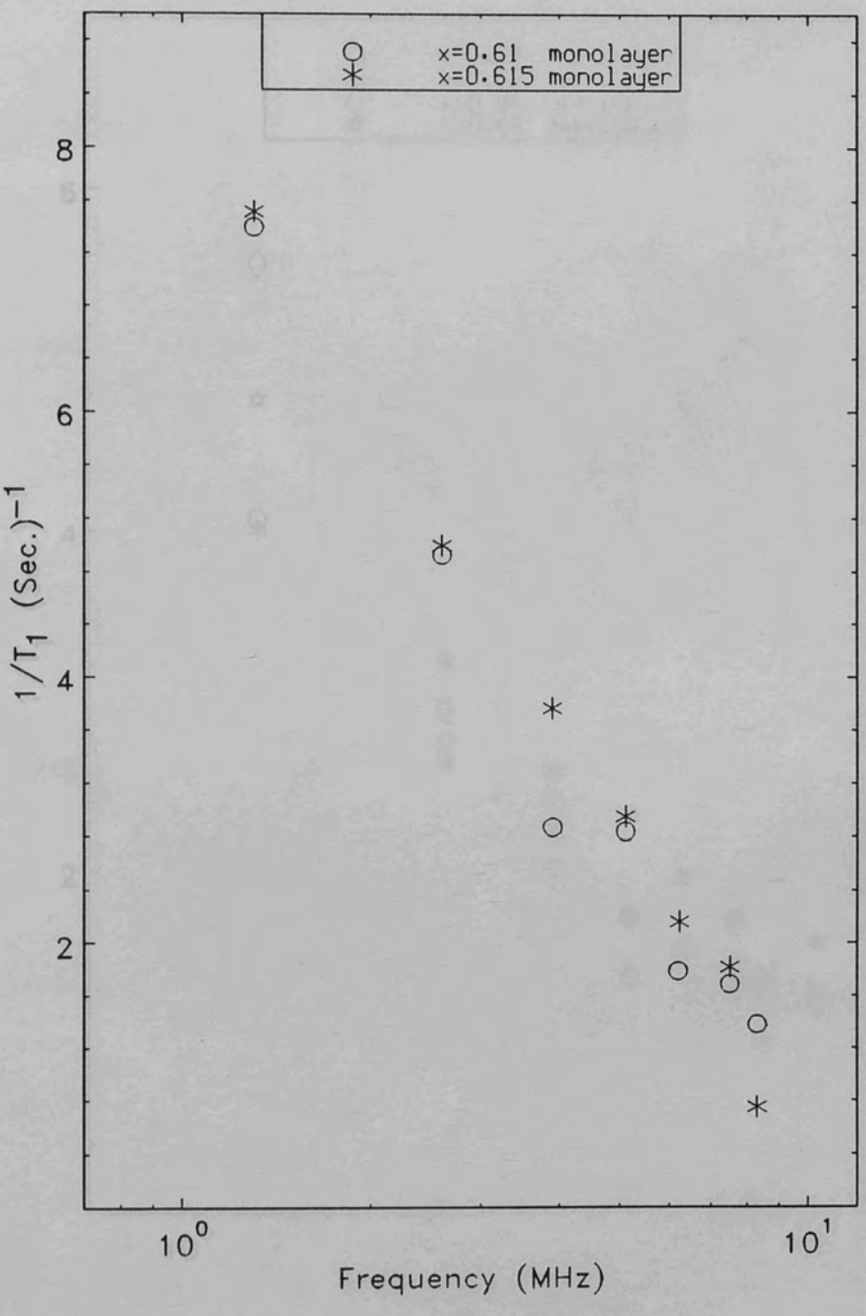

Figure 4.5.8

The rate of spin-lattice relaxation time as a function of coverage. T=1.2 K and β=90 deg.

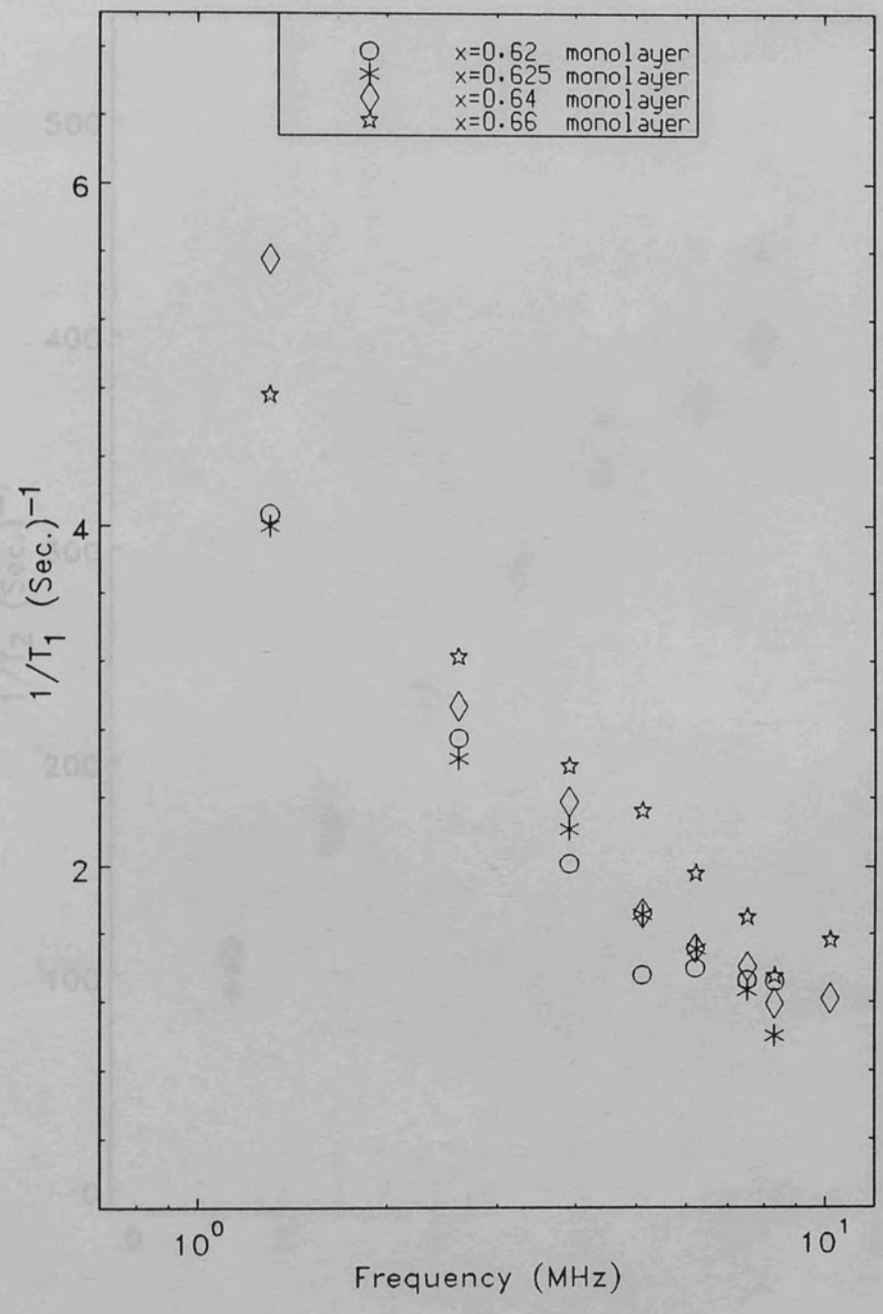

Figure 4.5.9

The rate of spin-lattice relaxation time as a function of coverage. T=1.2 K and β =90 deg.

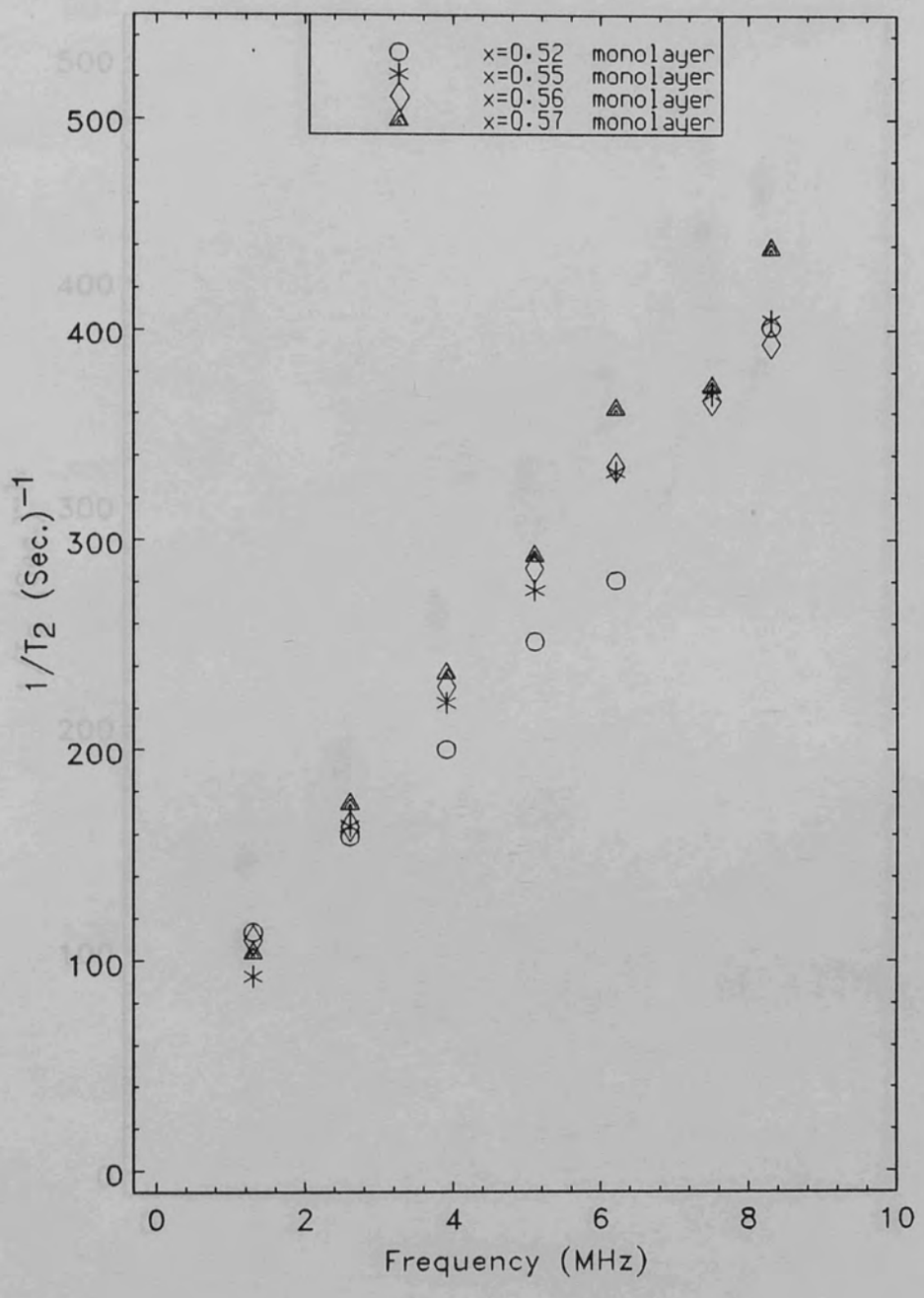

Figure 4.5.10

Spin–spin relaxation rate as a function of frequency. T=1.2 K and β =90 deg.

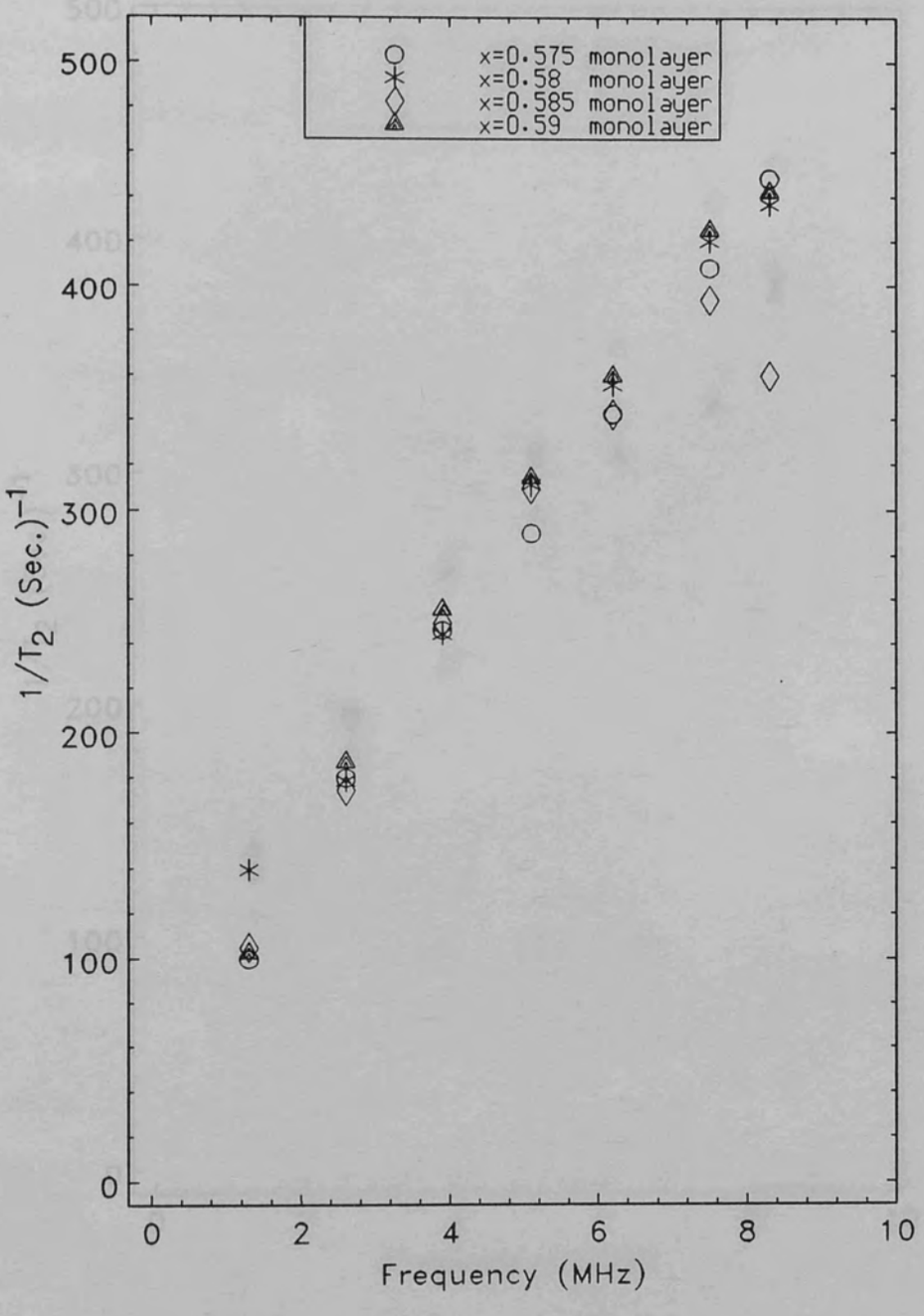

Figure 4.5.11

Spin–spin relaxation rate as a function of frequency. T=1.2 K and β=90 deg.

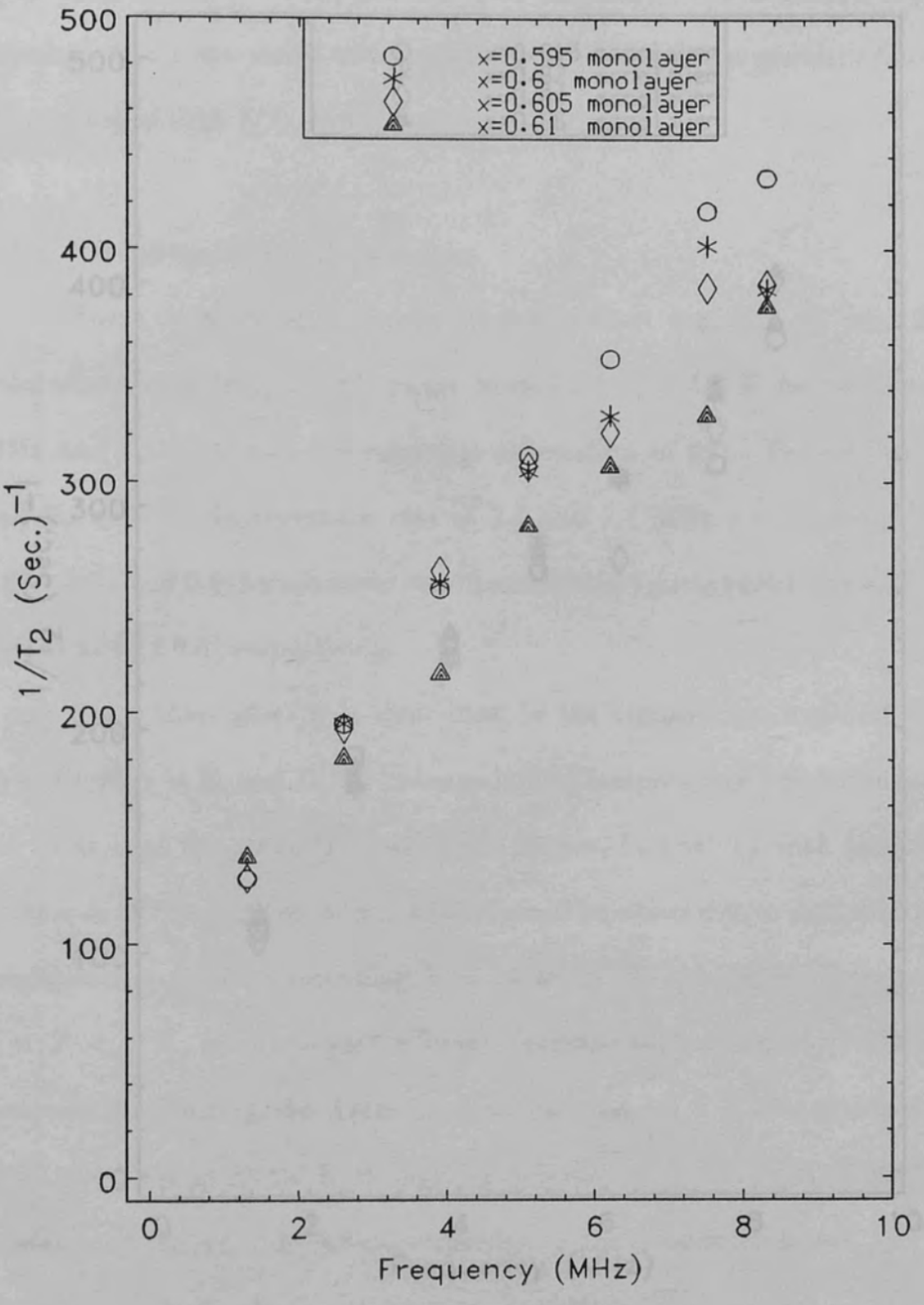

Figure 4.5.12

Spin–spin relaxation rate as a function of frequency. T=1.2 K and β=90 deg.

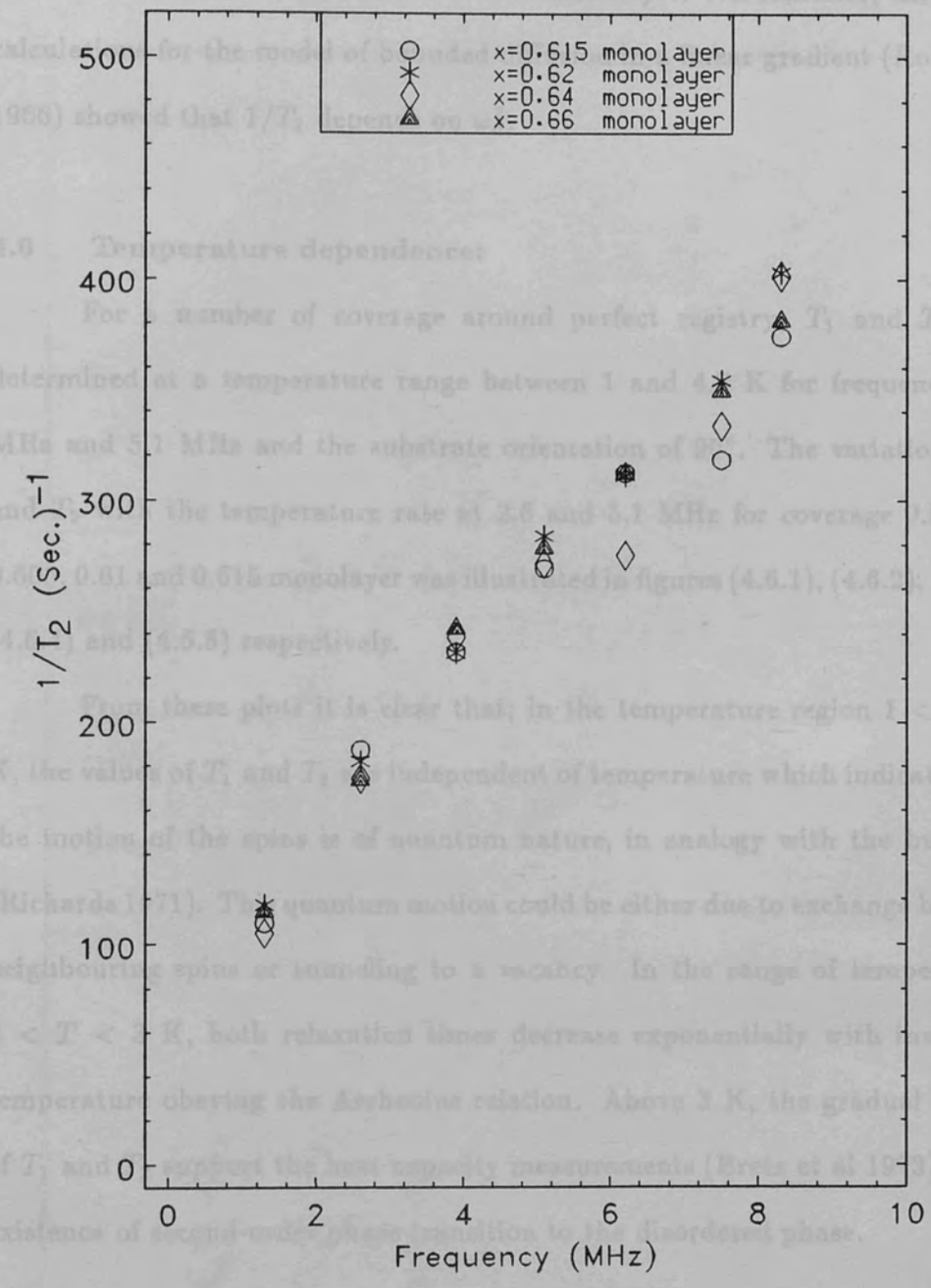

Figure 4.5.13

Spin–spin relaxation rate as a function of frequency. T=1.2 K and β=90 deg.

densities between $x = 0.52$ and $x = 0.66$ monolayer. Nevertheless, theoretical calculations for the model of bounded diffusion in a linear gradient (Robertson 1966) showed that $1/T_2$ depends on ω_0^2.

4.6 Temperature dependence:

For a number of coverage around perfect registry; T_1 and T_2 were determined at a temperature range between 1 and 4.2 K for frequencies 2.6 MHz and 5.1 MHz and the substrate orientation of 90°. The variation of T_1 and T_2 with the temperature rate at 2.6 and 5.1 MHz for coverage 0.59, 0.6, 0.605, 0.61 and 0.615 monolayer was illustrated in figures (4.6.1), (4.6.2), (4.6.3), (4.6.4) and (4.6.5) respectively.

From these plots it is clear that; in the temperature region $1 < T < 2$ K, the values of T_1 and T_2 are independent of temperature which indicates that the motion of the spins is of quantum nature, in analogy with the bulk ^{3}He (Richards 1971). This quantum motion could be either due to exchange between neighbouring spins or tunneling to a vacancy. In the range of temperatures $2 < T < 3$ K, both relaxation times decrease exponentially with inverse of temperature obeying the Arrhenius relation. Above 3 K, the gradual change of T_1 and T_2 support the heat capacity measurements (Bretz et al 1973) of the existence of second-order phase transition to the disordered phase.

4.7 Anisotropy:

The anisotropy of T_1 and T_2 with respect to the substrate orientation has been studied. It was found that the anisotropy of T_1 is weaker than the corresponding one for T_2.

T_1 was determined with the change of orientation angle at temperature

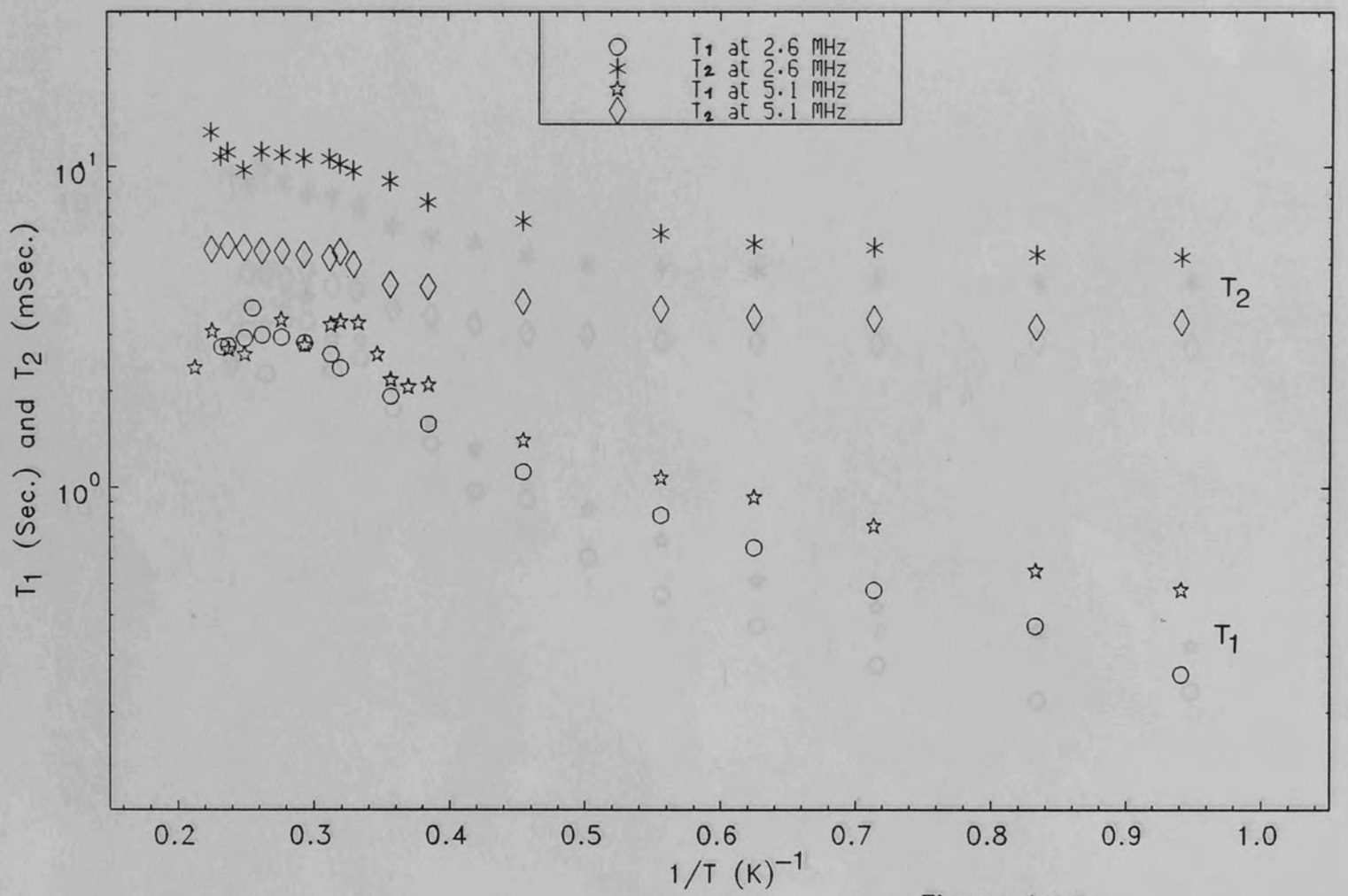

Figure 4.6.1

T_1 and T_2 as a function of inverse of temperature. x=0.59 monolayer and β=90°

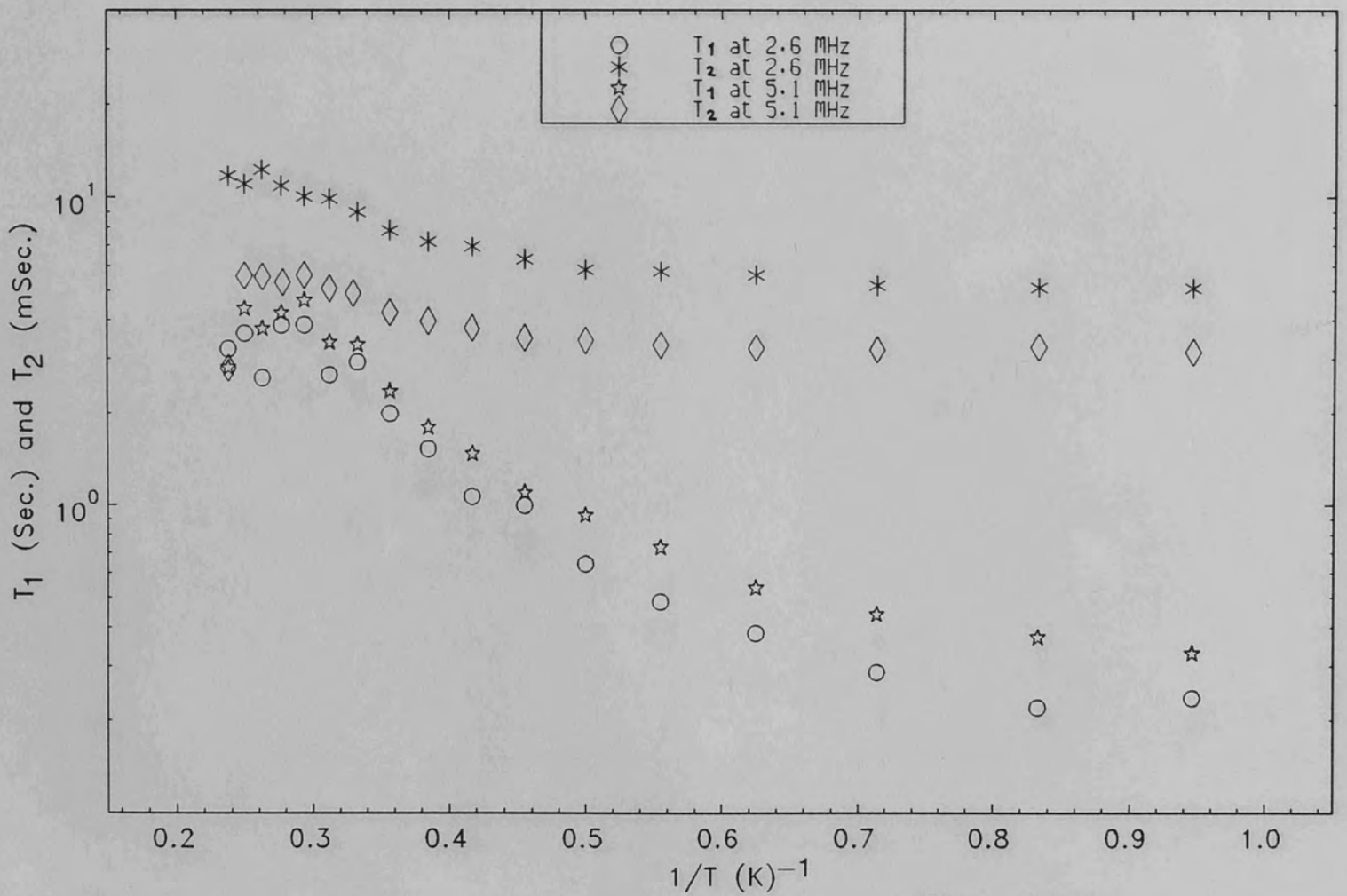

Figure 4.6.2

T_1 and T_2 as a function of inverse temperature. x=0.6 monolayer and β=90 deg.

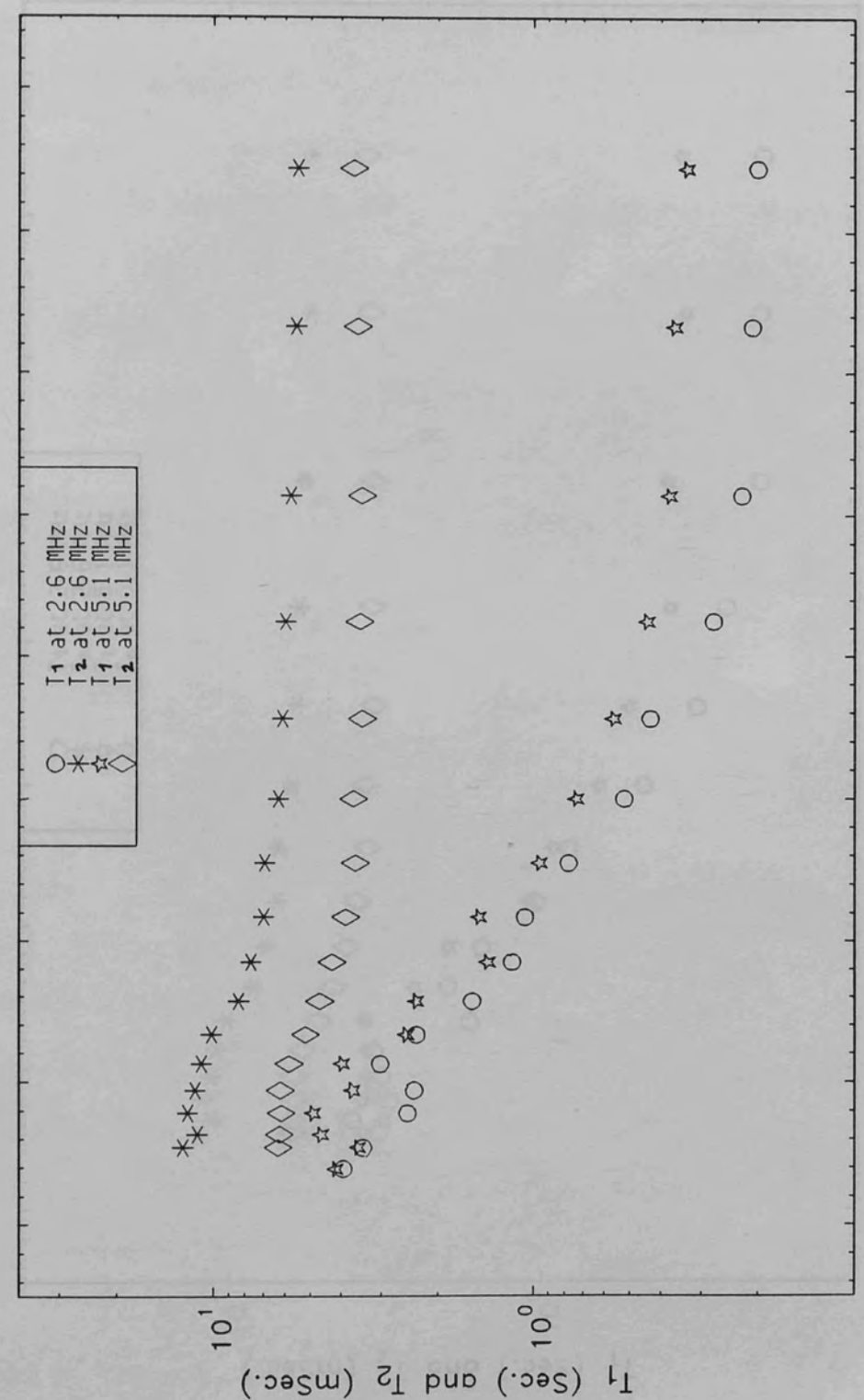

Figure 4.6.3

T_1 and T_2 as a function of inverse of temperature. x=0.605 monolayer and $\beta = 90^\circ$

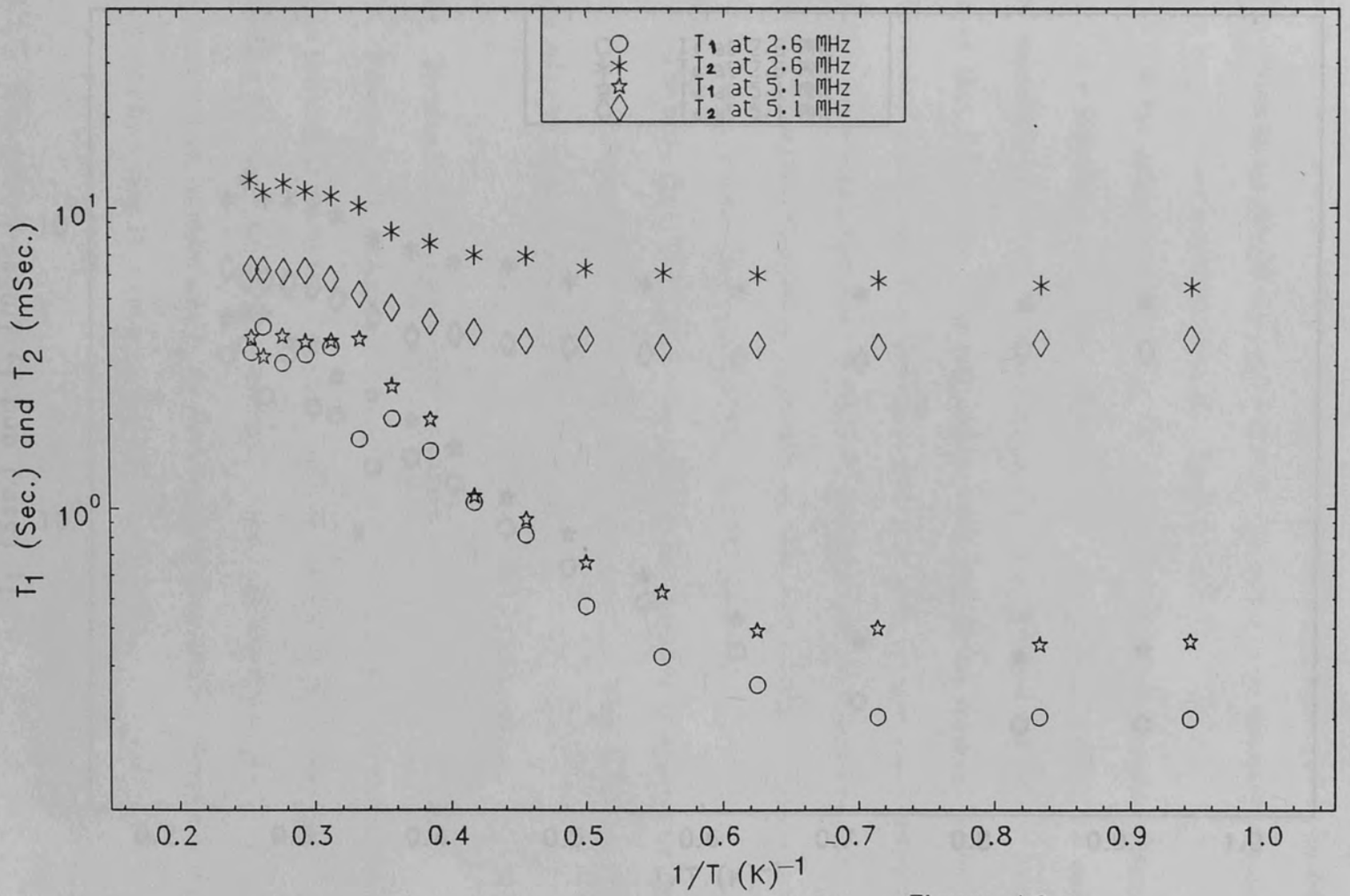

Figure 4.6.4

T_1 and T_2 as a function of inverse of temperature. x=0.61 monolayer and β=90 deg.

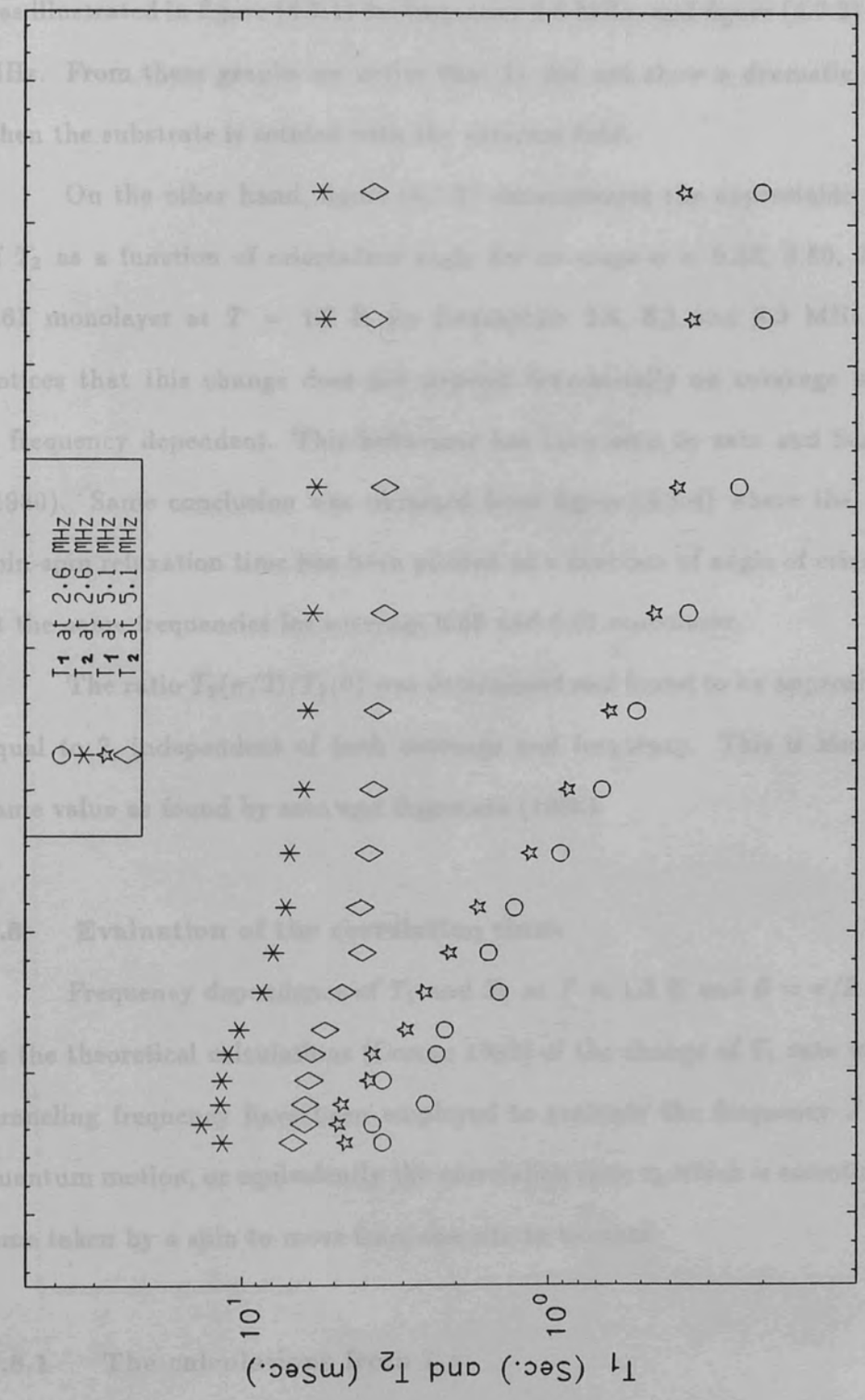

Figure 4.6.5

T_1 and T_2 as a function of inverse of temperature. x=0.615 monolayer and β=90 deg.

of 1.2 K and coverage $x = 0.58, 0.59, 0.6$ and 0.605 monolayer. This dependence was illustrated in figure (4.7.1) for frequency 2.6 MHz, and figure (4.7.2) for 5.1 MHz. From these graphs we notice that T_1 did not show a dramatic change when the substrate is rotated with the external field.

On the other hand, figure (4.7.3) demonstrates the appreciable change of T_2 as a function of orientation angle for coverage $x = 0.58$, 0.59, 0.6 and 0.61 monolayer at $T = 1.2$ K for frequencies 2.6, 5.1 and 8.3 MHz. One notices that this change does not depend dramatically on coverage while it is frequency dependent. This behaviour has been seen by sato and Sugawara (1980). Same conclusion was obtained from figure (4.7.4) where the rate of spin-spin relaxation time has been plotted as a function of angle of orientation at the same frequencies for coverage 0.59 and 0.61 monolayer.

The ratio $T_2(\pi/2)/T_2(0)$ was determined and found to be approximately equal to 2, independent of both coverage and frequency. This is almost the same value as found by sato and Sugawara (1980).

4.8 Evaluation of the correlation time:

Frequency dependence of T_1 and T_2 at $T = 1.2$ K and $\beta = \pi/2$ as well as the theoretical calculations (Cowan 1980) of the change of T_1 rate with the tunneling frequency have been employed to evaluate the frequency J of the quantum motion, or equivalently the correlation time τ_c which is essentially the time taken by a spin to move from one site to another.

4.8.1 The calculations from T_1:

Recalling equation (2.4.6), where T_1 is given by:

$$\frac{1}{T_1} = J_1(\omega_0) + 4J_2(2\omega_0)$$

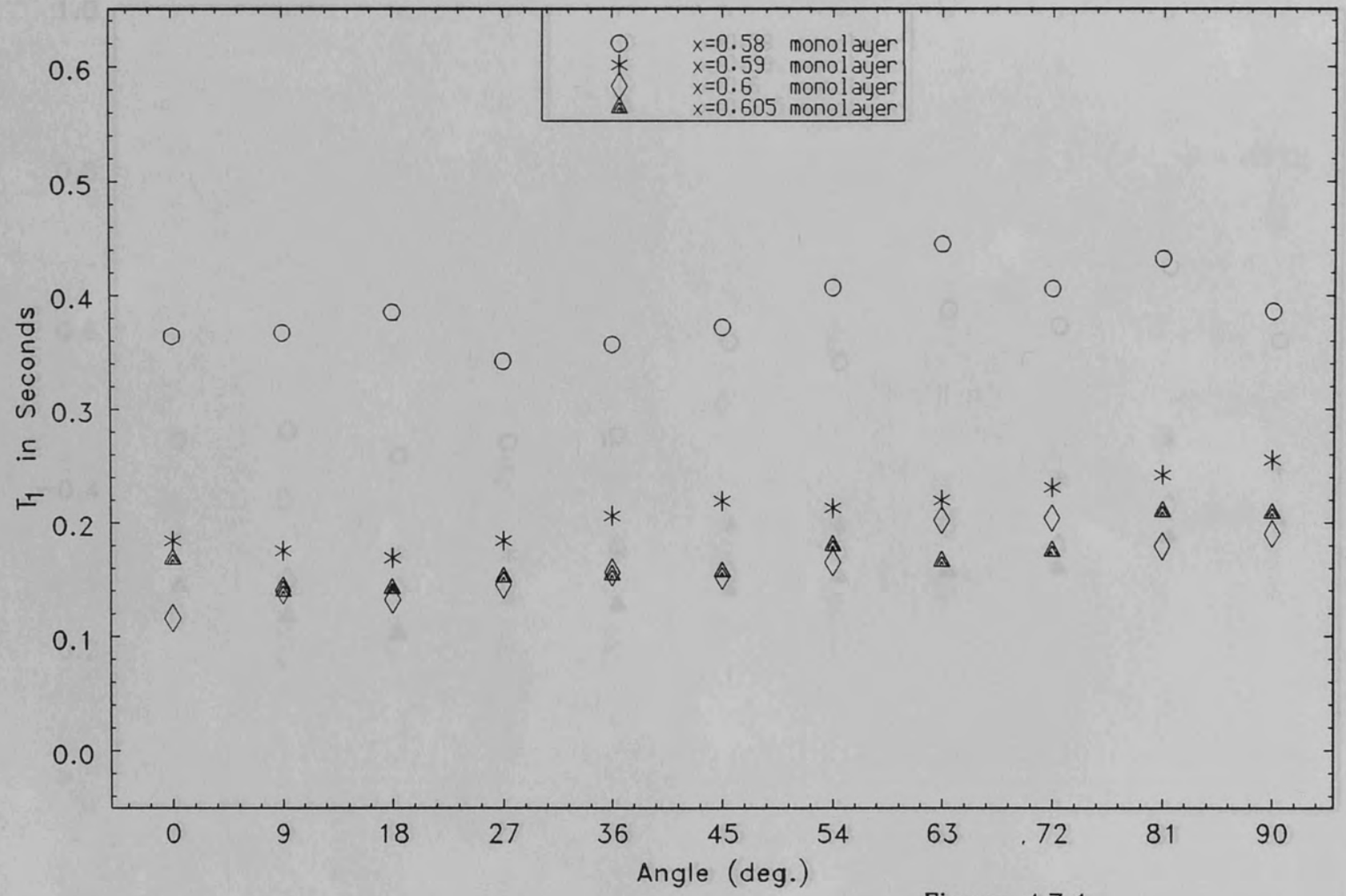

Figure 4.7.1

Spin–lattice relaxation time as a function of orientation angle. f_o = 2.6 MHz and T = 1.2 K

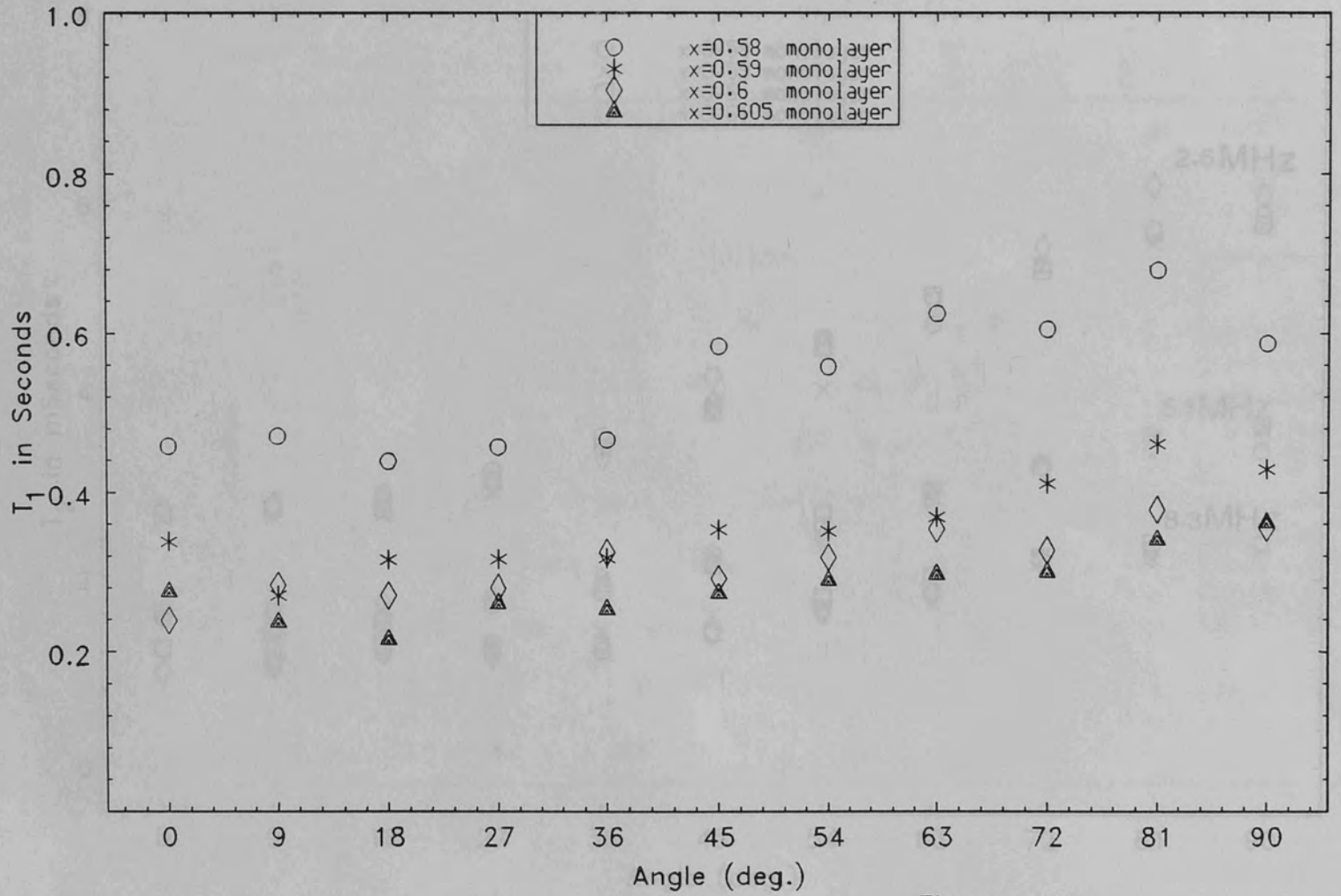

Figure 4.7.2

Spin–lattice relaxation time as a function of orientation angle. f_o =5.1 MHz and T=1.2 K

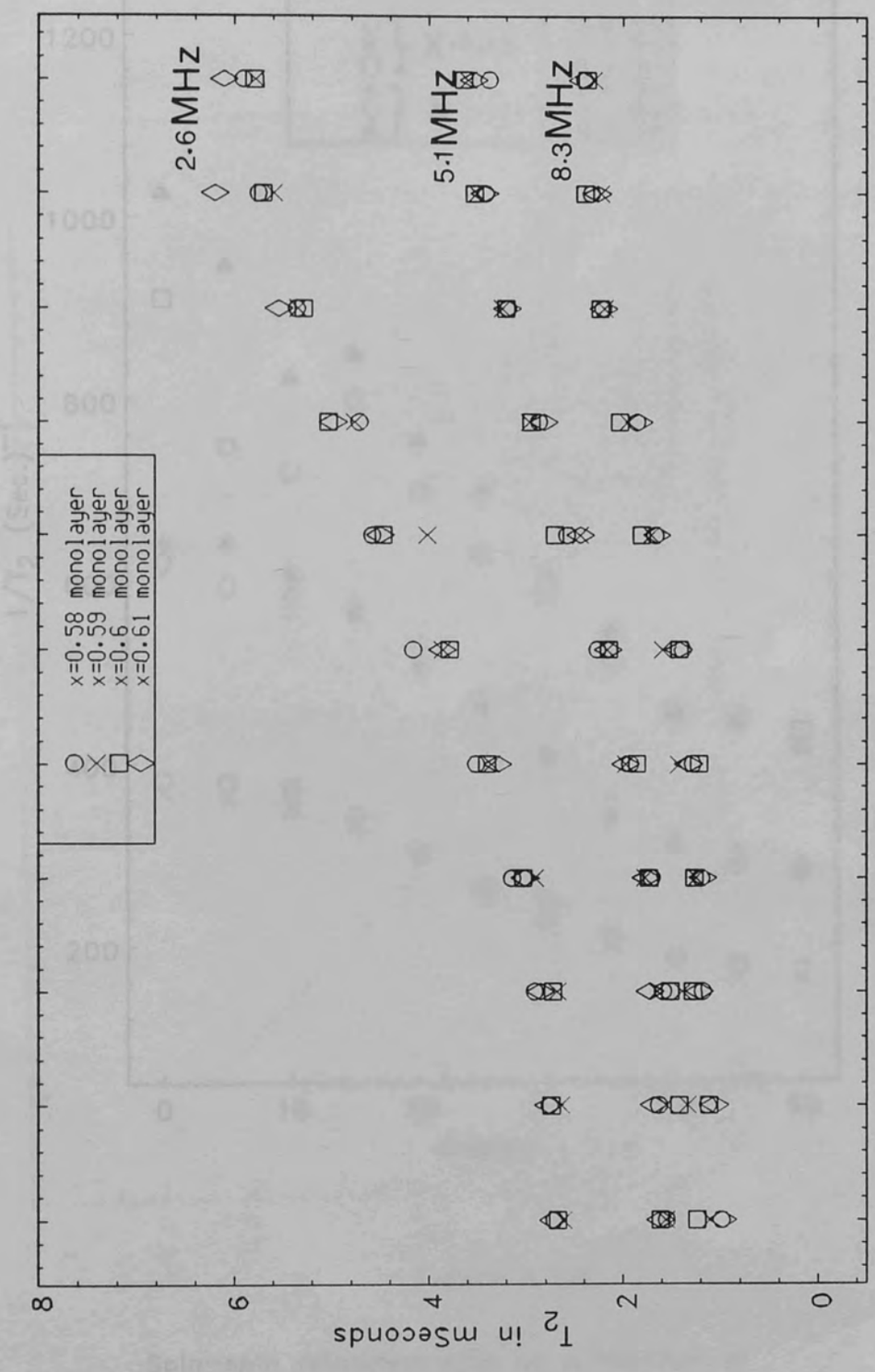

Figure 4.7.3

T_2 as a function of angle at f_o=2.6, 5.1 and 8.3 MHz for different coverages and T=1.2 K

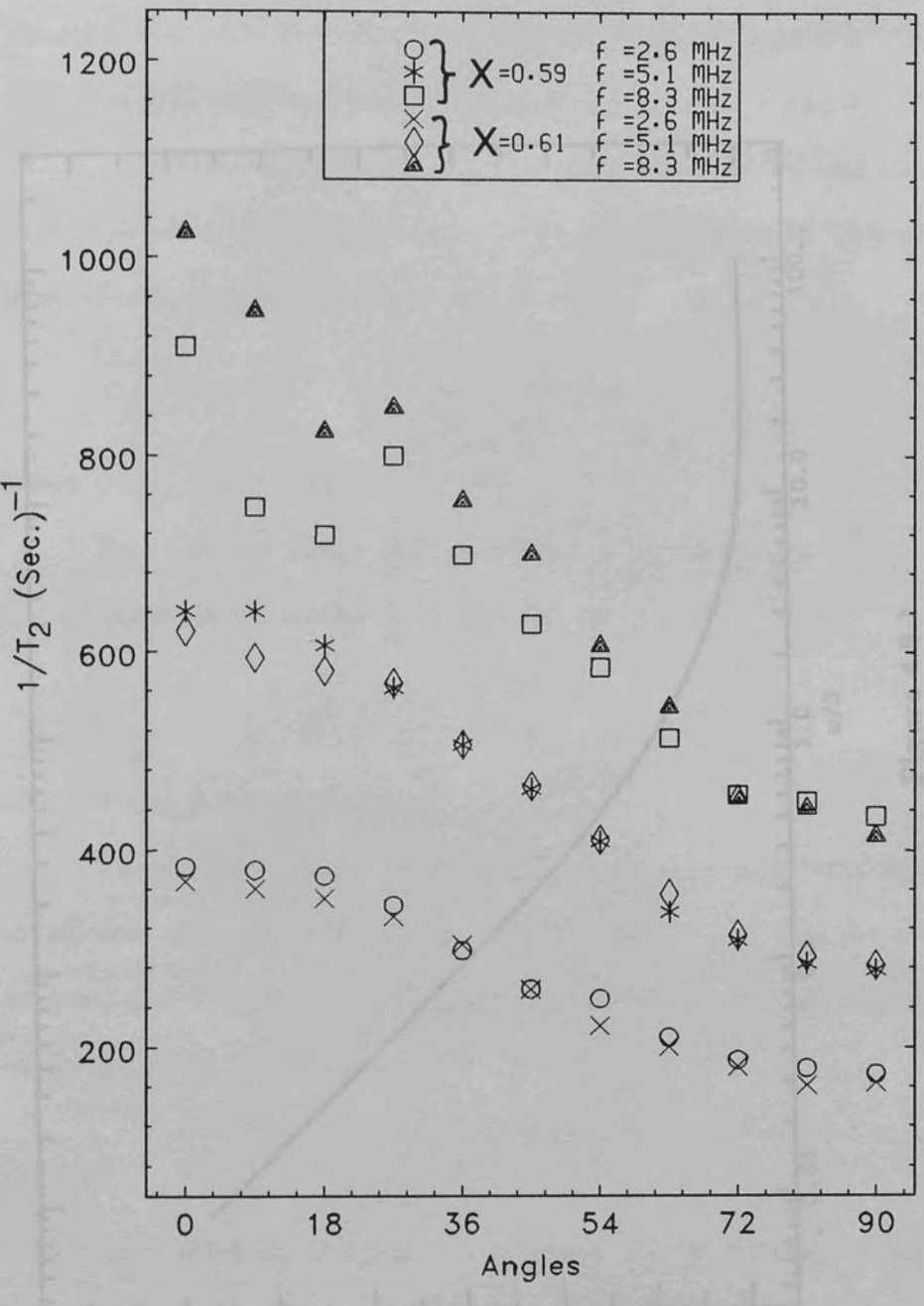

Figure 4.7.4

Spin–spin relaxation rate as a function of orientation angle at T=1.2 K.

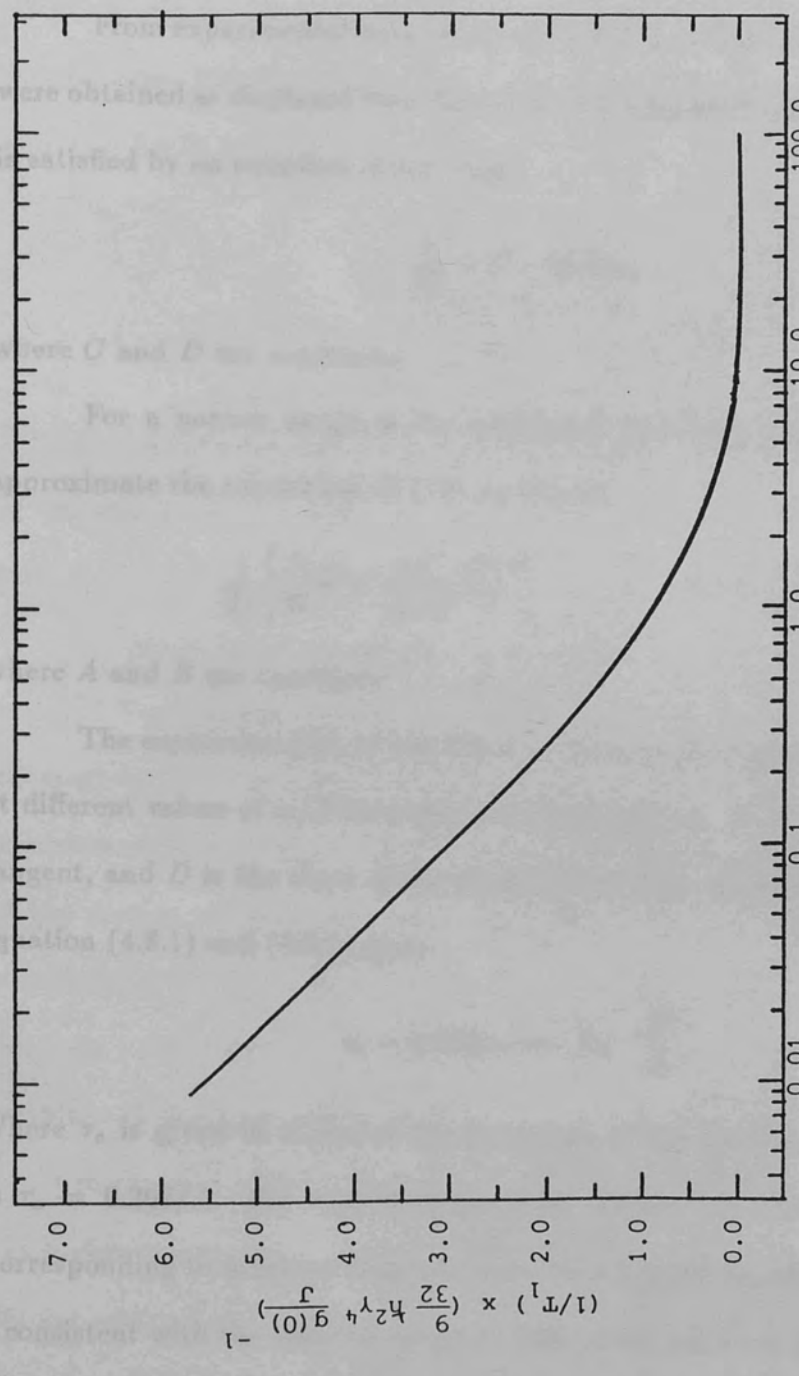

Figure 4.8.1

The Universal Curve as obtained by Cowan et al (1987).

substituting for $J_n(\omega_0)$ and $j_n(\omega_0)$ [the F.T of $g_n(t)$, equation (2.6.13)] and for the orientation β by the value 90°; a theoretical plot (Cowan et al 1987) for the change of $1/T_1$ with ω/J was produced as shown in figure (4.8.1).

From experimental data, $1/T_1$ was plotted versus $\ln\omega$ and straight lines were obtained as displayed from figure (4.5.4) to figure (4.5.9). This dependence is satisfied by an equation of the form,

$$\frac{1}{T_1} = C - D\, ln\omega_0 \tag{4.8.1}$$

where C and D are constants.

For a narrow range of the calculated frequency dependence, one can approximate the expression of $1/T_1$ as follows:

$$\frac{1}{T_1}\left[\frac{9}{32}\hbar^2\gamma^4\frac{{\mu_0}^2}{(4\pi)^2}\frac{g(0)}{J}\right]^{-1} = A - B\ln\left(\frac{\omega_0}{J}\right) \tag{4.8.2}$$

where A and B are constants.

The expression (4.8.1) was fitted to the curve's tangents of figure (4.8.1) at different values of ω/J in a self consistent manner. If B is the slope of the tangent, and D is the slope of the experimental line; a simple scaling between equation (4.8.1) and (4.8.2) gives:

$$\tau_c = 8.999 \times 10^{-10} x^{-3}\frac{D}{B} \tag{4.8.3}$$

Where τ_c is given in terms of the frequency of the motion J (Cowan 1980) as $\tau_c = 0.267/J$. For each coverage with certain D, different values of B (corresponding to different tangents) were tested, until the obtained value of τ_c is consistent with the selected tangent. This check has been made by choosing a value of ω in the middle of the frequency range ($\omega/2\pi = 5$ MHz), then $\omega\ \tau_c$ was computed and compared with the tangent point of the chosen tangent.

4.8.2 Employment of T_2:

It is believed that T_2 is affected, not only by the internuclear dipolar interaction, but also by the grafoil local fields which depend on the applied magnetic field. Therefore, it was essential to differentiate between both mechanisms. This has been done by writing the empirical frequency dependence equation for T_2 (Cowan et al 1987a),

$$\frac{1}{T_2} = A + B\omega_0 \tag{4.8.4}$$

Where the frequency independent part A is determined by the dipolar relaxation of ^{3}He atoms. B is thought to be the relaxation due to the motion in the grafoil local fields.

A plot of the slope B with the change of coverage is shown in figure (4.8.2). From which we notice that the slope increases with the increase of coverage to have its maximum value at registry, then starts to decrease to have approximately constant value. This could be explained by the slowing down of the motion of the spins where the spins are affected more strongly by the substrate local fields. Nevertheless, the substrate diamagnetic contribution is not fully understood yet. On the other hand, figure (4.8.3) demonstrates the variation of the intercept A as a function of coverage x. This intercept was found to increase smoothly with coverage at all densities except at registry. It has higher values due to the reduction of the mobility of the spins, where the dipolar interaction increases. Therefore, it seems to be reasonable to suggest that the net dipole-dipole contribution to T_2 could be extracted from the smooth baseline in this region corresponding to each coverage.

The analysis was made on the basis of the decomposition of the intercept

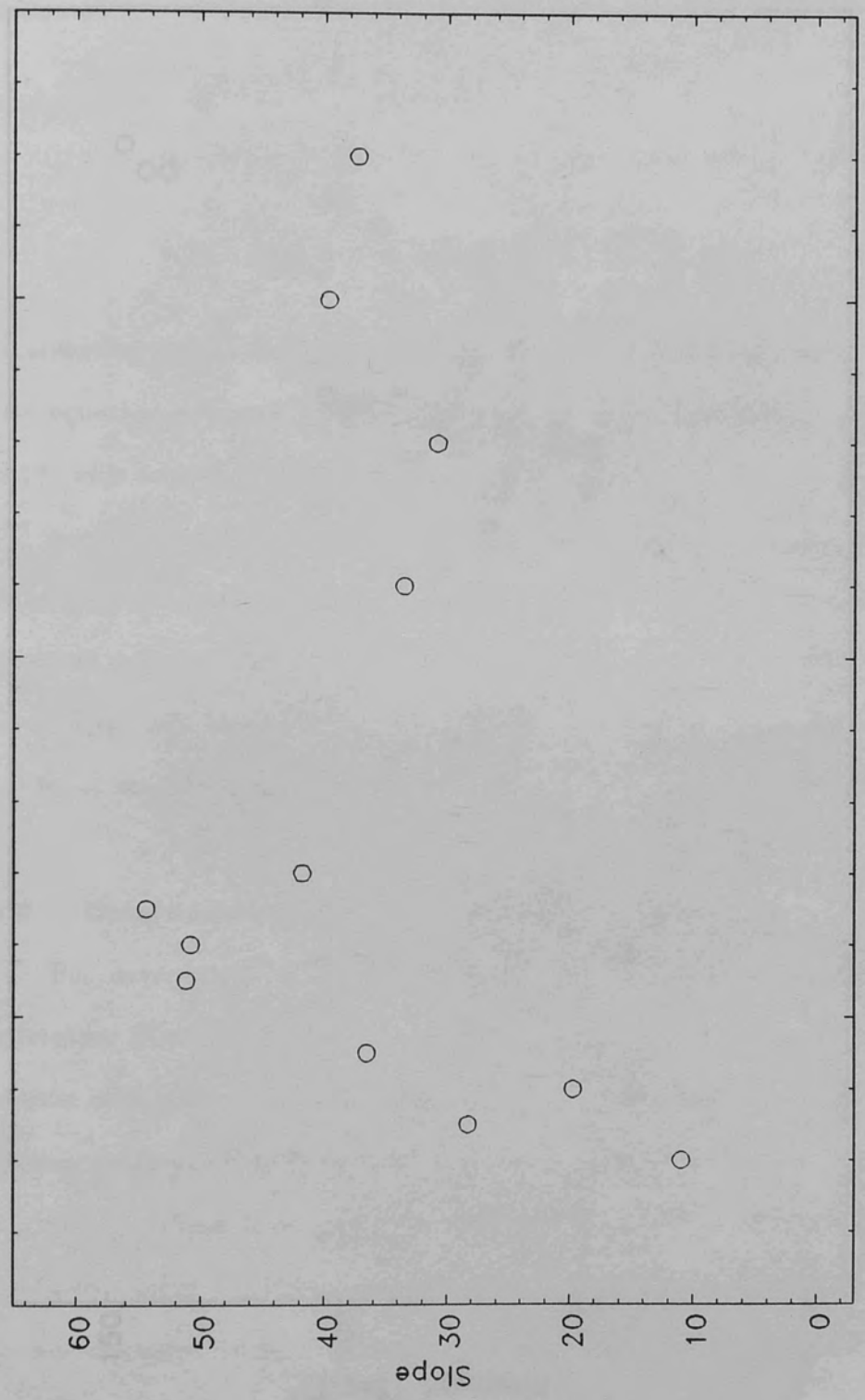

Figure 4.8.2

The slope of $(1/T_2$ vs. $f_o)$ as a function of coverage. T=1.2 K and β=90 deg.

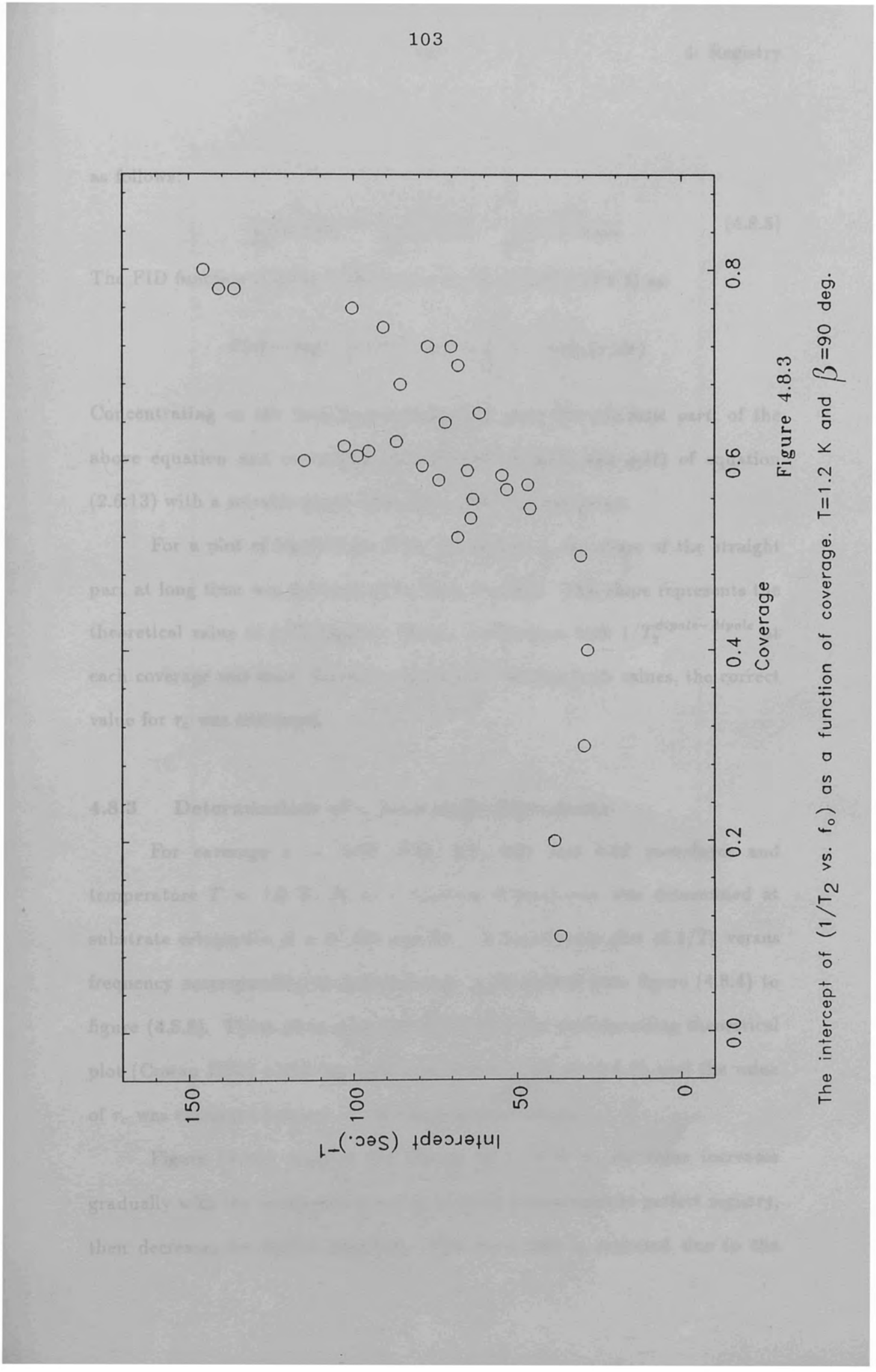

Figure 4.8.3

The intercept of $(1/T_2$ vs. $f_o)$ as a function of coverage. T=1.2 K and β=90 deg.

as follows:

$$\frac{1}{T_2^{freq.indep.}} = \frac{1}{T_2^{other\ contr.}} + \frac{1}{T_2^{dipole-dipole}} \tag{4.8.5}$$

The FID function (Cowan 1980) was given by equation (2.6.3) as:

$$F(t) = \exp(-t/T_2^{na}) \exp(-3 \int_0^t (t-\tau) G_0(\tau) d\tau)$$

Concentrating on the frequency independent part; *the adiabatic part*; of the above equation and evaluating the integrals of $g_0(t)$ and $g_2(t)$ of equation (2.6.13) with a suitable guess value of τ_c, $F(t)$ was evaluated.

For a plot of logarithmic $F(t)$ versus time t, the slope of the straight part at long time was determined for each coverage. This slope represents the theoretical value of $1/T_2$ dipolar. Hence, comparison with $1/T_2^{dipole-dipole}$ at each coverage was done. From the agreement between both values, the correct value for τ_c was evaluated.

4.8.3 Determination of τ_c from angle dependence:

For coverage $x = 0.58$, 0.59, 0.6, 0.61 and 0.62 monolayer and temperature $T = 1.2$ K, T_1 as a function of frequency was determined at substrate orientation $\beta = 0°, 45°$ and $90°$. A logarithmic plot of $1/T_1$ versus frequency corresponding to each coverage is illustrated from figure (4.8.4) to figure (4.8.8). These plots were compared with the corresponding theoretical plot (Cowan 1980) which has been reproduced in figure (2.6.1), and the value of τ_c was extracted for each of the mentioned coverages.

Figure (4.8.9) displays the change of τ_c with x, its value increases gradually with the increase of coverage to reach a maximum at perfect registry, then decreases for higher densities. This maximum is expected due to the

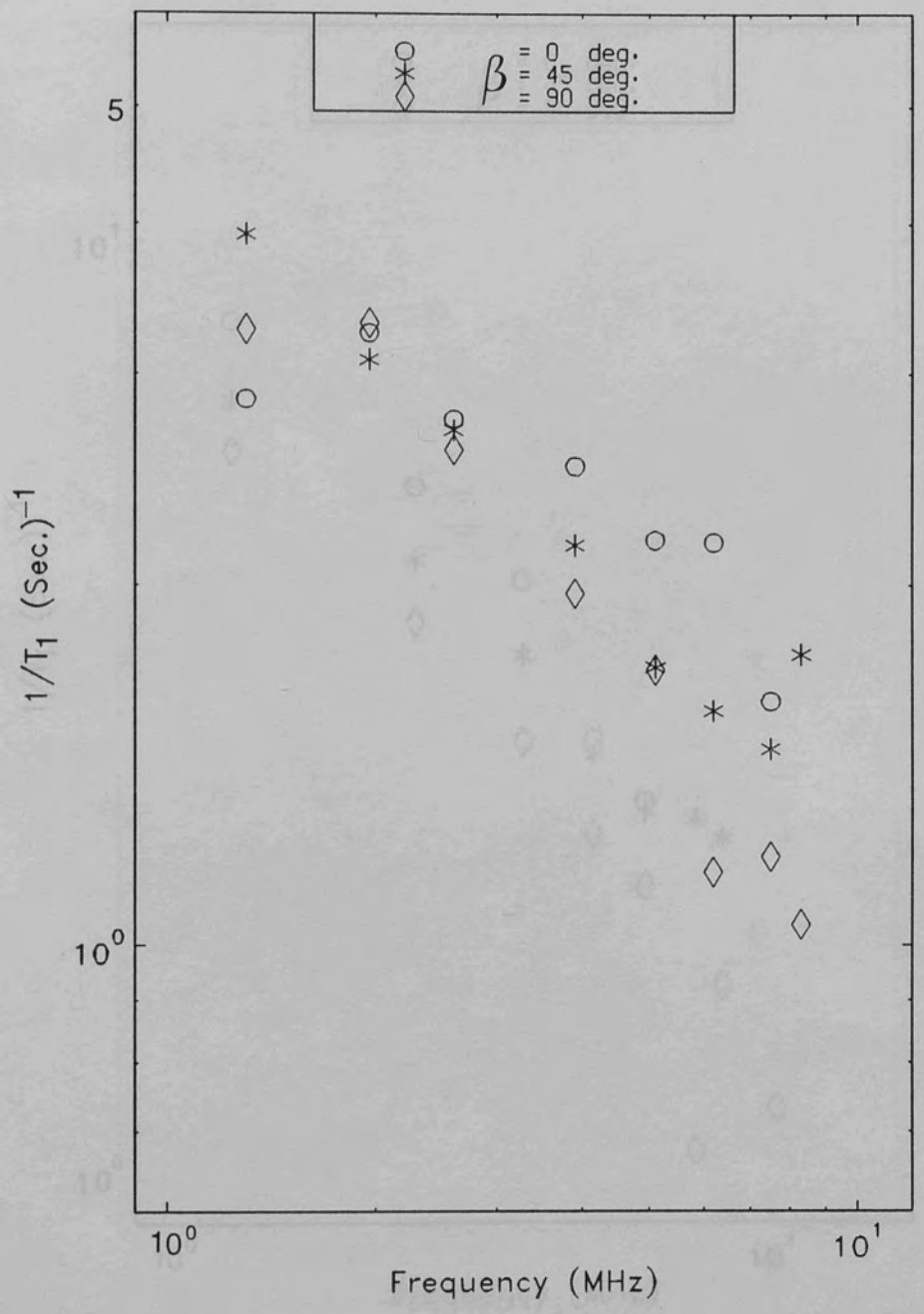

Figure 4.8.4

Spin–lattice relaxation rate as a function of Larmor frequency at different angles.
x=0.58 monolayer and T=1.2 K

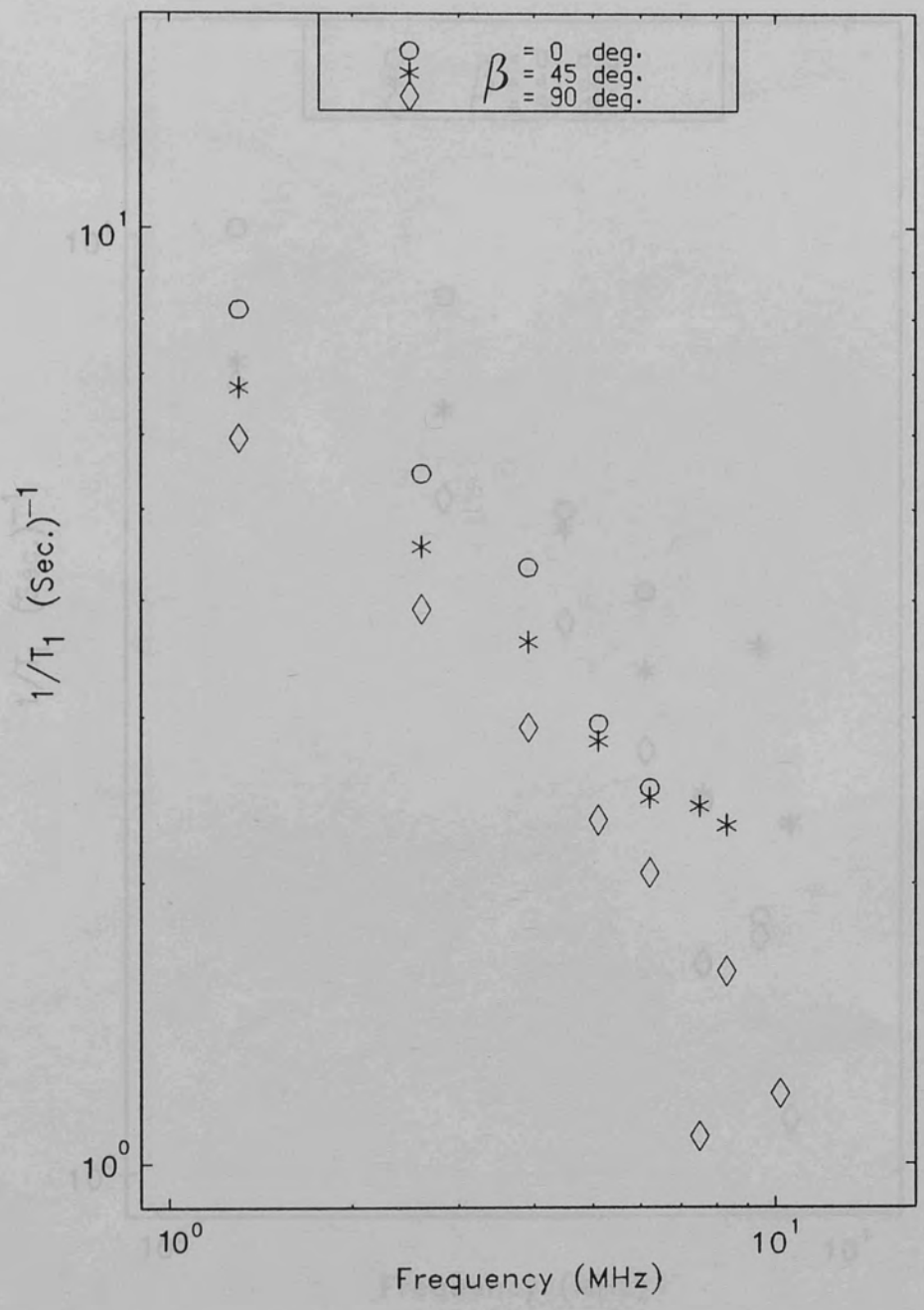

Figure 4.8.5

Spin–lattice relaxation rate as a function of Larmor frequency at different angles.
x=0.59 monolayer and T=1.2 K

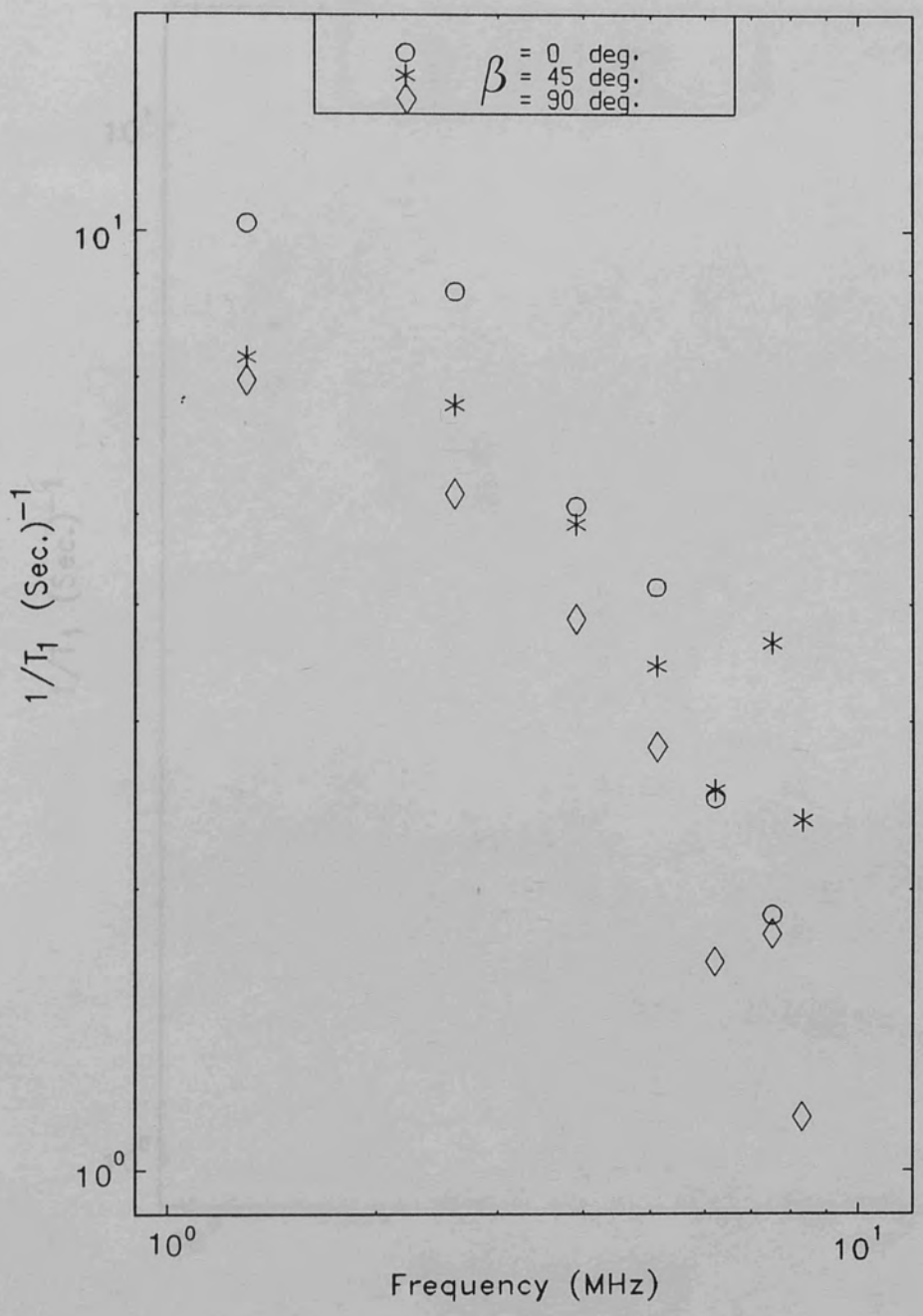

Figure 4.8.6

Spin–lattice relaxation rate as a function of Larmor frequency at different angles.
x=0.6 monolayer and T=1.2 K

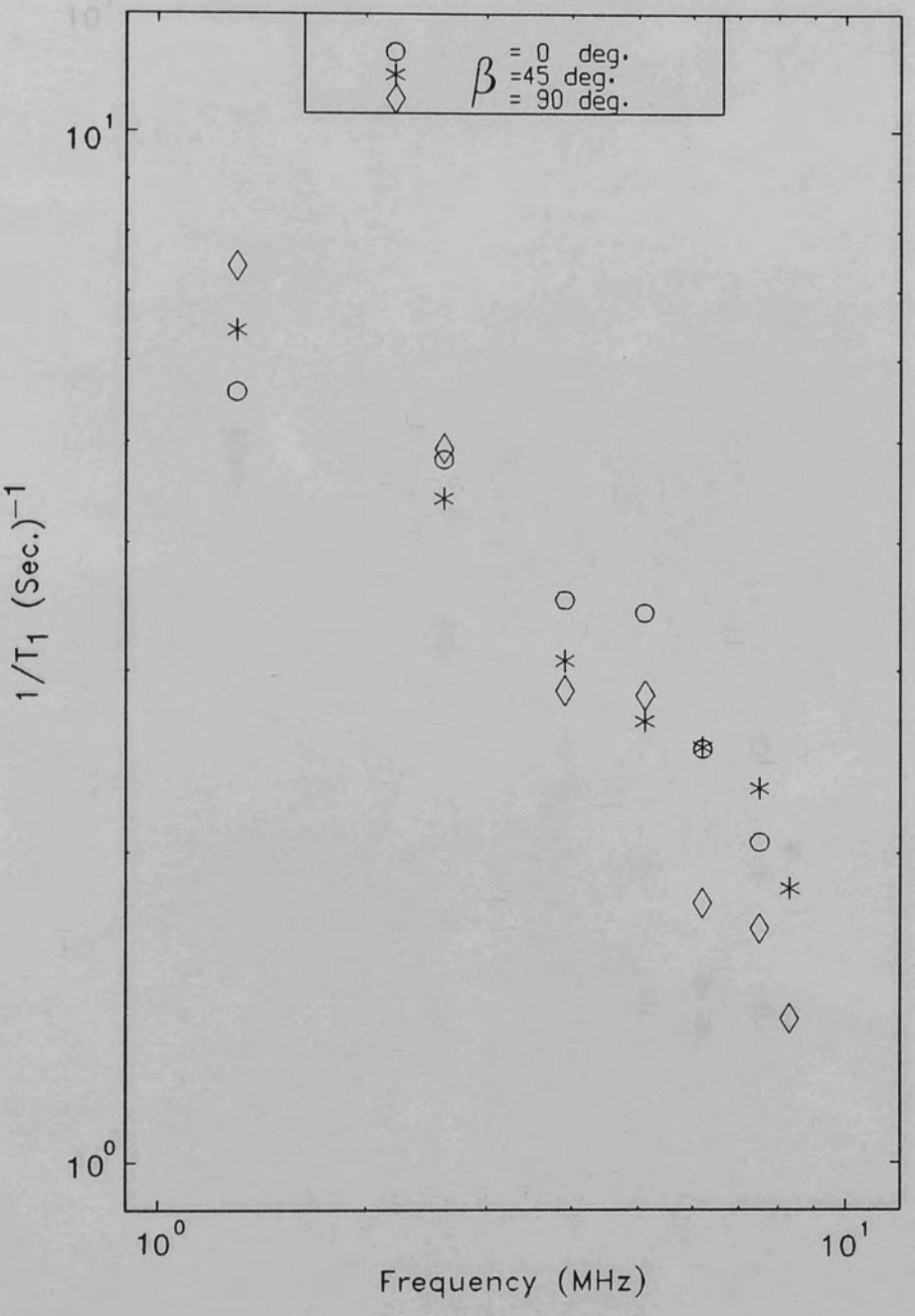

Figure 4.8.7

Spin–lattice relaxation rate as a function of Larmor frequency at different angles.

x=0.61 monolayer and T=1.2 K

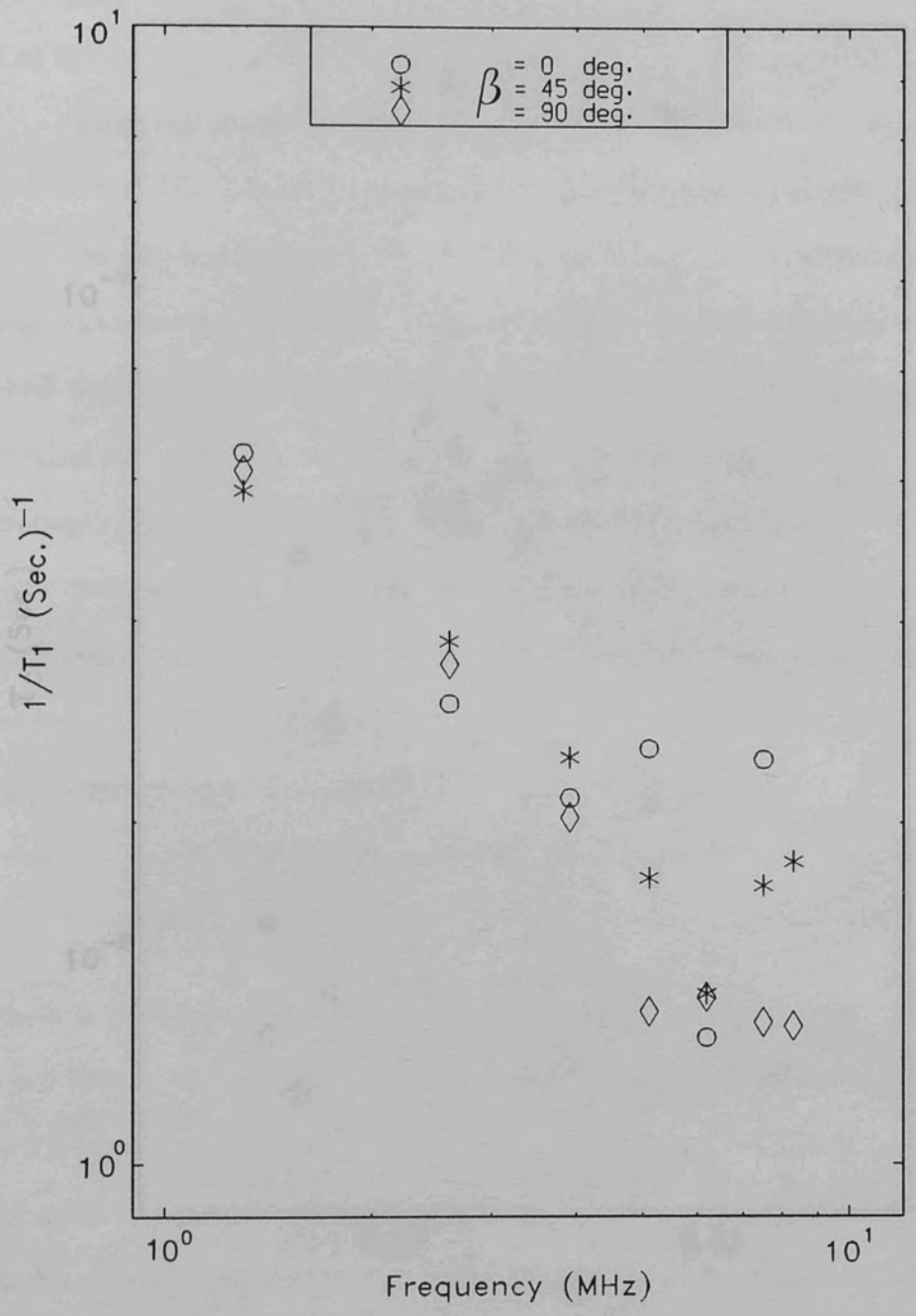

Figure 4.8.8

Spin–lattice relaxation rate as a function of Larmor frequency at different angles.
x=0.62 monolayer and T=1.2 K

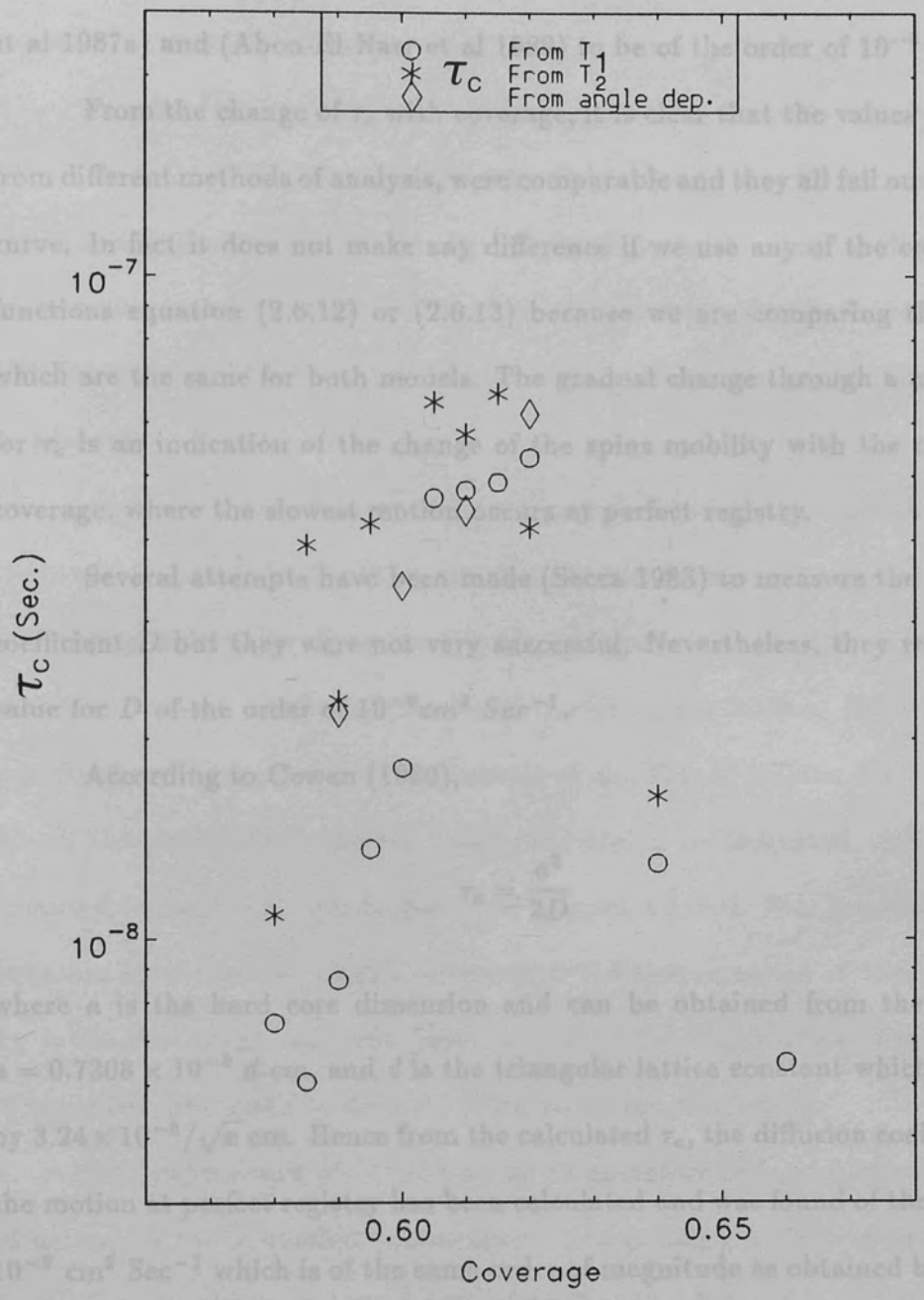

Figure 4.8.9

The correlation time as a function ofcoverage.

T=1.2 K and f_o=5.1 MHz.

slowing down of the motion at this region. The maximum τ_c was found (Cowan et al 1987a) and (Abou-El-Nasr et al 1988) to be of the order of 10^{-8} seconds.

From the change of τ_c with coverage, it is clear that the values obtained from different methods of analysis, were comparable and they all fall on the same curve. In fact it does not make any difference if we use any of the correlation functions equation (2.6.12) or (2.6.13) because we are comparing the slopes which are the same for both models. The gradual change through a maximum for τ_c is an indication of the change of the spins mobility with the change of coverage, where the slowest motion occurs at perfect registry.

Several attempts have been made (Secca 1983) to measure the diffusion coefficient D but they were not very successful. Nevertheless, they reported a value for D of the order of $10^{-9} cm^2\ Sec^{-1}$.

According to Cowan (1980),

$$\tau_c = \frac{a^2}{2D} \tag{4.8.6}$$

where a is the hard core dimension and can be obtained from the relation $a = 0.7308 \times 10^{-8}\ d$ cm, and d is the triangular lattice constant which is given by $3.24 \times 10^{-8}/\sqrt{x}$ cm. Hence from the calculated τ_c, the diffusion coefficient of the motion at perfect registry has been calculated and was found of the order of 10^{-9} cm^2 Sec^{-1} which is of the same order of magnitude as obtained by Sussex group (Secca 1983), and one order smaller than that obtained in Tokyo (Sato and Sugawara 1980).

4.9 The Activation Energy:

If the activation energy of the atom is given by E_a, then $E_a = E_f + E_m$ (Sullivan et al 1975), where E_f is the formation energy of vacancies and E_m

is the migration energy necessary to overcome the potential barrier due to repulsion between the ^{3}He atoms.

In solid ^{3}He, motion is thought to be quantum tunneling (Sullivan et al 1975), then $E_m = 0$. Assuming the same behaviour is true for two dimensions (Sato and Sugawara 1980), then E_a will be given by E_f only. A direct result of vacancies is the modulation of the internuclear magnetic dipolar interactions (Sullivan et al 1975). Therefore, the mobility of vacancies implies the mobility of adatoms.

At the registered phase, it is assumed that two types of vacancies exist (Sato and Sugawara 1980). First; the ground-state vacancy corresponding to the unoccupied sites naturally present in the triangular lattice. Second; thermally activated vacancy at the lattice site of the triangular lattice. But, at *perfect registry* there is no ground state vacancies at all. This is because the ^{3}He atoms fill all the preferable vacancies. Also, the thermally activated vacancies are expected to be zero at zero K (Sato and Sugawara 1980). This is a result of the equation $x_v = \exp(-E_f/k_BT)$, where x_v is the concentration of vacancies and k_B is the Boltzmann constant. However, at 1.2 K an estimation of the density of vacancies was found to be 4.2% (Sato and Sugawara 1980).

The dependence of T_1 and T_2 on temperature rate §4.6 was employed to determine the activation temperature corresponding to each coverage. The slope of the line at the middle range where $2 > T < 3$ was determined and was substituted in the Arrhenius law.

A plot of this activation temperature E_a/k_B versus x was illustrated in figure (4.9.1). The values of E_a/k_B obtained from T_1 data at $f_0 = 2.6$ and 5.1 MHz have a maximum around 8.8 K which is corresponding to perfect registry. While the lower value is for the data obtained from T_2 at the same frequencies.

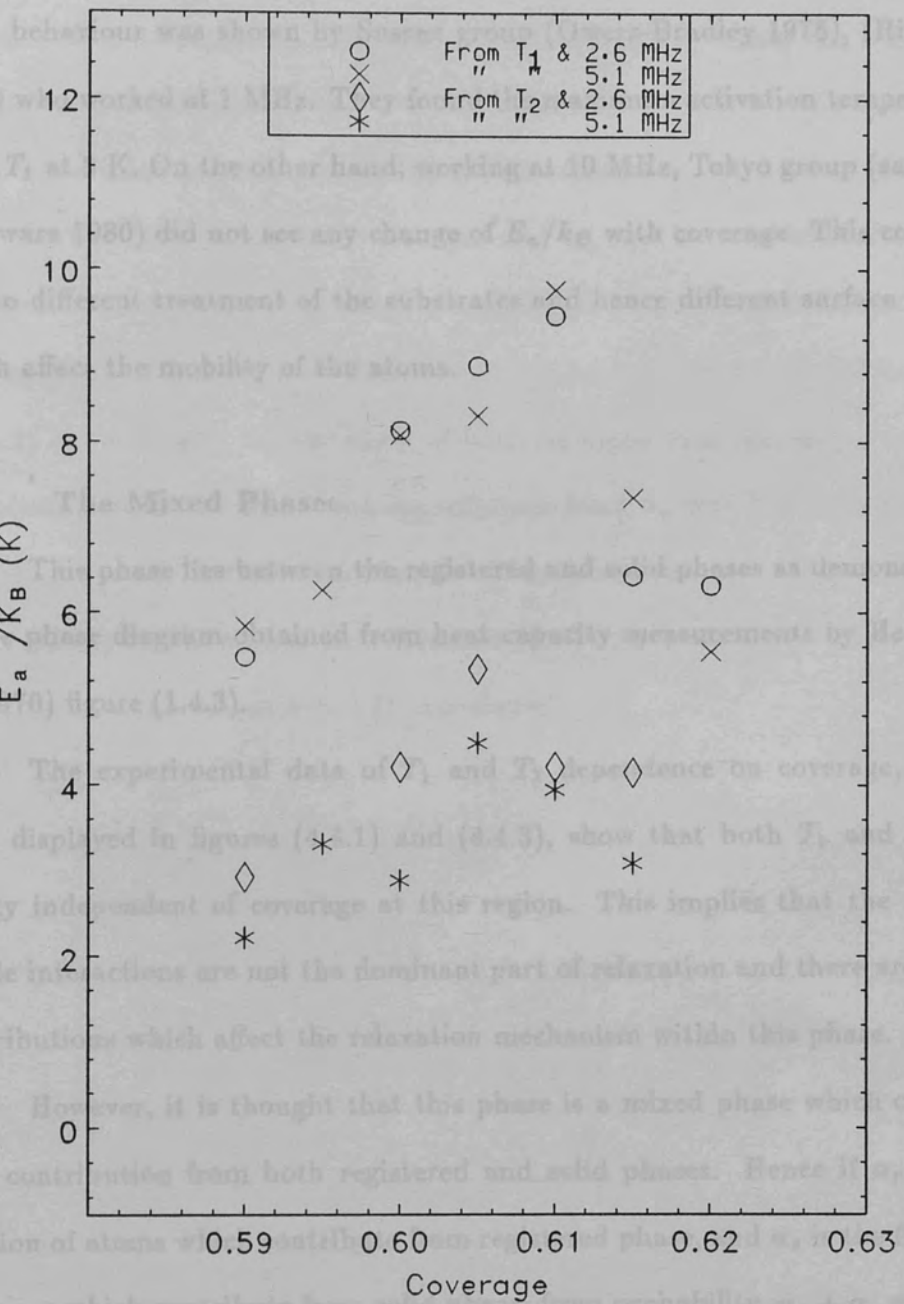

Figure 4.9.1

The activation temperature as a function of coverage. f_o=2.6 , 5.1 MHz and β=90 deg.

This difference is attributed to the effect of the substrate local fields on T_2. The same behaviour was shown by Sussex group (Owers-Bradley 1978), (Richards 1980) who worked at 1 MHz. They found the maximum activation temperature from T_1 at 8 K. On the other hand; working at 10 MHz, Tokyo group (sato and Sugawara 1980) did not see any change of E_a/k_B with coverage. This could be due to different treatment of the substrates and hence different surface nature which affect the mobility of the atoms.

4.10 The Mixed Phase:

This phase lies between the registered and solid phases as demonstrated in the phase diagram obtained from heat capacity measurements by Hering et al (1976) figure (1.4.3).

The experimental data of T_1 and T_2 dependence on coverage, which were displayed in figures (4.4.1) and (4.4.3), show that both T_1 and T_2 are nearly independent of coverage at this region. This implies that the dipole-dipole interactions are not the dominant part of relaxation and there are other contributions which affect the relaxation mechanism within this phase.

However, it is thought that this phase is a mixed phase which consists of a contribution from both registered and solid phases. Hence if α_r is the fraction of atoms which contribute from registered phase, and α_s is the fraction of atoms which contribute from solid phase; from probability, $\alpha_r + \alpha_s = 1$ and the following equations are satisfied for T_1 and T_2 respectively:

$$\frac{1}{T_1^{exper.}} = \frac{\alpha_r}{T_1^r} + \frac{\alpha_s}{T_1^s} \tag{4.10.1}$$

$$\frac{1}{T_2^{exper.}} = \frac{\alpha_r}{T_2^r} + \frac{\alpha_s}{T_2^s} \tag{4.10.2}$$

Where $T_1^{exper.}$ and $T_2^{exper.}$ are the experimental values of T_1 and T_2. While T_1^r,

T_1^s are the values of T_1 at registry and solid respectively. T_2^r and T_2^s are the corresponding values of T_2. From $x = 0.66$ monolayer; where the registered phenomenon is dying away; to $x = 0.72$ monolayer; where the solid phase starts to be formed; the behaviour of the atoms was studied.

It has been found that both α_r and α_s are independent of Larmor frequency for the region of coverage concerned. A plot of these fractions versus coverage as obtained from T_1 data was shown in figure (4.10.1). While figure (4.10.2) demonstrates the variation of both fractions with increasing coverage as obtained from T_2. Maximum contribution from α_r was found at $x = 0.66$ monolayer, which decreases gradually to reach zero at $x = 0.72$ monolayer. While as expected, α_s has zero value at $x = 0.66$ monolayer and increases gradually to reach one at $x = 0.72$ monolayer.

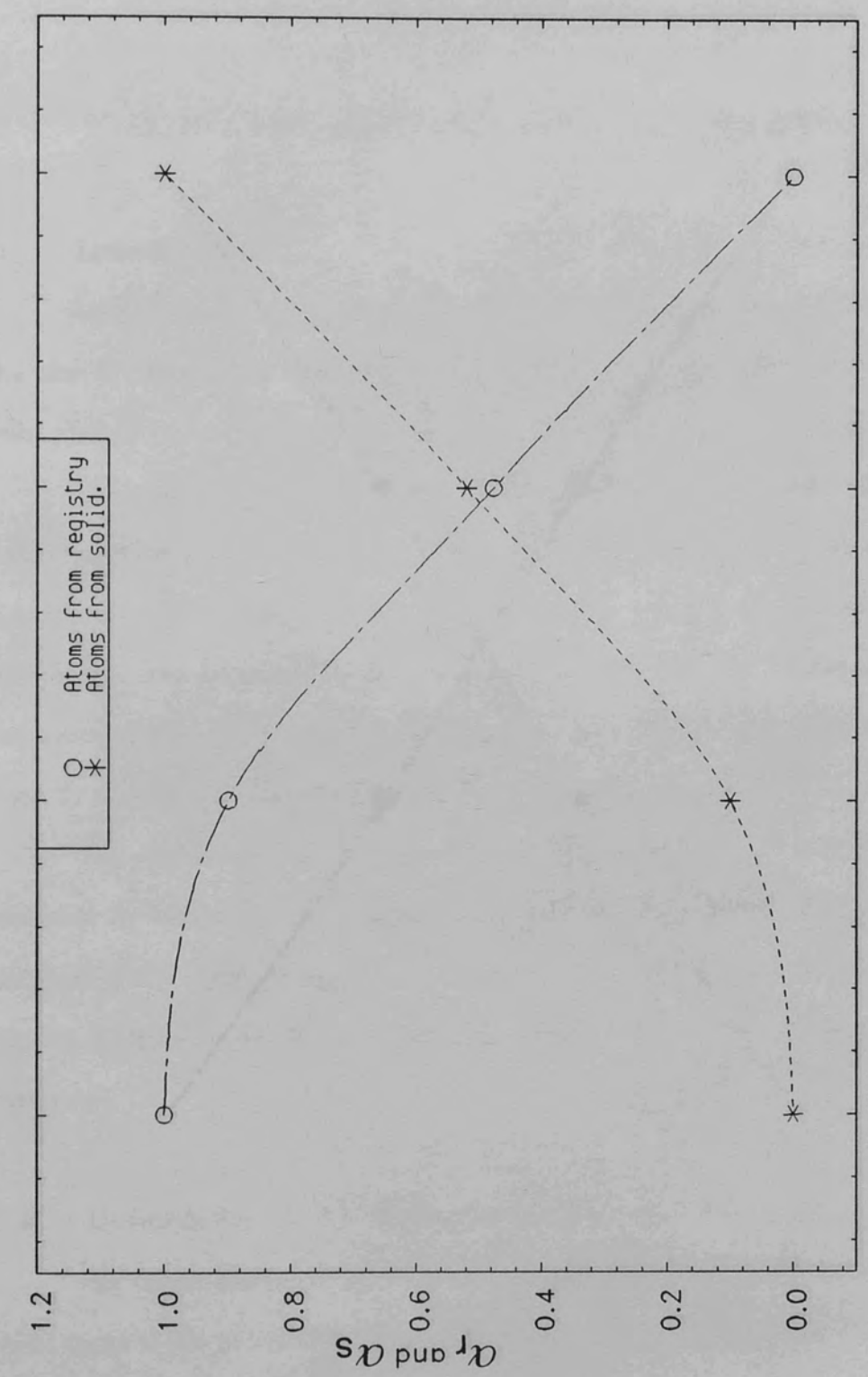

Figure 4.10.1

Fractions of atoms at registry and solid as obtained from T_1. f_o =5.1 MHz, T=1.2 K and $\beta = 90^\circ$

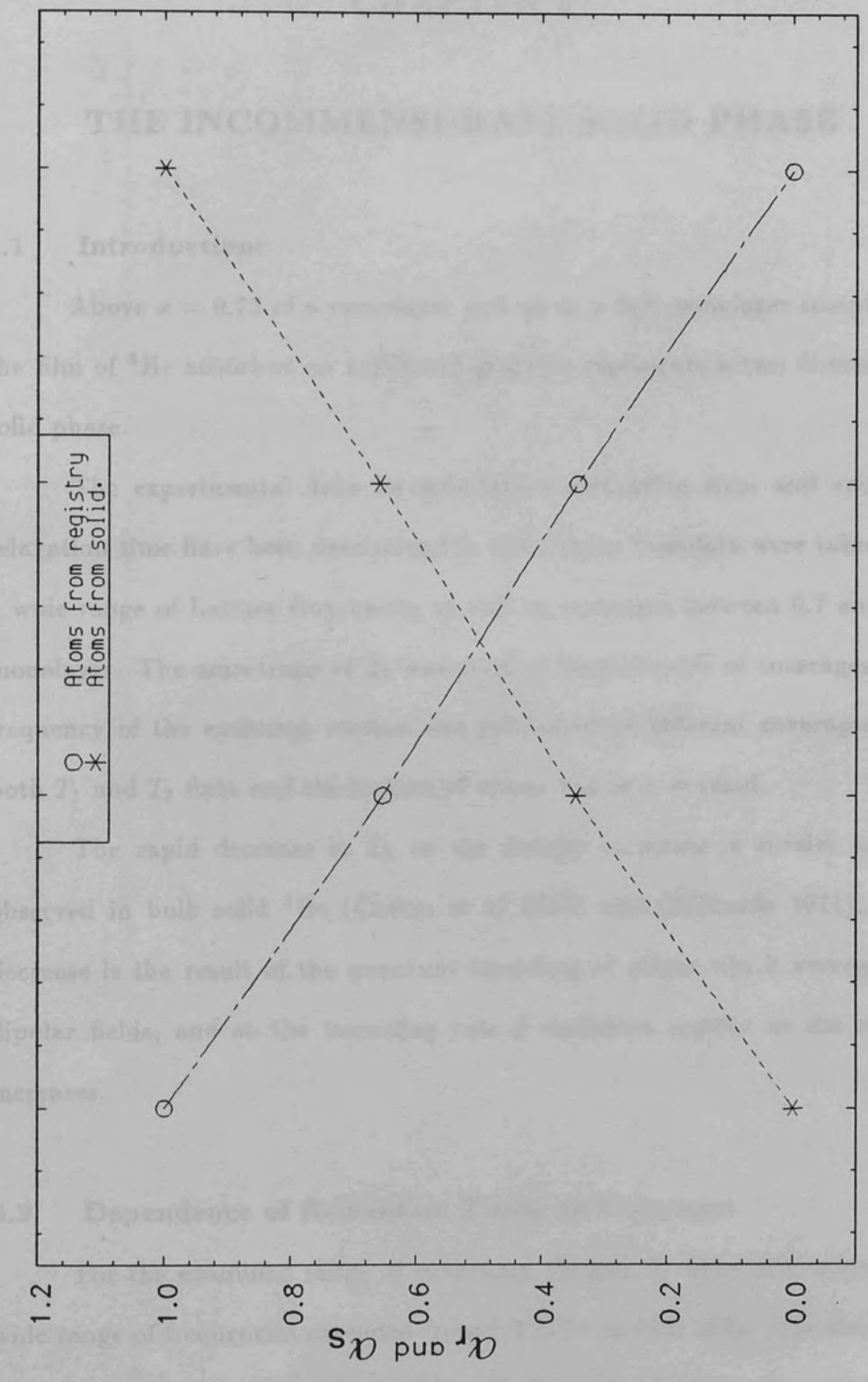

Figure 4.10.2

Fractions of atoms at registry and solid as obtained from T_2. f_o=5.1 MHz, T=1.2 K and $\beta = 90^\circ$

CHAPTER 5

THE INCOMMENSURATE SOLID PHASE

5.1 Introduction:

Above $x = 0.72$ of a monolayer and up to a full monolayer completion, the film of ^{3}He adsorbed on exfoliated graphite represents a two dimensional solid phase.

The experimental data for spin-lattice relaxation time and spin-spin relaxation time have been determined in this phase. The data were taken over a wide range of Larmor frequencies as well as coverages between 0.7 and 1.02 monolayer. The anisotropy of T_2 was studied for a number of coverages. The frequency of the exchange motion was calculated at different coverages from both T_1 and T_2 data and the motion of atoms has been studied.

The rapid decrease in T_2 as the density increases is similar to that observed in bulk solid ^{3}He (Cowan et al 1977) and (Richards 1971). This decrease is the result of the quantum tunneling of atoms which averages the dipolar fields, and so the tunneling rate J decreases rapidly as the density increases.

5.2 Dependence of Relaxation Times on Coverage:

For the examined range of coverages, T_1 and T_2 were determined in a wide range of frequencies extended from 1.3 MHz to 10.2 MHz. The data were taken at temperature of 1.2 and 4.2 K and the angle of orientation was 90°.

As illustrated in figure (5.2.1), for Larmor frequency $f_0 = 5.1$ MHz, T_1

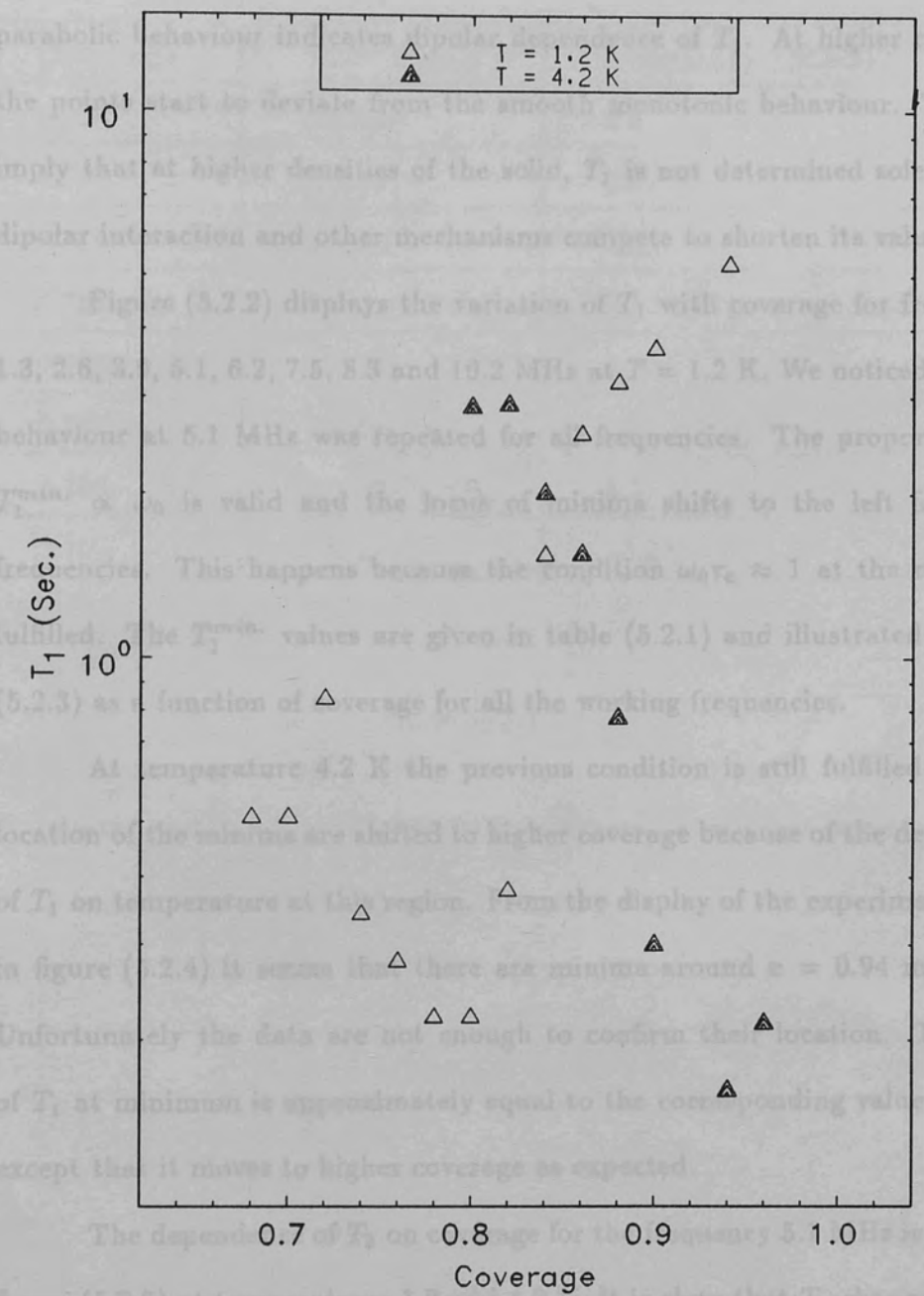

Figure 5.2.1

Spin–lattice relaxation time as a function of coverage. f_0=5.1 MHz and β=90 deg.

decreases with coverage to reach a minimum at $x \approx 0.79$ monolayer. This parabolic behaviour indicates dipolar dependence of T_1. At higher coverages, the points start to deviate from the smooth monotonic behaviour. This may imply that at higher densities of the solid, T_1 is not determined solely by the dipolar interaction and other mechanisms compete to shorten its value.

Figure (5.2.2) displays the variation of T_1 with coverage for frequencies 1.3, 2.6, 3.9, 5.1, 6.2, 7.5, 8.3 and 10.2 MHz at $T = 1.2$ K. We noticed that the behaviour at 5.1 MHz was repeated for all frequencies. The proportionality: $T_1^{min.} \propto \omega_0$ is valid and the locus of minima shifts to the left for higher frequencies. This happens because the condition $\omega_0 \tau_c \approx 1$ at the minima is fulfilled. The $T_1^{min.}$ values are given in table (5.2.1) and illustrated in figure (5.2.3) as a function of coverage for all the working frequencies.

At temperature 4.2 K the previous condition is still fulfilled, but the location of the minima are shifted to higher coverage because of the dependence of T_1 on temperature at this region. From the display of the experimental data in figure (5.2.4) it seems that there are minima around $x = 0.94$ monolayer. Unfortunately the data are not enough to confirm their location. The value of T_1 at minimum is approximately equal to the corresponding value at 1.2 K except that it moves to higher coverage as expected.

The dependence of T_2 on coverage for the frequency 5.1 MHz is shown in figure (5.2.5) at temperatures 1.2 and 4.2 K. It is clear that T_2 changes rapidly with the increase of coverage at both temperatures to reach its shortest value of the order of magnitude of 10^{-1} mSec in the neighbourhood of monolayer completion. Above this coverage T_2 starts to increase due to the formation of the second layer, where the mobility of the atoms becomes bigger. On display in figure (5.2.6), T_2 as a function of coverage at frequencies 1.3 and 5.1 MHz. On

Coverage	$T_1^{min.}$ (Sec.)	Frequency (MHz)
0.818	0.0499	1.3
0.805	0.0856	2.6
0.789	0.1503	3.9
0.785	0.207	5.1
0.773	0.2711	6.2
0.7676	0.2797	7.5
0.766	0.3639	8.3
0.759	0.479	10.2

Table 5.2.1

T_1 minima as a function of coverage for different Larmor frequencies.

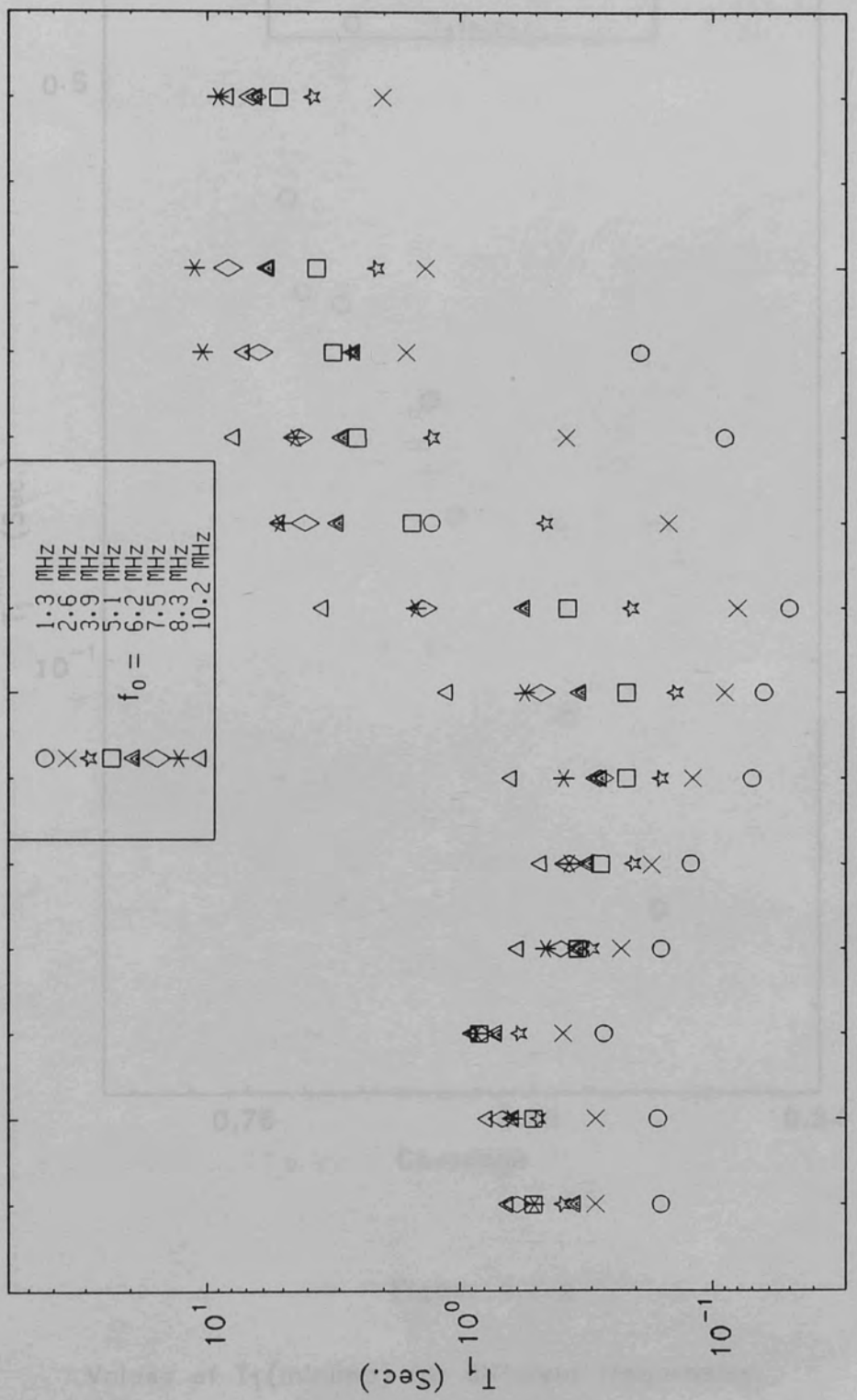

Figure 5.2.2

Spin–lattice relaxation time as a function of coverage. T=1.2 K and β=90 deg.

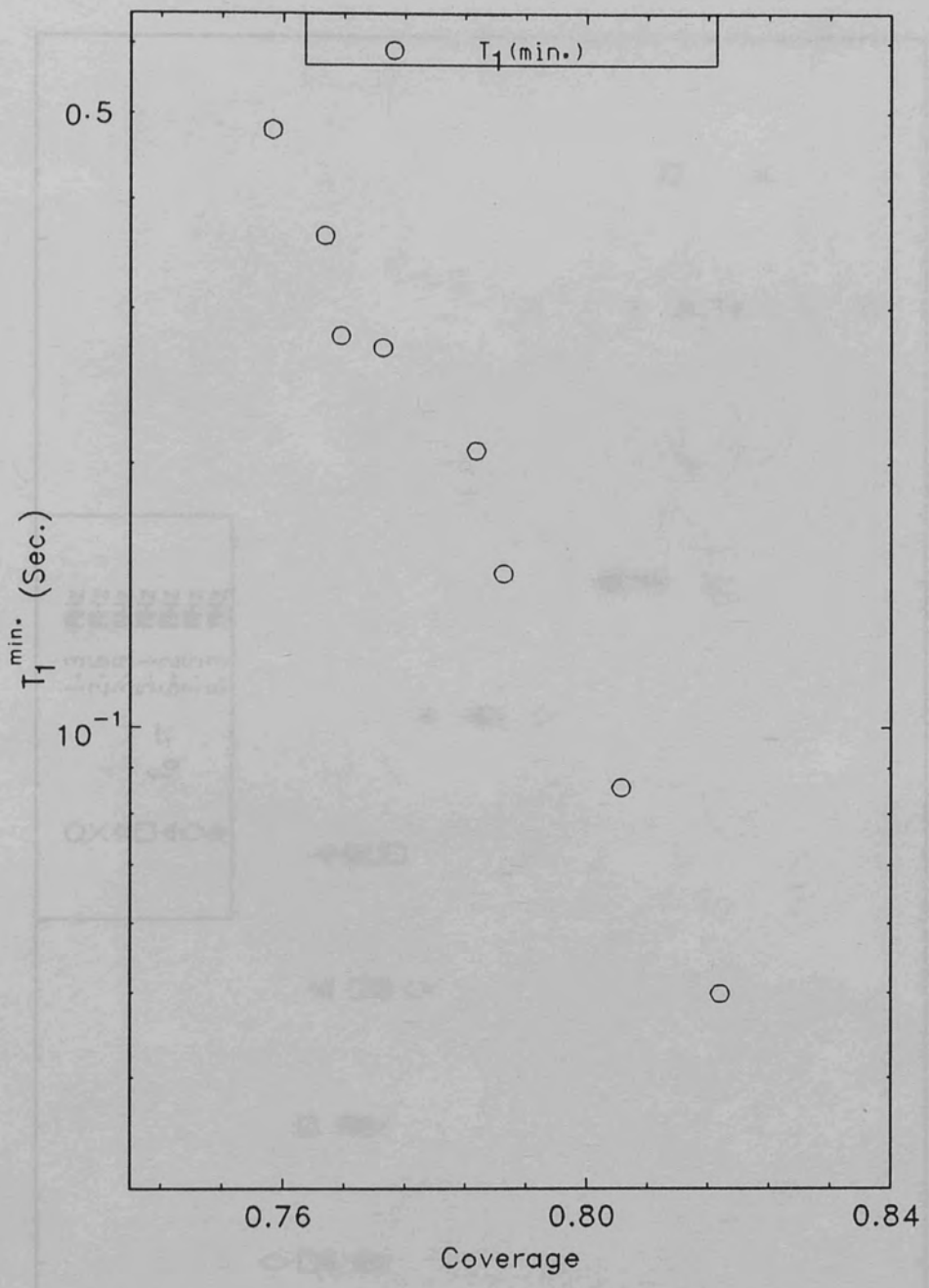

Figure 5.2.3

Values of T_1(minima) for different frequencies.

T=1.2 K and $\beta = 90^{\circ}$.

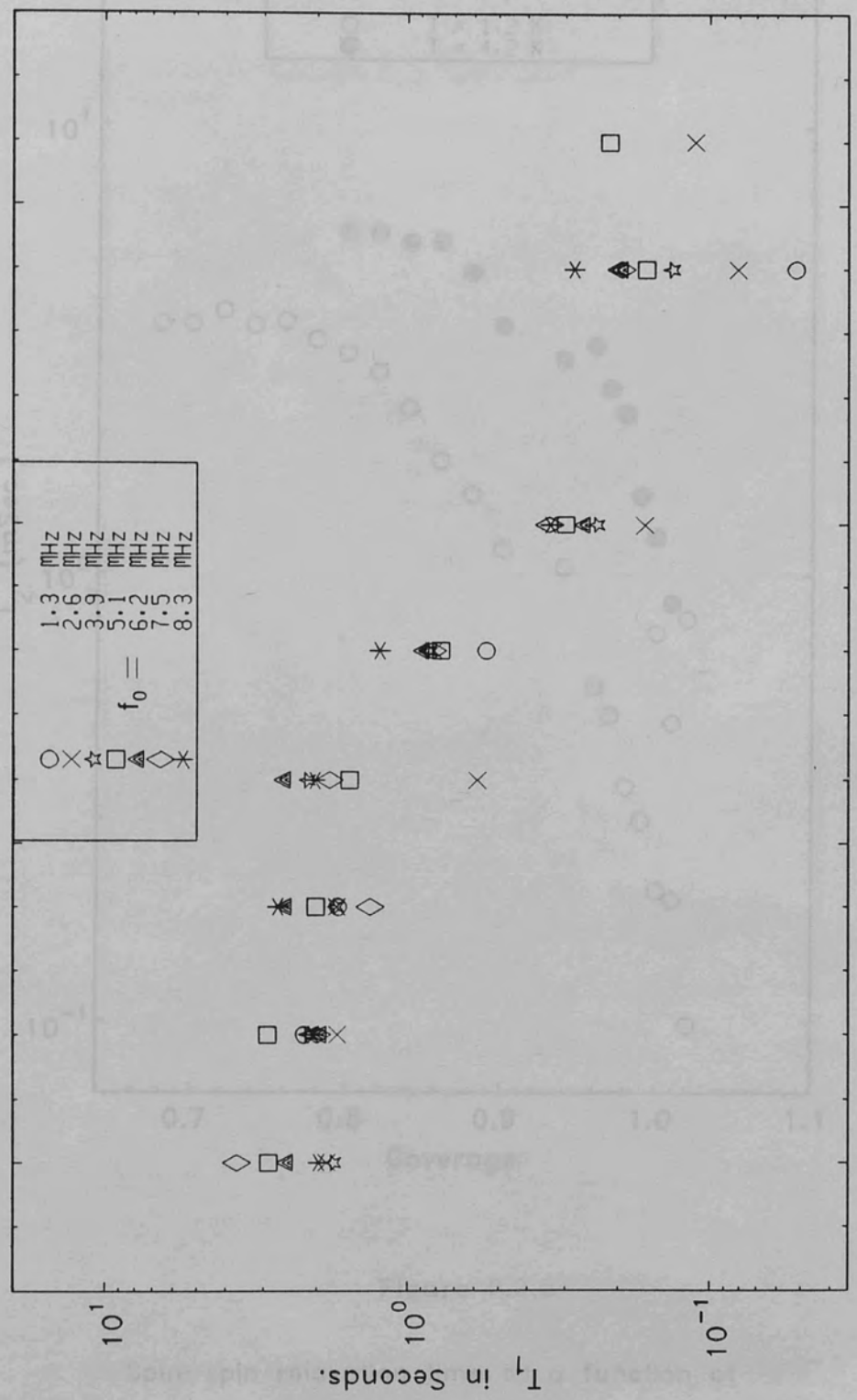

Figure 5.2.4

Spin-lattice relaxation time as a function of coverage. T=4.2 K and β=90 deg.

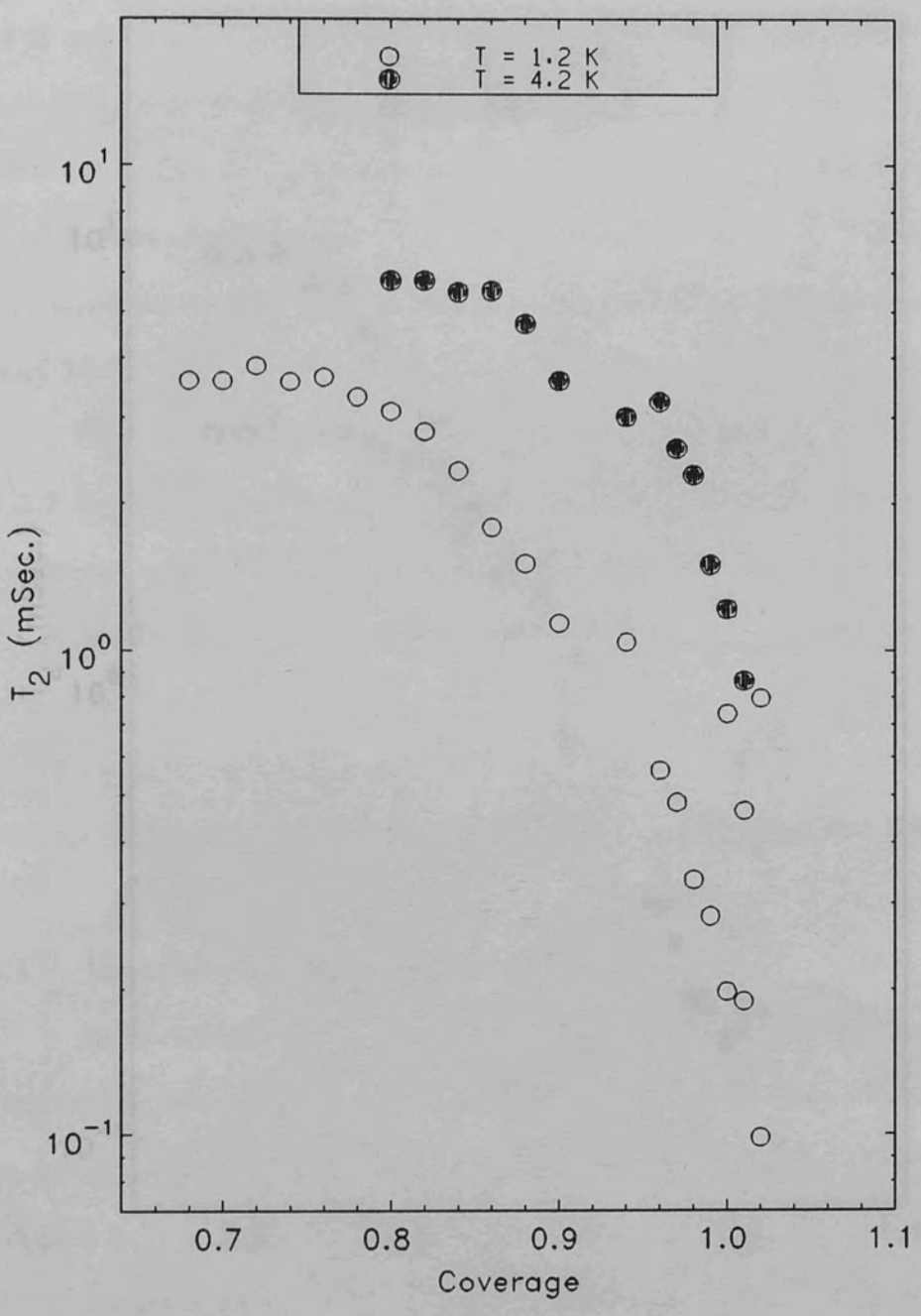

Figure 5.2.5

Spin–spin relaxation time as a function of coverage at f_o =5.1 MHz and β =90 deg.

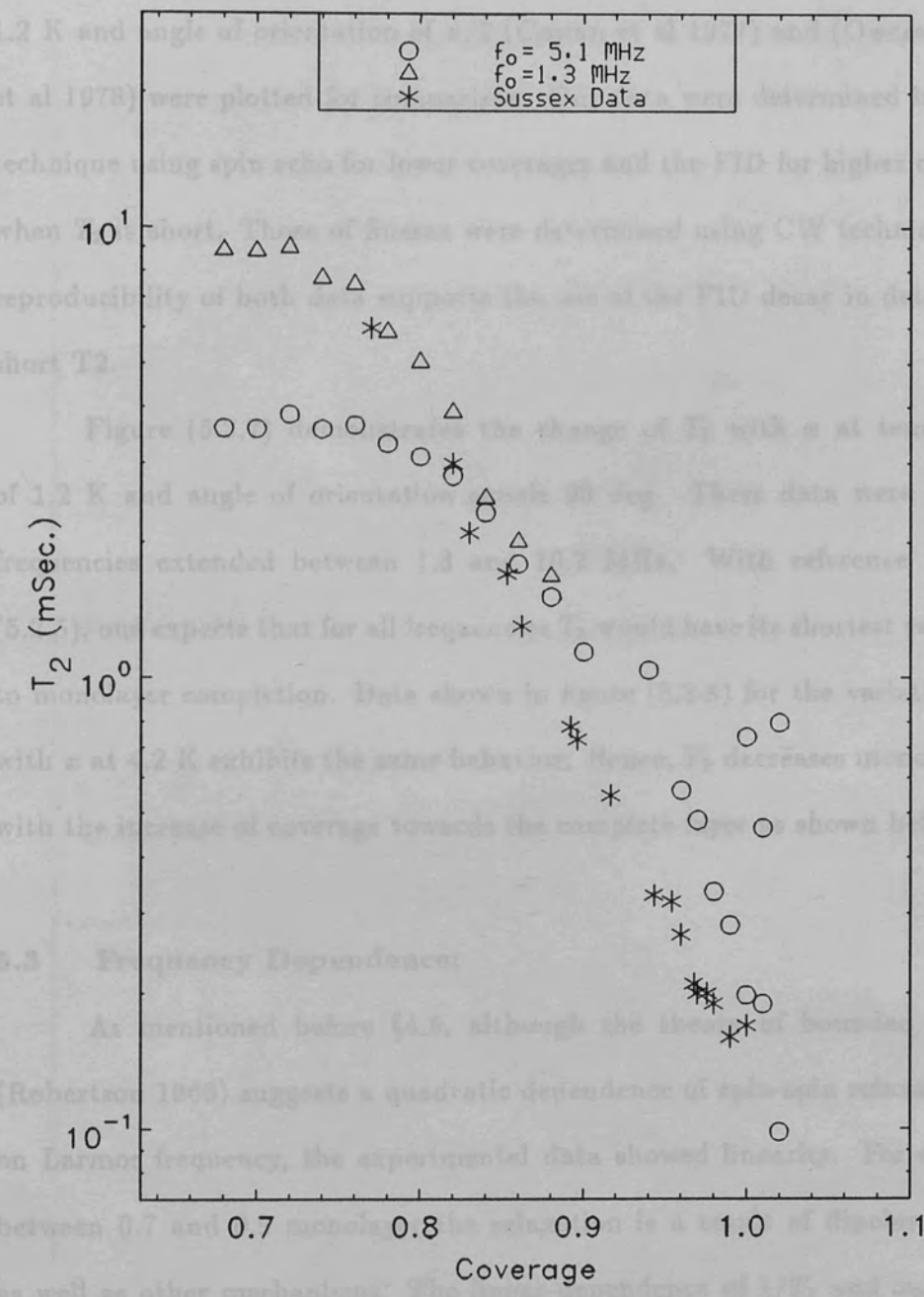

Figure 5.2.6

Comparison between T_2 taken at 1.3 and 5.1 MHz and T_2 taken at Sussex at 1 MHz. T=1.2 K and β=90 deg.

the same graph, T_2 data obtained by Sussex group at 1 MHz and temperature 1.2 K and angle of orientation of $\pi/2$ (Cowan et al 1977) and (Owers-Bradley et al 1978) were plotted for comparison. Our data were determined by pulsed technique using spin echo for lower coverages and the FID for higher coverages when T_2 is short. Those of Sussex were determined using CW technique. The reproducibility of both data supports the use of the FID decay in determining short T2.

Figure (5.2.7) demonstrates the change of T_2 with x at temperature of 1.2 K and angle of orientation equals 90 deg. These data were taken at frequencies extended between 1.3 and 10.2 MHz. With reference to figure (5.2.5), one expects that for all frequencies T_2 would have its shortest value close to monolayer completion. Data shown in figure (5.2.8) for the variation of T_2 with x at 4.2 K exhibits the same behavior. Hence, T_2 decreases monotonically with the increase of coverage towards the complete layer as shown before.

5.3 Frequency Dependence:

As mentioned before §4.5, although the theory of bounded diffusion (Robertson 1966) suggests a quadratic dependence of spin-spin relaxation rate on Larmor frequency, the experimental data showed linearity. For coverages between 0.7 and 0.9 monolayer the relaxation is a result of dipolar coupling as well as other mechanisms. The linear dependence of $1/T_2$ and ω_0 at these coverages for temperature 1.2 K and angle of rotation $\pi/2$ is illustrated in figures (5.3.1), (5.3.2), (5.3.3) and (5.3.4). Nevertheless, for higher coverages, the value of $1/T_2$ scattered as shown in figure (5.3.5) for $x = 0.94$ monolayer, so the relaxation is considered to be mainly dipolar. From figures (5.3.1) and (5.3.2), we notice that for lower densities of solid, T_2 does not change dramatically at

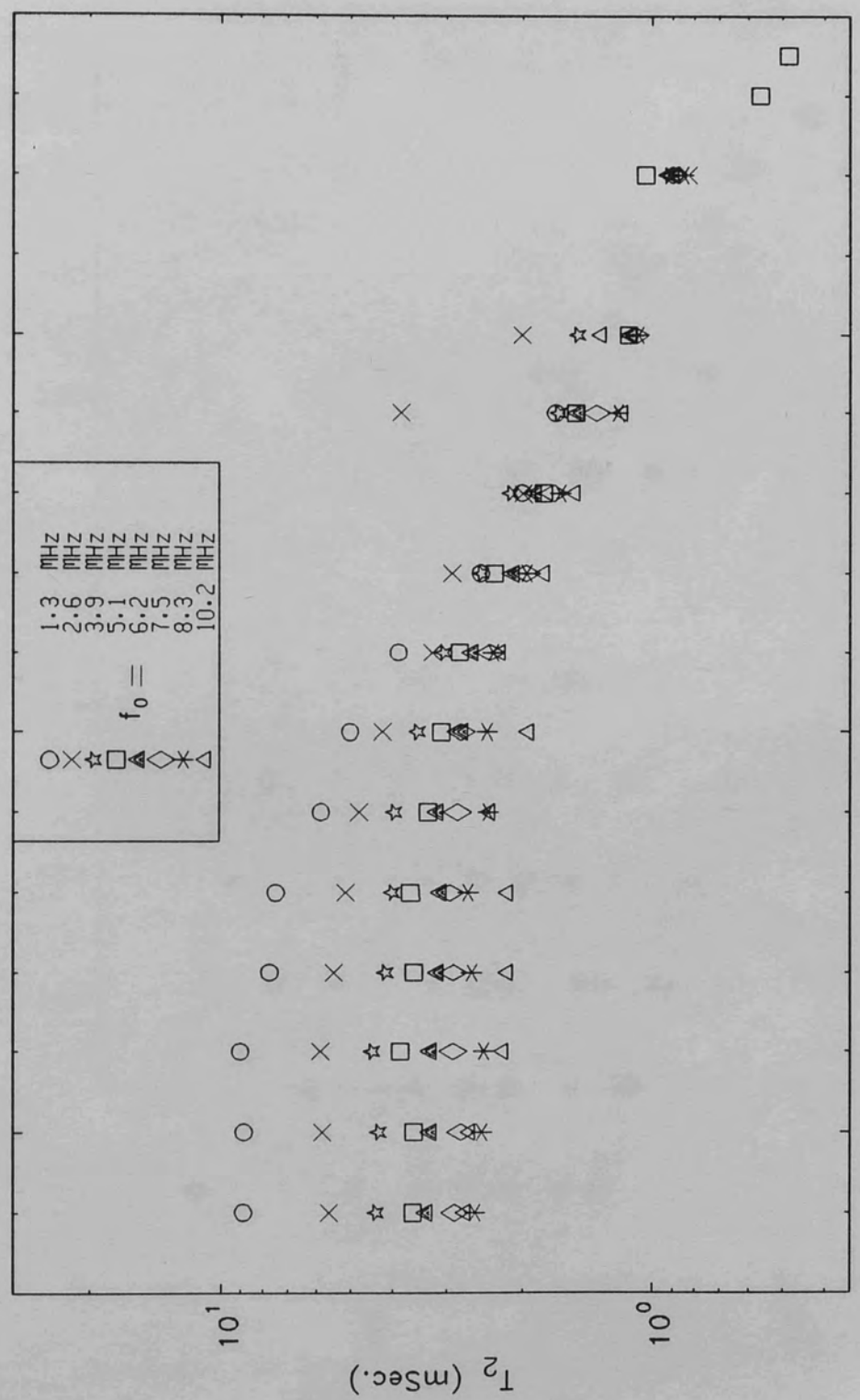

Figure 5.2.7

Spin-spin relaxation time as a function of coverage. T=1.2 K and β=90 deg.

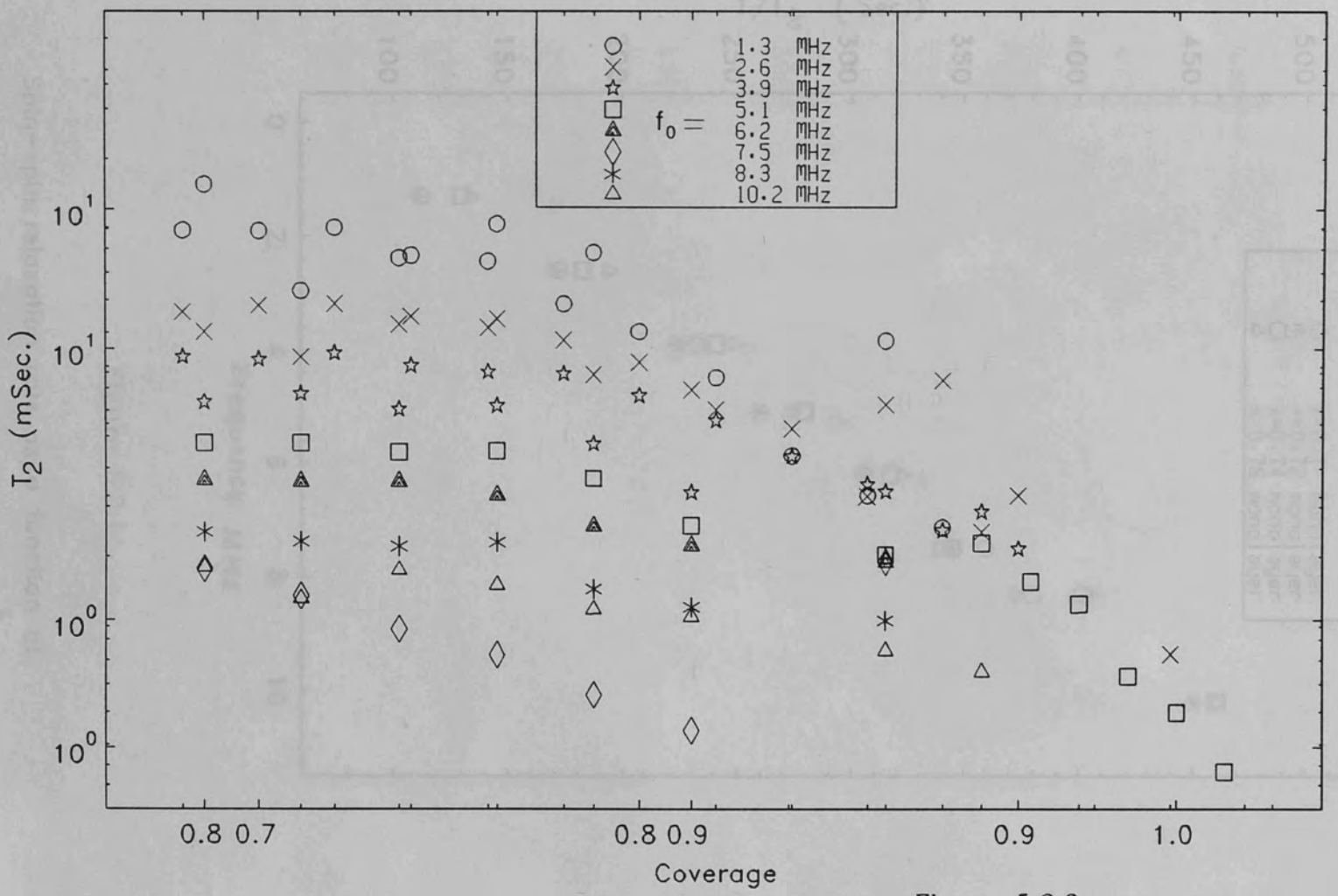

Figure 5.2.8

Spin–spin relaxation time as a function of coverage. T=4.2 K and β =90 deg.

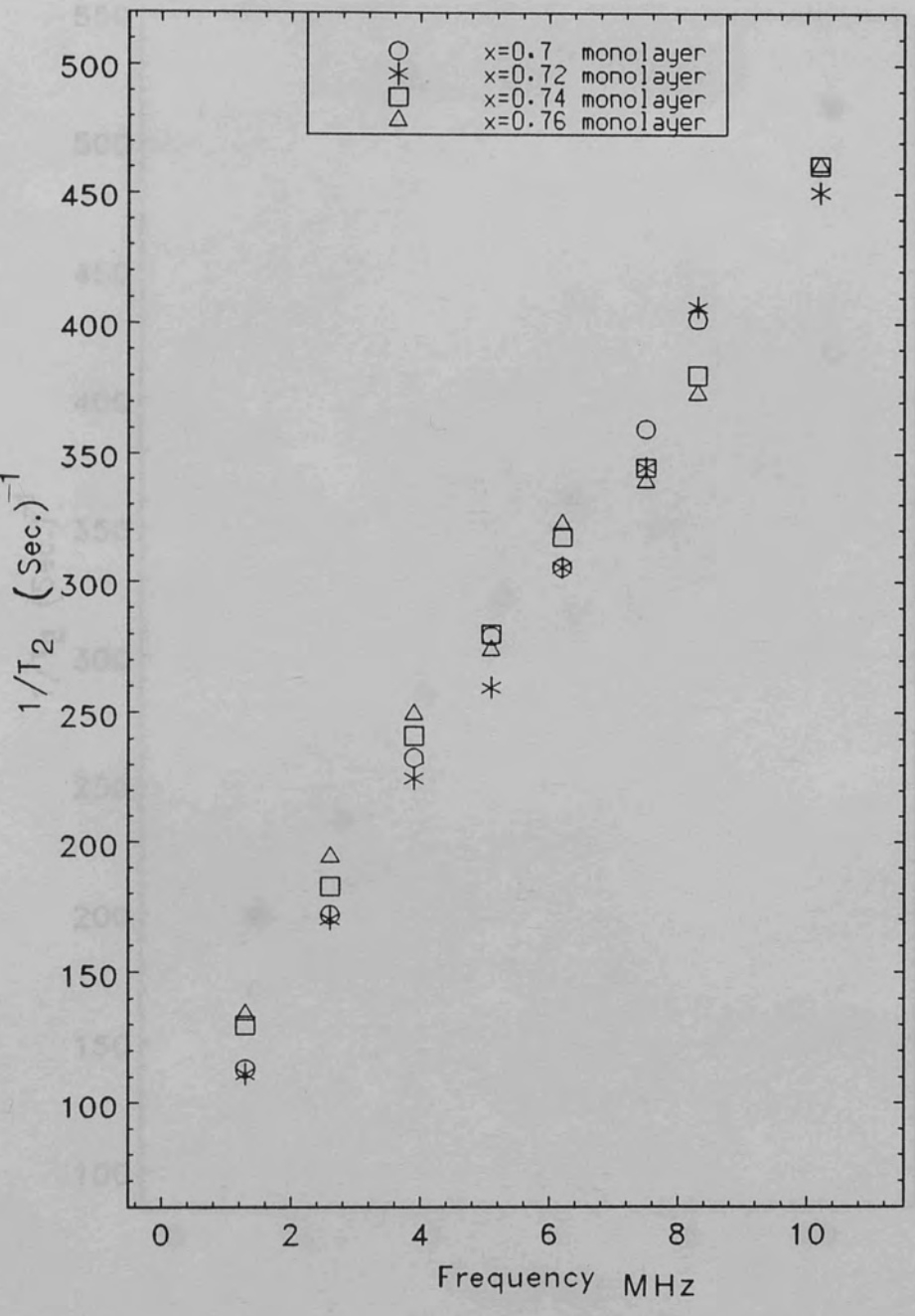

Figure 5.3.1

Spin–spin relaxation rate as a function of Larmor frequency. T=1.2 K and $\beta = 90^{\circ}$

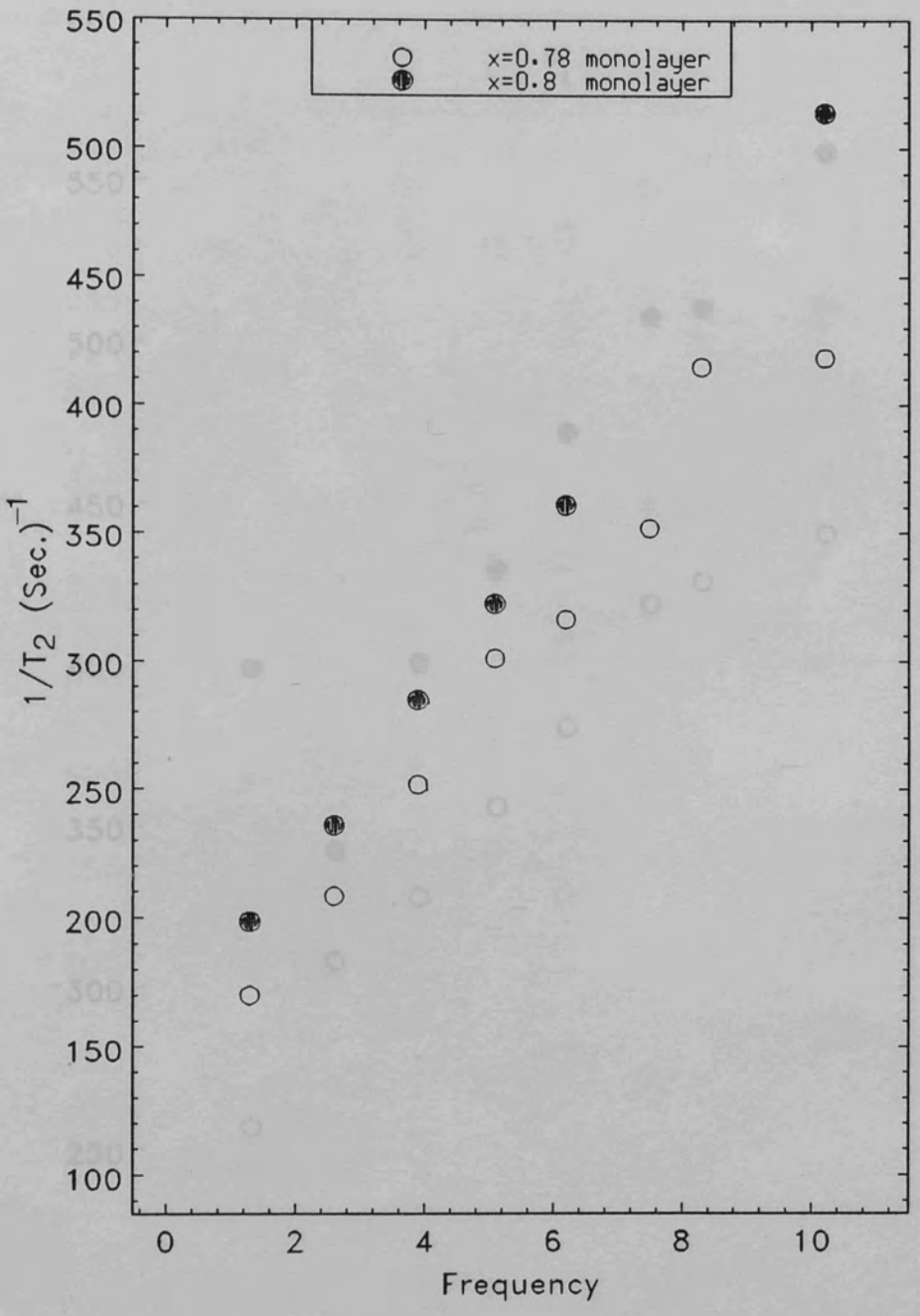

Figure 5.3.2

Spin-spin relaxation rate as a function of Larmor frequency. T=1.2 K and β=90°

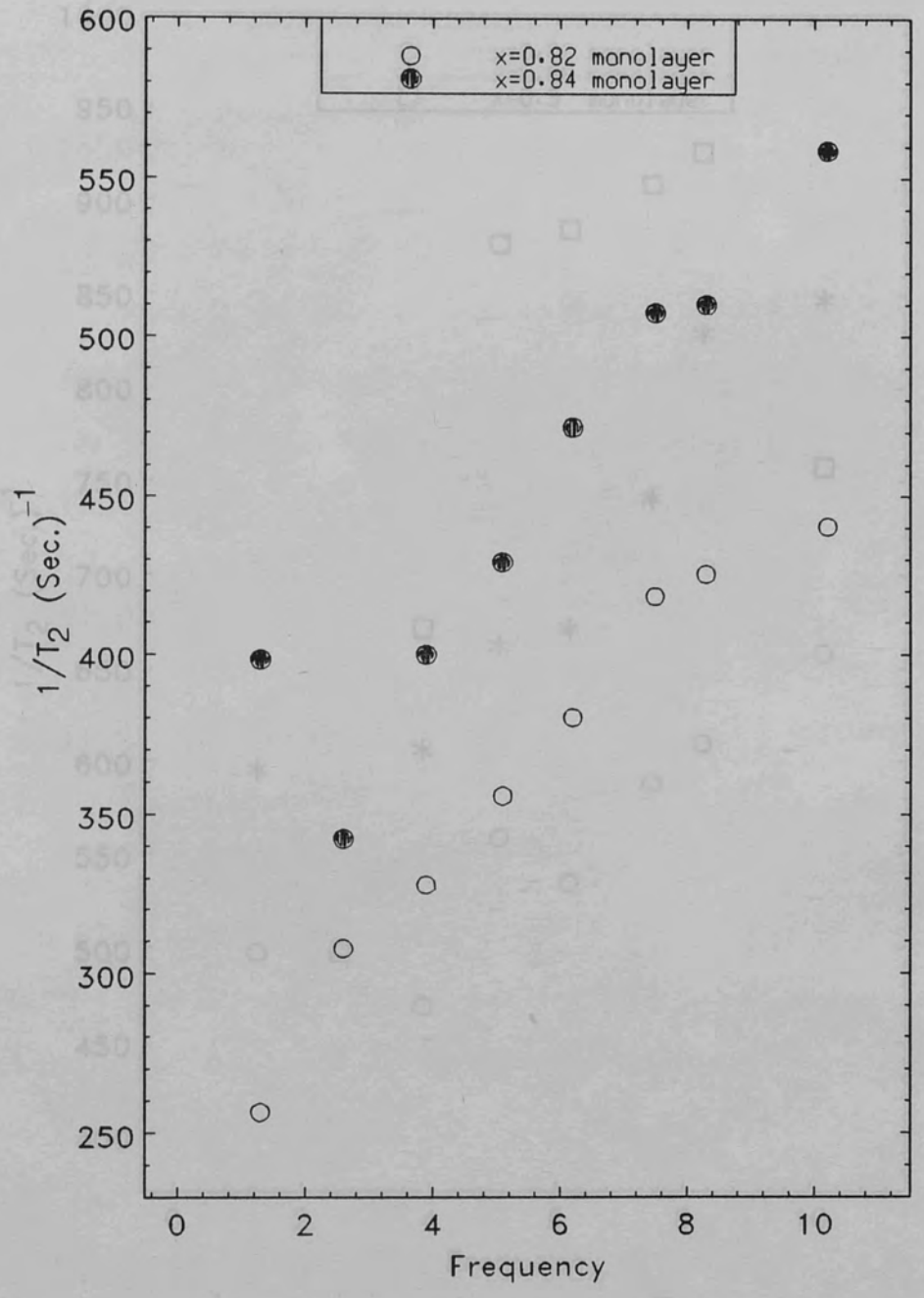

Figure 5.3.3

Spin-spin relaxation rate as a function of Larmor frequency. T=1.2 K and $\beta = 90^{\circ}$

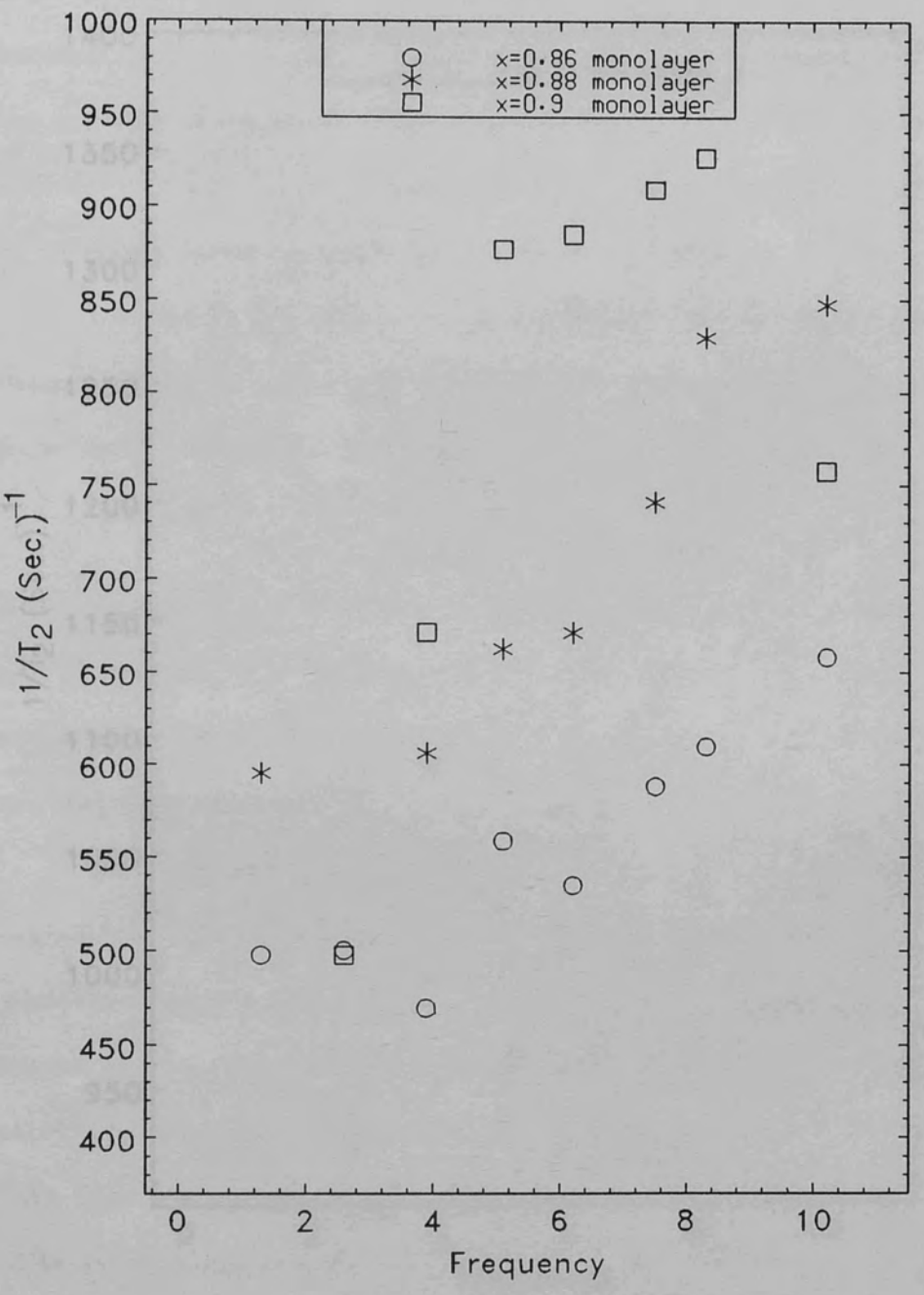

Figure 5.3.4

Spin–spin relaxation rate as a function of Larmor frequency. T=1.2 K and $\beta=90^{\circ}$

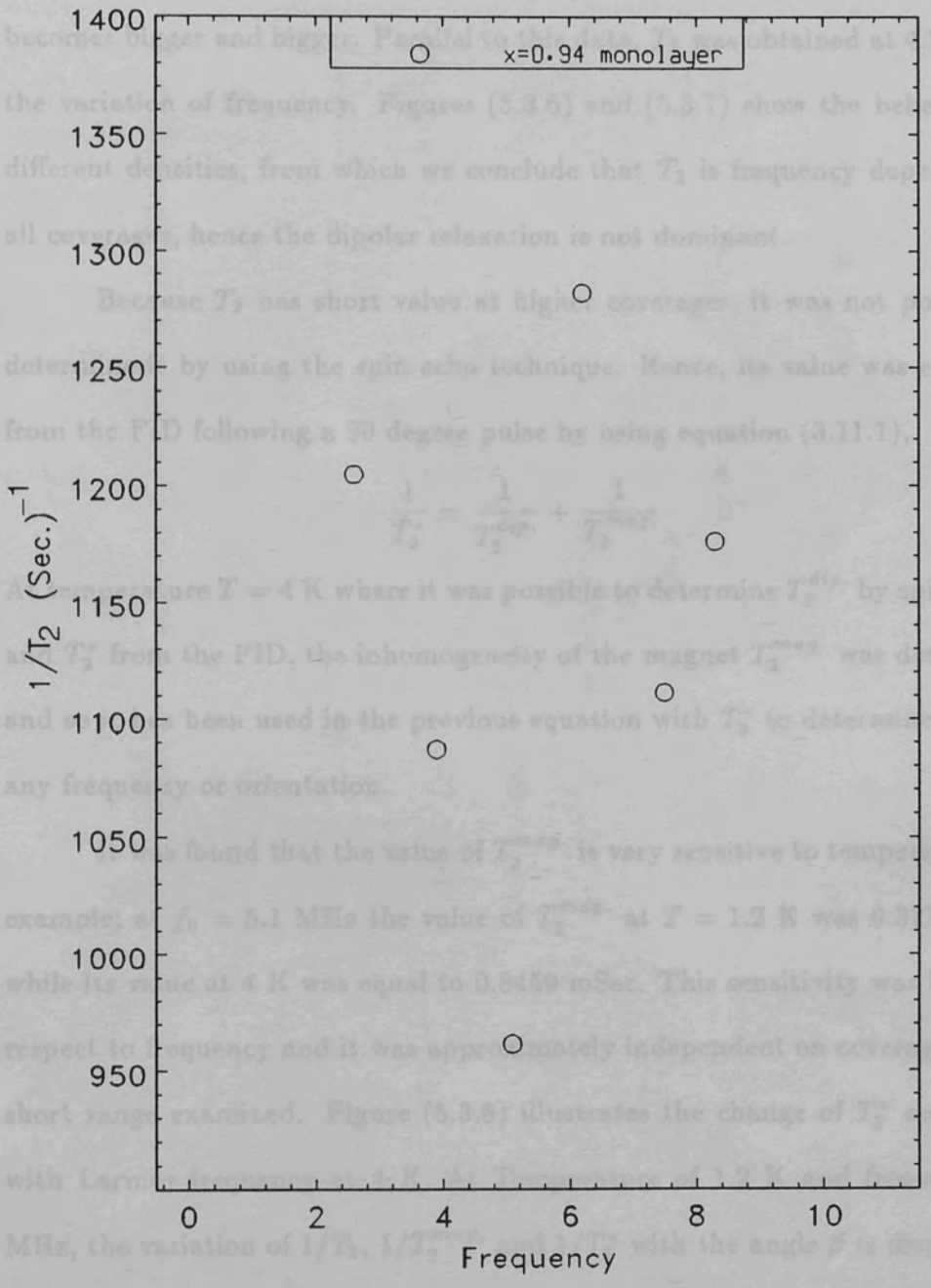

Figure 5.3.5

Spin–spin relaxation rate as a function of Larmor frequency. T=1.2 K and β=90°

different coverages for the same frequency. As the density increases the change becomes bigger and bigger. Parallel to this data, T_2 was obtained at 4.2 K with the variation of frequency. Figures (5.3.6) and (5.3.7) show the behaviour at different densities, from which we conclude that T_2 is frequency dependent at all coverages, hence the dipolar relaxation is not dominant.

Because T_2 has short value at higher coverages, it was not possible to determine it by using the spin echo technique. Hence, its value was extracted from the FID following a 90 degree pulse by using equation (3.11.1),

$$\frac{1}{T_2^*} = \frac{1}{T_2^{dip.}} + \frac{1}{T_2^{mag.}}$$

At temperature $T = 4$ K where it was possible to determine $T_2^{dip.}$ by spin echoes and T_2^* from the FID, the inhomogeneity of the magnet $T_2^{mag.}$ was determined and so it has been used in the previous equation with T_2^* to determine $T_2^{dip.}$ at any frequency or orientation.

It was found that the value of $T_2^{mag.}$ is very sensitive to temperature, for example; at $f_0 = 5.1$ MHz the value of $T_2^{mag.}$ at $T = 1.2$ K was 0.3274 mSec, while its value at 4 K was equal to 0.8459 mSec. This sensitivity was less with respect to frequency and it was approximately independent on coverage at this short range examined. Figure (5.3.8) illustrates the change of T_2^* and $T_2^{mag.}$ with Larmor frequency at 4 K. At Temperature of 1.2 K and frequency 5.1 MHz, the variation of $1/T_2$, $1/T_2^{mag.}$ and $1/T_2^*$ with the angle β is displayed in figure (5.3.9) which shows that all of them have a qualitative angle dependence at 1.2 K.

Experimental data were taken for the variation of the spin-lattice relaxation time T_1 with different Larmor frequencies. These working frequencies were 1.3, 2.6, 3.9, 5.1, 6.2, 7.5, 8.3 and 10.2 MHz. The data have been taken at orientation $\beta = 90°$ and temperatures 1.2 and 4.2 K. The range of coverages

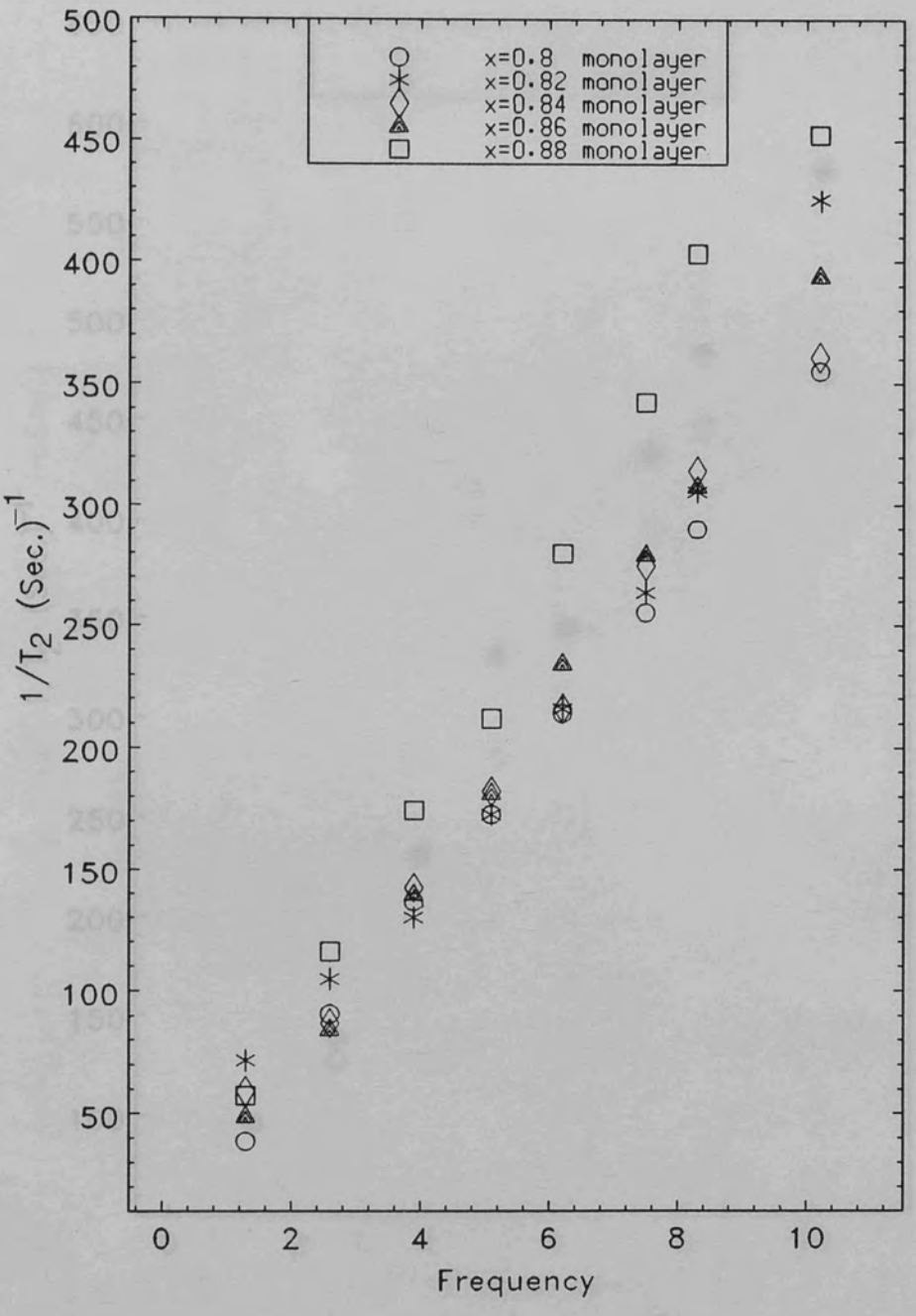

Figure 5.3.6

Spin–spin relaxation rate as a function of Larmor frequency. T=4.2 K and $\beta = 90^{\circ}$

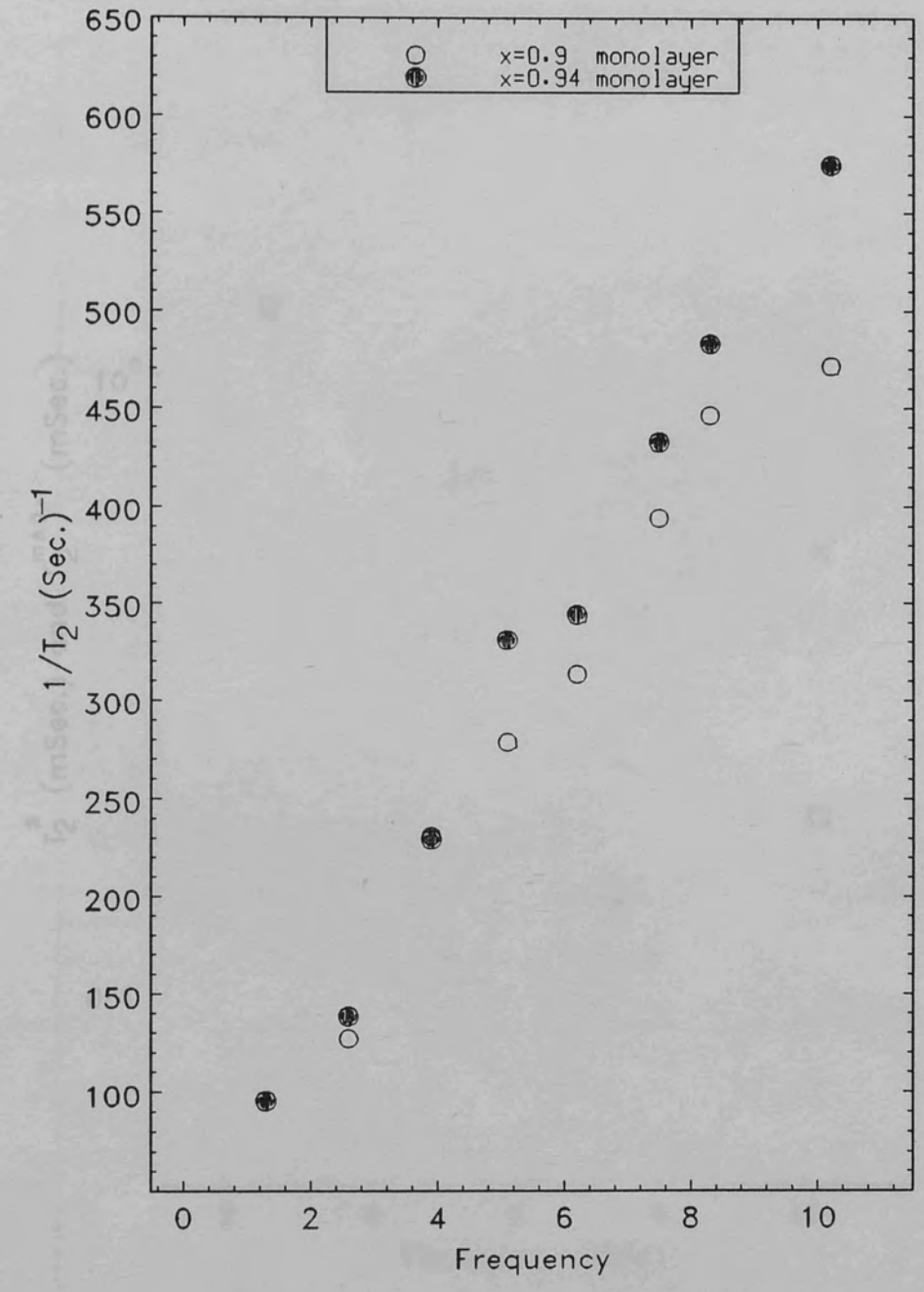

Figure 5.3.7

Spin–spin relaxation rate as a function of Larmor frequency. T=4.2 K and $\beta=90^{\circ}$

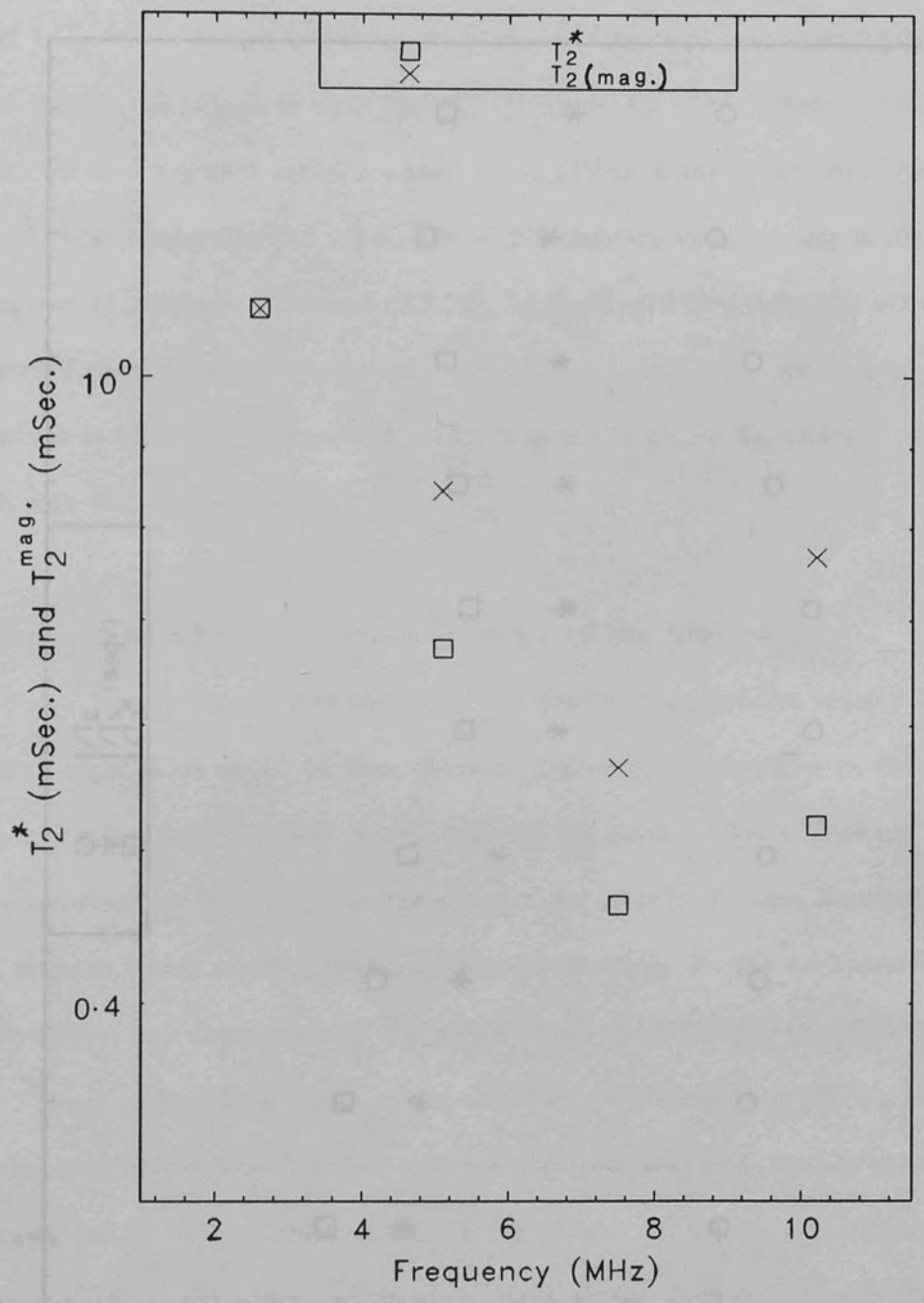

Figure 5.3.8

Variation of T_2^* and $T_2^{mag.}$ with Larmor frequency.
x=0.96 monolayer, T=4.2 K and β=90 deg.

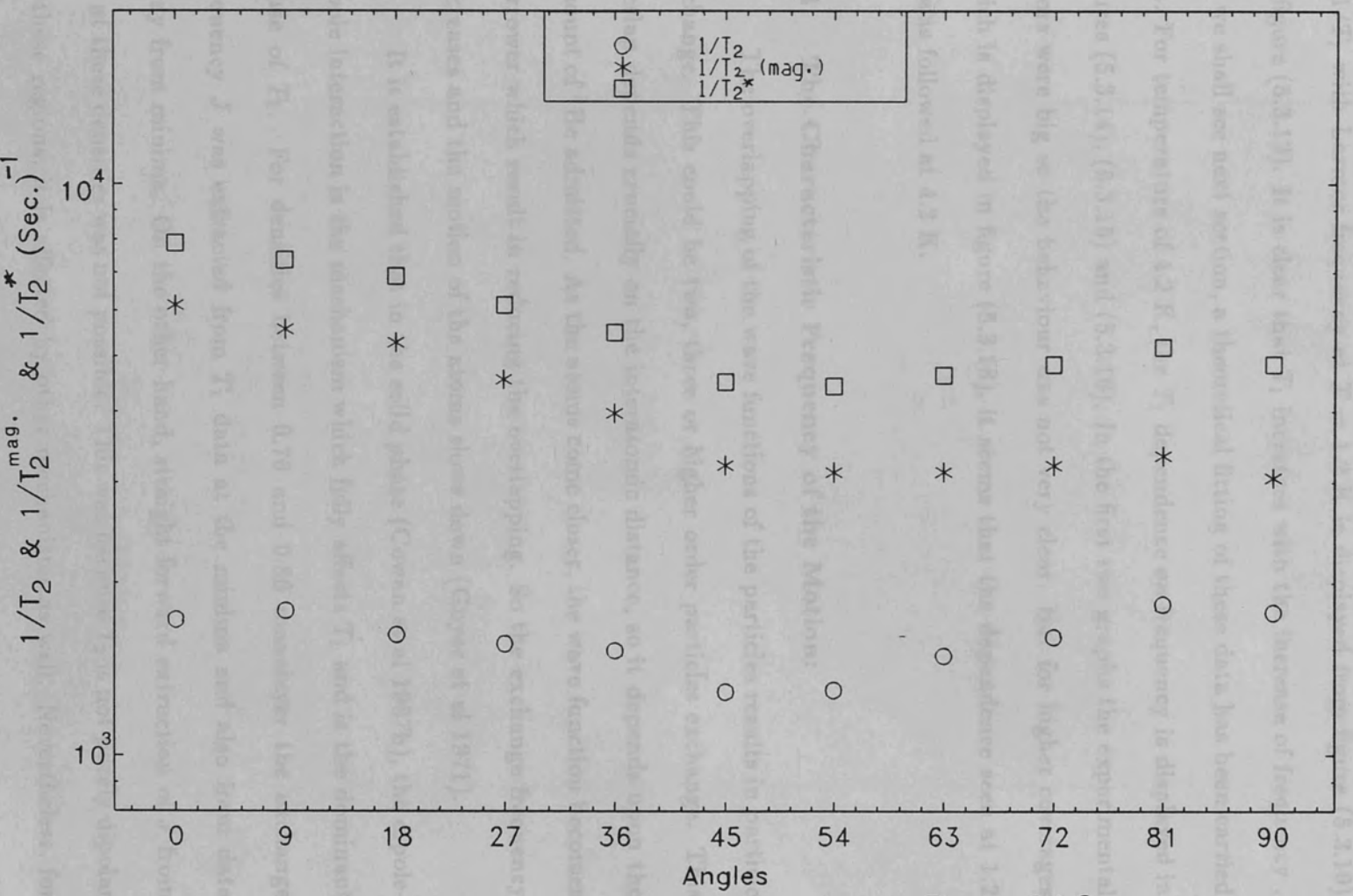

Figure 5.3.9

Angle dependence of $1/T_2$, $1/T_2$(mag.) and $1/T_2^*$. x=0.96 monolayer, f_0 =5.1 MHz and T =1.2 K

extends from $x = 0.7$ to $x = 0.9$ monolayer changed in 0.2 steps. The variation of $1/T_1$ with Larmor frequency at $T = 1.2$ K is displayed from figure (5.3.10) to figure (5.3.13). It is clear that T_1 increases with the increase of frequency . As we shall see next section, a theoretical fitting of these data has been carried out. For temperature of 4.2 K, the T_1 dependence on frequency is displayed in figures (5.3.14), (5.3.15) and (5.3.16). In the first two graphs the experimental errors were big so the behaviour was not very clear. But for higher coverages which is displayed in figure (5.3.16), it seems that the dependence seen at 1.2 K was followed at 4.2 K.

5.4 The Characteristic Frequency of the Motion:

The overlapping of the wave functions of the particles results in particle exchange. This could be two, three or higher order particles exchange. This overlap depends crucially on the interatomic distance, so it depends upon the amount of ^{3}He admitted. As the atoms come closer, the wave function becomes narrower which result in reducing the overlapping. So the exchange frequency decreases and the motion of the atoms slows down (Guyer et al 1971).

It is established that in the solid phase (Cowan et al 1987b), the dipole-dipole interaction is the mechanism which fully affects T_1 and is the dominant cause of T_2. For densities between 0.76 and 0.86 monolayer the exchange frequency J was extracted from T_1 data at the minima and also from data away from minima. On the other hand, straight forward extraction of J from T_2 at these densities was not possible. This was because T_2 is not purely dipolar in these regions; it is affected by other mechanisms as well. Nevertheless, for densities near the monolayer completion where the dipolar coupling is the only cause of the spin-spin relaxation, direct calculations could be done.

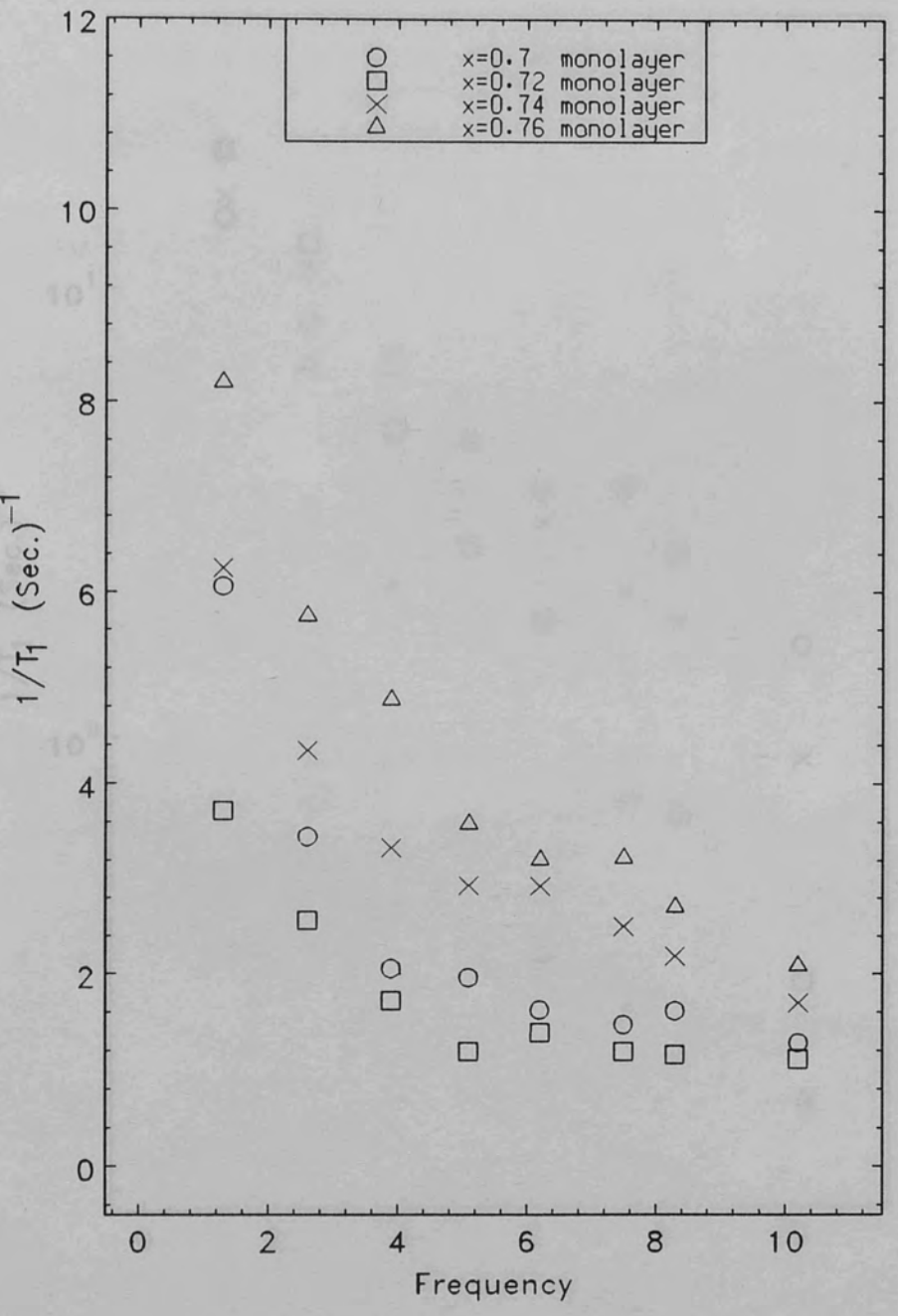

Figure 5.3.10

Spin–lattice relaxation rate as a function of Larmor frequency. T=1.2 K and β=90°

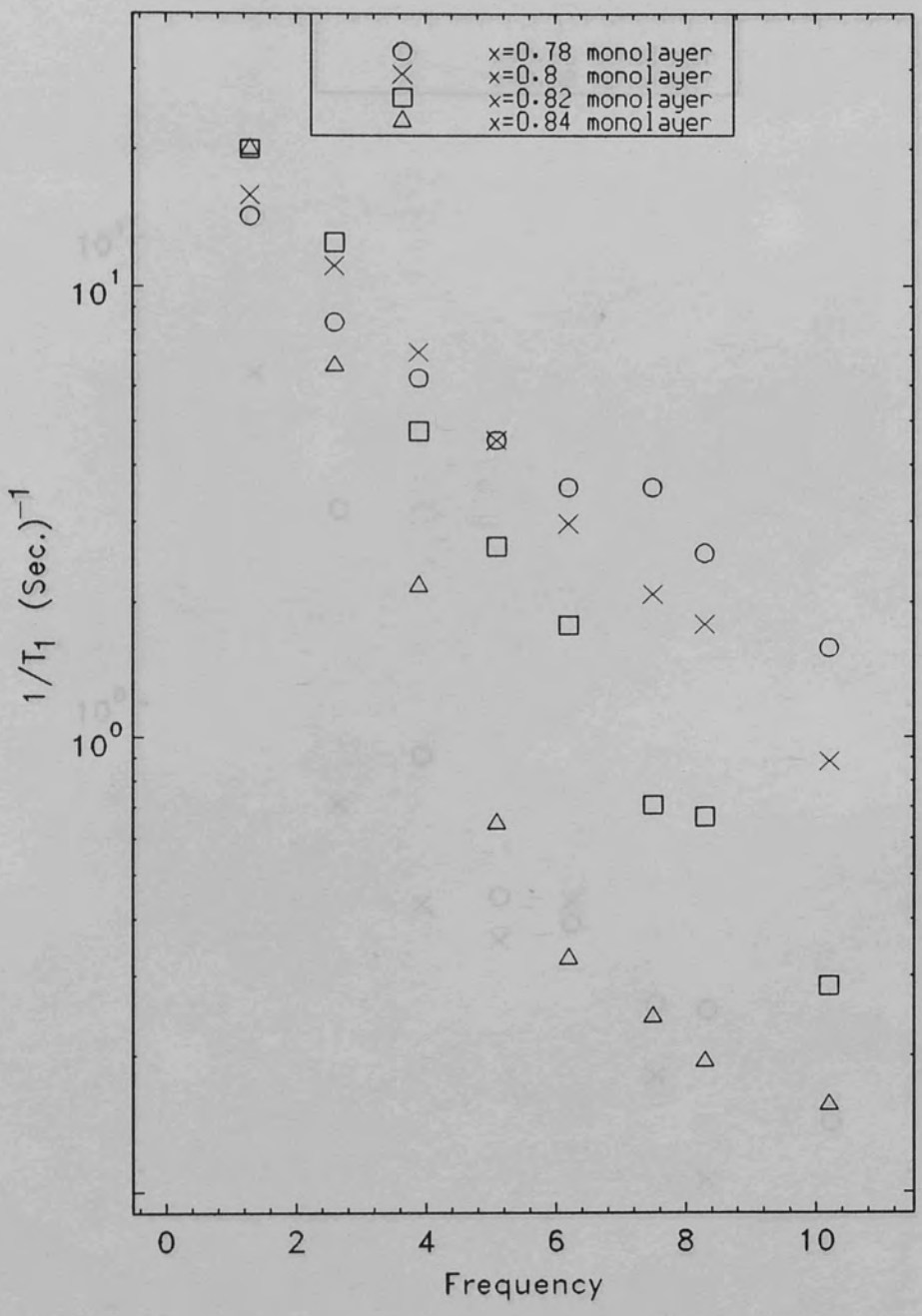

Figure 5.3.11

Spin–lattice relaxation rate as a function of Larmor frequency. T=1.2 K and β=90°

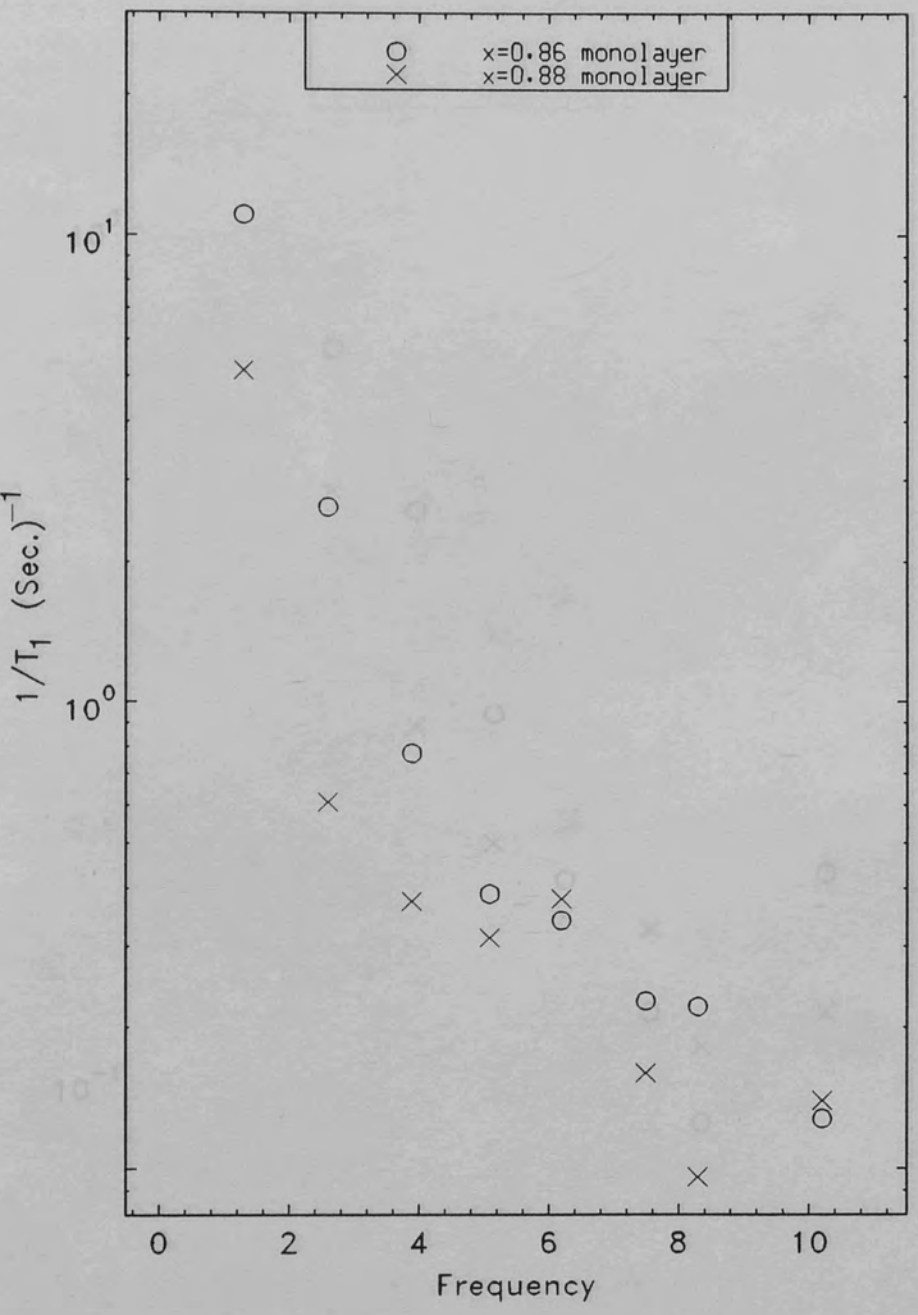

Figure 5.3.12

Spin–lattice relaxation rate as a function of Larmor frequency. T=1.2 K and $\beta = 90^\circ$

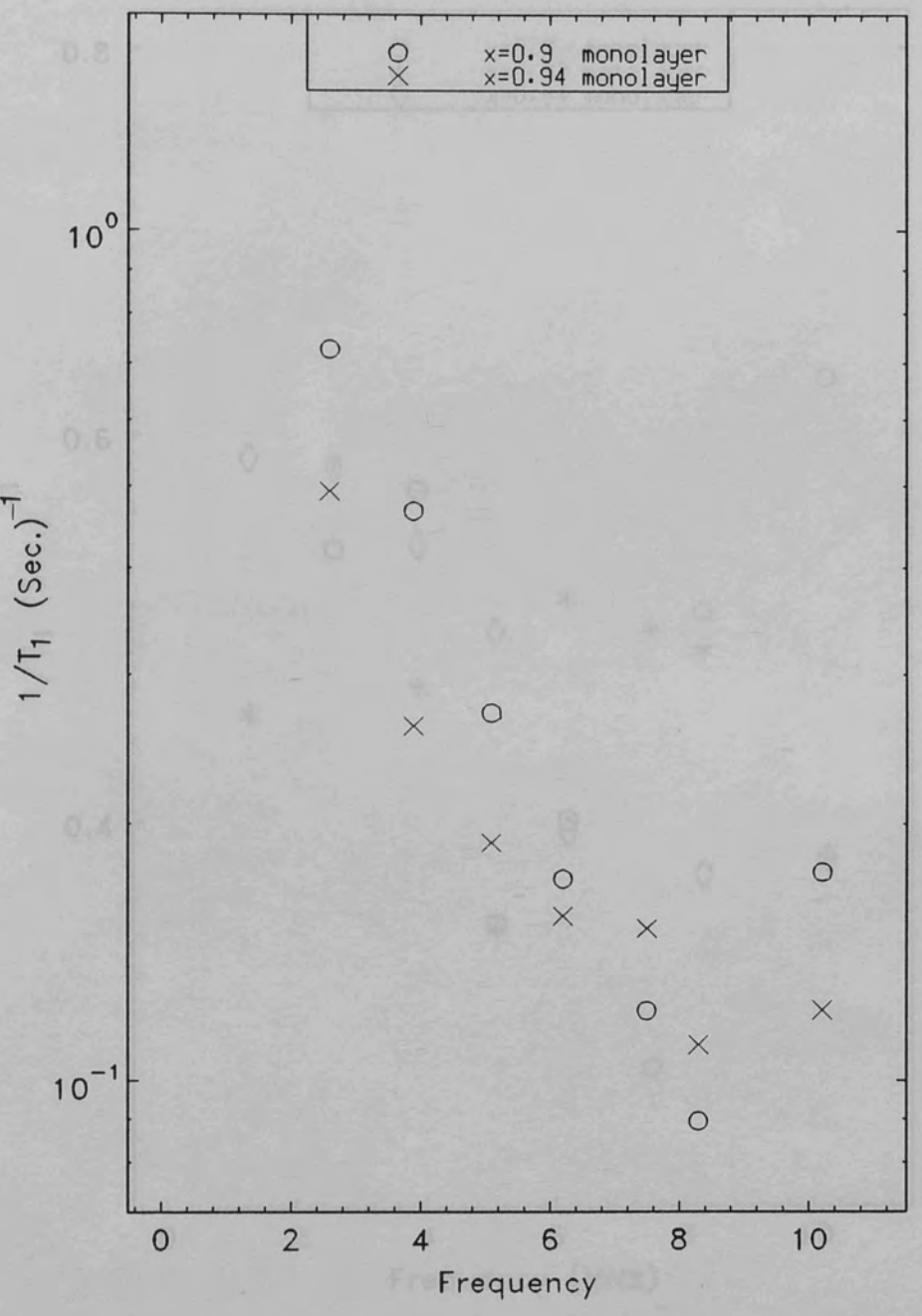

Figure 5.3.13

Spin–lattice relaxation rate as a function of Larmor frequency. T=1.2 K and $\beta=90^{\circ}$

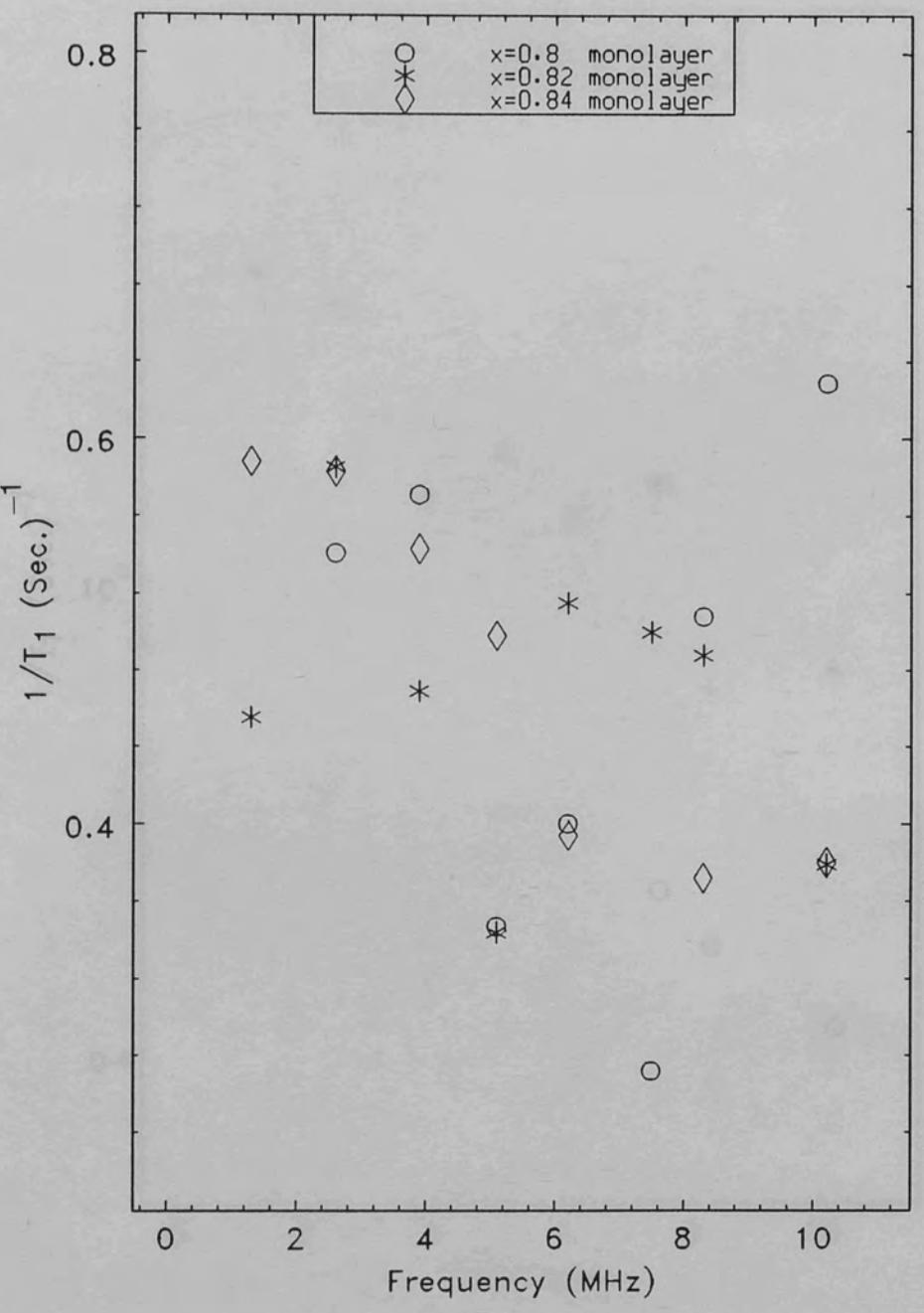

Figure 5.3.14

Spin–lattice relaxation rate as a function of Larmor frequency. T=4.2 K and β=90 deg.

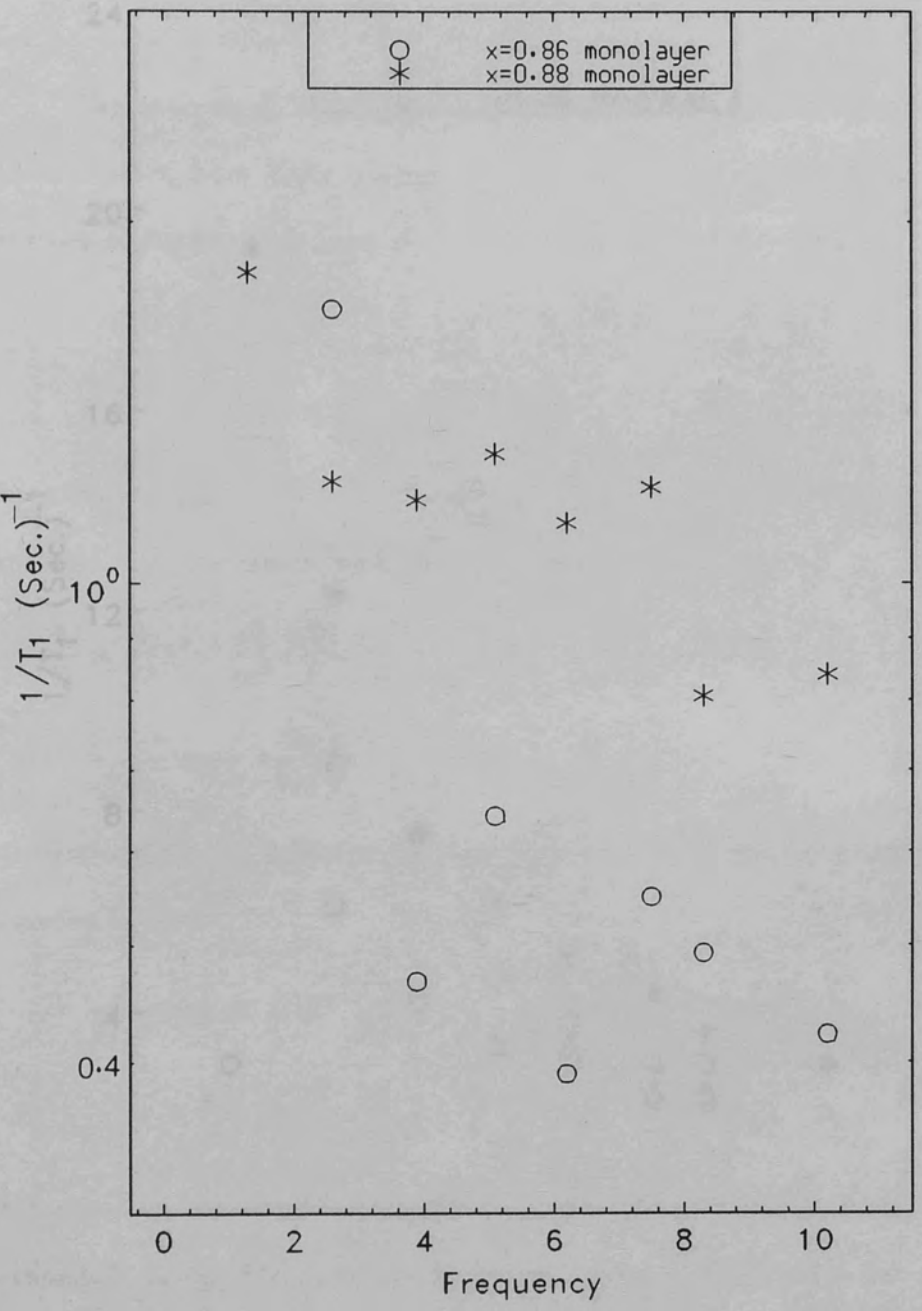

Figure 5.3.15

Spin–lattice relaxation rate as a function of Larmor frequency. T=4.2 K and $\beta=90^{o}$

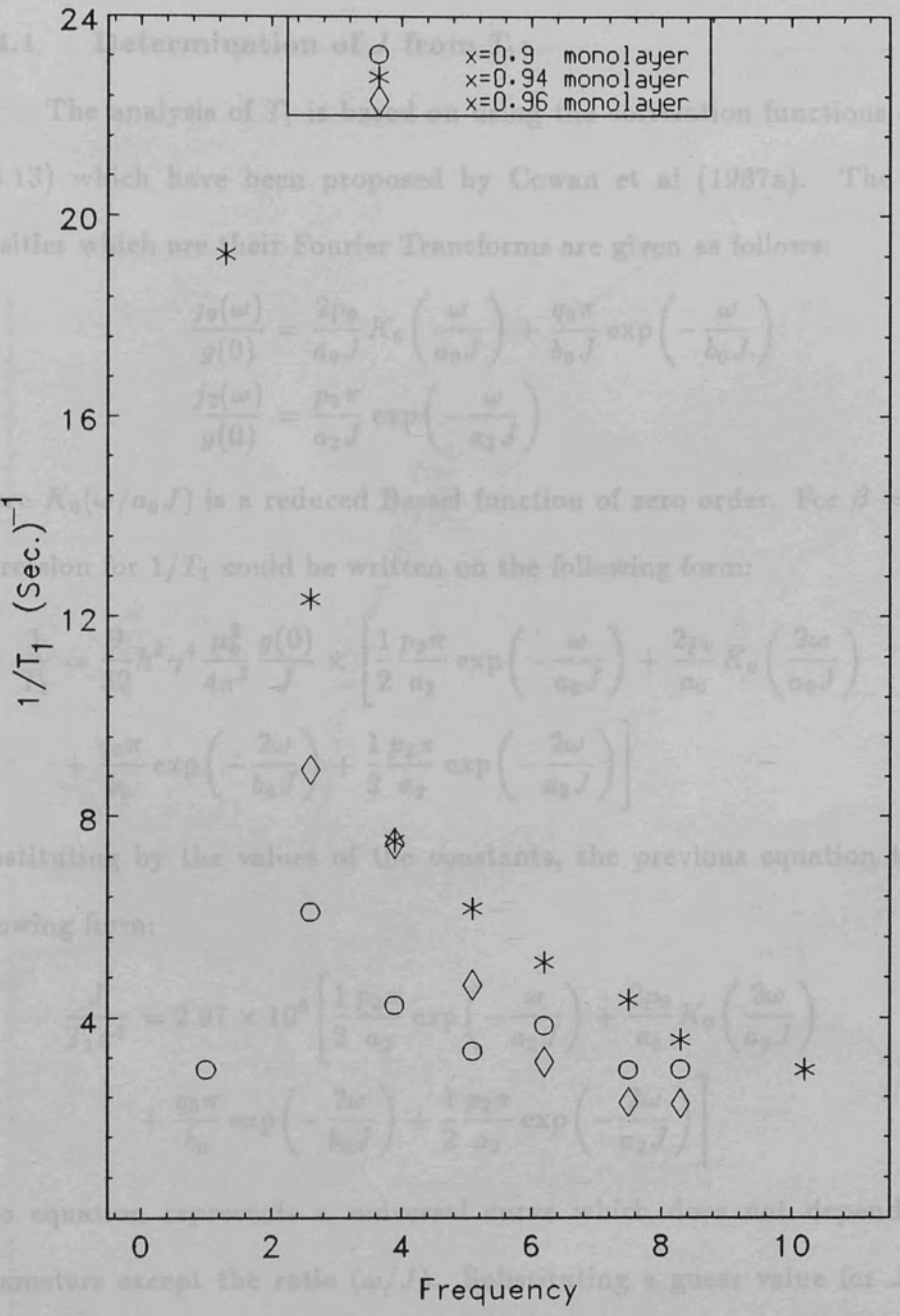

Figure 5.3.16

Spin–lattice relaxation rate as a function of Larmor frequency. T=4.2 K and β=90°

5.4.1 Determination of J from T_1:

The analysis of T_1 is based on using the correlation functions equation (2.6.13) which have been proposed by Cowan et al (1987a). The spectral densities which are their Fourier Transforms are given as follows:

$$\begin{aligned}\frac{j_0(\omega)}{g(0)} &= \frac{2p_0}{a_0 J} K_0\left(\frac{\omega}{a_0 J}\right) + \frac{q_0\pi}{b_0 J}\exp\left(-\frac{\omega}{b_0 J}\right) \\ \frac{j_2(\omega)}{g(0)} &= \frac{p_2\pi}{a_2 J}\exp\left(-\frac{\omega}{a_2 J}\right)\end{aligned} \tag{5.4.1}$$

where $K_0(\omega/a_0 J)$ is a reduced Bessel function of zero order. For $\beta = 90°$ the expression for $1/T_1$ could be written on the following form:

$$\begin{aligned}\frac{1}{T_1} = \frac{9}{32}\hbar^2\gamma^4\frac{\mu_0^2}{4\pi^2}\frac{g(0)}{J} \times \Bigg[&\frac{1}{2}\frac{p_2\pi}{a_2}\exp\left(-\frac{\omega}{a_2 J}\right) + \frac{2p_0}{a_0}K_0\left(\frac{2\omega}{a_0 J}\right) \\ &+ \frac{q_0\pi}{b_0}\exp\left(-\frac{2\omega}{b_0 J}\right) + \frac{1}{2}\frac{p_2\pi}{a_2}\exp\left(-\frac{2\omega}{a_2 J}\right)\Bigg]\end{aligned} \tag{5.4.2}$$

Substituting by the values of the constants, the previous equation takes the following form:

$$\begin{aligned}\frac{J}{T_1 x^3} = 2.97\times 10^8 \Bigg[&\frac{1}{2}\frac{p_2\pi}{a_2}\exp\left(-\frac{\omega}{a_2 J}\right) + \frac{2p_0}{a_0}K_0\left(\frac{2\omega}{a_0 J}\right) \\ &+ \frac{q_0\pi}{b_0}\exp\left(-\frac{2\omega}{b_0 J}\right) + \frac{1}{2}\frac{p_2\pi}{a_2}\exp\left(-\frac{2\omega}{a_2 J}\right)\Bigg]\end{aligned} \tag{5.4.3}$$

This equation represents a universal curve which does not depend on any parameters except the ratio (ω/J). Substituting a guess value for J as well as the experimental data to the above equation, the value of J was extracted from the best fit to the universal curve corresponding to each coverage. As shown in figure (5.4.1) for $x = 0.8$ monolayer, the best value of J was found to be 7.7×10^6 Sec^{-1}. The optimum values of J for densities extended between $x = 0.74$ and $x = 0.86$ monolayer were fitted to the universal curve as illustrated in figure (5.4.2).

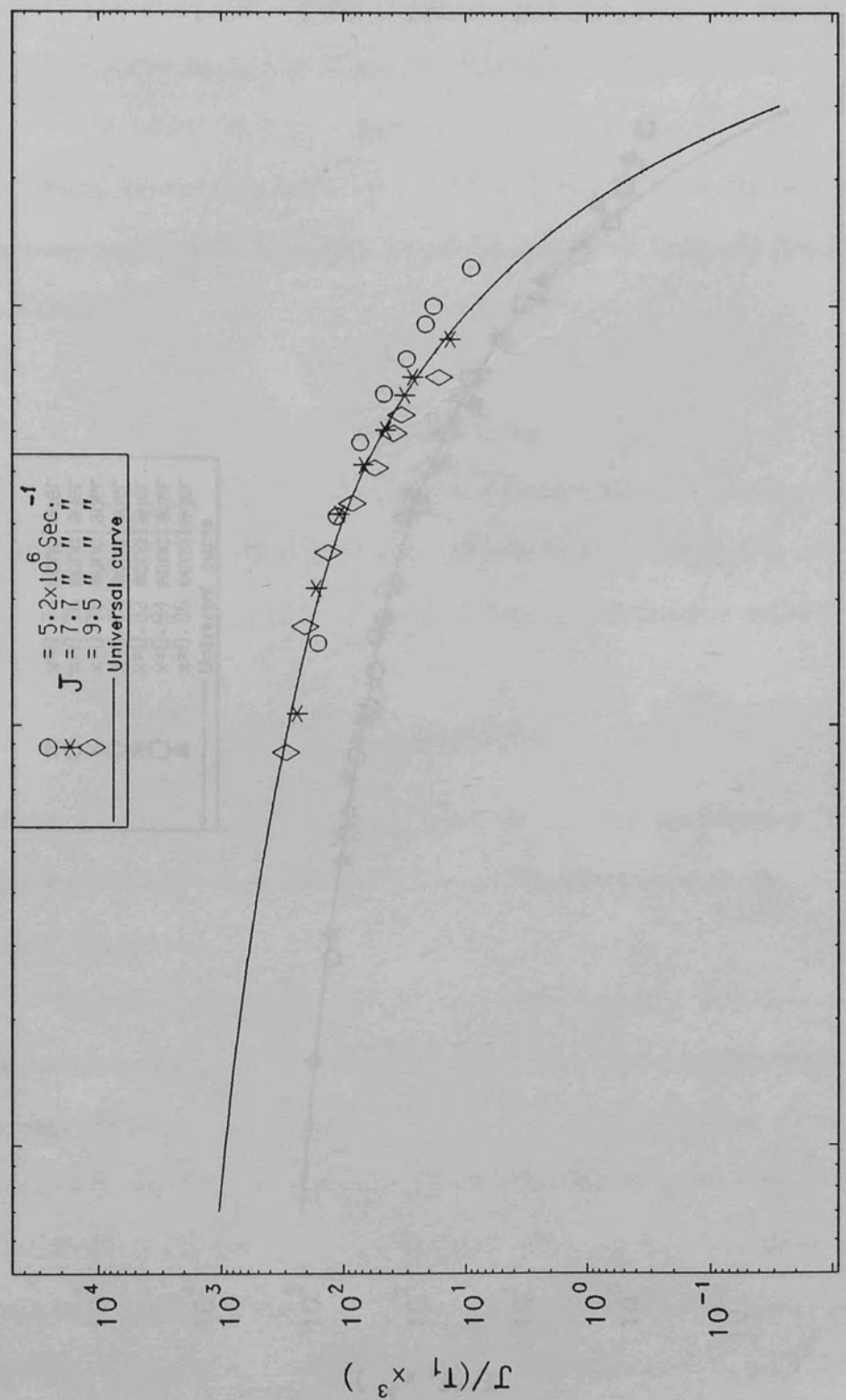

Figure 5.4.1

Choise of J from T_1 data. x=0.8 monolayer, T=1.2 K and β=90 deg.

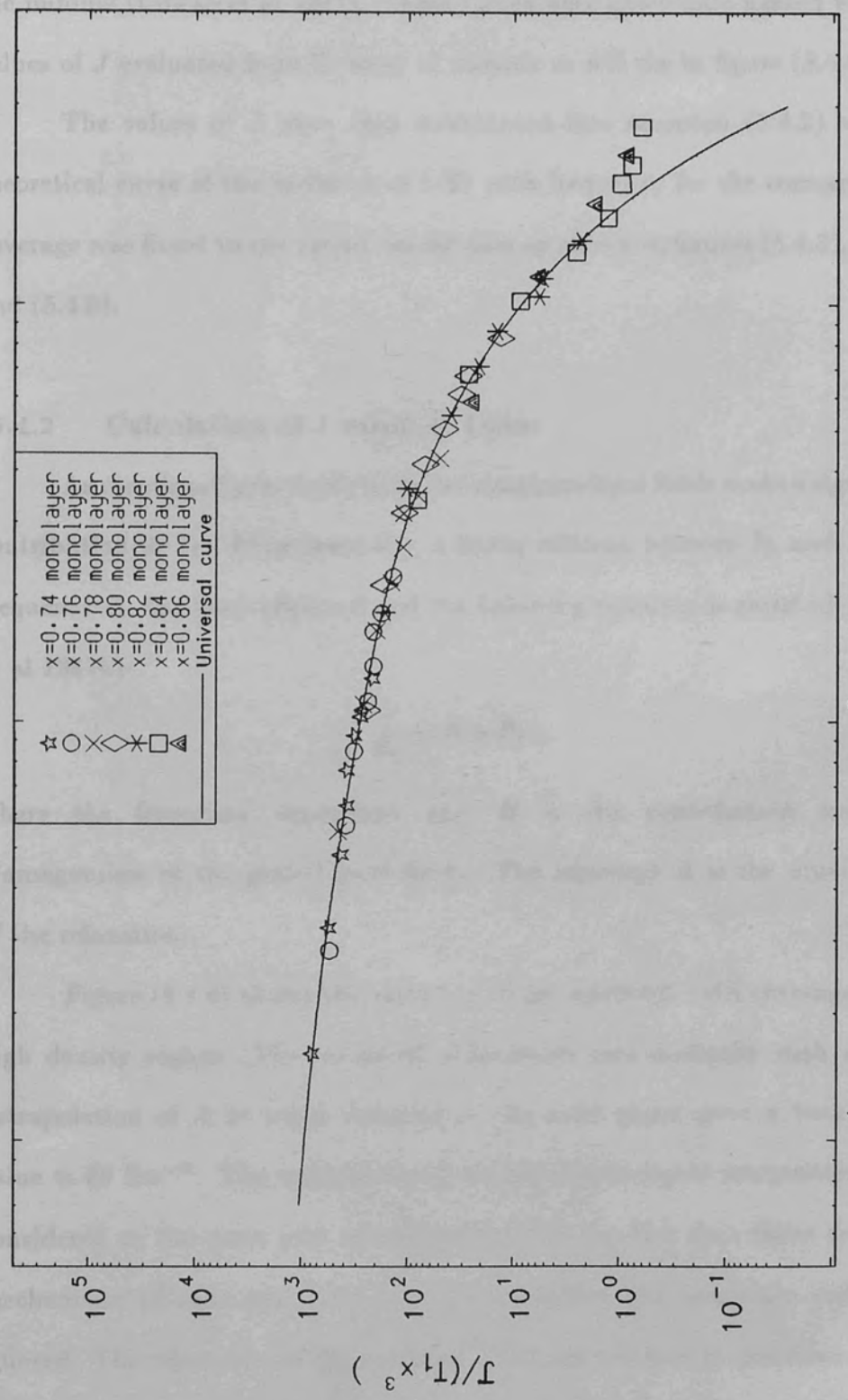

Figure 5.4.2

Universal curve for the determination of J at different coverages. T=1.2 K and $\beta = 90^{\circ}$

On the other hand, the exchange frequency J was evaluated from T_1 at the minima (Cowan et al 1987). These values were excellently agreed with the values of J evaluated from T_1 away of minima as will see in figure (5.4.8).

The values of J were then substituted into equation (5.4.2) and the theoretical curve of the variation of $1/T_1$ with frequency for the corresponding coverage was fitted to the experimental data as shown in figures (5.4.3), (5.4.4) and (5.4.5).

5.4.2 Calculation of J using T_2 Data:

As mentioned previously §4.5, the substrate local fields make a significant contribution to T_2. Experimentally, a linear relation between T_2 and Larmor frequency ω_0 has been observed and the following equation is satisfied (Cowan et al 1987b):

$$\frac{1}{T_2} = A + B\omega_0 \tag{5.4.4}$$

where the frequency dependent part B is the contribution from the diamagnetism of the grafoil local fields. The intercept A is the dipolar part of the relaxation.

Figure (5.4.6) shows the variation of the intercept with coverage at the high density region. The values of A increases monotonically with x. The extrapolation of A at lower densities of the solid phase gave a base line of value ≈ 80 Sec^{-1}. The contribution from the dipole-dipole interaction is still considered as the main part of relaxation. But the fact that there are other mechanisms (Cowan and Kent 1984) which affect the relaxation cannot be ignored. The relaxation of the particles which are trapped in positions of high adsorption energy such as touching platelet edges, is one of these mechanisms. By increasing the amount of sample, these effects become negligible with respect

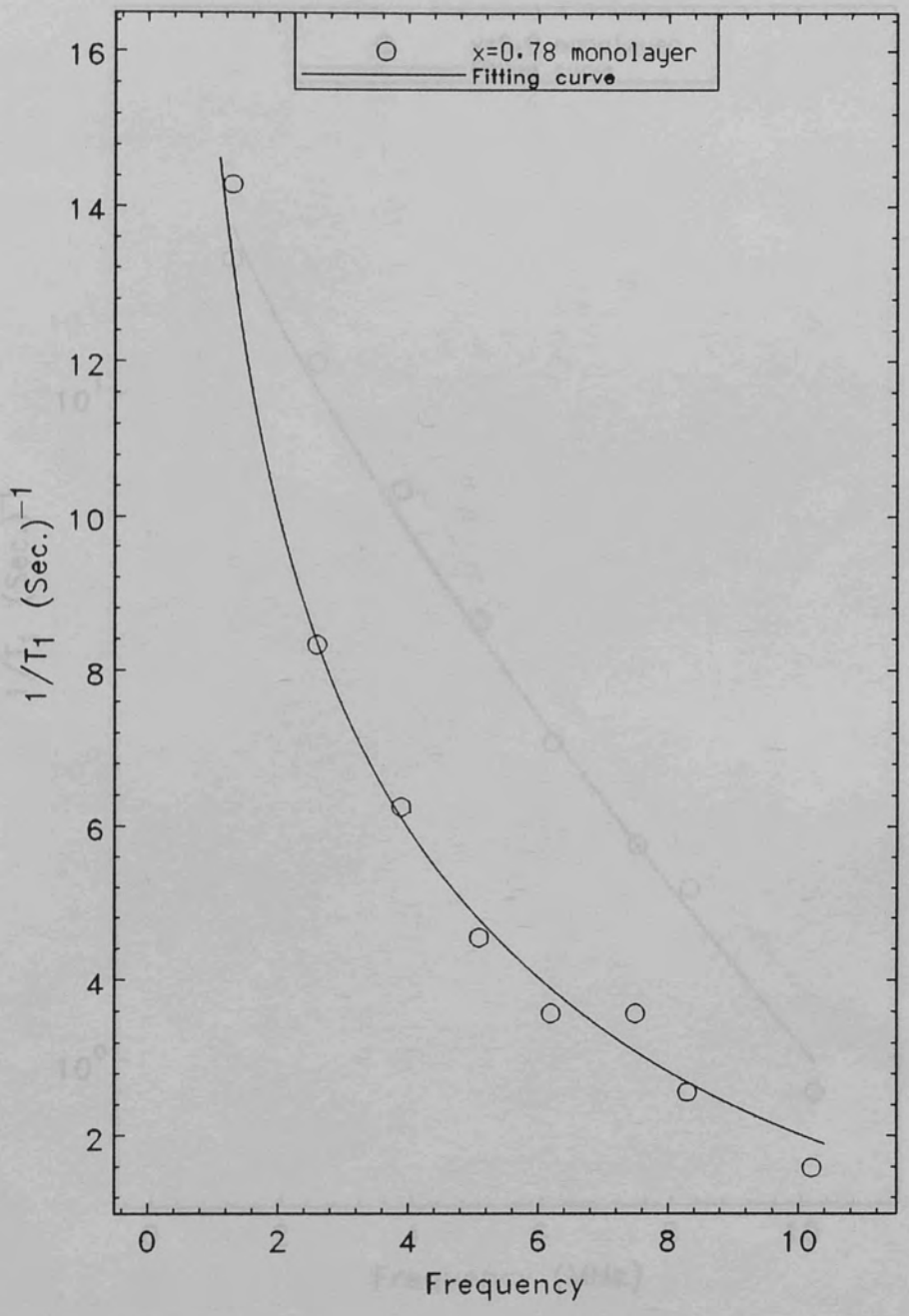

Figure 5.4.3

Theoretical fitting of the variation of experimental $1/T_1$ with frequency.

T=1.2 K and $\beta=90^{\circ}$

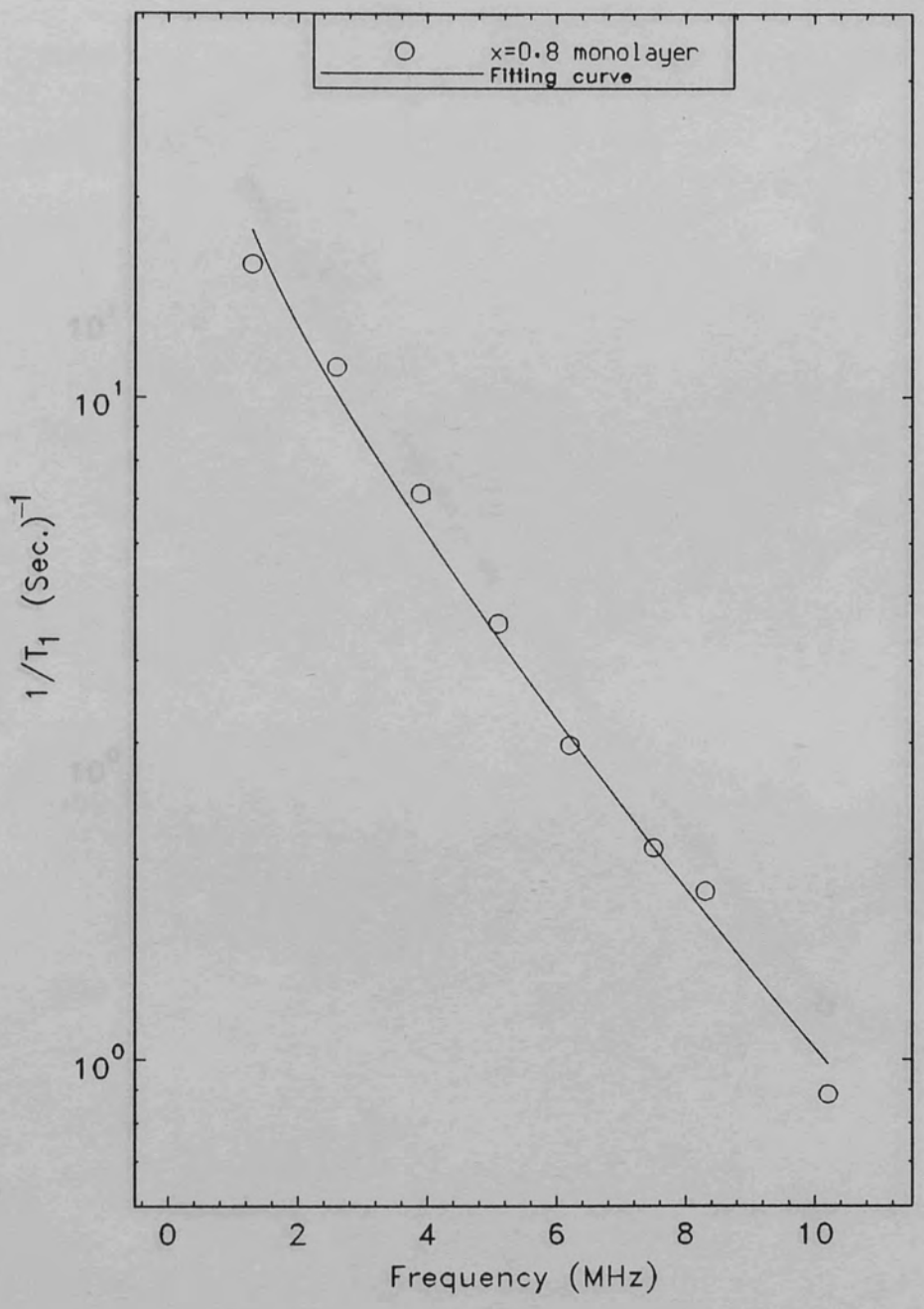

Figure 5.4.4

Theoretical fitting of the variation of experimental $1/T_1$ with frequency. T=1.2 K and β=90 deg.

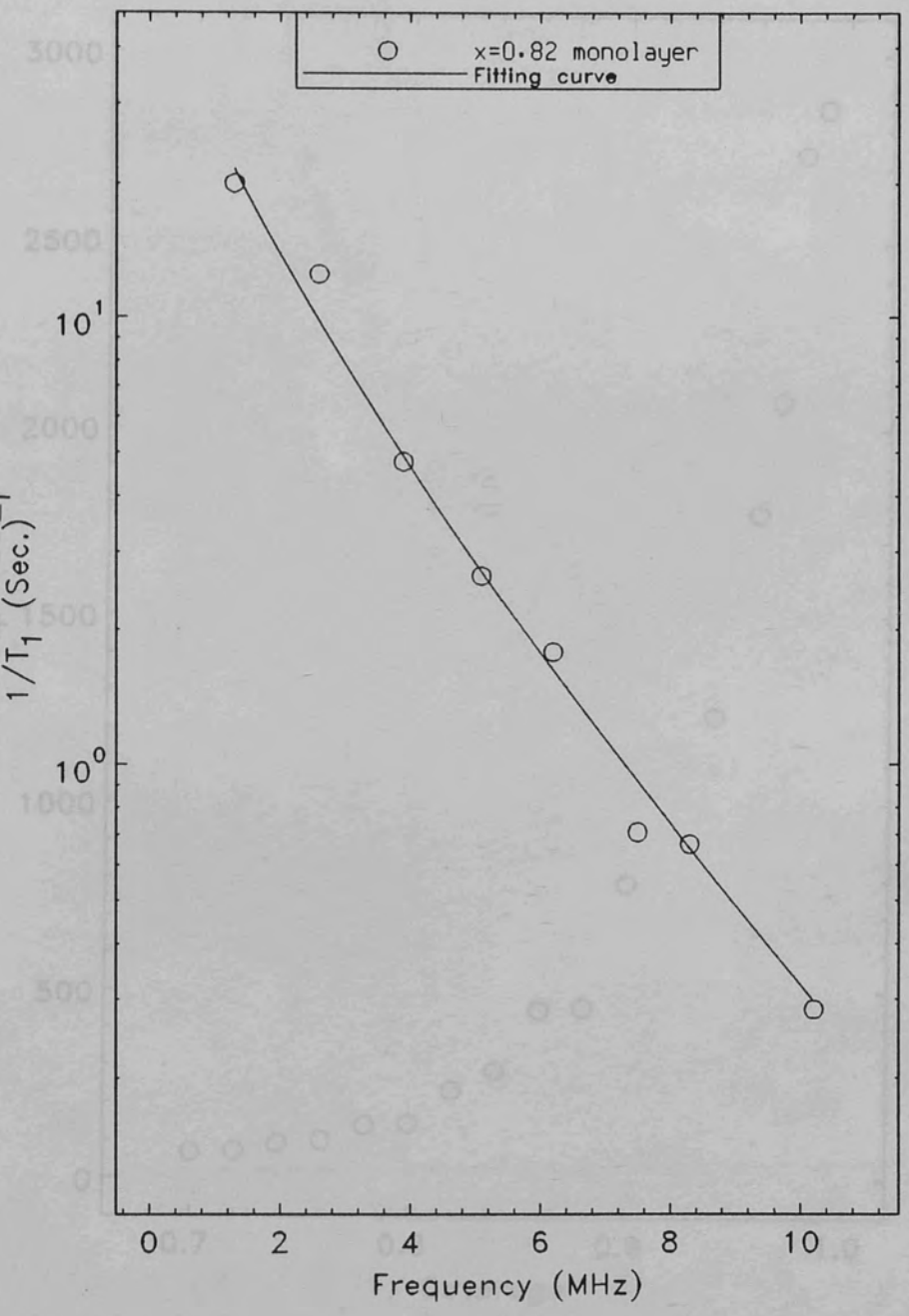

Figure 5.4.5

Theoretical fitting of the variation of experimental $1/T_1$ with frequency. T=1.2 K and β=90 deg.

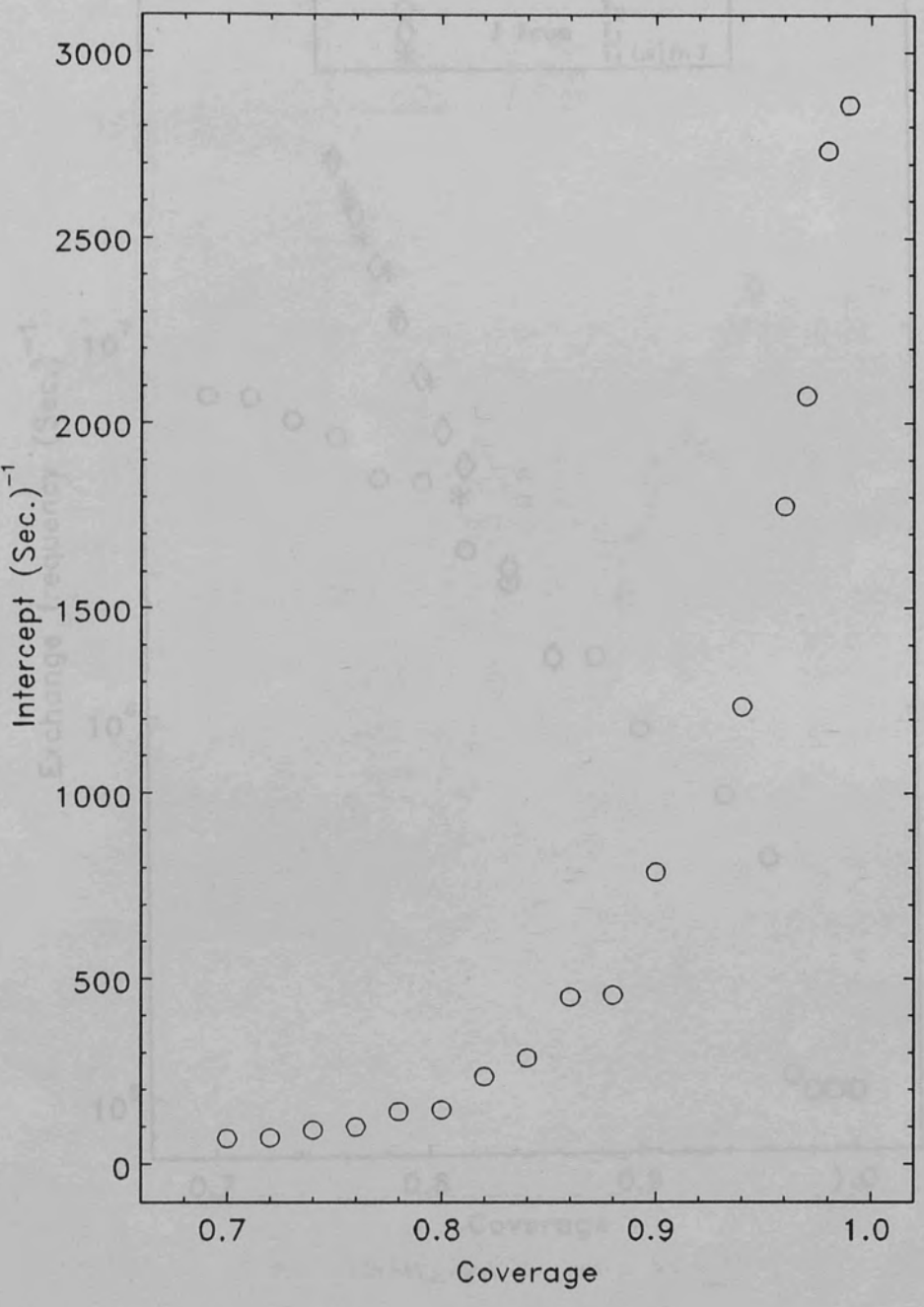

Figure 5.4.6

The variation of the intercept of $(1/T_2 \& f_0)$ with the change of coverage.
T=1.2 K and β=90 deg.

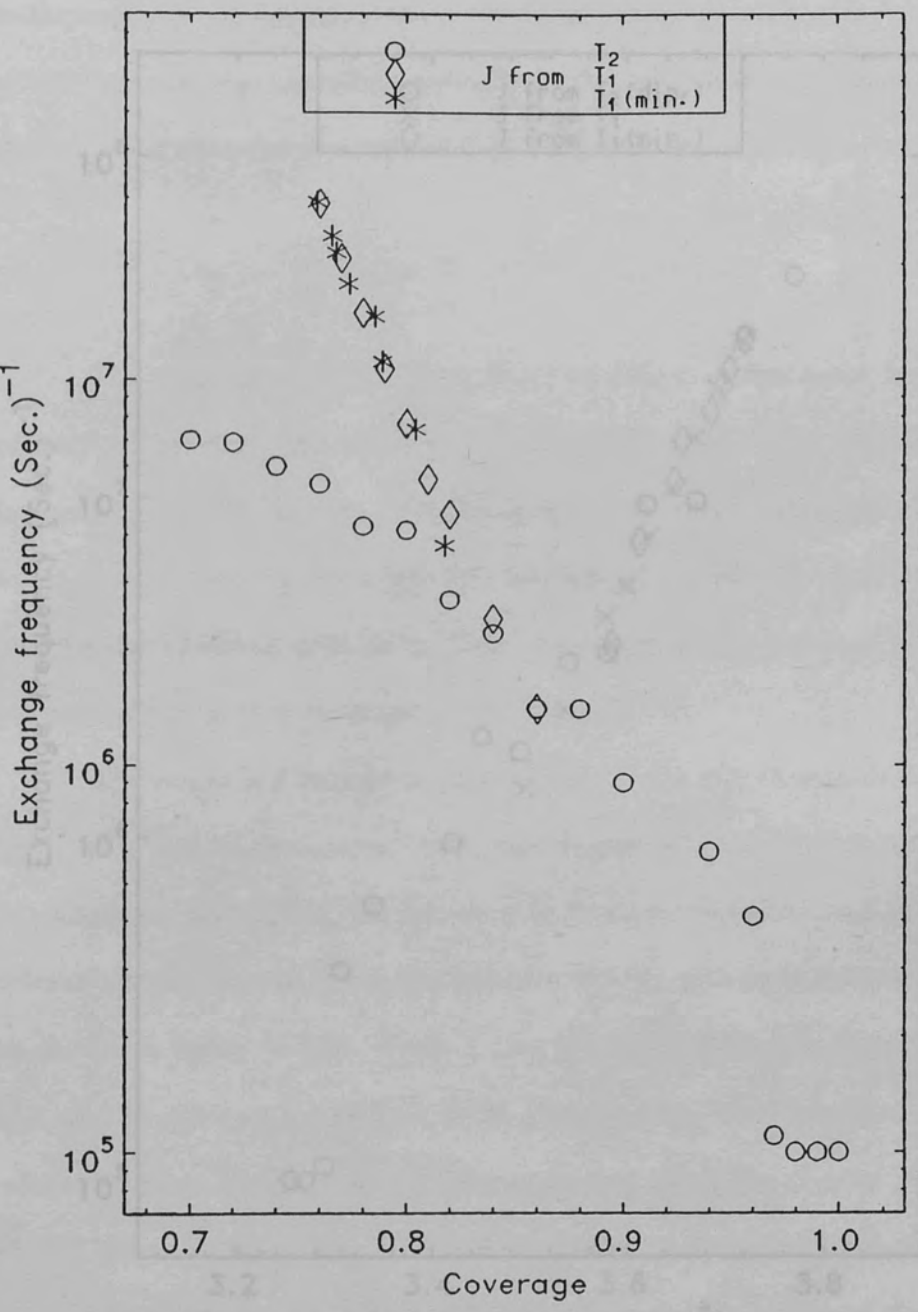

Figure 5.4.7

J obtained from T_2 data, T_1 (min.) and T_1 away from minima, as functions of coverage. T=1.2 K and $\beta = 90°$. Values of T_2 are not corrected for the "solid patches".

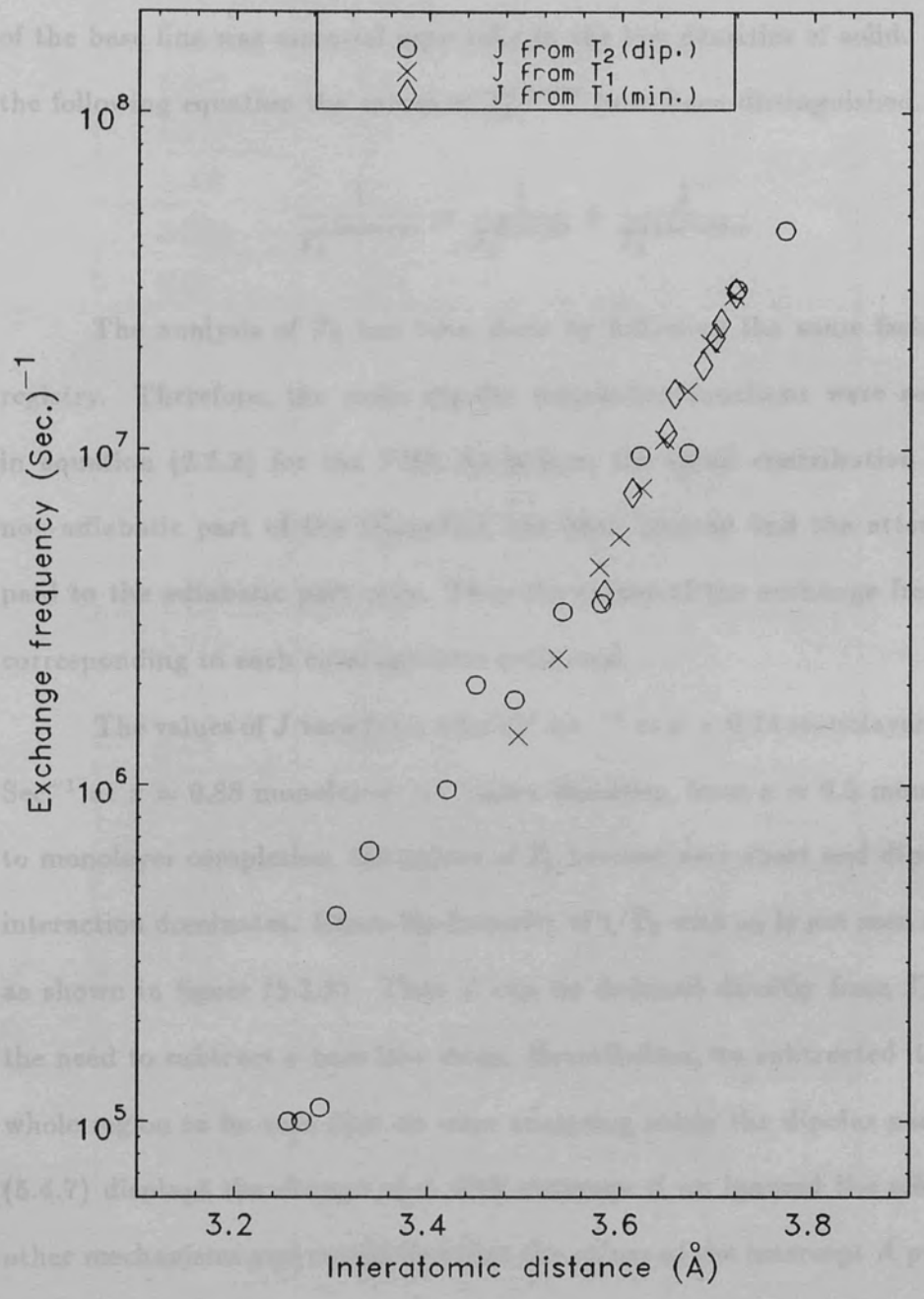

Figure 5.4.8

The variation of J obtained from T_2, T_1(min.) and T_1 away from minima with coverage.
T=1.2 K and $\beta = 90^\circ$

to the ordinary dipolar relaxation. To eliminate such contributions, subtraction of the base line was essential especially in the low densities of solid. Based on the following equation the values of $T_2^{dipolar}$ have been distinguished.

$$\frac{1}{T_2^{intercept}} = \frac{1}{T_2^{dipolar}} + \frac{1}{T_2^{base-line}} \tag{5.4.5}$$

The analysis of T_2 has been done by following the same fashion as at registry. Therefore, the same dipolar correlation functions were substituted in equation (2.5.2) for the FID. As before, the small contribution from the non-adiabatic part of the relaxation has been ignored and the attention was paid to the adiabatic part only. Thus the values of the exchange frequency J corresponding to each coverage were evaluated.

The values of J vary from 4.5×10^7 sec.$^{-1}$ at $x = 0.74$ monolayer to 2×10^6 Sec^{-1} at $x = 0.88$ monolayer. At higher densities, from $x = 0.9$ monolayer up to monolayer completion, the values of T_2 become very short and dipole-dipole interaction dominates. Hence the linearity of $1/T_2$ with ω_0 is not seen any more, as shown in figure (5.3.5). Then J can be deduced directly from T_2 without the need to subtract a base line value. Nevertheless, we subtracted it from the whole region to be sure that we were analyzing solely the dipolar part. Figure (5.4.7) displays the change of J with coverage if we ignored the effect of the other mechanisms and considered that the values of the intercept A present the pure dipolar effect for all densities. However, this is not the case at least for the low density solid since the discrepancy between the values of J obtained from both T_1 and T_2 is clear. Figure (5.4.8) displays the values of J obtained from T_1 away from minima and from T_1 at the minima (Cowan et al 1987) as well as from T_2 dipolar. The agreement between these values is striking. Table (5.4.1) shows most of the values of J with the corresponding coverage

R(Å)	$J \times 10^{+6}$ (Sec.)$^{-1}$	Coverage
3.256	0.1	0.984
3.27	0.1	0.976
3.289	0.11	0.964
3.306	0.41	0.955
3.34	0.64	0.935
3.42	0.97	0.892
3.45	2.0	0.877
3.494	1.8	0.855
3.54	3.3	0.833
3.58	3.5	0.814
3.599	5.53	0.805
3.612	7.456	0.8
3.622	7.71	0.795
3.62	9.6	0.793
3.645	10.7	0.785
3.648	11.184	0.784
3.656	14.6253	0.781
3.685	17.7797	0.768
3.692	20.73	0.765
3.698	21.5078	0.763
3.703	23.8019	0.761
3.717	28.82	0.755
3.72	30.0	0.754
3.77	45.0	0.734

Table 5.4.1

The Change of Exchange Frequency as a function of Interatomic Distance and Coverage.

or equivalently the interatomic distance. As observed; the value of J decreases with the increase of the amount of sample as expected.

All the above analyses have been done using the Heisenberg exchange Hamiltonian which represents a two particle exchange. On the other hand, based on three-particles exchange, Roger (1984) has deduced an expression for the exchange frequency J with the change of the interatomic distance a given as follows:

$$\frac{J_T}{k_B} \simeq 73\left(\frac{\sigma^*}{a}\right)^{19/2} \exp\left[-51.7\left(\frac{\sigma^*}{a}\right)^5\right]$$

This expression is given in units of the temperature K. Where $\sigma^* = \sigma =$ 2.65 Å is the Lenard-Jones parameter. k_B is Boltzmann constant and $J_T = J\hbar$ is in units of energy. Hence the exchange frequency J is given theoretically by the following equation:

$$J \simeq 73\frac{k_B}{\hbar}\left(\frac{\sigma^*}{a}\right)^{19/2} \exp\left[-51.7\left(\frac{\sigma^*}{a}\right)^5\right] \qquad (5.4.6)$$

Comparison between the experimental values of J and the theoretical curve is made. As displayed in figure (5.4.9), the agreement between both of them was satisfactory specially at lower densities.

The best fit for the change of J with the interatomic distance was found to be a straight line which satisfies the following equation:

$$J = \exp(c_1 + c_2 a) \qquad (5.4.7)$$

Where the parameters $c_1 = -39.6107$ and $c_2 = 11.5222$ were determined from a least square fitting of the values of J determined from both T_1 and T_2. This fitting is shown in figure (5.4.10). Comparison with J obtained by Sussex group (Cowan et al 1977), (Owers-Bradley 1978) was made. Although the

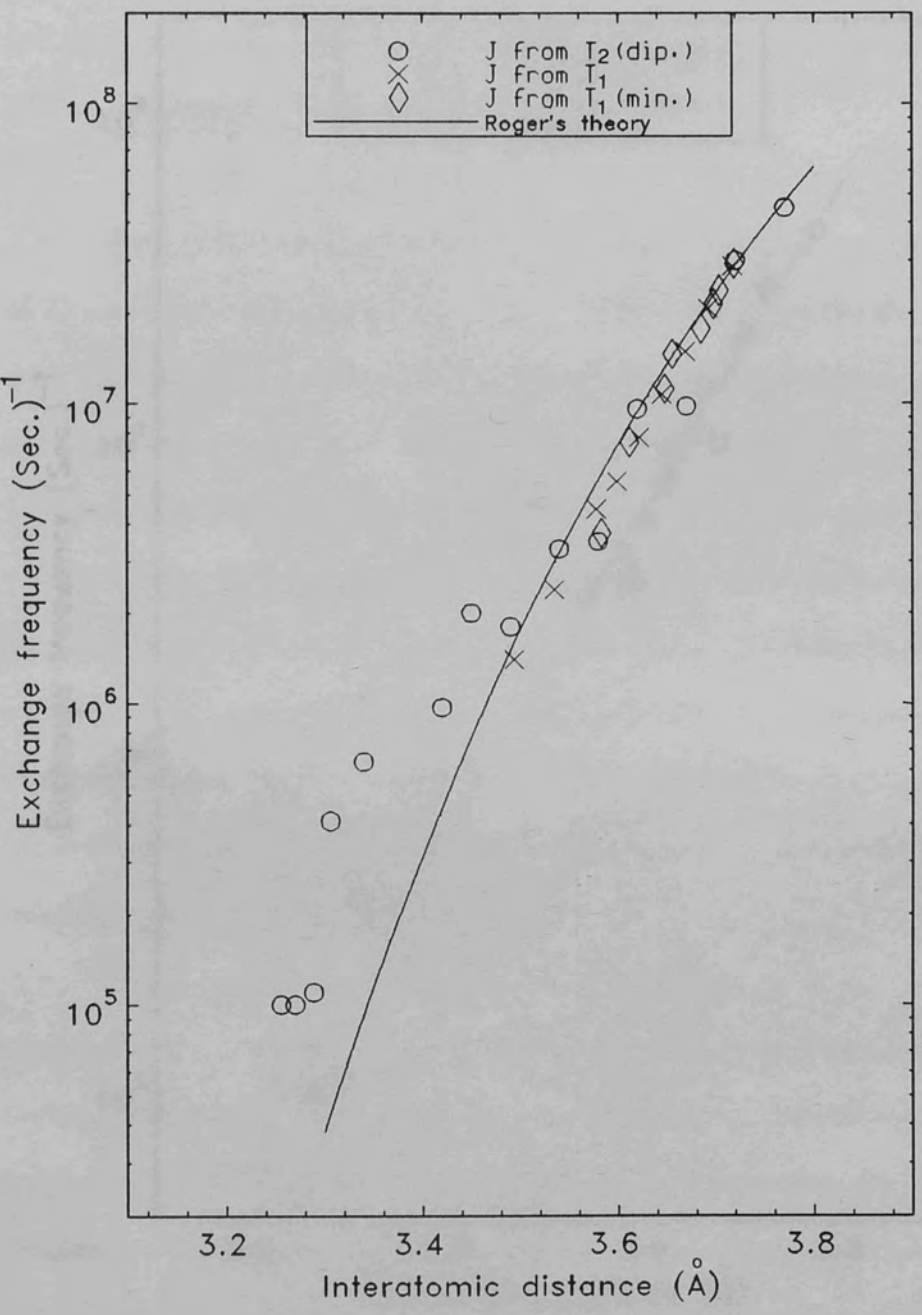

Figure 5.4.9

Comparison between J obtained from both T_1 and T_2 with J calculated by Roger.

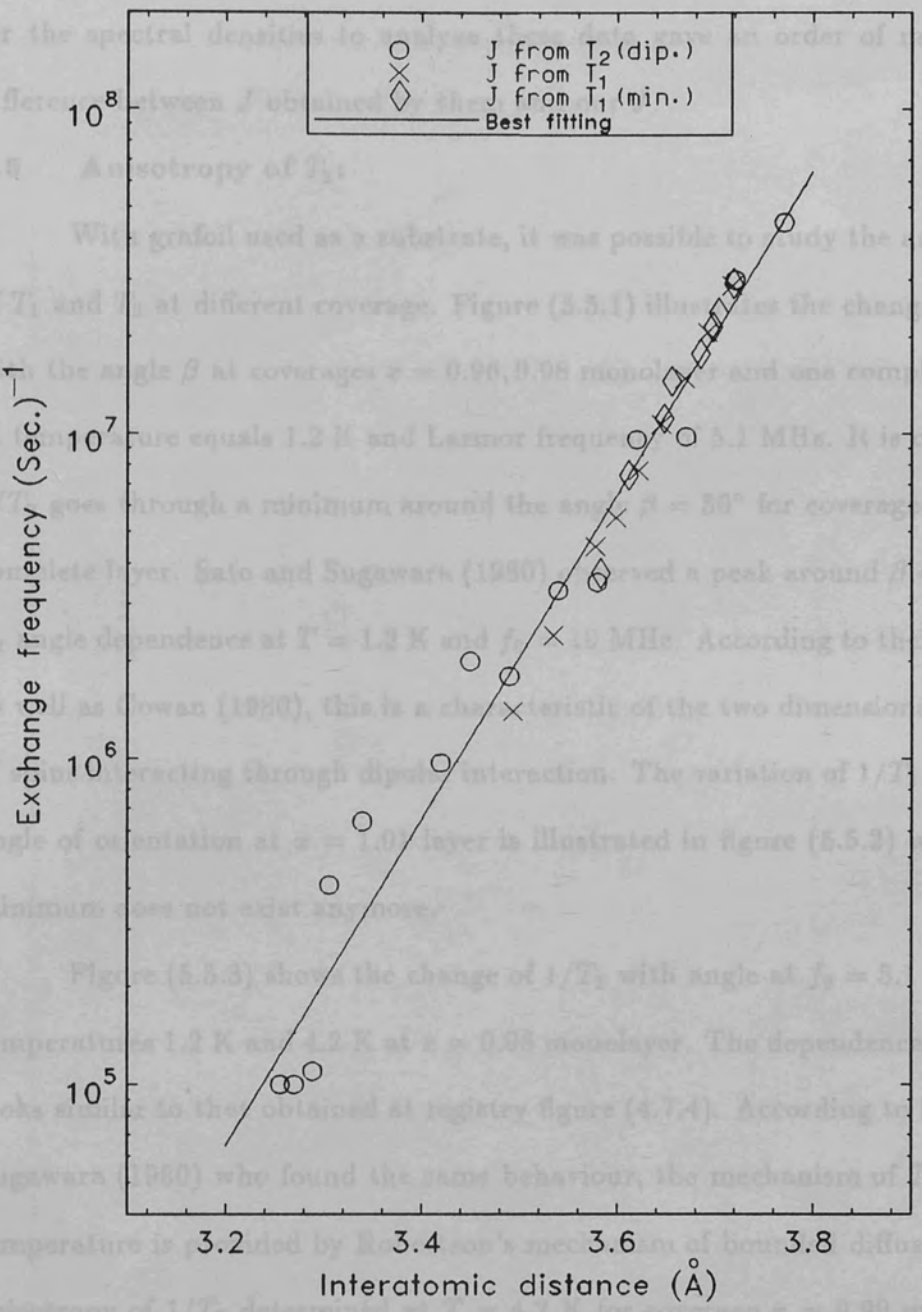

Figure 5.4.10

Least square fitting of J obtained from T_1 and T_2

experimental data are more or less the same, nevertheless using different model for the spectral densities to analyze these data gave an order of magnitude difference between J obtained by them and our J.

5.5 Anisotropy of T_2:

With grafoil used as a substrate, it was possible to study the anisotropy of T_1 and T_2 at different coverage. Figure (5.5.1) illustrates the change of $1/T_2$ with the angle β at coverages $x = 0.96, 0.98$ monolayer and one complete layer at temperature equals 1.2 K and Larmor frequency of 5.1 MHz. It is clear that $1/T_2$ goes through a minimum around the angle $\beta = 50°$ for coverages $x < 1.0$ complete layer. Sato and Sugawara (1980) observed a peak around $\beta = 45°$ for T_2 angle dependence at $T = 1.2$ K and $f_0 = 10$ MHz. According to their report, as well as Cowan (1980), this is a characteristic of the two dimensional system of spins interacting through dipolar interaction. The variation of $1/T_2$ with the angle of orientation at $x = 1.01$ layer is illustrated in figure (5.5.2) where the minimum does not exist anymore.

Figure (5.5.3) shows the change of $1/T_2$ with angle at $f_0 = 5.1$ MHz for temperatures 1.2 K and 4.2 K at $x = 0.96$ monolayer. The dependence at 4.2 K looks similar to that obtained at registry figure (4.7.4). According to Sato and Sugawara (1980) who found the same behaviour, the mechanism of T_2 at this temperature is provided by Robertson's mechanism of bounded diffusion. The anisotropy of $1/T_2$ determined at $T = 4.2$ K for coverage $x = 0.99$ monolayer and one layer completion is displayed in figure (5.5.4).

Recall equation (2.5.2) and Compare the experimental T_2 at $T = 1.2$ K and $f_0 = 5.1$ MHz with the calculated T_2 using different J at various angles. This was made to check the accuracy of the obtained value of J from T_2 data. Figure (5.5.5) illustrates the experimental values as well as values obtained using

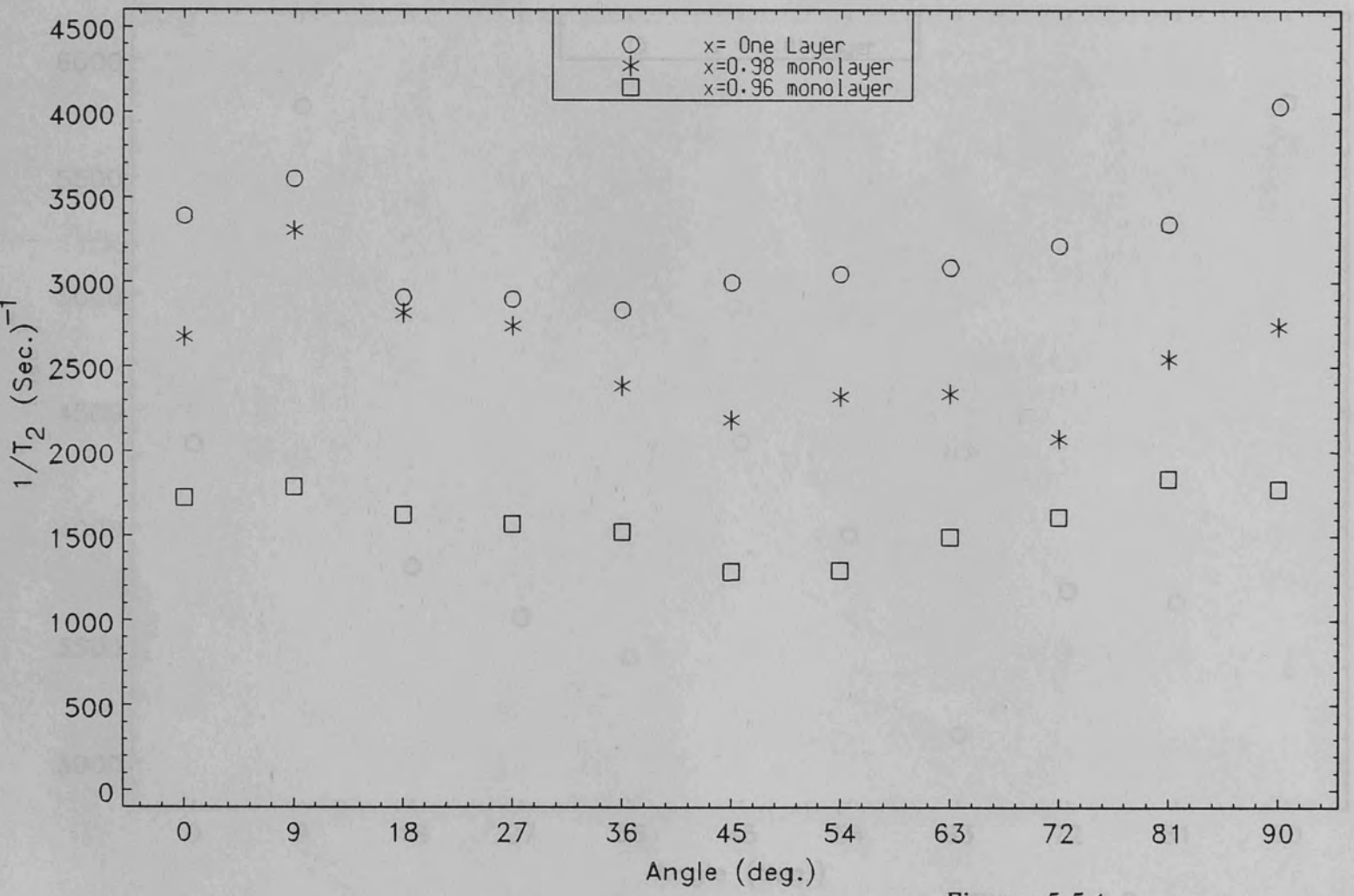

Figure 5.5.1

The variation of spin–spin relaxation rate vs. angles. T=1.2 K and f_o=5.1 MHz.

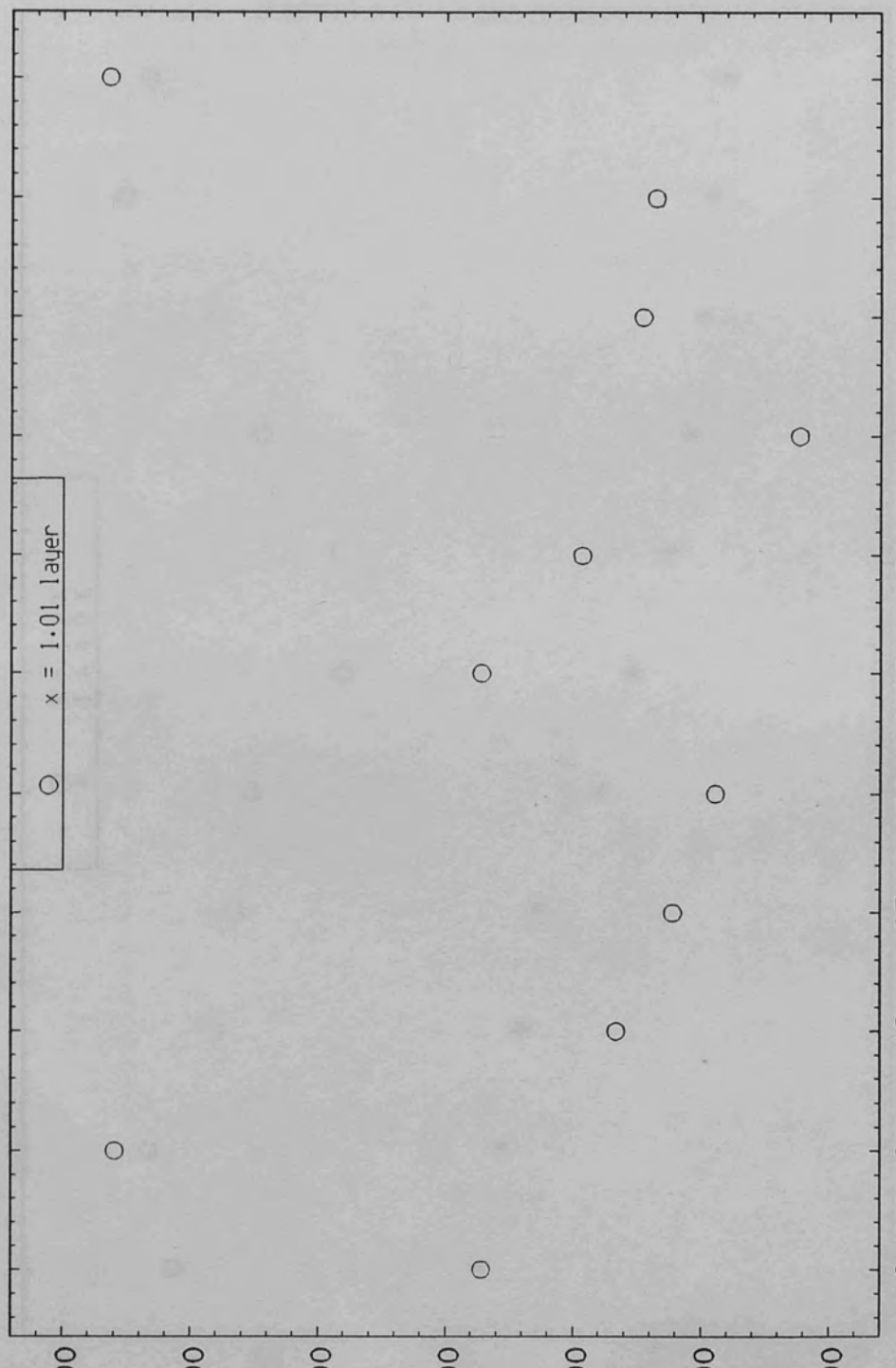

Figure 5.5.2

The variation of spin-spin relaxation rate with angles. T=1.2 K and f_o=5.1 MHz.

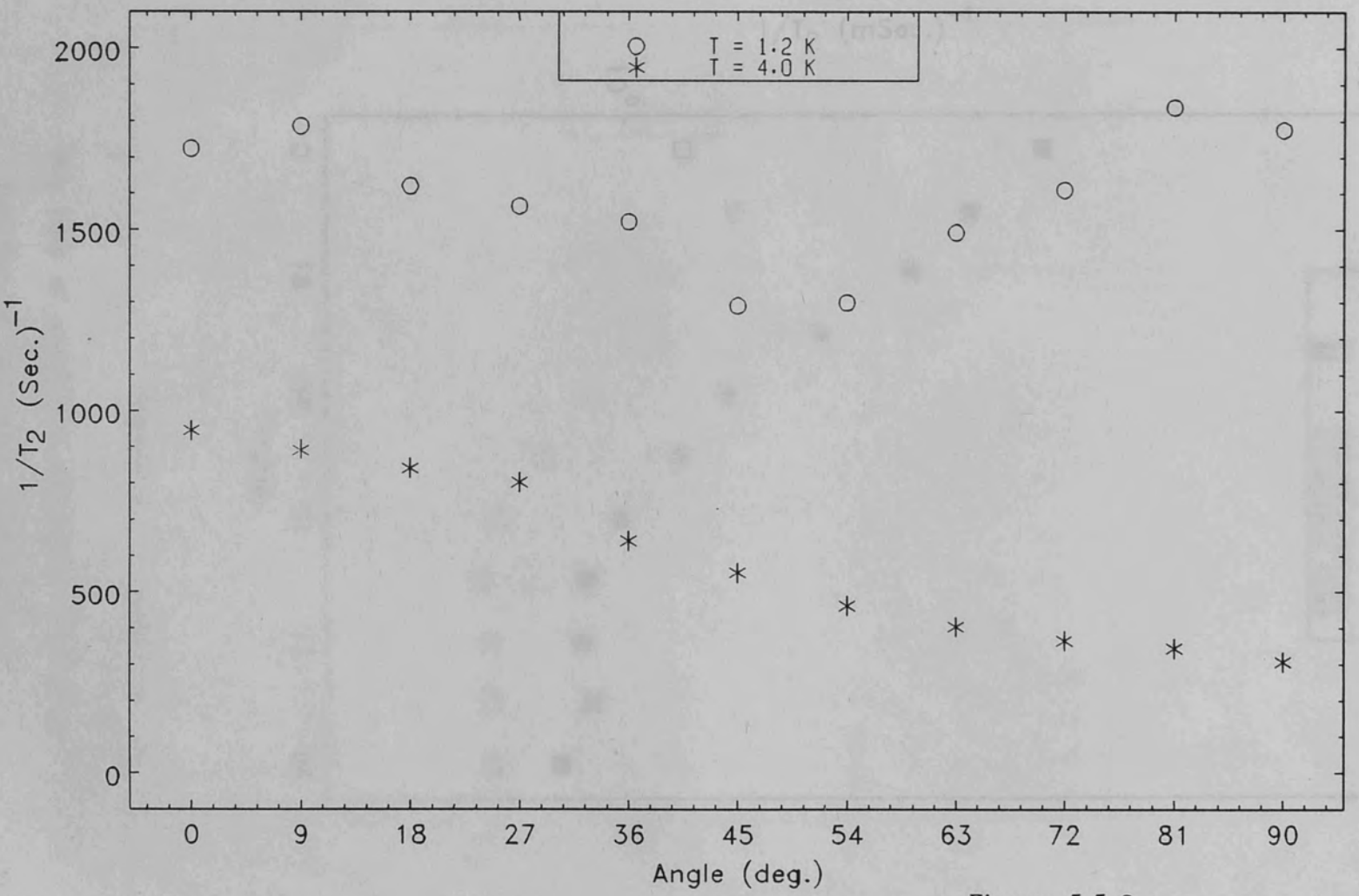

Figure 5.5.3

The variation of spin–spin relaxation rate & angles. x=0.96 monolayer and f_o =5·1 MHz

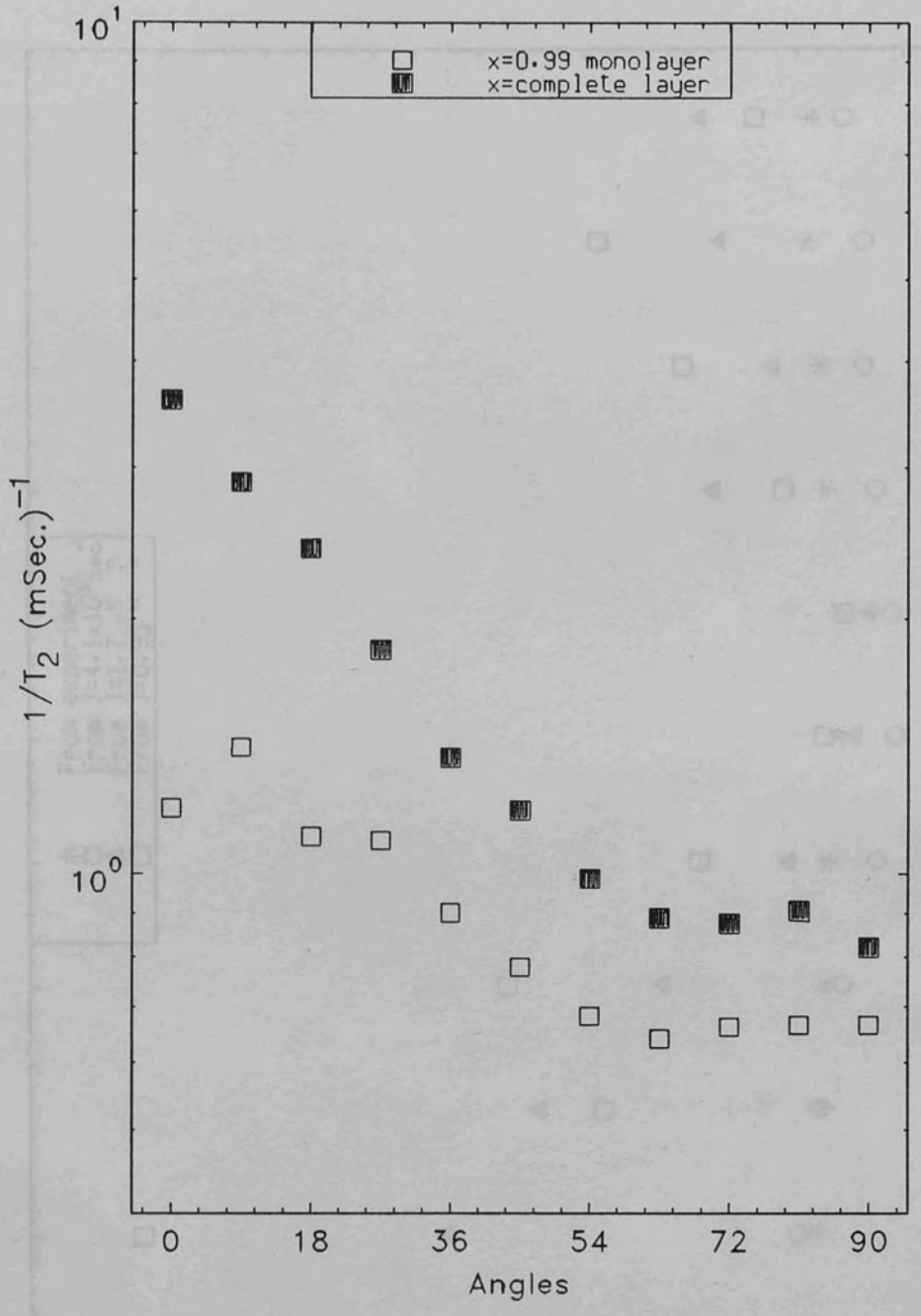

Figure 5.5.4

The rate of spin-spin relaxation time as a function of the angle of orientaion.

T=4.2 K and f_o=5.1 MHz.

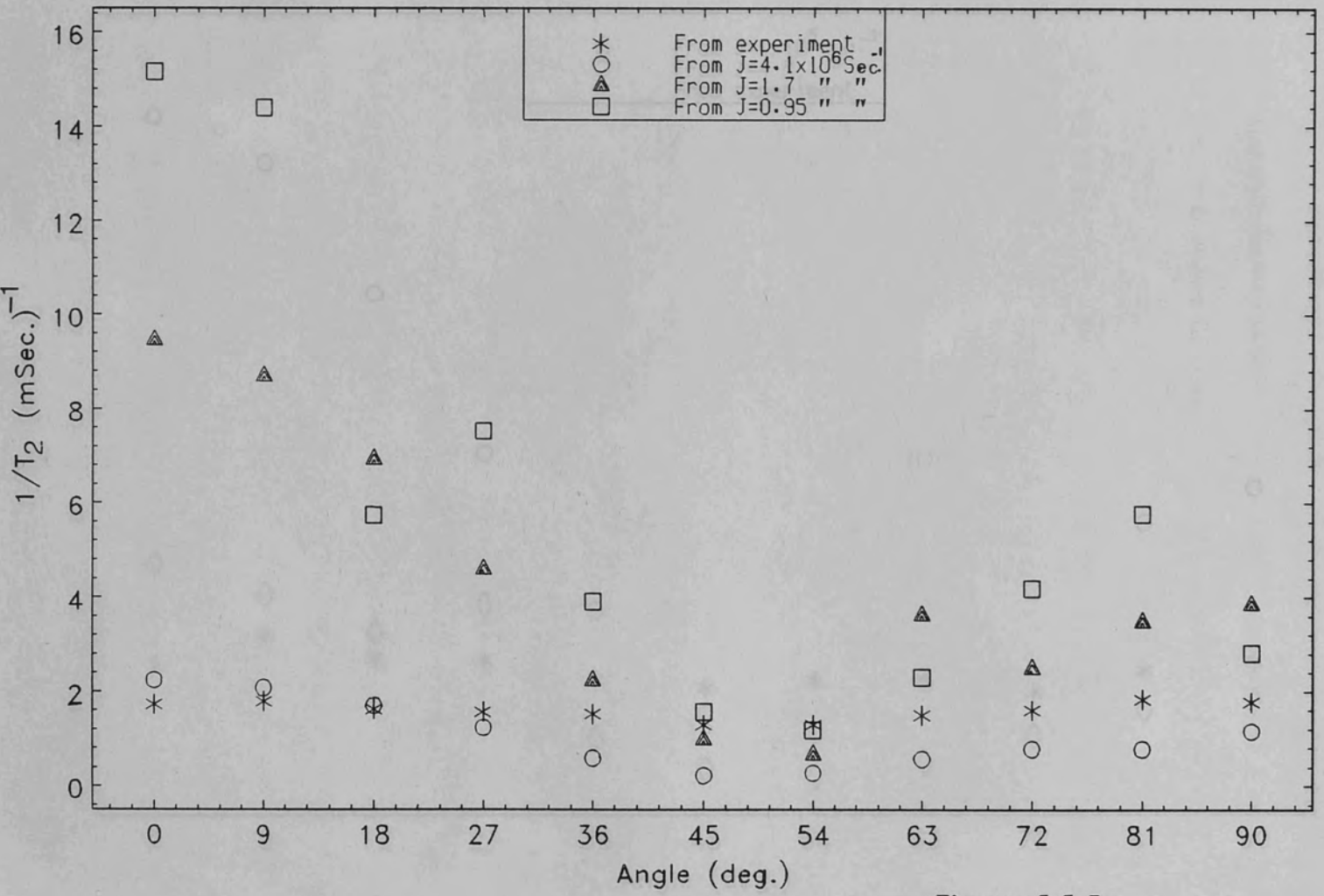

Figure 5.5.5

Comparison between $1/T_2$ obtained experimentally & by using arbitrary J. x=0.96

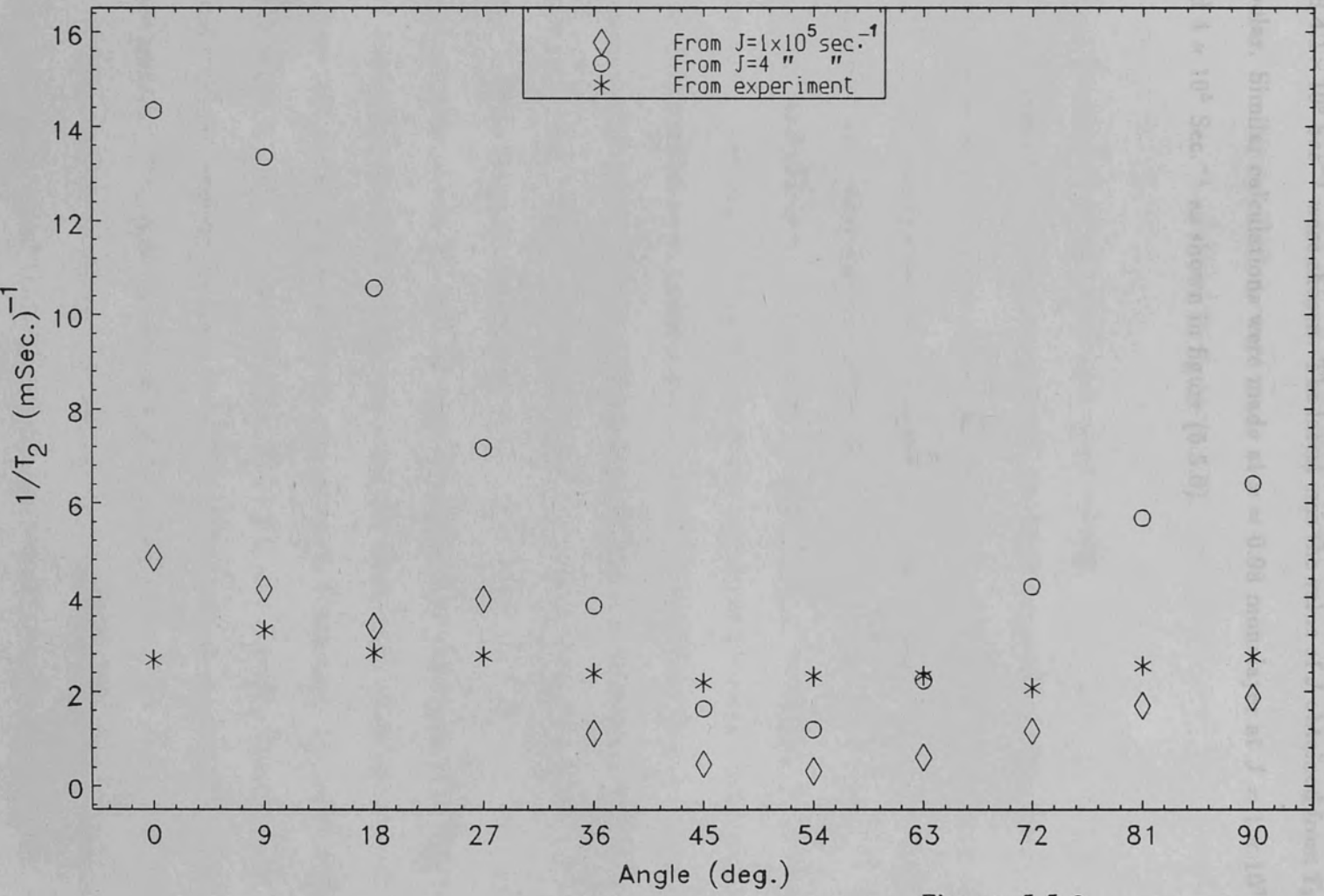

Figure 5.5.6

Comparison between $1/T_2$ obtained experimentally and by using arbitrary J. x=0.98

arbitrary J at coverage $x = 0.96$ monolayer. The values $J = 9.5 \times 10^4$, 1.7×10^5 and 4.1×10^5 Sec^{-1} were chosen. The latest was the value of J obtained from T_2 dipolar. Similar calculations were made at $x = 0.98$ monolayer at $J = 1 \times 10^5$ and 4×10^5 Sec.^{-1} as shown in figure (5.5.6).

CHAPTER 6

Summary and Future Work

6.1 Summary of the Experimental Work:

This work has been done to study the NMR properties of ^{3}He adsorbed on exfoliated graphite through the determination of the relaxation times T_1 and T_2 of the spins system. In this final chapter, a summary for the work and comparison with other groups will be given.

T_1 and T_2 were determined as functions of coverage, frequency, temperature and angle of orientation at the registered phase and solid phase. Some data were taken at mixed phase as well. If did not state; then the working frequency is 5.1 MHz, the temperature is 1.2 K and β is 90 degree.

6.1.1 The Registered Phase:

At this phase, T_1 and T_2 were determined at coverages $x = 0.5$ to 0.57 monolayer where the change was every 0.2 monolayer, while for coverages between 0.57 and 0.625 monolayer the change was in 0.005 steps. For frequencies 1.3, 2.6, 3.9, 5.1, 6.2, 7.5 and 8.3 MHz; $T = 1.2$ K and $\beta = 90°$, a minima were found at perfect registry for both T_1 and T_2 which indicate the reduction of the spins mobility. This minima were found by Sussex group.

Frequency dependence of T_1 and T_2 was determined for the mentioned coverages. It was found that T_1 obeys a logarithmic law with frequency while T_2 is linear. For coverages $x = 0.59$, 0.6, 0.61 and 0.62; frequency dependence of T_1 was determined at angles 0 and 45 besides 90°.

For a number of coverages at x = 0.59, 0.6, 0.605, 0.61 and 0.615 monolayer, T_1 and T_2 were determined as a function of temperature rate for frequencies 5.1 and 2.6 MHz. The activation temperature was evaluated from these graphs and was found to have a maximum of 8.8 K at perfect registry in agreement with Sussex group.

The anisotropy of T_1 was determined at x = 0.58, 0.59, 0.6 and 0.605 monolayer for frequencies 2.6 and 5.1 MHz, but it did not show a dramatic change. On the other hand, the anisotropy of T_2 was determined at x = 0.58, 0.59, 0.6 and 0.61 at frequencies 2.6, 5.1 and 8.3 MHz. It was found that the change of T_2 is frequency dependent while it was coverage independent, the same behaviour was found by Sato and Sugawara.

The correlation time of the quantum motion τ_c was evaluated using different data. It was obtained from T_1 by using the dipolar correlation functions model; as well as from T_1 angle dependence. T_2 data were used to extract τ_c by separating the dipolar relaxation from other mechanisms. The change of τ_c with coverage gave a maximum value of the order of 10^{-8} Sec corresponding to perfect registry. By using this value of τ_c, it was found that the diffusion coefficient D in this region is of the order of 10^{-9} cm^2 Sec^{-1} which is the same order as obtained by Sussex group.

6.1.2 The Mixed Phase:

On the mixed phase which extends between the registered phase and the solid phase; T_1 and T_2 data showed coverage independence. It is thought that this phase is a combination of both registry and solid. The contribution from both phases was determined.

6.1.3 The Solid Phase:

For a wide range of frequencies extended between 1.3 and 10.2 MHz; T_1 and T_2 were determined at coverages between 0.7 and one layer completion in 0.2 steps. At $T = 1.2$ K, T_1 showed a minimum which shifts to lower coverage for higher frequencies, while at $T = 4.2$ K the minima seems to occur at higher coverage. For both temperatures T_2 decreases to reach its lowest value near by the complete layer. The same behaviour was observed by Sussex group for both T_1 and T_2.

T_1 and T_2 were determined with the change of frequency at both $T = 1.2$ and $T = 4.2$ K. For coverages between 0.7 and 0.94 monolayer T_2 was determined using the spin echo technique, while because of the short value of T_2 at higher coverages, the FID method was used. At these high coverages, the inhomogeneity of the magnet $T_2^{mag.}$ was determined.

The characteristic frequency of the exchange motion J was determined. Using the same correlation functions which have been used at registry for T_1 and fitting guess values for J on a universal curve, the optimum values of J were obtained from T_1. Following the same way of analysis as the registered phase and separate T_2 dipolar, the values of J were determined. Comparison with J obtained from T_1 at the minima (Cowan et al 1987), it was found that J decreases with the increase of density which indicates slowing down of the spins motion. These values of J were found one order of magnitude difference than the corresponding values obtained by Sussex.

Some T_2 anisotropy data were taken at1.2 K for coverages $x = 0.96, 0.98$ and one layer showed minima for $1/T_2$ around $\beta = 50°$ which indicate dipolar relaxation (Cowan 1980), these minima were observed by Sato and Sugawara as well. The anisotropy of T_2 at 4.2 K and coverages $x = 0.96, 0.99$ and complete

layer for frequency 5.1 MHz showed the same behaviour as found at registry which concludes that at high temperature, the dipole-dipole relaxation is not dominant.

6.2 Suggestions for Future Work:

In the light of this work and the work of other groups, attention should be paid to several points either theoretically or experimentally and the need of new work to be done such as:

(1) Theoretical study of the effect of the diamagnetic local fields of grafoil which affect the spin-spin relaxation time.

(2) Study of the effect of the edges of grafoil layers and the wall domains on the amount of ^{3}He adsorbed on the grafoil surface.

(3) On the same time, a better substrate than grafoil might be used. Provided that it has a bigger surface area and lower diamagnetic effects.

(4) Experiments should be carried on the mixed phase at temperature less than 1.2 K to investigate the nature of the film and determine the actual contribution from both registry and solid phases.

(5) Experiments to determine the diffusion coefficient at different fractions of monolayer should be tried.

(6) New theories to investigate the linear dependence seen between $1/T_2$ and ω_0 in all experiments at the registered phase and the solid phase.

APPENDIX "A"

The Magnetization System After Applying 90° or 180° Pulse:

For a system in thermal equilibrium, the expectation value $a(t)$ of an operator $A(t)$ is given (Cowan 1987) as:

$$a(t) = Tr\left\{A(t)\ exp(-\beta\mathcal{H}\ )\right\}/Tr\left\{exp(-\beta\mathcal{H}\ )\right\}$$

where $\beta = \frac{1}{K_B T}$.

The time evolution of an operator is described by the Heisenberg equation of motion as follows:

$$\frac{d}{dt}A(t) = \frac{i}{\hbar}[\mathcal{H}\ , A(t)]$$

by integrating the previous equation we obtain:

$$A(t) = exp\frac{i}{\hbar}\mathcal{H}\ t\ A\ exp - \frac{i}{\hbar}\mathcal{H}\ t$$

where $A = A(0)$ is the Schrödinger representation for the operator. Hence the equation of $a(t)$ takes the form:

$$a(t) = Tr\left\{exp\frac{i}{\hbar}\mathcal{H}\ t\ A\ exp - \frac{i}{\hbar}\mathcal{H}\ t\ exp{-\beta\mathcal{H}}\right\}\Big/ \quad (A1)$$
$$Tr\left\{exp{-\beta\mathcal{H}}\right\}$$

Since in NMR the spin system is disturbed, then, a non-equilibrium system should be introduced. However, the non-equilibrium state could be treated as an equilibrium state of different or fictitious Hamiltonian (Cowan 1987). If the system initially had the fictitious Hamiltonian $\mathcal{H}'$ and the time

evolution is generated by the real Hamiltonian $\mathcal{H}''$; equation (A1) can be written on the form:

$$a(t) = Tr\left\{exp\frac{i}{\hbar}\mathcal{H}''t\ A\ exp-\frac{i}{\hbar}\mathcal{H}''t\ exp-\beta\mathcal{H}'\right\}\Big/ Tr\left\{exp-\beta\mathcal{H}'\right\}$$

The general Hamiltonian of the NMR system is given by equation (2.2.1).

$$\mathcal{H} = \mathcal{H}_z + \mathcal{H}_d + \mathcal{H}_m$$

Where $\mathcal{H}_z + \mathcal{H}_m \gg \mathcal{H}_d$; and so $\mathcal{H}_d$ could be ignored. Thus the spin energy states are the equally spaced eigenstates of the Zeeman Hamiltonian. Assuming high temperature limit and bearing in mind that $TrA(t) = 0$, the expectation value equation could be reduced (Cowan 1987) to the form:

$$a(t) = Tr\left\{-\beta\mathcal{H}\ A(t)\right\}/Tr\left\{1\right\} \qquad (A2)$$

In a real NMR system, the non-equilibrium states are created either by applying 90° pulse or/and 180° pulse to the spin system. The first pulse rotates the equilibrium magnetization which was pointing in z-direction to the x-y plane; while the second one rotates it to -z-direction. Where the Hamiltonian in both cases is given as:

$$\mathcal{H}_{90^\circ} = -B_0\gamma\hbar I_x$$

$$= -\hbar\omega_0 I_x$$

$$\mathcal{H}_{180^\circ} = -\hbar\omega_0 I_y$$

Following Cowan (1987), and by comparison with equation (A2), the transverse magnetization $m_x(t)$ could take the following form:

$$m_x(t) = \beta\hbar\omega_0 Tr\left\{M_x(t)\ I_x\right\}/Tr\left\{1\right\}$$

but $M_x(t)$ is the magnetic moment per unit volume in x-direction.

$$M_x(t) = \frac{1}{V}\sum_j \mu_{xj} = \frac{1}{V}\gamma\hbar I_x(t)$$

Hence we can write:

$$m_x(t) = \frac{\gamma\beta\hbar^2\omega_0}{V} Tr\left\{I_x(t)\, I_x(0)\right\} / Tr\left\{1\right\} \qquad (A3)$$

$$m_y(t) = \frac{\gamma\beta\hbar^2\omega_0}{V} Tr\left\{I_y(t)\, I_y(0)\right\} / Tr\left\{1\right\} \qquad (A4)$$

similarly, after applying 180° the equilibrium magnetization will have the form

$$m_z(t) = -\frac{\gamma\beta\hbar^2\omega_0}{V} Tr\left\{I_z(t)\, I_z(0)\right\} / Tr\left\{1\right\} \qquad (A5)$$

APPENDIX "B"

Transformation of I_x into I_- in Magnetization expression:

In equation (2.2.6), the expression of the complex magnetization is given by:

$$m(t) = \frac{\gamma\beta\hbar^2\omega_0}{V} Tr\{I_+(t)I_x(0)\} / Tr\{1\}$$

to transfer this equation to the following form,

$$m(t) = \frac{\gamma\beta\hbar^2\omega_0}{2V} Tr\{I_+(t)I_-(0)\} / Tr\{1\}$$

this implies that the following equality should be valid,

$$2Tr\{I_+(t)I_x(0)\} = Tr\{I_+(t)I_-(0)\}$$

It seems resonable to try the effect of adding the other part of the operator I_-, by which is meant I_y. First; this operator is treated as follows:

$$\begin{aligned} II &= iTr\{I_+(t)I_y(0)\} \\ &= iTr\{[I_x(t) + iI_y(t)]I_y\} \\ &= iTr\{I_x(t)I_y + iI_y(t)I_y\} \\ &= iTr\{I_x(t)I_y(0)\} - Tr\{I_y(t)I_y(0)\} \end{aligned}$$

since the rotation about z-direction does not affect the behaviour of the system; $I_y \rightarrow I_x$ and $I_x \rightarrow -I_y$,

$$\begin{aligned} II &= iTr\{-I_y(t)I_x(0)\} - Tr\{I_x(t)I_x(0)\} \\ &= -iTr\{I_y(t)I_x(0)\} - Tr\{I_x(t)I_x(0)\} \end{aligned}$$

$$II = -Tr\{I_x(t)I_x(0) + iI_y(t)I_x(0)\}$$

$$= -Tr\{[I_x(t) + iI_y(t)]\, I_x(0)\}$$

finally this means that,

$$iTr\{I_+(t)I_y(0)\} = -Tr\{I_+(t)I_x(0)\}$$

Therefore if we add and subtract the above equation from the original term $Tr\{I_+(t)I_x(0)\}$ we obtain,

$$Tr\{I_+(t)I_x(0)\} = Tr\{I_+(t)I_x(0)\} - iTr\{I_+(t)I_y(0)\} -$$

$$Tr\{I_+(t)I_x(0)\}$$

$$2Tr\{I_+(t)I_x(0)\} = Tr\{I_+(t)I_x(0) - iI_+(t)I_y(0)\}$$

$$= Tr\{I_+(t)[I_x(0) - iI_y(0)]\}$$

$$= Tr\{I_+(t)I_-(0)\}$$

and hence, our target will be reached.

REFERENCES

Abou-El-Nasr L., Cowan B. and Fardis M., in "Proc. of 10th AMPÈRE summer sch. and symp.", Portorož, Yugoslavia, 298 (1988).

Abragam A., **The Principles of Nuclear Magnetism**, (Oxford, 1961).

Avogadro A. and Villa M., J. Chem. Phys., **16**, 2359 (1977).

Bloembergen N., Purcell E.M. and Pound R.V., Phys. Rev., **73**, 679 (1948).

Bretz M. and Dash J.G., Phys. Rev. Lett., **26**, 963 (1971).

Bretz M., Dash J.G., Hickernell D.C., Mclean E.O. and Vilches O.E., Phys. Rev. A, **8**, 1589 (1973); Errat., Phys. Rev. A, **9**, 2814 (1974).

Brewer D.F., Creswell D.G. and Thomson A.L., in "Proc. 12th. Int. Conf. on Low Temp. Phys. (LT 12)", (Acad. Press of Japan, Tokyo), 157 (1970).

Campbell C.E. and Schick M., Phys. Rev. A, **5**, 1919 (1972).

Careri G., Santini M. and Signorelli G., in "Low Temp. Phys., LT9", Vol. **A**, (Plenum Press, New York), 364 (1965).

Commercially done using Hilger & Watts model, **E777** Emission Spectrograph..

Cowan B.P., Ph.D thesis, Sussex Univ. (1976).

Cowan B.P., J. Phys. C:Solid State Phys., **10**, 3383 (1977).

Cowan B.P., Richards M.G., Thomson A.L. and Mullin W.J., Phys.Rev.Lett., **38**, 165 (1977).

Cowan B.P., Owers-Bradley J.R., Thomson A.L. and Richards M.G. in **Quantum Fluids and Solids** ed. by S.B. Trickey, E.D.Adams and J.W.Duffy, (Plenum Press, New York), 441 (1977).

Cowan B., J. Phys. C, **13**, 4575 (1980).

Cowan B.P., unpublished notes, **Quantum Theory of Relaxation**, 1987.

Cowan B.P. and Kent A.J., Phys. Lett. A, **106**, 54 (1984).

Cowan B., Abou-El-Nasr L., Fardis M., "Int. Conf. on Low Temp. phys. (LT 18)", **part one**, 307 (1987a).

Cowan B., Abou-El-Nasr L., Fardis M., "Int. Conf. on Low Temp. Phys. (LT 18)", **part one**, 309 (1987b).

Cowan B.P., Abou-El-Nasr L.A., Fardis M. and Hussain A., Phys. Rev. Lett., **58**, 2308 (1987).

Guyer R.A., Richardson R.C. and Zane L.I., Rev. Mod. Phys., **43**, 532 (1971).

Dash J.G., Scientific American, **228**, 30 (1973).

Dash J.G., **Films on Solid Surfaces**, (Academic Press, New York 1975).

Dash J.G., in **Quantum Fluids**, edited by T.Regge and J. Ruvalds (North-Holland, Amsterdam), 63 (1978).

Dash J.G. and Schick M., in **The Phys. of Liquid and Solid Helium**, edited by K.H. Bennemann and J.B. Ketterson (John Willy & son, New York, Chichester, Brisbane, Toronto), 497 (1978).

Farrar T.C.and Becker E.D., **Pulse and Fourier Transform NMR**, (Academic Press, London, 1971).

Fukushima E. and Roeder S.B.W., **Experimental Pulse NMR**, (Addison-Wesley Publishing Company, 1981).

Hering S.V., Van Sciver S.W. and Vilches O.E., J.L.T.P., **25**, 793 (1976).

Hoare F.E., Jackson L.C. and Kurti N., **Experimental Cryophysics**, (Butterworths, London, 1961).

Grimmer D.P. and Luszczynski K., in "**Monolayer and Submonolayer Helium Films**", Ed. by Daunt J.G. and Lerner E., 123 (1973)

Hahn E.L., Phys. Rev., **80**, 580 (1950).

Hickernell D.C., Mclean E.O. and Vilches O.E., Phys. Rev. Lett., **28**, 789 (1972).

Kay and Laby, **Tables of Physical and Chemical Constants**, 14th edition (Longman, London, 1975).

Kent A.J., Ph.D. Thesis, London Univ. (1985).

Kjems J.K., Passell L., Taub H., Dash J.G. and Novaco A.D., Phys. Rev. B, **13**, 1446 (1976).

Kubo R. and Tomita K., J. Phys. Soc. Japan, **9**, 888 (1954).

Landesman A., Ann. Phys. Paris, **8**, 53 (1973).

Mullin W.J. and Cowan B.P., to be published, (1989).

Nielsen M., McTague J.P. and Ellenson W.E., Journal De Physique, **38**, C4 Supp.10, 10 (1977).

Novaco A.D., Phys. Rev. A, **7**, 1653 (1973).

Owers-Bradley J.R., Ph.D. Thesis, Sussex Univ. (1978).

Owers-Bradley J.R., Thomson A.L., Richards M.G. in "Proc. LT-15", J. Phys. (Paris), **39**, C6-299 (1978).

Richards M.G., Advances in Magnetic Resonance, **5**, 305 (1971).

Richards M.G., in **Phase Transitions in Surface Films**, ed. by J.G.Dash and J.Ruvalds, (Plenum Publishing Corporation 165, 1980)

Robertson B. Phys. Rev., **151**, 273 (1966).

Roger M., Delrieu J.M. and Hetherington J.H., J. Physique-Lett. **41**, L-139 (1980).

Roger M., Phys.Rev. B, **30**, 6432 (1984).

Rollefson R.G., Phys. Rev. Lett., **29**, 410 (1972).

Rose-Innes A.C., **Low Temperature Laboratory Techniques**, (The English Universities Press, 1973).

Rusby R.L., J.L.T.P., **58**, 203 (1985).

Sato K. and Sugawara T., J.L.T.P., **38**, 37 (1980).

Secca M.F., Ph.D. Thesis, Sussex Univ. (1983).

Somorjai Gabor A., **Chemistry in Two Dimensions Surfaces**, Cornell Univ. Press (1981).

Sullivan N., Deville G. and Landesman A., Phys. Rev. B **11**, 1858 (1975).

Thomy A. and Duval X., J. Chim. Phys. Physiochem. Biol., **66**, 1966 (1969).

Thomy A. and Duval X., J.Chim. Phys. Physicochem. Biol., **67**, 286, 1011 (1970).

Van Vleck J.H., Phys. Rev., **74**, 1168 (1948).